THE IONIC BUILDING BLOCKS OF LIFE: EXPLORING ASTROCHEMISTRY THROUGH MASS SPECTROMETRY

by

Callie A. Cole

B.S., Chemistry – ACS Certified
University of Montana, Missoula, 2010

Certificate of College Teaching
Graduate Teacher Program
University of Colorado, Boulder, 2013

A thesis submitted to the
Faculty of the Graduate School of the
University of Colorado in partial fulfillment
of the requirements for the degree of
Doctor of Philosophy
Department of Chemistry and Biochemistry
2015

This thesis entitled:

The Ionic Building Blocks of Life: Exploring Astrochemistry through Mass Spectrometry

written by Callie A. Cole

has been approved for the Department of Chemistry and Biochemistry by:

_____

Veronica M. Bierbaum

_____

Theodore P. Snow

_____

Date

The final copy of this thesis has been examined by the signatories, and we find that both the content and the form meet acceptable presentation standards of the scholarly work in the above mentioned discipline.

Cole, Callie A. (Ph.D., Analytical Chemistry)
The Ionic Building Blocks of Life: Exploring Astrochemistry through Mass Spectrometry
Thesis directed by Dr. Veronica M. Bierbaum

ABSTRACT

The first polyatomic molecule was discovered in interstellar space in 1968, catalyzing the growth of a new scientific field called astrochemistry. Since its inception, collaborations among laboratory chemists, astrophysical modelers, and observational astronomers in this field have led to the detection of nearly 200 molecules in the interstellar medium (ISM). Similarly, detections of complex biomolecules in cometary dust and meteorites have sparked theories of the origin of terrestrial life, a central focus of the recently-established field of astrobiology. Chemical processing occurs in a variety of environments within our galaxy. The purpose of this work is to explore the chemistry of ions and molecules that are pertinent to a multitude of these regions including nebulae, prestellar cores, and the atmosphere of Saturn's moon, Titan.

This thesis presents mass spectrometric investigations of gas-phase ion chemistry that contribute to the fields of both astrochemistry and astrobiology. Many gas-phase chemical reactions are initiated by ions due to the attractive forces induced by their charge on a reacting partner. This attraction often lowers the barriers of ion-neutral reactions, and can lead to high reaction rates even at low temperatures. The ions examined herein increase in complexity starting with simple species (CN^-) and concluding with larger biomolecules, the deprotonated nucleobases.

This work begins with a series of Flowing Afterglow-Selected Ion Flow Tube (FA-SIFT) experiments exploring nitrogen-containing carbanion ($C_xN_y^-$) chemistry and the formation of interstellar propene and methyl formate (Chapters 3 and 4). Reactions between $C_xN_y^-$ and H atoms reveal pathways for destruction of several C_xN^- and $C_xN_2^-$ anions, but no reactions are observed for

$C_xN_3^-$ species. Two previously-proposed reactions between organic cations and H_2 are shown to be immeasurably slow and unlikely to produce propene. Lastly, a reaction pathway producing protonated trans-methyl formate is experimentally and computationally verified. The later chapters describe studies of heterocyclic biomolecules performed using a modified ion trap apparatus. These ions include deprotonated azoles, pyrimidines, and purines (Chapters 5-7). In addition to their reactivity, the dissociation processes and fragments of these anions provide clues to potential precursors and abiotic syntheses. Notably, nearly all fragments observed are detected interstellar species.

To my mother, who taught me to view the world with wonder, curiosity, and joy.

We are all connected; to each other, biologically. To the earth, chemically.
To the rest of the universe, atomically.

Neil deGrasse Tyson

ACKNOWLEDGEMENTS

There are many individuals who contributed to the completion of this thesis work, but the central figure is my advisor and mentor, Ronnie Bierbaum. Thank you for your guidance, reassurance, and (of course) scientific expertise. I also want to thank Theodore Snow, for his constant smiles of encouragement and his wisdom. You both helped make the University of Colorado my scientific home for the past 5 years. I would also like to thank a scientist and friend, Eric Herbst, for his great advice and suggestions during his visits and at conferences. Lastly, my undergraduate research advisors Chris Palmer and Philip Ramsey deserve my gratitude for introducing me to the chemistry laboratory at the University of Montana. What all five of these people have in common, in addition to their great breadth of scientific knowledge, is their ability to light up a room with their enthusiasm and positivity. Their love of science is contagious, and I thank them all deeply for that.

The Bierbaum lab group has always been there for scientific support, as well as afternoon snack breaks and laughs. Oscar Martinez, Nick Demarais, Jennifer Herbst, Zhibo Yang, Charles Nichols, Zhe-Chen Wang, and Nadine Wehres all deserve my thanks. The "supergroup" meetings also allowed me to interact with other graduate students, and to practice public speaking. The supergroup members include those of the Barney Ellison, Mathias Weber, and Carl Lineberger research groups. I thank them for their interesting weekly talks and great research suggestions over the years. In addition, I thank my instructors in the Analytical and Physical Chemistry divisions, and the members of my thesis committee: Maggie Tolbert, Jose Jimenez, and Mathias Weber. Without funding, none of the research in this thesis would be possible. Therefore, I also thank the National Aeronautics and Space Administration (NASA) and the National Science Foundation (Grants CHE-1012321, CHE-1300886, and DGE-1144083) for their financial assistance.

My love of teaching and scientific outreach was also greatly enriched during my time at the University of Colorado. Dr. Margaret Asirvatham, Laurel Hyde Boni, Dr. Pam Nagafuji, Alan Foster, and Julie Andrew provided invaluable assistance in setting up (and thinking up) demonstrations and preparing lessons for my teaching efforts. I would like to thank several specific events and schools for the spectacular opportunities they gave me: the CU Teach Program (Julie Andrew), Boulder High School (Dr. Laura Duncan), CU Upward Bound (Tanaya Winder), CU Wizards, the Women in Science Conference, the AP Preparation Program, Longmont and Skyline High Schools (Dr. Richard Martyr), and the Graduate Teacher Program (Dr. Laura Border). Thank you so much for everything you continue to do to spread the love of science to people of all ages!

I can't finish my acknowledgements without thanking those people who helped me blow off steam outside of work. Every morning, I rely on women like Clara Chew, Candace Garbow, and Allison Betts to drag me out of bed and run. Thank you for your constant inspiration! My lunch would taste sour if I had to eat it alone, so thanks to my lunch buddies from the Niels Damrauer group. I really enjoyed my mid-day time with you. My roommate and friend Stephen Hinton has somehow put up with me for four years. I adore him and always will. Sean Bannon has been both supportive and loving to me since before I even began the Ph.D. program here at CU. He is my confidant, friend, and partner. I would not be where I am today without him. Finally, my family has been there through thick and thin, always encouraging me to press on in my pursuits: my mother, Geri, my grandmother, Lois, my twin brother, Ben, my brothers Trevor and Graham, my sister-in-law Tami, my adorable nephew Ryker, and my father, Patrick. Thank you all for your love. I'd like to extend a special thank you to my twin brother Ben (http://www.vogengineering.com), for creating many of the figures and images included in this thesis.

PUBLICATIONS

1. **Cole, C. A.** & Wang, Z.-C.; Snow, T. P.; Bierbaum, V. M. Gas Phase Chemical Processes of the Cyanate Ion (OCN^-). *Journal of Chemical Physics*. **2015**, in preparation.

2. Wang, Z.-C.; **Cole, C. A.**; Snow, T. P.; Bierbaum, V. M. Reactions of Azine Anions with Nitrogen and Oxygen Atoms: Implications for Titan and Interstellar Gas-Phase Chemistry. *Journal of the American Chemical Society*. **2015**, in preparation.

3. **Cole, C. A.**; Wang, Z.-C.; Snow, T. P.; Bierbaum, V. M. Deprotonated Purine Dissociation: Experiments, Computations, and Astrobiological Implications. *Journal of Physical Chemistry A*. **2015**, *119*, 334-343.

4. Wang, Z.-C.; **Cole, C. A.**; Snow, T. P.; Bierbaum, V. M. Experimental and Computational Studies of the Formation Mechanism of Protonated Interstellar Diazines. *The Astrophysical Journal*. **2015**, *798*, 102-109.

5. **Cole, C. A.**; Wang, Z.-C.; Snow, T. P.; Bierbaum, V. M. Anionic Derivatives of Uracil: Fragmentation and Reactivity. *Physical Chemistry Chemical Physics*. **2014**, *16*, 17835-17844.

6. **Cole, C. A.**; Demarais, N. J.; Yang, Z.; Snow, T. P.; Bierbaum, V. M. Heterocyclic Anions of Astrobiological Interest. *The Astrophysical Journal*. **2013**, *779*, 181-190.

7. Lin, Z.; Talbi, D.; Roueff, E.; Herbst, E.; Wehres, N.; **Cole, C. A.**; Yang, Z.; Snow, T. P.; and Bierbaum, V. M. Can Interstellar Propene (CH_3CHCH_2) Be Formed Via Gas-Phase Reactions? *The Astrophysical Journal*. **2013**, *764*, 80-85.

8. **Cole, C. A.**; Wehres, N.; Yang, Z.; Thomsen, D. L.; Snow, T. P.; Bierbaum, V. M. A Gas-Phase Formation Route to Interstellar Trans Methyl Formate. *The Astrophysical Journal Letters*, **2012**, *754*, L5-L9.

9. Yang, Z.; **Cole, C. A.**; Martinez, O.; Carpenter, M. Y.; Snow, T. P.; Bierbaum, V. M. Experimental and Theoretical Studies of Reactions between H atoms and Nitrogen-containing Carbanions. *The Astrophysical Journal*. **2011**, 739, 19-29.

TABLE OF CONTENTS

LIST OF TABLES

LIST OF FIGURES

CHAPTER 1

The Astrochemistry of Gas-Phase Ions

1.1 Introduction

Space was once thought to be an empty vacuum, completely devoid of any matter. Gradually, spectroscopic discoveries of small molecules began to challenge that perspective. CH and CN were detected in 1937 and 1940, and the first ion, CH^+, was detected soon thereafter in 1941.[1-3] Following the observation of these molecules, nearly three decades passed before the first polyatomic molecule (NH_3) was discovered.[4] Arguably, this detection brought about the birth of modern astrochemistry.[5] Rather than considering space a void, astronomers and chemists began to view it as a diverse chemical environment. In the ensuing years, more and more interstellar species were discovered, yielding a current count of nearly 200 molecules. After verifying the existence of these molecules, a major question remains: How were these species formed? Indeed, space conditions often do not seem conducive to chemical reactivity. The densities of the gases throughout our galaxy can range from 10^{-4} to 10^8 cm^{-3}.[6] In diffuse areas, these low densities mean that millions of years can pass between particle collisions. In denser regions, hours may still go by before two particles collide.[7] To put these values in perspective, one cubic centimeter of air at sea level on Earth contains ~10^{19} cm^{-3}. At this density, one particle (i.e. N_2) collides with approximately 10^8 other species per second. In addition to very low particle densities, interstellar space can reach extremely cold temperatures, ranging from 10-150 K. Neither low densities nor low temperatures promote chemical reactivity.

Despite these harsh conditions, chemical reactions occur in space and represent a key driving force behind the evolution of interstellar matter. Although ~95% of matter and energy in the universe, called "dark matter" and "dark energy", is still unknown, the remaining ~5% comprises stars, planets,

moons, comets, asteroids, and other celestial bodies. The area between these bodies, known as the interstellar medium (ISM), is made up of gas (99% by mass), dust, and ice (1% by mass).[8] The ISM is of particular interest to astronomers and chemists, because the physical processes occurring there contribute to star formation, heating and cooling processes, and the overall evolution of galaxies. Of the known interstellar matter, hydrogen is the most abundant element, and helium is second most abundant (~10% that of hydrogen). Carbon, nitrogen, and oxygen follow helium, at about 10^{-3}-10^{-4} the abundance of hydrogen.[5] The two most abundant molecules in space are H_2 and CO (10^{-4} the abundance of H_2).

Perhaps the chemical complexity of space is best represented by an image. Figure 1.1 depicts an enlarged image taken by the Hubble space telescope of the Carina nebula. In this image, the variation of interstellar density and composition is evident. Photons from nearby stars cannot penetrate dense regions with high abundances of dust particles, but they may both penetrate and ionize the gases in more diffuse areas. The false colors in this image illustrate some of the chemical makeup of this nebula. The electronic transitions of oxygen and sulfur atoms, as well as atomic hydrogen recombination lines are shown in blue, red, and green, respectively.[6]

Nebulae such as Carina are the nurseries of star and planet formation, and the mechanism whereby these celestial bodies are created and destroyed is central to the chemical processing of matter in the universe. It is important to differentiate the general stages in this process to understand the relevant environments of the chemistry described in this work. As shown in Figure 1.1, interstellar matter condenses into large accumulations of gas and dust, called clouds (or nebulae). Diffuse clouds (10-10^2 cm^{-3}) further condense into dense clouds (> 10^3 cm^{-3}) which may persist for millions of years. Radiation from nearby stars can penetrate diffuse clouds, ionizing and fragmenting molecules, whereas dense clouds allow for more intermolecular collisions and reactions in the absence of abundant

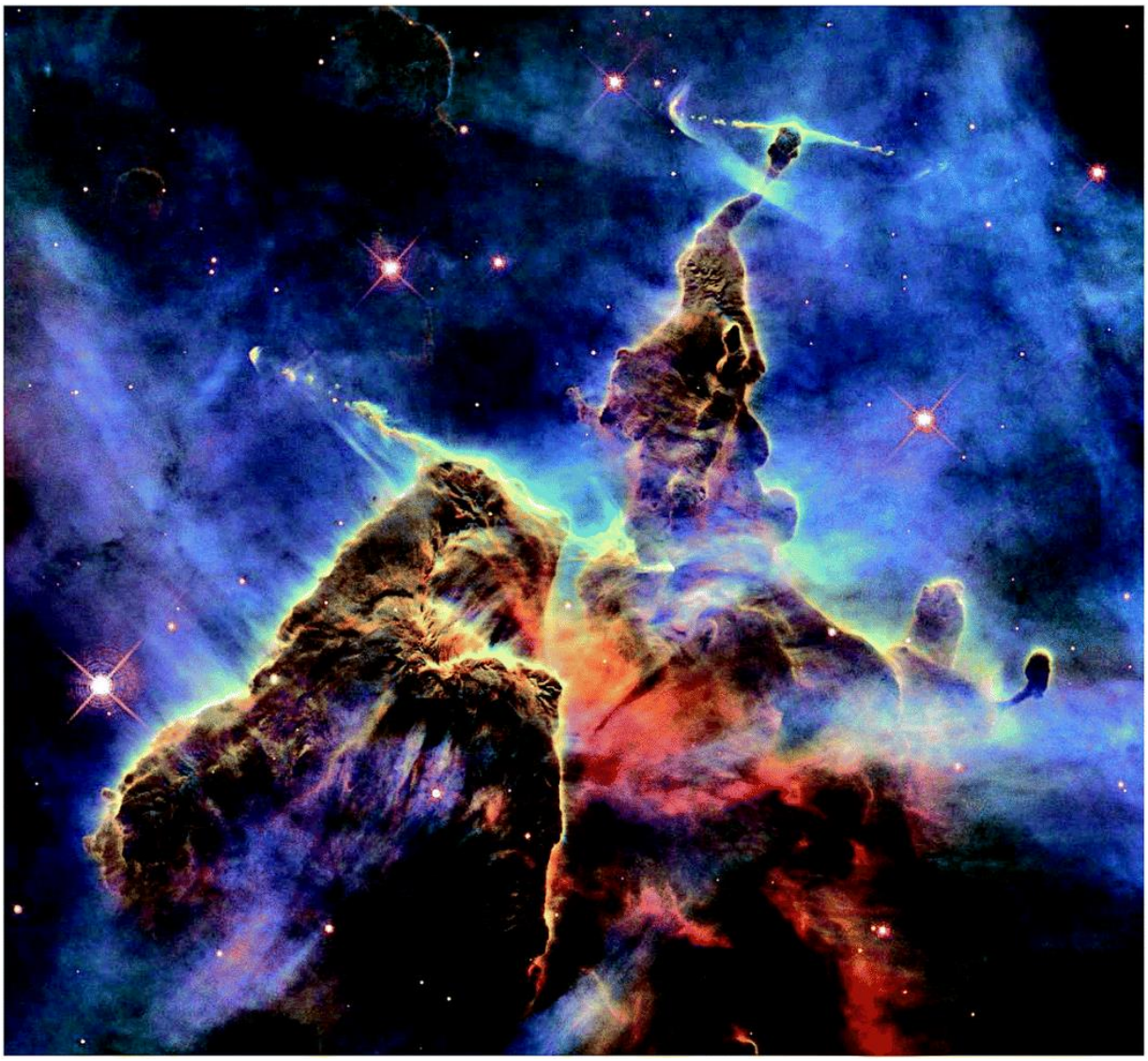

Figure 1.1
Hubble space optical image of the Carina nebula, showing dark molecular clouds as well as diffuse clouds containing ionized gases. The colors correspond to the electronic transitions of O (blue) and S (red), and H atom recombination (green). Image credit: NASA, European Space Agency, M. Livio.[6]

photochemical processing. As dense clouds gather more and more mass, gravity condenses them further until cold cores begin to develop within them. Cold cores are dense pockets (~10^4 cm^{-3}) of gas and dust that reach very low temperatures (~10 K) such that icy mantles build on grain surfaces, where further chemical reactions may take place. Cold cores eventually collapse into a central condensation point, known as a hot core, which begins to heat up to temperatures of 100-300 K. Hot and cold cores are collectively called prestellar cores, because they precede the formation of a protostar and eventually, a star itself. At a certain point in the process of gravitational collapse, a star is formed when the fusion of hydrogen nuclei begins at the center of the condensation point. This star is initially surrounded by a plane of rapidly rotating matter, known as the protoplanetary disk, which eventually gives rise to planets and other solar-orbiting bodies. When the star reaches the end of its life, its chemical contents are released back into the ISM to repeat the cycle once again. A schematic of this process is shown in Figure 1.2.

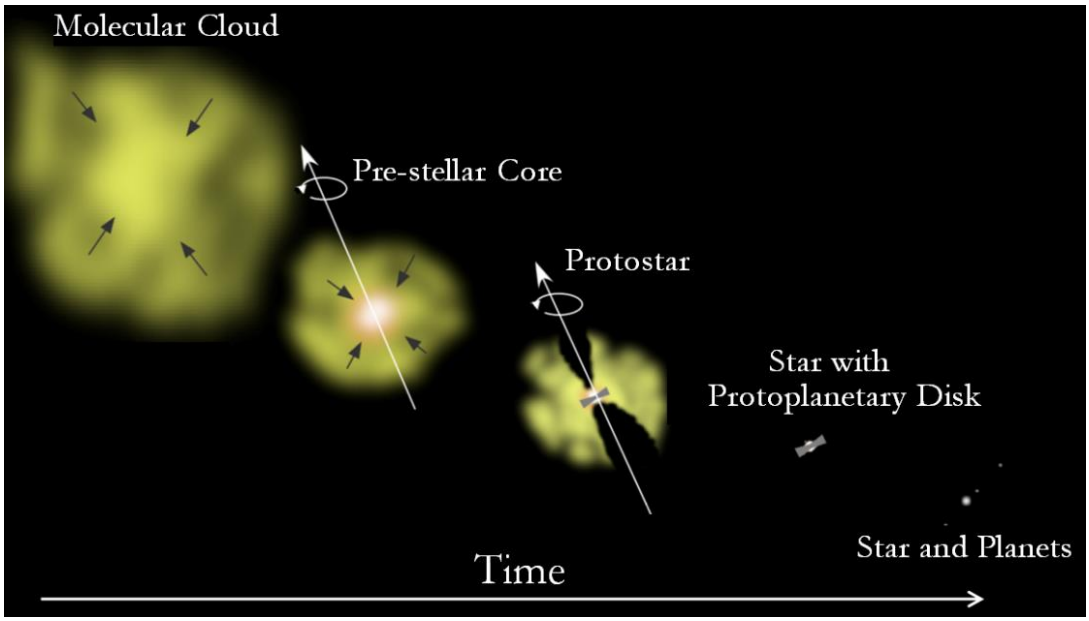

Figure 1.2
The process of star and planet formation from interstellar molecular clouds. (Adapted from Bergin (2013)).[9]

The purpose of this work is to explore the chemistry of ions and molecules that are pertinent to a multitude of interstellar environments from nebulae and prestellar cores to the atmospheres of moons. This chapter provides an introduction to and a synopsis of the material presented in this thesis. First, a background in astrochemistry is provided, including a motivation for studying ions, as well as a description of the environments that give rise to the examined ion-neutral reactions (i.e., gas, ice, and dust in the ISM and Titan's atmosphere). Next, an overview of astrobiology and the origin of life is discussed to motivate the investigations of important biomolecules. The chapter concludes with an overall summary of this thesis work, including the instrumentation used and chemical species investigated.

1.2 Astrochemical Background

1.2.1 What is Astrochemistry?

As its name implies, astrochemistry is a blend of astronomy, the study of celestial bodies in the universe, and chemistry, the study of matter. In addition to astronomy and chemistry, theoretical modelers and physicists contribute greatly to the field. Current knowledge of astrochemistry arises from an amalgamation of these three main sources: laboratory data, astronomical observations, and chemical models (shown in Figure 1.3). The overarching mission of astrochemistry is to unravel the complex chemical interactions of matter in space.

Laboratory astrochemists use mass spectrometry and spectroscopy to accomplish a number of goals. First, laboratory data provide observational astronomers with the spectroscopic signatures of species to aid in their discovery of new molecules. The first molecules to be detected in the late 1930s and early 1940s would not have been confirmed without laboratory spectra. Secondly, laboratory results delineate the chemical reactivity of previously observed and potential interstellar

molecules, allowing the many connections among interstellar species to be uncovered and more fully understood. Lastly, reactivity data involving astrochemically-relevant species including reaction rate constants and branching fractions are reported by laboratory astrochemists and incorporated into chemical models to increase their accuracy. Databases such as the *Kinetic Database for Astrochemistry* (KIDA)[10] compile all current laboratory data, increasing its availability to chemical modelers. The work presented herein addresses the latter two goals of laboratory astrochemistry in detail.

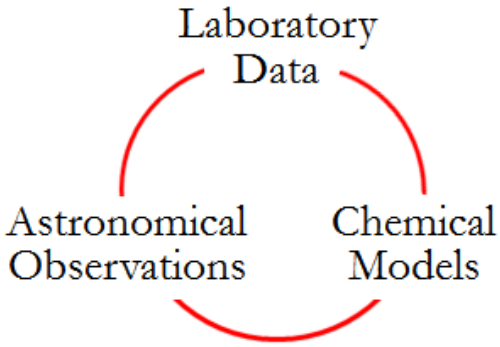

Figure 1.3
The field of astrochemistry is a fusion of three main substituents: laboratory data (kinetic measurements, reaction mechanisms, and spectroscopy), chemical models, and astronomical observations.

Observational astronomers gather data about the universe using telescopes and spacecraft. Arrays of ground-based and satellite telescopes are used to examine spectroscopic signatures of interstellar species and to examine the radiation emitted by various celestial bodies and events (Figure 1.1). Ground-based telescopes have been successfully used for many observations, beginning with the detection of diatomic molecules, and progressing through the use of radio spectroscopy to much larger, more complex species. The Atacama Large Millimeter/submillimeter Array (ALMA) located in the high desert of Chile is the most notable current ground-based array, consisting of 66 radio telescopes capable of detecting millimeter and submillimeter radiation.[11] The Hubble space telescope was launched into orbit in 1990, and remains in operation today, providing some of the deepest views

into the universe by detecting radiation that was emitted as many as 13.2 billion years ago.[12] Finally, spacecraft and probes are sent to celestial objects that can be directly sampled. The Cassini-Huygens Mission has incorporated mass spectrometry and spectroscopy to detect both ions and neutral molecules as it passes through the atmosphere of Titan, a moon of Saturn.[13] Currently, data from the very first comet landing accomplished by the Rosetta mission and the Philae probe in late 2014 are under analysis.[14]

The vast quantities of data collected by laboratory astrochemists and observational astronomers provide chemical modelers with the monumental task of synthesizing it all. Chemical models account for the sources and sinks of various constituents, and can be used to predict interstellar abundances of different species. Many parameters are required by models, including densities, reaction rate constants, temperature, and radiation flux. A model's output is only as meaningful as the quality of the parameters, so the accuracies of these values are of utmost importance. Particularly, reaction rate constants and other experimental data are integral to a model's success.[15]

1.2.2 Why Ions?

Within this work, an emphasis is placed on atoms and molecules with a non-zero electronic charge, known as ions. These species are central to astrochemistry, because the charge of the ion results in an attractive force between itself and a neutral reacting partner, increasing the rate of collisions with respect to their neutral-neutral counterparts. In regions with extremely low densities such as interstellar space, these collisions are responsible for much of the chemical processing that takes place. Consider the two diagrams shown in Figure 1.4 (a) and (b).

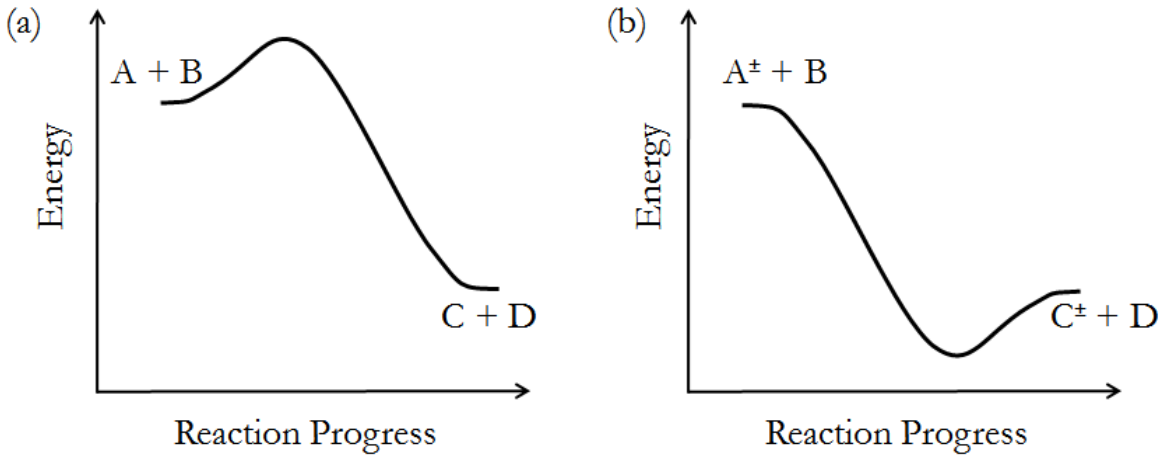

Figure 1.4
Qualitative potential energy surfaces for gas-phase neutral-neutral (a) and ion-neutral (b) reactions. (Adapted from Prof. Veronica Bierbaum's 2012 Distinguished Research Lecture).[16]

Both of the reactions depicted are two-body processes, but (a) shows a reaction between two neutral atoms or molecules, and (b) represents a reaction between an ion and a neutral. There is a key difference between these two processes. When one neutral atom or molecule approaches another ($A + B \rightarrow C + D$), an energy barrier often exists, which can slow or even prevent the reaction progress. However, when an ion approaches a neutral, this barrier is frequently eliminated due to the attractive forces resulting from the ionic charge. The reaction rate of an ion-neutral reaction ($A^{\pm} + B \rightarrow C^{\pm} + D$) is often high, even at the very low temperatures characteristic of the ISM.[7]

The attractive potential between an ion and a neutral species is a strong long-range force that may lead to a collision.[17] The magnitude of this potential is determined by the dipole moment of the neutral (μ_D), which may be either naturally-occurring or induced by the approach of the ion. The charge of the ion (q), the polarizability of the neutral reagent (α), and the distance between the ion and neutral (r) also play an important role. When the neutral possesses a permanent dipole moment, the angle (θ) between the dipole moment vector and r additionally influences the degree of attraction. Equations (1.1) and (1.2) describe the ion-induced dipole and ion-dipole potentials, respectively.

$$V(r) = \frac{-q^2\alpha}{2r^4} \tag{1.1}$$

$$V(r) = \frac{-q^2\alpha}{2r^4} + \frac{-q\mu_D}{r^2}\cos\theta \tag{1.2}$$

When an ion and a neutral approach one another, they may enter into a metastable orbit leading to a collision. This is shown in Figure 1.5. At a critical impact parameter (b_c) value, the ion and neutral enter into orbit. This value is dependent on many of the same variables as the attractive potentials described above, with the addition of the initial ion velocity, v_o. A trajectory where $b > b_c$ leads to a deflected ion, and a trajectory where $b < b_c$ leads to capture. The expression for b_c based on an ion-induced dipole potential is given in equation (1.3) below.

$$b_c = \left(\frac{4q^2\alpha}{\mu v_o^2}\right)^{1/4} \tag{1.3}$$

These expressions represent the starting point for the derivation of an ion-neutral collision rate constant, discussed in further detail in section 2.4.4. Although ion-neutral attraction promotes collisions, not all collisions result in reactions. The overall reaction enthalpies and barriers determine whether a collision leads to products. In interstellar gases, generally only exothermic reactions form products.[18] The results of temperature-variable experiments reveal that many ion-neutral reactions are temperature independent or have a very simple temperature dependence, which allows measurements at room temperature such as those described in this work to be applied to chemical models of the ISM.[7]

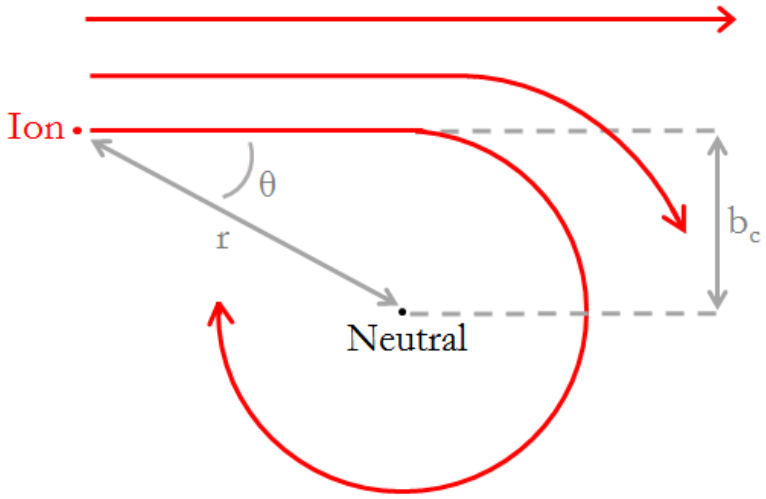

Figure 1.5
Schematic of ion and neutral trajectories. An impact parameter (b) is used to determine whether or not the species enter a metastable orbit with one another. The ion-neutral distance, r, and the angle between r and the dipole moment vector, θ, define the attractive potential between the species when the neutral possesses a permanent dipole moment (equation (1.2)).

1.2.3 Chemistry in the Interstellar Medium (ISM)

In layman's terms, the interstellar medium (ISM) is the 'stuff' between stars in space. As previously described, the vast majority of this material is in the gas-phase (99% by mass), with minor contributions from ice and dust (1% by mass). Particles accumulate within this medium, forming inhomogeneous clouds, such as those shown in Figure 1.1. A review of these regions written by Snow and McCall[19] divides them into four distinct categories based on properties such as composition, density, and temperature. Figure 1.6 illustrates the rise and fall of various constituents (normalized to hydrogen abundance, $n(X)/n_H$) as a function of the total column density of hydrogen (N_H). The term 'column density' refers to the number of particles per unit area (cm^2) integrated along a line of sight. N_H allows the density of various cloud types to be compared.

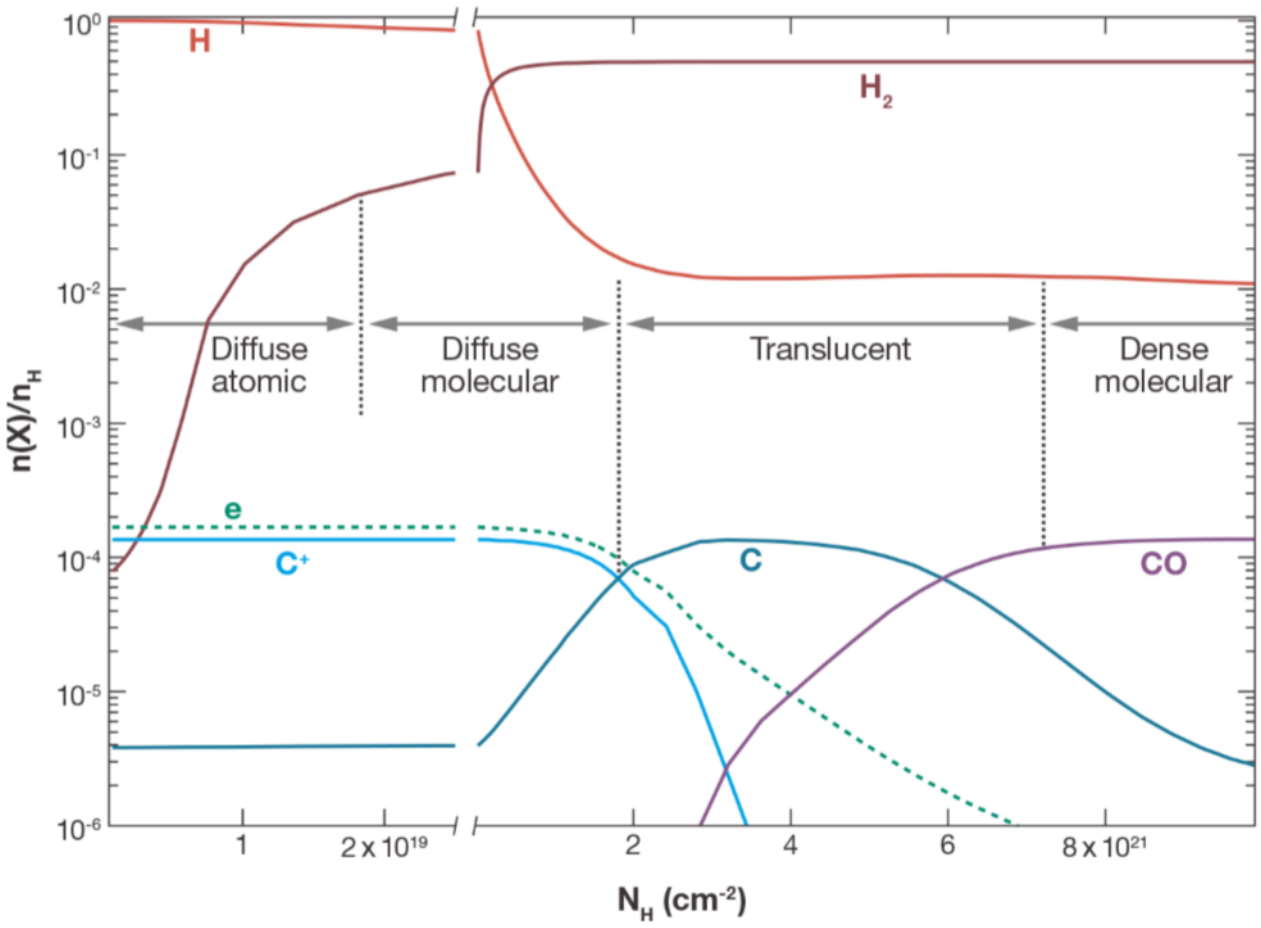

Figure 1.6
The atomic and molecular constituents of various interstellar cloud types are shown. The independent variable is the total column density of hydrogen (N_H), and the dependent variable is the density of a given species normalized to total hydrogen ($n(X)/n_H$). (Adapted from Snow and McCall (2006)).[19]

Recall that interstellar clouds eventually undergo gravitational collapse to form stars (Figure 1.2), and that their central regions are the densest, while the outermost regions are more diffuse. Therefore, each region described in Figure 1.6 represents a layer of a nebula. The diffuse atomic region (10-100 cm^{-3}, 30-100 K) is the outermost layer and consequently receives the highest degree of radiation flux from neighboring stars. This oncoming radiation readily ionizes most species, creating an abundance of cations (including carbon cation, C^+) and electrons. The majority of hydrogen is in its atomic form, with a small portion of H_2. The diffuse molecular layer (100-500 cm^{-3}, 30-100 K) is characterized by the rise of molecular hydrogen with respect to atomic hydrogen, a slight increase in

density, and therefore a slight decrease in transmitted photon flux. Hence, atomic species such as C begin to rise. Although less is known about translucent layers (500-5000 cm^{-3}, 15-50 K), they represent an important transitory zone that divides the largely ionized (C^+) diffuse areas and the predominantly molecular (CO) dense regions. The decline in electron and cation abundance correlates to an increased density, and therefore increased radiation shielding. Dust particles are essential to the blocking of UV and visible radiation from these areas. The innermost, dense molecular layer (> 10^4 cm^{-3}, 10-50 K) is the most chemically complex of the four. Most of the interstellar molecules that have been observed were detected in this region. High densities result in low temperatures allowing icy mantles to form on dust particles as well. Complex molecules can deposit on these surfaces, awaiting the heat released from the cloud's gravitational collapse to re-enter the gas phase.

The molecules that have been discovered in the ISM to date are listed by their order of detection from left to right in Table 1.1.[20] Cations, anions, and neutral molecules ranging in size from two to seventy atoms (C_{70}) have been confirmed. The majority of these nearly 200 molecules were identified based on their rotational emission spectra (meter to submillimeter radio wavelengths), although vibrational and electronic emission have also led to successful detections in the infrared (IR), visible, and ultraviolet (UV) regimes.[20] Using a background star as a light source, absorption spectra are also important tools. For example, many organic compounds can be identified by their absorption of IR wavelengths. IR radiation is particularly useful for analyzing the inner regions of clouds containing high concentrations of dust and ice, as small particulates are not detected at these longer wavelengths. Figure 1.7 shows a spectrum of the Orion nebula taken by the Herschel Space Observatory's HIFI (Heterodyne Instrument for the Far Infrared) apparatus. In this IR spectrum, peaks resulting from the vibrational emissions of many complex species containing H, C, N, O, and S are shown. Notably, a feature of methyl formate, a molecule investigated in Chapter 4, is present in this spectrum.

Table 1.1
List of detected interstellar molecules in order of detection from left to right. **Cations** are shown in red font, **anions** are shown in blue font, and neutral species are shown in black font. * indicates tentative detections.

CH	CN	**CH^+**	OH	NH_3	H_2O	H_2CO
CO	H_2	**HCO^+**	CH_3OH	HC_3N	HCN	HCOOH
SiO	CS	CH_3CN	OCS	NH_2CHO	H_2S	HNCO
CH_3CHO	CH_3CCH	CH_2NH	H_2CS	HNC	SO	CH_3OCH_3
CH_3NH_2	**N_2H^+**	C_2H	CH_2CHCN	CH_3CH_2OH	$HCOOCH_3$	SO_2
HDO	SiS	NS	NH_2CN	HC_5N	C_2H_2	C_3N
H_2CCO	C_2	HNO	CH_3CH_2CN	HC_7N	HC_9N	C_4H
NO	**OCN^-(s)**	CH_3SH	HNCS	C_2H_4	**HCS^+**	**$HOCO^+$**
HOC^+	CH_3C_3N	SiH_4	CH_3C_4H	C_3O	c-SiC_2	C_3H
HCl	c-C_3H_2	C_6H	**$HCNH^+$**	MgNC	C_5H	**H_3O^+**
C_2S	C_3S	$(CH_3)_2CO$	NaCl	AlCl	KCl	AlF
c-C_3H	PN	*CH_3NC	C_3	CH_2CN	HC_2CHO	C_5
SiC	SiC_4	CO_2	CH_2	CP	H_2C_3	H_2C_4
HC_2N	NH	CH_4	C_2O	HCCNC	SiN	HNCCC
SO^+	NH_2	**CO^+**	**HC_3NH^+**	H_2CN	NaCN	N_2O
MgCN	C_8H	**H_3^+**	**H_2COH^+**	C_7H	CH_3COOH	H_2C_6
$HC_{11}N$	HF	c-C_2H_4O	*LiH	C_5N	SiC_3	CH_3
CH_2OHCHO	SiCN	C_4H_2	C_6H_2	C_6H_6	*C_2H_5N	CH_2CHOH
AlNC	FeO	$HOCH_2CH_2OH$	N_2	CH_2CHCHO	CH_3CH_2CHO	SiNC
HC_4N	CH_2CCHCN	c-H_2C_3O	CH_3CONH_2	CH_3C_6H	CH_2CNH	**CF^+**
CH_3C_5N	**C_6H^-**	**C_4H^-**	HCP	**C_8H^-**	CH_2CHCH_3	PO
CNCHO	CCP	**C_3N^-**	NH_2CH_2CHN	*PH_3	**C_5N^-**	HCNO
AlO	HOCN	C_2H_5OCHO	C_3H_7CN	HSCN	AlOH	**CN^-**
H_2O^+	**OH^+**	**H_2Cl^+**	C_{60}	C_{70}	KCN	**SH^+**
FeCN	HOOH	O_2	HO_2	**HCl^+**	SH	$HCOOCH_3$
HNCNH	CH_3O	**ℓ-C_3H^+**	**C_{60}^+**	CH_3CHNH	E-HNCHCN	TiO
TiO_2	CH_3COOCH_3	**NH_3D^+**	HMgNC	***H_2NCO^+**	**ArH^+**	*$(NH_2)_2CO$
CH_3CH_2SH	C_3H_7CN	***NO^+**	C_5S	*MgCCH	*NCCP	*SiH_3CN
*CCN						

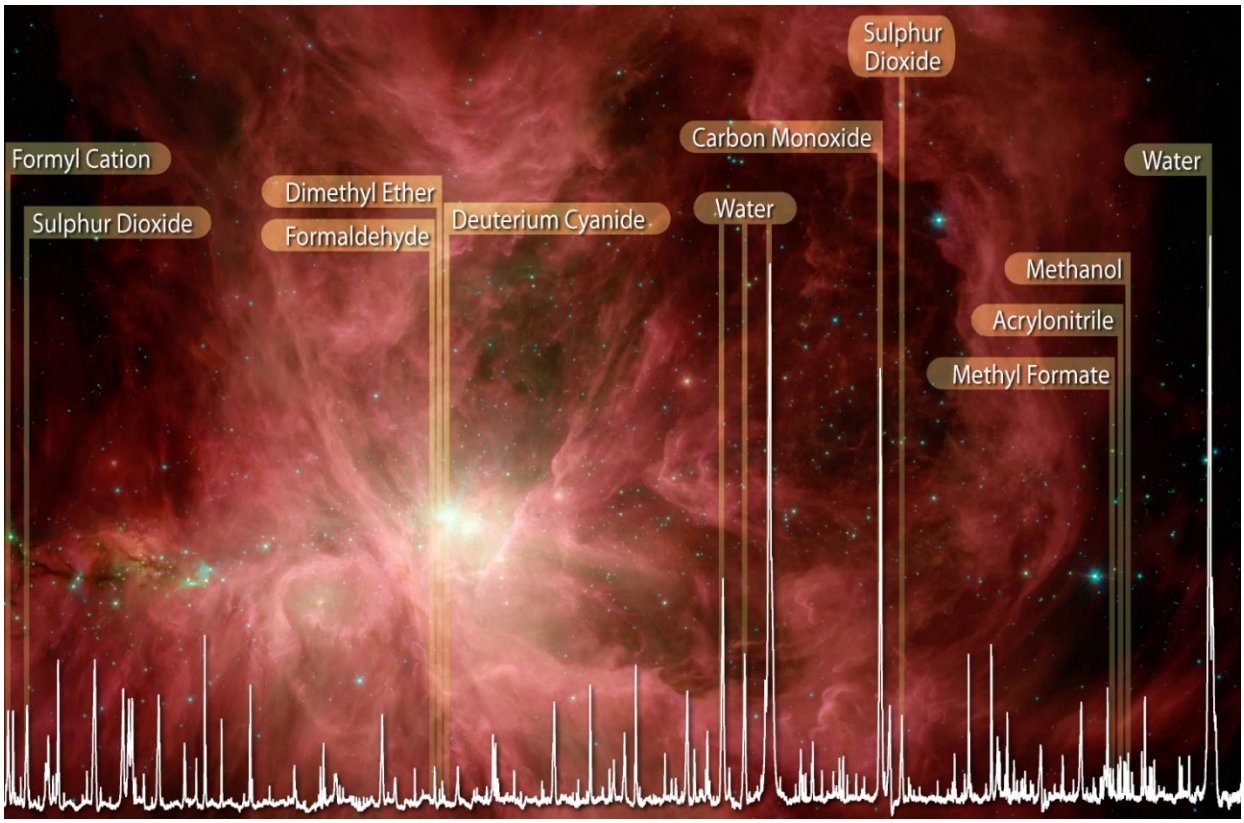

Figure 1.7
HIFI (Heterodyne Instrument for the Far Infrared) spectrum of species detected in the Orion Nebula. © ESA, HEXOS, and the HIFI Consortium.

This background would not be complete without a brief discussion of the remaining 1% of known matter in the ISM: ice and dust. Dust grains are made up of amorphous silicates and carbonaceous material, and incorporate approximately 100% of the available interstellar silicon, magnesium, and iron, 70% of carbon, and 30% of oxygen.[6] Although they are not spherical, their approximate 'diameters' are between 10 and 500 nm.[21] Dust particles serve to block ultraviolet and visible radiation from dense cloud cores, and they provide a means for H atoms to associate, yielding H_2 (the most abundant form of hydrogen in dense cloud environments).[21] Additionally, these grains behave as a reservoir on which gas-phase molecules can accumulate. They enable reactions with activation barriers in the gas phase such as the hydrogenation of C, O, and N. For example, methanol has been proposed to form via sequential hydrogenation of CO on grain surfaces.[22]

Throughout the process of star formation within a nebula, dust grains can accumulate layers of ices onto their surface. These layers are thought to develop sequentially. Adsorbed atomic oxygen is hydrogenated early in the process of cloud formation, generating a water-rich 'polar' inner layer. As the clouds increase in density, CO-rich 'non-polar' layers form on top. Figure 1.8 shows a schematic of deposited ice layers on a silicate grain as a dense cold core (< 20 K) collapses and warms to become a hot core (> 100 K). The observed abundances of some organic species detected in hot cores cannot be explained by gas-phase reactions alone. This will be discussed in greater detail in Chapter 4. It has therefore been suggested that some organics are formed on a dust grain surface during the warming of a core, and that they thermally desorb into the gas-phase as temperatures rise above 100 K.[23] Although methanol is the most complex molecule to be unambiguously detected in interstellar ice mantles, larger species are likely produced in lower quantities.[23] To date, OCN^- is the only verified ionic component of interstellar ice.[24,25]

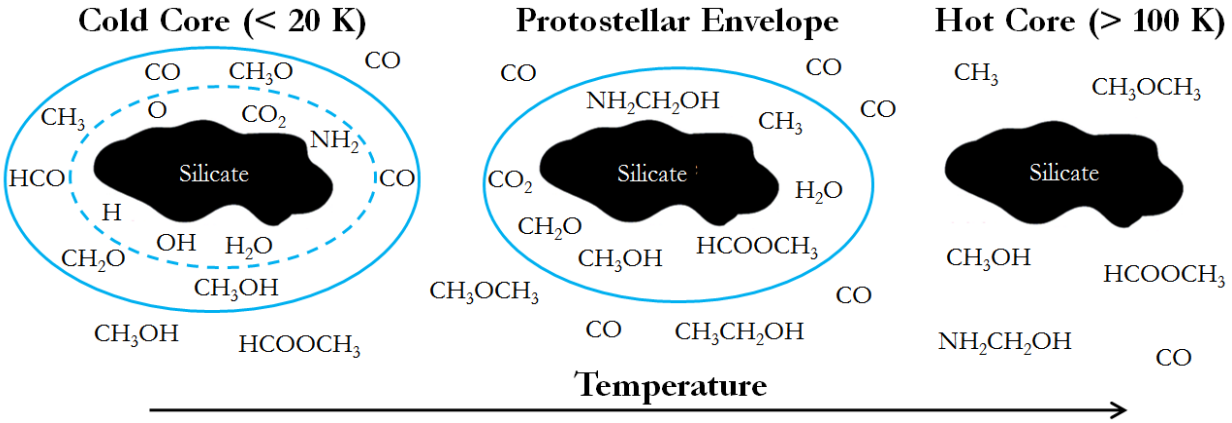

Figure 1.8
Chemical processing in ice mantles on silicate grains during star formation. In the cold core, the dashed blue line represents the inner polar ice layer, and the solid blue line represents the outer non-polar ice layer. The protostellar envelope is warm enough (> 20 K) to promote chemical mixing among these layers. In the hot core, molecules evaporate and undergo continued processing through gas-phase reactions, outlined in this work. (Adapted from van Dishoeck (2014)).[6]

1.2.4 Atmospheric Chemistry of Titan

In addition to the ISM, extraterrestrial atmospheres undergo chemical processing that relies heavily on ion-neutral reactions. Titan, a moon of Saturn, is the only satellite in our Solar System with a substantial atmosphere.[26] This moon is shrouded in a haze of organic molecules that may be similar to Earth's atmosphere prior to the build-up of oxygen (~10^9 years ago).[27,28] For this reason, Titan's atmospheric chemistry has important implications for the origin of terrestrial life. The abiotic pathways that yield complex organic species in the atmosphere of Titan may have also produced essential biomolecules on early Earth.[29,30] Notably, recent results suggest that molecules on Titan may accumulate into membranes, the precursors of cells.[31] Theories of biomolecule origins will be covered in the next section, but a brief overview of Titan's atmospheric chemistry is provided here.

The Cassini spacecraft of NASA's Cassini-Huygens Mission has been orbiting Saturn since 2004, and has successfully passed through the atmosphere of Titan over 100 times. Each 'fly by' results in valuable data that unveil much about its chemical composition. The Ion Neutral Mass Spectrometer (INMS) and the Cassini Plasma Spectrometer (CAPS) instruments aboard the spacecraft show Titan's atmosphere to be predominantly made up of nitrogen (N_2), with minor constituents including CH_4 (2%) and H_2 (0.4%). Photons and high energy electrons from Saturn's magnetosphere induce complex chemistry in the upper atmosphere, producing species such as C_2H_4, C_2H_2, HCN, and C_2H_6 through dissociation processes and ions such as CN^-, C_3N^-, and C_5N^- through ionization events involving N_2 and CH_4.[32] Benzene has been detected, and likely reacts with radicals and ions to produce larger, more complex aromatics.[33] Additionally, massive aerosol species (~8000 Da) termed "tholins" have been detected and are considered the primary source of Titan's opaque haze.[34] A schematic of these mechanisms are shown in Figure 1.9. Anions relevant to Titan including CN^-, C_3N^-, C_5N^-, and deprotonated nitrogen-containing aromatic species, are examined in this thesis.

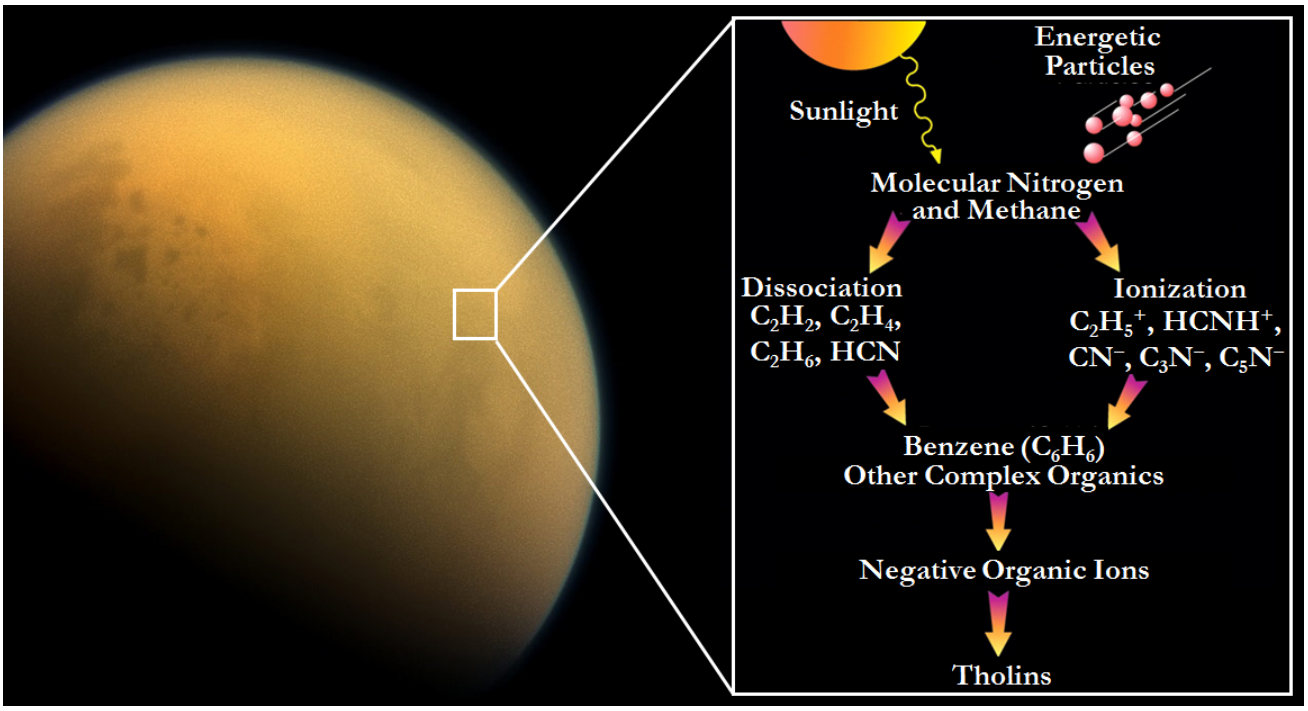

Figure 1.9
The upper atmospheric chemistry of Titan is initiated when the most abundant species (N_2 and CH_4) are dissociated and ionized by solar radiation and energetic particles, forming larger hydrocarbon and nitrile species, ring molecules, and eventually aerosols (tholins). Image credit: NASA JPL – Caltech Space Science Institute. (Adapted from Waite et al. (2007)).[34]

1.3 Astrobiology and the Origin of Life

Much like astrochemistry, astrobiology represents a fusion of scientific disciplines. Astronomers, biologists, and chemists collaborate within this field to study the origin, evolution, distribution, and future of life in the universe.[35] The origin of life has been a central focus of the NASA Astrobiology Institute (NAI) since its establishment in 1998.[36,37] The fundamental question driving origin of life research is: How do simple molecules of terrestrial or extraterrestrial origin assemble into the replicating structures characteristic of life? Two general approaches have been taken to address this question. The top-down approach, favored by biologists, begins with modern life forms and looks for common components to gain an understanding of their ancestors. The research described in this

work employs the bottom-up method, exemplified by the renowned work of Stanley Miller,[38] whereby the chemical formation, destruction, and reactivity of biological compounds is examined.

The biomolecules required to form life were either endogenously produced on early Earth or exogenously formed and delivered to Earth, likely by comets and meteors.[39] Possibly, a combination of these two mechanisms contributed. The feasibility of synthesizing prebiotic species in the early terrestrial atmosphere may be explored through the analysis and observation of current atmospheric systems with analogous environmental conditions. Titan's atmosphere is thought to have a composition and vertical structure similar to the early Earth,[29] allowing astrobiologists to observe and model a contemporary system undergoing possibly prebiotic processes. Many essential biomolecules including purines are predicted to exist there,[30] highlighting Titan's importance to the field of astrobiology. Exogenous delivery of biomolecules to early Earth is also a strong possibility considering the heavy bombardment phase of Earth's history between 3.8 and 4.5 billion years ago.[40] It is estimated that as much as 10^9 kg of carbon was delivered per year to Earth during that period from comets and asteroids. Comets are expected to have carried the bulk of these carbonaceous compounds, and more than 50 molecules, many of which are prebiotic, have been identified in cometary comae to date.[41,42] Similarly, the pyrimidine nucleobase uracil has been detected in the Murchison, Murray, and Orgueil meteorites,[43-45] adding to the argument that biomolecules may have seeded Earth through bombardment of extraterrestrial material.

In addition to the regions of their synthesis, the mechanisms behind prebiotic molecule formation remain largely unknown. The vast majority of the currently detected interstellar species (Table 1.1) are organic in nature, and there are many extraterrestrial environments that promote the synthesis of complex organics in the gas phase (Figure 1.7), on grain surfaces, and in icy mantles (Figure 1.8).[9,23] Astrochemists have extensively studied the abiotic formation of biomolecules,[46,47] yet

there is still no consensus on the formation mechanisms leading to key prebiotic species. Chapters 6 and 7 in this thesis explore nucleobase molecules, including pyrimidines and purines, to better understand their precursors and synthesis pathways.

1.4 Summary of this Work

An array of experimental results relevant to astrochemistry and astrobiology are reported in this thesis. The investigated ions and molecules increase in complexity over the course of this work, beginning with simple species (CN^-) and concluding with larger biomolecules, the deprotonated nucleobases. Figure 1.10 depicts a schematic of the environments and molecules examined. Several ionization techniques and instrumental setups are employed to explore the formation, reactivity, and fragmentation of these species. The following is a brief overview of the projects described herein.

1.4.1 Flowing Afterglow and Ion Trap

All experimental data are collected using one of two mass spectrometric methods. The Flowing Afterglow-Selected Ion Flow Tube (FA-SIFT) apparatus is suited for the study of ion-neutral reactions and measuring kinetic data.[7,48] This instrument is compatible with several ion sources, of which we employ electron ionization and graphite discharge ionization. The smaller species described in Chapters 3 and 4 ($C_xN_y^-$, propene, and methyl formate) employ the FA-SIFT technique. For larger biological molecules, atmospheric pressure ionization methods have been shown to be more effective. An ion trap apparatus coupled with an electrospray ionization source is utilized for the remainder of the studies discussed in Chapters 5-7 (deprotonated azoles, pyrimidines, and purines). We have modified this instrument to allow for the introduction of liquid and gaseous neutral reagents into the ion trap for reactivity studies with ions.[49] An in depth characterization of the experimental methods is included in Chapter 2.

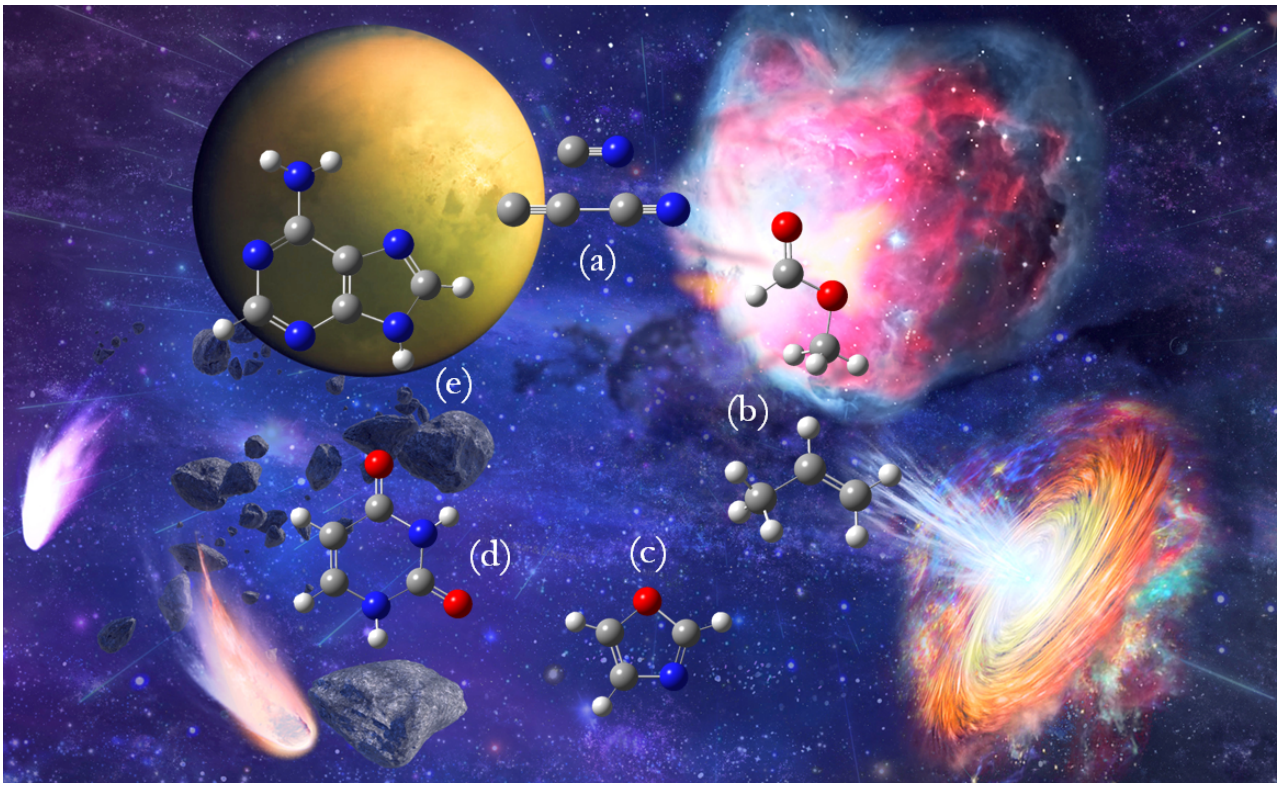

Figure 1.10
The work presented in this thesis is relevant to a multitude of environments from nebulae and prestellar cores to comets, asteroids, and Saturn's moon, Titan. Chapter 3 discusses nitrogen-containing carbanion reactivity (a), Chapter 4 focuses on propene and methyl formate formation (b), Chapter 5 outlines deprotonated azole chemistry (c), and Chapters 6 and 7 cover deprotonated pyrimidine (d) and purine (e) nucleobase dissociation. (Image courtesy of Ben Cole, founder of Tidbit Universe LLC).

1.4.2 Ions of Interest

The first set of ions investigated in this thesis are nitrogen-containing carbanions.[50] Several of these anions (CN^-, C_3N^-, and C_5N^-) have been detected in the ISM near carbon stars[51-53] as well as in the atmosphere of Titan.[26] We have experimentally and computationally explored the reactions between a series of these carbanions and the most abundant atomic species in the universe, hydrogen. Reaction rate constants are measured using the FA-SIFT, and the energetics of various reaction mechanisms are determined using *ab initio* calculations. We find that anions containing one and two nitrogen atoms (C_xN^- and $C_xN_2^-$ with x = 1-6 and x = 1, 3-5 respectively) are destroyed in reactions

with H atoms through associative detachment ($A^- + H \rightarrow AH + e^-$) and fragmentation mechanisms. Anions containing three nitrogen atoms ($C_xN_3^-$, x = 2 and 4) are unreactive with H atom, and therefore may persist in diffuse, H atom rich regions of the ISM. These results are detailed in Chapter 3.

Next, the formation pathways to propene[54] (CH_3CHCH_2) and methyl formate[55] ($HC(O)OCH_3$) are considered. Propene has been detected in abundance within the cold prestellar core TMC-1[56] despite its weak dipole moment and efficient destruction through reactions with atomic oxygen. Methyl formate has been observed in many regions, including star forming areas such as Orion KL[57] and Sgr B2(N),[58] prestellar cold cores,[59] protostars, and protoplanetary disks.[60] The observed abundances of both propene and methyl formate are underpredicted by current astrochemical models. To remedy these inconsistencies, we utilize the FA-SIFT apparatus with supportive computational techniques to study the kinetics of possible formation routes to these molecules. Our results indicate that two suggested reaction steps leading to propene via reactions with H_2 ($C_3H_3^+$ and $C_3H_5^+ + H_2$) do not occur at measurable rates. However, the reaction between protonated methanol and formic acid is shown to produce protonated trans methyl formate at a measurable rate. The branching fractions and reaction rate constant for this process have been measured and added to the KIDA database[10] to make these data available for incorporation into astrochemical models to improve their accuracy. Chapter 4 provides a thorough review of these experiments and results.

The gas phase chemistry of a series of 5-membered ring species known as azoles were also analyzed.[61] Azoles are heterocycles containing an N atom and often an additional O, N, or S atom in their ring. They have yet to be detected in the ISM, Titan's atmosphere, or even in meteorites, but there is some evidence that they are present in cometary dust.[41] Laboratory studies are necessary to lay the groundwork for these detections.[62] Although their interstellar presence has not been conclusively

verified, these species are important in the synthesis of deoxyribonucleic and ribonucleic acids (DNA and RNA), so they are very important to origin of life research. Within a modified ion trap apparatus, we have measured the gas-phase acidities ($\Delta G°_{acid}$) of oxazole, thiazole, and isothiazole. In addition, we observed the reactions of these deprotonated anions with several interstellar molecules (OCS, CO_2, and SO_2) as well as CS_2, CH_3Cl, $(CH_3)_3CCl$, and $(CH_3)_3CBr$ and observed association, atom abstraction, nucleophilic substitution, and elimination. Lastly, the dissociation processes of these anions were probed, and all neutral fragments are detected interstellar species. A comprehensive outline of these investigations is included in Chapter 5.

The final projects described in this work focus on the gas phase chemistry of nucleobase molecules, which are essential substituents of the genetic material of terrestrial life forms. Pyrimidines, including uracil, thymine, and cytosine, make up the first category of these compounds and are discussed in Chapter 6.[63] Purines, including adenine and guanine, are explored in Chapter 7.[64] No nucleobases have been detected in the ISM to date, however both pyrimidines and purines have been detected in comets[41] and meteorites,[43,65,66] supporting the theory of their exogenous formation and delivery to early Earth. Additionally, the presence of complex carbon and nitrogen-containing cyclic molecules in Titan's atmosphere increases the likelihood of a purine and pyrimidine presence there.[67] The abiotic formation of these biomolecules is of central importance to astrobiology. Often, dissociation processes provide insights into the process of molecular synthesis.[68] Therefore, in an effort to elucidate potential precursors and formation processes, these deprotonated nucleobases are collisionally dissociated within an ion trap apparatus, and computational methods are employed to delineate possible mechanisms. Proposed fragment structures are verified through tandem mass spectrometric (MS^n) and acid bracketing methods. Notably, all of the pyrimidine species fragment to produce OCN^-, the only anion whose presence has currently been verified in interstellar ices. Possibly, this anion is important in the initial stages of abiotic formation of pyrimidines. Similarly, our results

indicate that CN^- is the simplest anionic fragment of deprotonated adenine, providing an enigmatic connection between these large purine biomolecules and the small interstellar nitrogen-containing carbanions that began this thesis work.

1.5 References

1 P. Swings; L. Rosenfeld, *Considerations Regarding Interstellar Molecules*. Astrophys. J., **1937**, *86*, 483-486.

2 A. McKellar, *Evidence for the Molecular Origin of some Hitherto Unidentified Interstellar Lines*. Pub. Astron. Soc. Pac., **1940**, *52*, 187-192.

3 A. Douglas; G. Herzberg, *Note on CH^+ in Interstellar Space and in the Laboratory*. Astrophys. J., **1941**, *94*, 381.

4 A. C. Cheung; D. M. Rank; C. H. Townes; D. D. Thornton; W. J. Welch, *Detection of NH_3 Molecules in Interstellar Medium by their Microwave Emission*. Phys. Rev. Lett., **1968**, *21*, 1701-1705.

5 E. Herbst; J. T. Yates, *Introduction: Astrochemistry*. Chem. Rev., **2013**, *113*, 8707-8709.

6 E. F. Van Dishoeck, *Astrochemistry of Dust, Ice and Gas: Introduction and Overview*. Faraday Disc., **2014**, *168*, 9-47.

7 T. P. Snow; V. M. Bierbaum, *Ion Chemistry in the Interstellar Medium*. Annu. Rev. Anal. Chem., **2008**, *1*, 229-259.

8 D. Gerlich; M. Smith, *Laboratory Astrochemistry: Studying Molecules Under Inter-and Circumstellar Conditions*. Phys. Scripta, **2006**, *73*, C25-C31.

9 E. A. Bergin In *Astrobiology: An Astronomer's Perspective*, AIP Conference Proceedings, National Observatory of Rio de Janeiro, 2013.

10 V. Wakelam; E. Herbst; J.-C. Loison; I. Smith; V. Chandrasekaran; B. Pavone; N. Adams; M.-C. Bacchus-Montabonel, et al., *A Kinetic Database for Astrochemistry (KIDA)*. Astrophys. J. Sup. Ser., **2012**, *199*, 21-30.

11 R. L. Brown; W. Wild; C. Cunningham, *ALMA–the Atacama Large Millimeter Array*. Adv. Space Res., **2004**, *34*, 555-559.

12 E. Buenzli; D. Saumon; M. S. Marley; D. Apai; J. Radigan; L. R. Bedin; I. N. Reid; C. V. Morley, *Cloud Structure of the Nearest Brown Dwarfs: Spectroscopic Variability of Luhman 16AB from the Hubble Space Telescope*. Astrophys. J., **2015**, *798*, 127-140.

13 M. Meltzer, *The Cassini-Huygens Visit to Saturn: An Historic Mission to the Ringed Planet*. Springer Praxis Books: Chichester, UK, 2015.

14 D. Jewitt, *Rosetta Mission: When the Dust has Settled*. Nature Phys., **2015**, *11*, 96-97.

15 V. Wakelam; E. Herbst; F. Selsis, *The Effect of Uncertainties on Chemical Models of Dark Clouds*. Astron. Astrophys., **2006**, *451*, 551-562.

16 V. M. Bierbaum, *Astrochemistry: From the Laboratory to the Stars*. Distinguished Research Lecture, **2012**.

17 P. Langevin, *A Fundamental Formula of Kinetic Theory*. Annal. Chim. Physi., **1905**, *5*, 245-288.

18 E. Herbst; W. Klemperer, *The Formation and Depletion of Molecules in Dense Interstellar Clouds*. Astrophys. J., **1973**, *185*, 505-534.

19 T. P. Snow; B. J. McCall, *Diffuse Atomic and Molecular Clouds*. Annu. Rev. Astron. Astrophys., **2006**, *44*, 367-414.

20 D. E. Woon *The Astrochymist*. http://www.astrochymist.org/ (accessed February 23, 2015).

21 I. W. M. Smith, *Laboratory Astrochemistry: Gas-Phase Processes*. In *Ann. Rev. Astron. Astrophys.*, Faber, S. M.; VanDishoeck, E., Eds. 2011; Vol. 49, 29-66.

22 N. Watanabe; A. Kouchi, *Measurements of Conversion Rates of CO to CO_2 in Ultraviolet-Induced Reaction of Amorphous $D_2O(H_2O)$/CO Amorphous Ice*. Astrophys. J., **2002**, *567*, 651-655.

23 E. Herbst, *Three Milieux for Interstellar Chemistry: Gas, Dust, and Ice*. Phys. Chem. Chem. Phys., **2014**, *16*, 3344-3359.

24 J. Novozamsky; W. Schutte; J. Keane, *Further Evidence for the Assignment of the XCN Band in Astrophysical Ice Analogs to OCN^- Spectroscopy and Deuterium Shift*. Astron. Astrophys., **2001**, *379*, 588-591.

25 F. Van Broekhuizen; K. Pontoppidan; H. Fraser; E. van Dishoeck, *A 3-5 Micrometer VLT Spectroscopic Survey of Embedded Young Low Mass Stars II: Solid OCN^-*. Astron. Astrophys., **2005**, *441*, 249-260.

26 V. Vuitton; P. Lavvas; R. Yelle; M. Galand; A. Wellbrock; G. Lewis; A. Coates; J.-E. Wahlund, *Negative Ion Chemistry in Titan's Upper Atmosphere*. Planet. Space Sci., **2009**, *57*, 1558-1572.

27 M. G. Trainer; A. A. Pavlov; H. L. DeWitt; J. L. Jimenez; C. P. McKay; O. B. Toon; M. A. Tolbert, *Organic Haze on Titan and the Early Earth*. Proc. Nat. Acad. Sci., **2006**, *103*, 18035-18042.

28 A. A. Pavlov; M. T. Hurtgen; J. F. Kasting; M. A. Arthur, *Methane-Rich Proterozoic Atmosphere?* Geol., **2003**, *31*, 87-90.

29 F. Raulin, *Question 2: Why an Astrobiological Study of Titan will Help Us Understand the Origin of Life*. Origins Life Evol. Bio., **2007**, *37*, 345-349.

30 S. Pilling; D. P. P. Andrade; A. C. Neto; R. Rittner; A. N. de Brito, *DNA Nucleobase Synthesis at Titan Atmosphere Analog by Soft X-rays*. J. Phys. Chem. A, **2009**, *113*, 11161-11166.

31 J. Stevenson; J. Lunine; P. Clancy, *Membrane Alternatives in Worlds without Oxygen: Creation of an Azotosome*. Sci. Adv., **2015**, *1*, 1400067-1400075.

32 V. Vuitton; R. Yelle; M. McEwan, *Ion Chemistry and N-Containing Molecules in Titan's Upper Atmosphere*. Icarus, **2007**, *191*, 722-742.

33 V. Vuitton; R. Yelle; P. Lavvas, *Composition and Chemistry of Titan's Thermosphere and Ionosphere*. Philos. Trans. A Math Phys. Eng. Sci., **2009**, *367*, 729-741.

34 J. Waite; D. Young; T. Cravens; A. Coates; F. Crary; B. Magee; J. Westlake, *The Process of Tholin Formation in Titan's Upper Atmosphere*. Science, **2007**, *316*, 870-875.

35 C. F. Chyba; K. P. Hand, *Astrobiology: The Study of the Living Universe*. Annu. Rev. Astron. Astrophys., **2005**, *43*, 31-74.

36 D. J. D. Marais; J. A. Nuth, III; L. J. Allamandola; A. P. Boss; J. D. Farmer; T. M. Hoehler; B. M. Jakosky; V. S. Meadows, et al., *The NASA Astrobiology Roadmap*. Astrobiology, **2008**, *8*, 715-730.

37 B. S. Blumberg, *The NASA Astrobiology Institute: Early History and Organization*. Astrobiology, **2003**, *3*, 463-470.

38 S. L. Miller; H. C. Urey, *Organic Compound Synthesis on the Primitive Earth*. Science, **1959**, *130*, 245-251.

39 C. Chyba; C. Sagan, *Endogenous Production, Exogenous Delivery, and Impact-Shock Synthesis of Organic Molecules - An Inventory for the Origins of Life*. Nature, **1992**, *355*, 125-132.

40 P. Ehrenfreund; S. Rasmussen; J. Cleaves; L. Chen, *Experimentally Tracing the Key Steps in the Origin of Life: The Aromatic World*. Astrobiology, **2006**, *6*, 490-520.

41 J. Kissel; F. R. Krueger, *The Organic-Component in Dust from Comet Halley as measured by the Puma Mass-Spectrometer onboard Vega-1*. Nature, **1987**, *326*, 755-760.

42 J. Oro, *Comets and Formation of Biochemical Compounds on Primitive Earth*. Nature, **1961**, *190*, 389-390.

43 R. Hayatsu, *Orgueil Meteorite - Organic Nitrogen Contents*. Science, **1964**, *146*, 1291-1293.

44 C. E. Folsome; J. Lawless; M. Romiez; C. Ponnampe, *Heterocyclic Compounds Indigenous to Murchison Meteorite*. Nature, **1971**, *232*, 108-109.

45 P. G. Stoks; A. W. Schwartz, *Uracil in Carbonaceous Meteorites*. Nature, **1979**, *282*, 709-710.

46 T. P. Snow; M. Stepanovic; N. B. Betts; B. R. Eichelberger; O. Martinez, Jr.; V. M. Bierbaum, *Formation of Gas-Phase Glycine and Cyanoacetylene via Associative Detachment Reactions*. Astrobiology, **2009**, *9*, 1001-1005.

47 L. E. Orgel, *Prebiotic Chemistry and the Origin of the RNA World*. Crit. Rev. Biochem. Mol. Biol., **2004**, *39*, 99-123.

48 V. M. Bierbaum, *Go with the Flow: Fifty Years of Innovation and Ion Chemistry using the Flowing Afterglow*. Int. J. Mass Spectrom. , **2014**, *in press*.

49 S. Gronert, *Quadrupole Ion Trap Studies of Fundamental Organic Reactions*. Mass Spectrom. Rev., **2005**, *24*, 100-120.

50 Z. Yang; C. A. Cole; O. Martinez, Jr.; M. Y. Carpenter; T. P. Snow; V. M. Bierbaum, *Experimental and Theoretical Studies of Reactions Between H atoms and Nitrogen-Containing Carbanions*. Astrophys. J., **2011**, *739*, 19-29.

51 M. Agundez; J. Cernicharo; M. Guelin; C. Kahane; E. Roueff; J. Klos; F. J. Aoiz; F. Lique, et al., *Astronomical Identification of CN^-, the Smallest Observed Molecular Anion*. Astron. Astrophys., **2010**, *517*, L2-L6.

52 P. Thaddeus; C. A. Gottlieb; H. Gupta; S. Bruenken; M. C. McCarthy; M. Agundez; M. Guelin; J. Cernicharo, *Laboratory and Astronomical Detection of the Negative Molecular Ion C_3N^-*. Astrophys. J., **2008**, *677*, 1132-1139.

53 J. Cernicharo; M. Guelin; M. Agundez; M. C. McCarthy; P. Thaddeus, *Detection of C_5N^- and Vibrationally Excited C_6H in IRC+ 10216* Astrophys. J. Lett., **2008**, *688*, L83-L86.

54 Z. Lin; D. Talbi; E. Roueff; E. Herbst; N. Wehres; C. A. Cole; Z. Yang; T. P. Snow, et al., *Can Interstellar Propene (CH_3CHCH_2) be Formed via Gas-Phase Reactions?* Astrophys. J., **2013**, *765*, 80-84.

55 C. A. Cole; N. Wehres; Z. Yang; D. L. Thomsen; T. P. Snow; V. M. Bierbaum, *A Gas-Phase Formation Route to Interstellar Trans-Methyl Formate*. Astrophys. J. Lett., **2012**, *754*, L5-L8.

56 N. Marcelino; J. Cernicharo; M. Agúndez; E. Roueff; M. Gerin; J. Martín-Pintado; R. Mauersberger; C. Thum, *Discovery of Interstellar Propylene (CH_2CHCH_3): Missing Links in Interstellar Gas-Phase Chemistry*. Astrophys. J. Lett., **2007**, *665*, L127-L130.

57 C. Favre; D. Despois; N. Brouillet; A. Baudry; F. Combes; M. Guelin; A. Wootten; G. Wlodarczak, *$HCOOCH_3$ as a Probe of Temperature and Structure in Orion-KL*. Astron. Astrophys., **2011**, *532*, A32.

58 Y. T. Miao; D. M. Mehringer; Y. J. Kuan; L. E. Snyder, *Complex Molecules in Sagittarius B2(N) - The Importance of Grain Chemistry*. Astrophys. J., **1995**, *445*, L59-L62.

59 A. Bacmann; V. Taquet; A. Faure; C. Kahane; C. Ceccarelli, *Detection of Complex Organic Molecules in a Prestellar Core: A New Challenge for Astrochemical Models*. Astron. Astrophys., **2012**, *541*, L12-L16.

60 E. Herbst; E. F. van Dishoeck, *Complex Organic Interstellar Molecules*. Annu. Rev. Astron. Astrophys., **2009**, *47*, 427-480.

61 C. A. Cole; N. J. Demarais; Z. Yang; T. P. Snow; V. M. Bierbaum, *Heterocyclic Anions of Astrobiological Interest*. Astrophys. J., **2013**, *779*, 181-190.

62 H. Mollendal; A. Konovalov, *Microwave Spectrum of 2-Aminooxazole, a Compound of Potential Prebiotic and Astrochemical Interest*. J. Phys. Chem. A, **2010**, *114*, 2151-2156.

63 C. A. Cole; Z.-C. Wang; T. P. Snow; V. M. Bierbaum, *Anionic Derivatives of Uracil: Fragmentation and Reactivity*. Phys. Chem. Chem. Phys., **2014**, *16*, 17835-17844.

64 C. A. Cole; Z.-C. Wang; T. P. Snow; V. M. Bierbaum, *Deprotonated Purine Dissociation: Experiments, Computations, and Astrobiological Implications*. J. Phys. Chem. A, **2015**, *119*, 334-343.

65 R. Hayatsu; M. H. Studier; L. P. Moore; E. Anders, *Purines and Triazines in Murchison Meteorite*. Geochim. Cosmochim. Ac., **1975**, *39*, 471-488.

66 P. G. Stoks; A. W. Schwartz, *Nitrogen-Heterocyclic Compounds in Meteorites – Significance and Mechanisms of Formation*. Geochim. Cosmochim. Ac., **1981**, *45*, 563-569.

67 J. Cui; R. V. Yelle; V. Vuitton; J. H. Waite; W. T. Kasprzak; D. A. Gell; H. B. Niemann; I. C. F. Muller-Wodarg, et al., *Analysis of Titan's Neutral Upper Atmosphere from Cassini Ion Neutral Mass Spectrometer Measurements*. Icarus, **2009**, *200*, 581-615.

68 A. Simakov; G. B. S. Miller; A. J. C. Bunkan; M. R. Hoffmann; E. Uggerud, *The Dissociation of Glycolate – Astrochemical and Prebiotic Relevance*. Phys. Chem. Chem. Phys., **2013**, *15*, 16615-16625.

CHAPTER 2

Experimental and Computational Methods

2.1 Introduction

The work presented in this thesis integrates experimental and computational research on gas-phase ion chemistry. This chapter thoroughly describes the instrumentation and theoretical methods, in addition to the data analysis approaches that are employed. Chapters 3-5 incorporate the Flowing Afterglow-Selected Ion Flow Tube (FA-SIFT) technique, and a modified Thermo Finnigan LCQ Deca XP Plus Quadrupole Ion Trap is primarily used for the studies detailed in Chapters 5-7. Therefore, we will begin with an overview of these two instrumental setups, before describing kinetic data acquisition and error propagation. We will conclude with an overview of the computational practices that are integrated throughout this work.

2.2 Flowing Afterglow-Selected Ion Flow Tube (FA-SIFT)

The flowing afterglow experiment originated 50 years ago in the National Bureau of Standards laboratories (present day National Oceanic and Atmospheric Administration, NOAA) in Boulder, CO for the purpose of studying the chemical reactions occurring in Earth's ionosphere.[1,2] Since that time, applications of this method have proliferated beyond atmospheric chemistry to include fundamental organic chemistry,[3] thermochemistry,[4] analytical chemistry,[5] and astrochemistry,[6] to name a few. This exceptional technique is particularly effective for the study of reactions between ions and neutral atoms/molecules, due in part to several beneficial features. First, the determination of accurate kinetic data is made possible by the relationship between distance and time in a flow system. Additionally, the reactants (ionic and neutral) have a thermal energy distribution as a result of multiple collisions with

the helium carrier gas, allowing for reactivity studies at a well-defined temperature (300 K). High ion densities are possible, increasing the sensitivity of the technique. Finally, this instrument provides a platform to study unstable, exotic ions and neutrals.[7] This work discusses ions produced by electron ionization (EI) and graphite discharge ionization, as well as neutral H atom generation and reactivity.

The basic layout of the FA-SIFT is shown in Figure 2.1 and has been discussed in detail in earlier publications.[8,9] For simplicity, we will describe the instrument from left to right following the directional flow of ions in the apparatus. As Figure 2.1 depicts, there are four main regions of the FA-SIFT: (1) the ion production region, (2) the ion selection region, (3) the reaction flow tube, and (4) the ion detection region. In a flow of helium (99.997%, with further liquid nitrogen purification), cations and anions are produced from a variety of sources, discussed in the following section. Ions of a desired polarity are drawn through a nose cone and focused by electrostatic lenses prior to entering a quadrupole mass spectrometer. Favorable RF (radio frequency) and DC (direct current) potentials are applied to the poles such that only the ions of desired m/z pass through the length of the quadrupole to be refocused by a second set of electrostatic lenses. The focused ions of chosen m/z are then injected into the reaction flow tube through a Venturi inlet. Within the reaction flow tube, the ions are again entrained in a flow of helium and collisionally thermalized prior to encountering neutral reagents, which are added through one of seven inlets along the length of the meter-long flow tube. The remaining parent and newly-formed product ions are sampled through a second nose cone, focused with electrostatic lenses, mass analyzed with a second quadrupole mass spectrometer, and finally detected with a continuous dynode electron multiplier. Kinetic data are gathered by monitoring the decline of reactant ion signal as a function of reaction distance (proportional to reaction time).

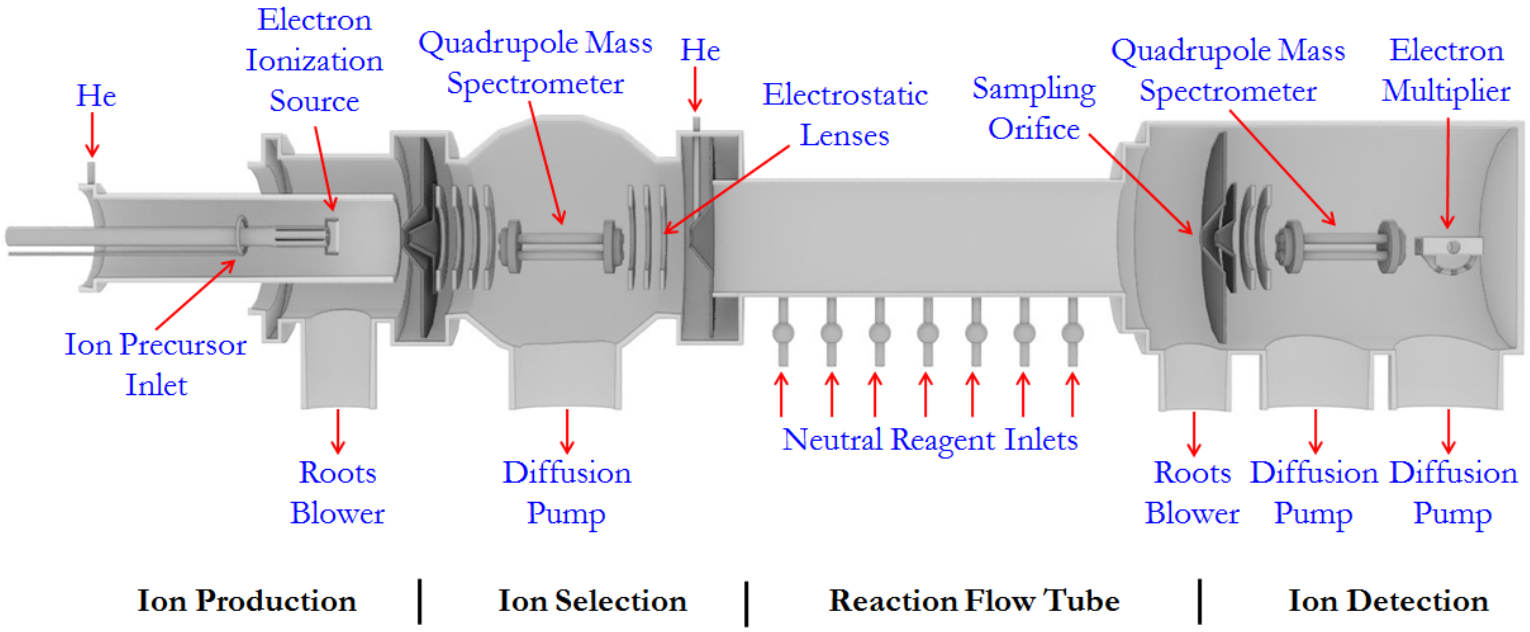

Figure 2.1
Flowing Afterglow-Selected Ion Flow Tube. (Image courtesy of Ben Cole, founder of Tidbit Universe LLC).

2.2.1 Ion Production

The ion production region of the FA-SIFT is housed in a stainless steel tube with an inner diameter of 4.75 cm. Helium serves as both a carrier gas and a discharge medium in this region, and is maintained at ~0.25-0.30 Torr for all experiments. A two-stage mechanical pumping system consisting of a Roots blower (~200 L s^{-1}) and a backing pump continually remove gases from this section of the instrument, promoting a flow. Precursor gases are introduced into the flow from an axially movable inlet consisting of a 4 cm diameter ring with 24 upstream equidistant holes to promote sufficient mixing. This precursor inlet and an EI source are shown in Figure 2.2 below. The EI source consists of a filament (iridium with yttrium oxide coating) and an extraction grid. To generate a plasma of ions, a current is run through the filament (~6 A). Emitted electrons (~25 μA) accelerate towards the extraction grid, which is held at a potential 70 V more attractive than the filament (~90 V and ~20 V, respectively). Between the filament and the extraction grid, electrons interact with the helium carrier gas (and any introduced precursor gas), forming an array of ions (i.e. $He + e^- \rightarrow He^+ + 2\ e^-$).

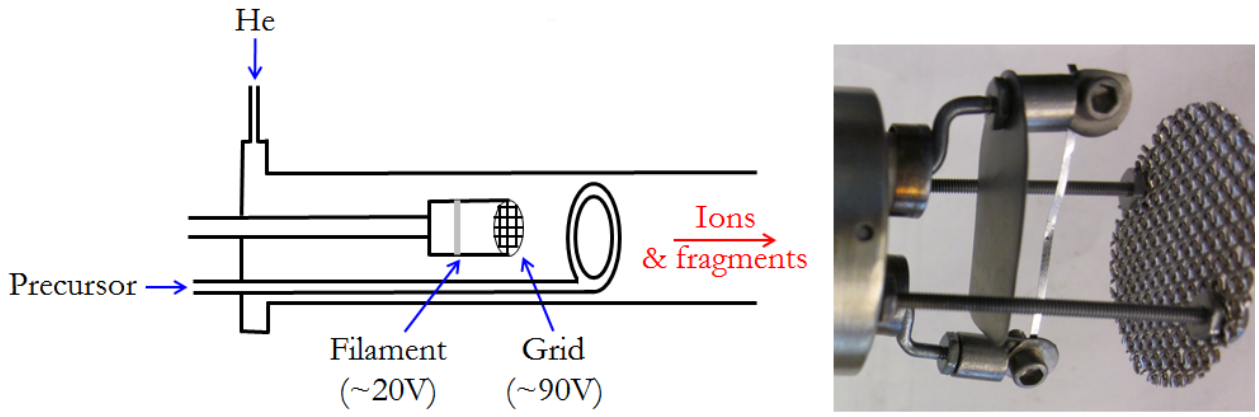

Figure 2.2
Electron Ionization (EI) Source; diagram (left) and photograph (right).

A second ion production method that is coupled with the FA-SIFT is a graphite discharge source, shown in Figure 2.3. A rod of graphite (~0.5 cm diameter, ~7 cm long) is biased relative to the source flow tube by 2-3 kV, producing a discharge in the helium carrier gas. This rod is held by a hollow stainless steel support that is isolated from the flow tube by a quartz sleeve along its entire length. A larger quartz sleeve is used to isolate the barrel-type connector that joins the graphite rod to the support. The graphite is conductively cooled during discharge by flowing water through the center of the hollow stainless steel support. Unlike the EI source, N_2 gas is introduced here as the discharge medium. Although the exact mechanism of ionization is unclear, the discharging graphite likely sputters carbon from its surface, forming bare carbon chain anions. The added N_2 gas then may react with these anions to form the $C_xN_y^-$ anions that are discussed in Chapter 3.

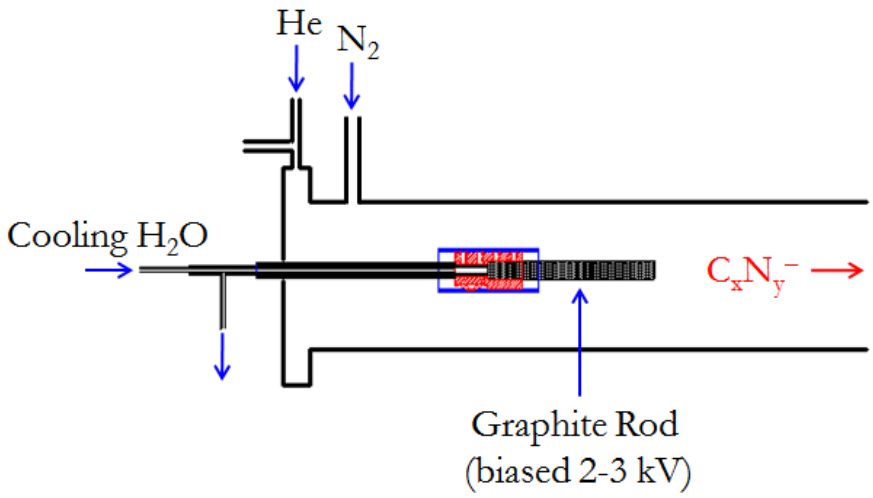

Figure 2.3
Graphite Discharge Ionization Source.

2.2.2 Ion Selection

The newly-formed ions are sampled through a nose cone with an orifice of approximately 2 mm. A conical extractor electrode with a 4 mm diameter aperture sits just beyond the nosecone, and its electric field serves to draw the ions from the ion production region (~0.25-0.30 Torr) to the lower pressure ion selection region (~1 x 10^{-5} Torr). This region consists of two sets of electrostatic lenses and a quadrupole mass spectrometer, which serves to select the m/z of interest for the experiment. This selection capability was added to the FA design in 1976 by Adams and Smith in order to remove unwanted electrons, ions, and parent gas species from the reaction flow tube.[10] A set of two diffusion pumps, a 10 inch pump for the lens region and a 6 inch pump for the quadrupole housing region (~2000 L s^{-1} air and ~700 L s^{-1} air, respectively), evacuate the ion selection chamber. Following ion extraction, two ring electrodes and a set of three electrostatic lenses (together forming an Einzel lens) serve to focus the beam of ions into the entrance of the quadrupole mass spectrometer. The potential applied to each of these lenses is variable, and can be optimized such that the ion current is maximized and the energy imparted to the ions is minimized. The quadrupole is capable of analyzing species up to m/z 500. When the quadrupole operates in RF-only mode (with no DC potential applied to the poles), all ions of a single polarity can be transmitted. During an experiment, a DC potential is applied to the poles such that only ions of a specific m/z can follow a stable trajectory through the mass spectrometer. Figure 2.4 shows two overlaid mass spectra resulting from graphite discharge ionization with ~0.150 Torr helium and N_2 in the source flow tube. These ions are discussed in detail in Chapter 3. The blue, "unSIFTed" (RF-only) spectrum shows an array of nitrogen-containing carbanions including several interstellar anions (CN^-, C_3N^-, and C_5N^-). When the correct DC potential is applied, the red "SIFTed" spectrum is obtained where only the m/z of interest, in this case $C_4N_3^-$, is transmitted with minimal noise and interference from other species. Following the quadrupole, ions enter a second Einzel lens (three electrostatic lenses) that focuses the mass-selected ions into a Venturi inlet that aids

in the flow of ions from the low pressure selection region (~1 x 10^{-5} Torr) to the high pressure (~0.50 Torr) reaction flow tube. This conical inlet is made up of concentric inner and outer annuli through which helium flows to produce a low pressure region near the sampling orifice, thereby increasing ion transmission into the reaction flow tube.

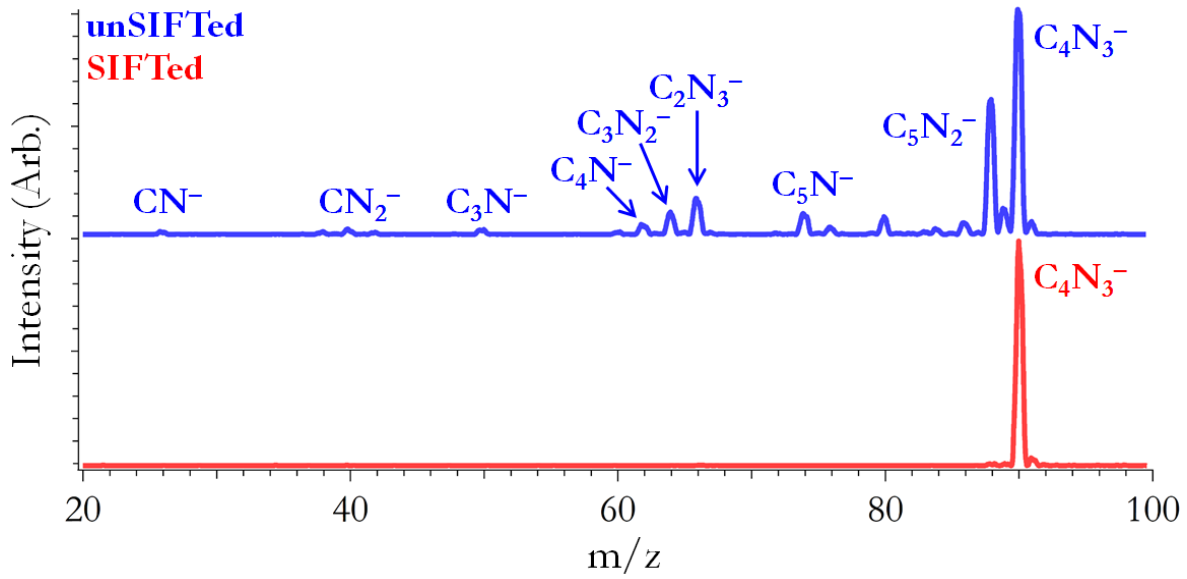

Figure 2.4
Overlaid mass spectra in RF-only mode (unSIFTed) and with an applied DC potential (SIFTed) to the quadrupole at the entrance of the flow tube on the FA-SIFT apparatus.

2.2.3 Reaction Flow Tube and H Atom Source

Upon exiting the Venturi inlet, the ions once again are entrained in a flow of helium carrier gas (~200 std cm^3 s^{-1}) at a higher pressure (~0.50 Torr) than the ion selection region. The flow tube is stainless steel, slightly over 1 m in length, and has an inner diameter of 7.3 cm. Within the first ~ 30 cm of the flow tube, ions reach thermal temperatures through ~10^4 collisions with helium, and the initially turbulent helium flow becomes laminar and parabolic. The remaining 77 cm of the reaction flow tube includes 7 neutral reagent inlets, spaced 11 cm apart. These inlets consist of solenoid valves connected to a glass manifold where neutral reagent pressures can be monitored before, during, and

after reagent introduction. To measure the reagent flow rate, the gas is diverted into a calibrated volume system. The measured increase in pressure with time allows for the determination of neutral reagent flow. The flow is chosen such that the reactant ion intensity is depleted to ~10% of its original value when neutral reagent is introduced at inlet 7 (allowing a reaction distance of 77 cm). In lieu of using these 7 inlets, atomic hydrogen is introduced into the reaction flow tube at a fixed inlet that is ~70 cm upstream from the detection region entrance, to allow adequate reaction time as well as laminar flow.

Hydrogen, the most abundant element in the universe, is extremely important to interstellar chemical processes, but H atom is very difficult to produce and study due to its reactivity and instability. We employ thermal dissociation to produce this atomic species, as follows. A flow of high purity (99.999%, Airgas Inc.) H_2 gas is introduced at ~9 std cm^3 s^{-1} into a molecular sieve trap that is immersed in liquid nitrogen to remove residual impurities. The H_2 then flows into a water-cooled tube[11] containing a coiled tungsten filament, to which a variable and measurable voltage is applied (0-40 V). This applied voltage resistively heats the filament, causing H_2 to thermally dissociate into atomic H. A catalytic mechanism for this dissociation has been recently proposed, whereby an H_2 associates with the surface of the tungsten filament (W + H_2), the energy imparted to the H_2 molecule breaks its H-H bond yielding WH + H, and the WH subsequently cleaves as well to yield another association site on the tungsten filament surface and a free H atom.[12] The newly-formed H atoms are transferred to the fixed reaction flow tube inlet by Teflon tubing to minimize recombination. The overall process, including formation and transfer of the H atoms, is about 1% efficient. Therefore, it is crucial that the reactant ions of interest do not react with H_2. Lastly, the concentration of H atoms introduced into the reaction flow tube is quantified using the associative detachment reaction between H and Cl^- as a calibration. The reaction rate constant of this reaction has been measured several times with a reported error of 20%,[2,13,14] and the value used in this thesis is 9.6×10^{-10} cm^3 s^{-1}.

After the neutral reagents are introduced into the reaction flow tube, either through the 7 inlets or the fixed H atom inlet, the remaining parent ions and product ions are sampled through a second nose cone orifice (~0.5 mm diameter aperture) at the downstream end of the flow tube. All residual helium and neutral reagents and products are pumped out of the reaction flow tube by another Roots blower pump (~800 L s^{-1}).

2.2.4 Ion Detection

The final region of the FA-SIFT apparatus, the ion detection region, is pumped down to a pressure of ~1 x 10^{-5} Torr which effectively quenches all ion-neutral reactions upon their entrance through the nose cone. This region is made up of five electrostatic lenses, a quadrupole mass spectrometer, and an electron multiplier. A 6 inch diffusion pump evacuates the ion lens area (2400 L s^{-1} air), and a 4 inch diffusion pump evacuates the quadrupole and electron multiplier region (1200 L s^{-1} air). The ions are focused into the entrance of the quadrupole mass spectrometer by the electrostatic lenses, which can be optimized to increase ion signal. The quadrupole allows for the separation and monitoring of specific product ion or parent ion signal, and is capable of analyzing ions up to m/z 1000. The ions exiting the quadrupole are detected using a continuous dynode electron multiplier with a gain of ~10^8, whose pulsed signal is processed by Extrel Merlin Software to produce a mass spectrum.

2.3 Modified Quadrupole Ion Trap

The origins of the quadrupole ion trap mass spectrometer date back even earlier than the FA-SIFT apparatus. The original public disclosure of the instrumental setup was made by Paul and Steinwedel in 1953,[15] and the Finnigan Corporation produced the first commercially available ion trap about 30 years later.[16,17] Throughout the ensuing years, ion traps have been used in a variety of

applications from clinical detection of biomarkers[18] and environmental analyses[19] to the European Space Agency's recent Rosetta mission.[20] Several reviews have outlined the basic operating principles[21,22] and versatility of ion traps with respect to the study of gas phase ion chemistry.[23] The ion trap owes its commercial success to the ease with which it can be coupled to separation techniques as well as ionization sources such as electrospray ionization (ESI). Hence, the ion trap is able to analyze compounds of many different properties and volatilities, including larger biomolecules that are much more difficult to analyze using the FA-SIFT instrument. Additionally, tandem mass spectrometry (MS^n) is facile within an ion trap apparatus, allowing for structural verification of ions through fragmentation.

The instrument employed in this work is a Finnigan LCQ Deca XP Plus ion trap mass spectrometer with an ESI source.[24] A schematic depiction of the instrument is shown in Figure 2.5. The setup is discussed from left to right following the directional flow of ions in the apparatus. As shown in Figure 2.5, there are four main regions of the instrument: (1) the ion production region, (2) the ion desolvation region, (3) the ion fragmentation/reaction region, and (4) the ion detection region. At ambient temperature and pressure, cations and anions are produced from an ESI source, which is discussed in the following section. Ions of a chosen polarity are drawn into a sampling orifice biased by 3.5-5 kV with respect to the electrospray needle. The ions then flow through an ion transfer tube, where they undergo thermal desolvation (250-300 °C). A tube lens focuses the ions as they exit the ion transfer tube, and guides them through the opening of a grounded skimmer, which acts as a vacuum baffle leading into the low pressure (~10^{-3} Torr helium) mass analyzer region. A quadrupole and an octopole serve as ion optics to further focus the ion beam before entry into the ion trap. Within the ion trap, ions of interest may be isolated, reacted, and/or fragmented, as described in the following sections. A resonant frequency is applied to expel ions of a specific m/z, and ion detection is accomplished using a continuous dynode electron multiplier.

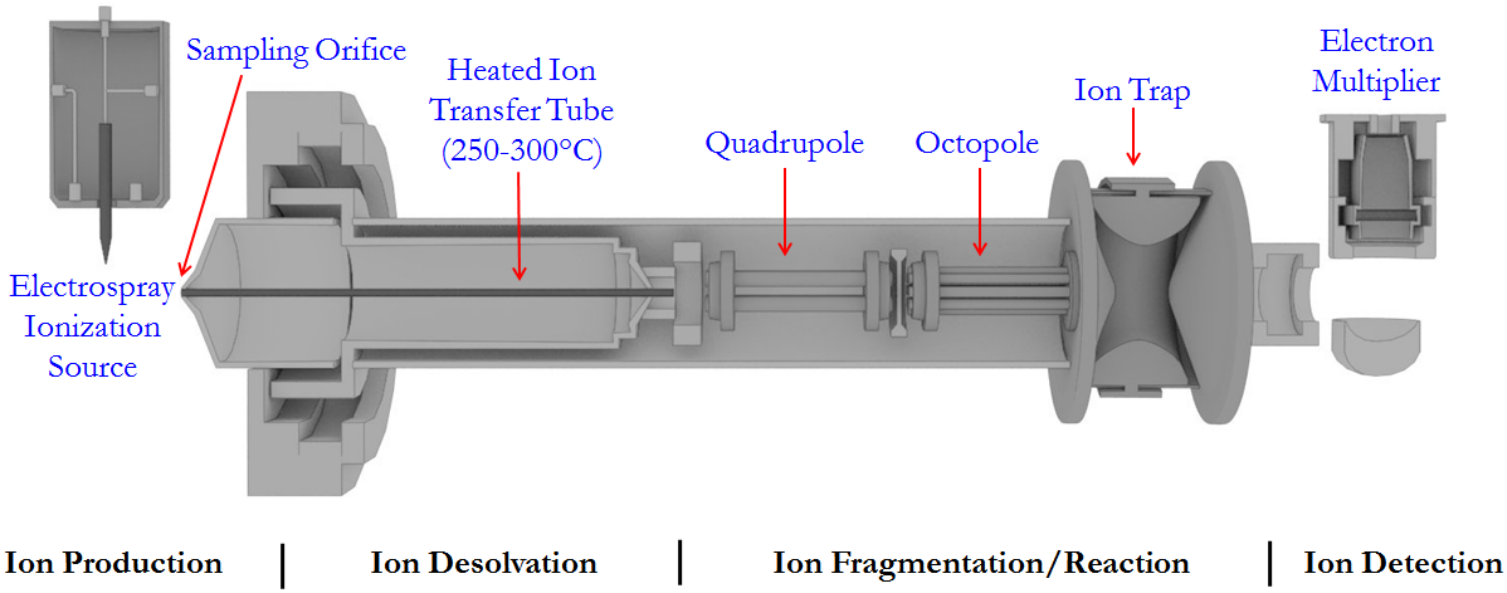

Figure 2.5
LCQ Deca XP Plus Ion Trap Mass Spectrometer. (Image courtesy of Ben Cole, founder of Tidbit Universe LLC).

2.3.1 Ion Production

The ions explored using the ion trap apparatus include deprotonated azoles (Chapter 5), pyrimidines (Chapter 6), and purines (Chapter 7), all of which are efficiently produced with an ESI source. Figure 2.6 depicts the basic layout of this ionization setup, which has been described in previous publications.[25] The basic premise of ESI is that under atmospheric pressure, the application of a strong electric field to a liquid solution passing through a capillary can be used to create bare, gas-phase ions. Specifically, our work uses solvent mixtures of 1:1 CH_3OH:H_2O and solute concentrations of the order of 10^{-4} M. To augment ion signal in specific cases (Chapters 6 and 7), the solution pH can be increased with the addition of sodium hydroxide. Flow rates through the electrospray capillary (fused silica, ~50 μm inner diameter) range from 5-10 μL min^{-1}. Approximately 3.5-5 kV is applied to the electrospray needle to provide a large potential difference between the needle and the entrance to the ion transfer tube, which is positioned ~2-3 cm away. The electric fields in the source region produced with these settings are approximately 10^6 V m^{-1}. As the liquid exits the electrospray needle, nebulizer gas (N_2, 99.999%, Airgas Inc.) flows parallel to the needle to enhance initial solvent evaporation. In response to the strong electric field, ions begin to accumulate in the droplet that forms at the exit of the electrospray needle. The charge increases in density in the droplet, causing its shape to elongate, and eventually burst into a spray of droplets (~1.5 μm diameter and ~50,000 elementary charges) when the surface tension is broken. This elongation and spray of the solution is known as a 'Taylor cone' and is shown in Figure 2.6. These droplets begin to shrink as the solvent evaporates, increasing their charge per unit volume in the process. Each droplet elongates in response to the electric field and the charge accumulation in an analogous fashion to the original spray, and again the surface tension is broken, releasing even smaller droplets (~0.1 μm diameter, ~400 elementary charges). This process repeats itself until bare (or nearly bare) gas-phase ions are produced. These ions

are drawn into a heated ion transfer tube (250-300 °C, ~1 Torr) which evaporates any residual solvent molecules from the ions. Finally, the ion beam is focused by a tube lens, and sampled into the low pressure mass analysis region (~10^{-3} Torr) through a skimmer.

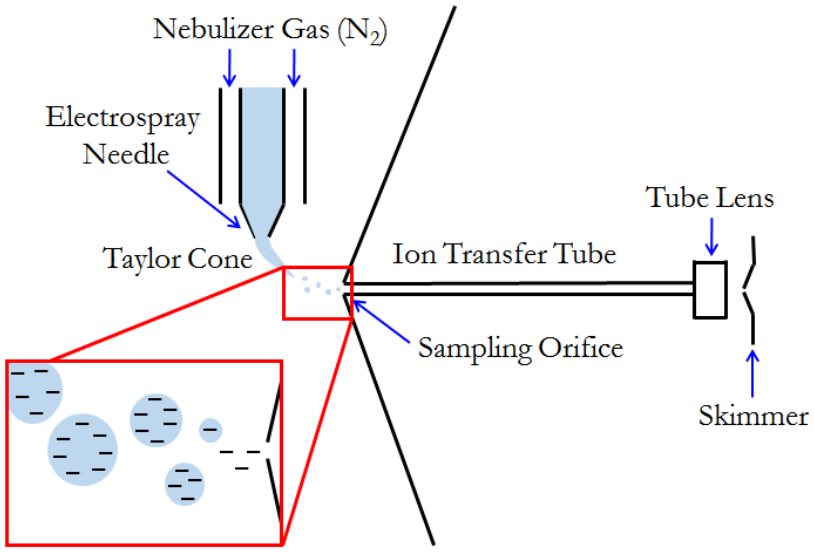

Figure 2.6
Electrospray Ionization Source.

2.3.2 Ion Optics, Trapping, and Detection

The gas-phase ions produced from the ESI source enter a series of ion optics prior to the ion trap itself. A quadrupole focuses the ions into the interoctopole lens, which serves several functions. This lens is a baffle between the multipole regions of the vacuum manifold (~10^{-3} Torr and ~10^{-5} Torr in the quadrupole and octopole regions, respectively), a focusing element, and finally, an ion gate. These evacuated regions are pumped using a combination of two direct-drive mechanical pumps (~10 L s^{-1} air) and one turbomolecular pump (200 L s^{-1} air). The potential applied to the interoctople lens either repels ions from the ion trap, or draws them to the next stage of ion optics. Next, an

octopole continues to focus the ion beam into the entrance of the ion trap mass spectrometer. A specific injection time (≤ 5 ms) can be optimized to collect ions in the trap for a set amount of time before 'closing the gate,' or applying a repulsive potential to the interoctopole lens of the setup.

The ion trap consists of three electrodes: entrance and exit end cap electrodes and a ring electrode, as shown in Figure 2.5. The ions enter the trap through an orifice in the center of the entrance end cap. An attractive DC potential applied to these electrodes (± 10 V) draws the ions from the ion optics into the ion trap. Here, they encounter helium buffer gas (5.1×10^{-3} Torr, see section 2.4.2 for calibration, 99.999%, Airgas Inc.), which is leaked into the system through an orifice on the exit end cap. The sensitivity and resolution of the instrument are augmented by the presence of helium. The kinetic energies of the ions are reduced upon collisions with helium, damping the amplitude of their oscillations and focusing them into the center of the trap. The trajectories of the trapped ions are manipulated in three dimensions by applied RF potentials to the ring electrode (constant frequency of 0.76 MHz and variable amplitude of 0-8500 V) and the end cap electrodes (variable frequency and amplitude, π out of phase). The ion trap's rotational symmetry ($x^2 + y^2 = z^2$) allows ion motion to be expressed in z (axial) and r (radial) coordinates. The Mathieu equation can be used to derive a general expression for an ion trajectory stability parameter in the axial direction, q_z.[23]

$$q_z = \frac{8zeV}{m(r_o^2+2z_o^2)\omega^2}$$

Based on this expression, the stability of the ion trajectories within the trap is governed by several factors. The ion mass (m), nominal charge (z), elementary charge (e), RF zero-to-peak amplitude voltage (V), and the angular frequency ($\omega=2\pi\nu$, where ν is the frequency) all play an important role. The size of the ion trap impacts the trajectory stability as well: r_o represents the radius of the ring electrode and z_o is the distance between the centers of the end cap electrodes, measuring in the radial

and axial directions, respectively. The q_z values employed for our research (Chapters 5-7) range from 0.25-0.35 to successfully trap the ions of interest. When an ion falls outside of the q_z range ~0.15-0.908, that ion is ejected from the trap.

Utilizing potentials applied to the end cap and ring electrodes, trapped ions can be isolated, collisionally excited, and ejected from the trap. In order to isolate an ion of a specific m/z, all other ions may be ejected by scanning RF frequencies applied to the end caps that are resonant with all ion oscillations besides the ion of interest. Once an ion is isolated, that ion may be excited through collisions with helium in much the same way. A resonance excitation RF voltage is applied to the endcaps, which does not have sufficient amplitude to eject the ion, but does enhance ion motion in the axial direction leading to more energetic collisions with the buffer gas. This process will be discussed in more detail in the following section. Finally, all ions may be removed from the ion trap from low mass to high mass by increasing the RF voltage amplitude applied to the ring electrode. This process destabilizes the ions in the axial direction, sending them out of the trap through the orifice in the center of the exit end cap electrode. Upon exiting the ion trap, ions are focused with an electrostatic lens towards a conversion dynode. The secondary particles produced on impact with the conversion dynode are accelerated into a continuous dynode electron multiplier, whose output signal is converted into a mass spectrum using LCQ Tune Software.

2.3.3 Collision-Induced Dissociation (CID)

The process of fragmenting an ion through collisions with background gas, known as collision induced dissociation (CID), can be accomplished either before or after entry into the ion trap apparatus. Prior to entering the ion trap, the difference in the DC potentials applied to the skimmer and the quadrupole can cause an acceleration and subsequent collision induced fragmentation. For

example, as is discussed in Chapter 5, a 5-10 V difference between these potentials can cause decarboxylation in deprotonated azole-5-carboxylic acids.[26]

Within the ion trap, fragmentation is accomplished using variable RF amplitudes applied to the end cap electrodes of the trap. These applied potentials increase the axial kinetic energy of the oscillating ions such that higher energy collisions with helium take place, sometimes resulting in dissociation. The LCQ Tune Software allows the user to vary the Normalized Collision Energy (NCE, %), which is directly proportional to the applied RF amplitude, but is normalized to remove the effect of the parent mass.[27] This NCE may be applied for a certain activation time (typically 10-100 ms). Based on the LCQ calibration used in this work, 35-75% NCE corresponds to an applied end cap potential of approximately 1.20-1.65 V. This provides a rough estimate of the potential applied to the electrodes, but in order to determine the energy imparted to the ions, a more extensive calibration is necessary. Figure 2.7 depicts an example breakdown curve taken for the purposes of such a calibration.[28] For a series of solvated metal cations, the decline in parent ion and the rise of fragment ion was monitored. Implementing previously established methods,[29] the fragment's appearance energy

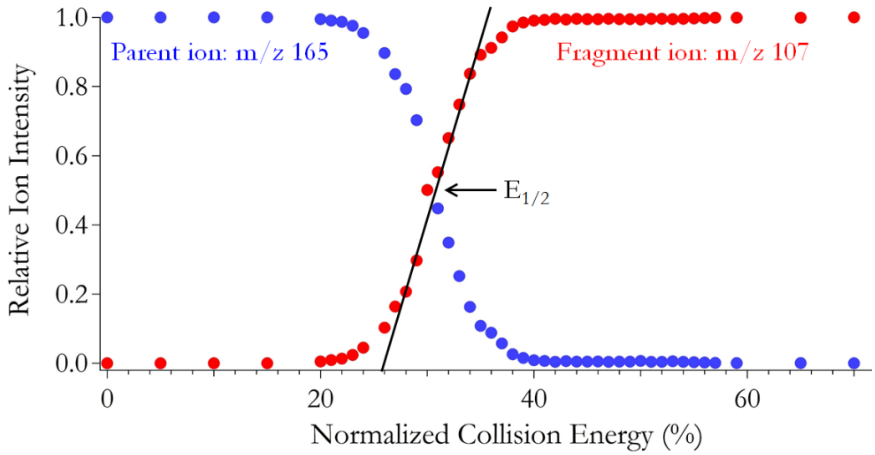

Figure 2.7
Breakdown curve with 20 ms activation time and $q_z = 0.25$ for the complex Ag^+(acetone). Although there are two abundant isotopes of Ag, the parent peak that is monitored is m/z 165, and the corresponding fragment peak is m/z 107.

was determined by extrapolating from the point at which the fragment ion intensity is half of its maximum value ($E_{1/2}$) back to the baseline, to obtain an appearance NCE (%) for that species. Figure 2.7 shows the breakdown curve of monosolvated Ag^+(acetone) to form unsolvated Ag^+. After averaging six trials of this dissociation process, an appearance energy of 30% NCE was attributed to the fragmentation of this complex. This procedure was repeated for a variety of solvated metal cations, and the published literature values of their bond energies were obtained for comparison (kcal mol^{-1}). The summarized calibration data are shown in Figure 2.8. The relationship between the association energy of the solvent to the cation and the NCE (%) is linear, allowing for a straightforward determination of the energy imparted to ions during the CID process. Most dissociation events described in this work fall within the range 35-75% NCE, which corresponds to the cleavage of 41-88 kcal mol^{-1} bonds over a 20 ms activation time. The linear expression relating the NCE (%) to the fragment appearance energies (AE, kcal mol^{-1}) reported in the literature is shown below.

$$NCE = 0.85(AE); R^2 = 0.98$$

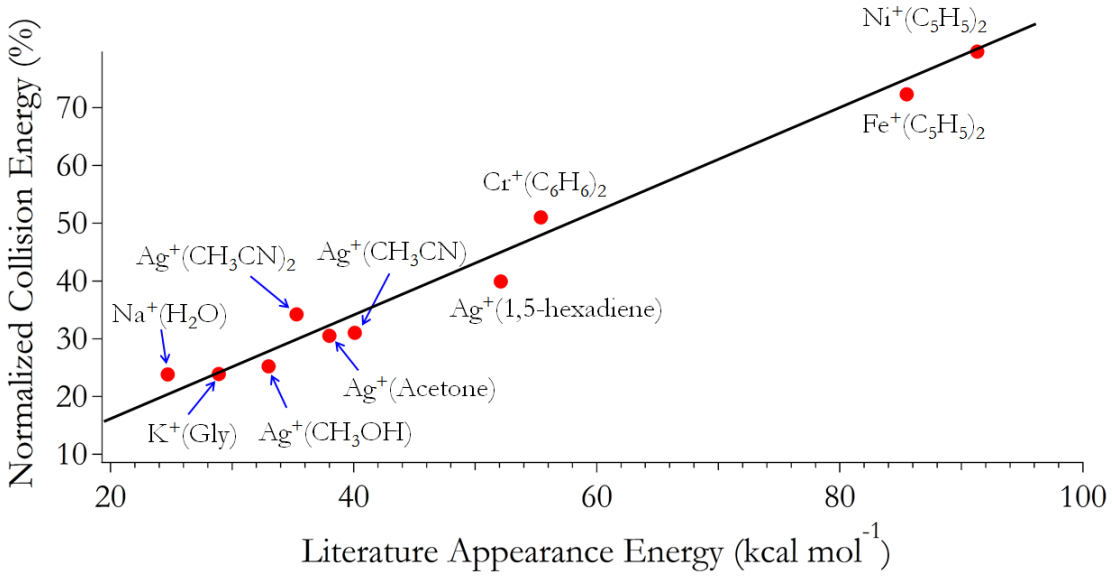

Figure 2.8
Ion trap normalized collision energy (NCE, %) calibration for metal ion complexes.

2.3.4 Instrument Modifications

The commercial LCQ Deca XP Plus instrument is modified for the purposes of introducing volatile liquids and gases into the ion trap to examine their reactivity with trapped ions. As previously described, helium buffer gas is leaked into the ion trap through an opening in the exit end cap electrode. The goal of this minimally-invasive modification is to allow neutral reagents to enter the ion trap along with the helium in a quantifiable flow, allowing the measurement of kinetic data such as reaction rate constants and branching fractions. We acknowledge and thank Prof. Scott Gronert for not only pioneering this technique,[23] but also for his personal correspondence and guidance.

Figure 2.9
Liquid neutral reagents are introduced into the helium line (vertical tubing shown) by syringe pump through a septum (a). Next, a small fraction of the helium reagent mixture is sampled into the ion trap through a silica capillary, shown in photograph (b). (Image courtesy of Ben Cole, founder of Tidbit Universe LLC).

The schematic in Figure 2.9 illustrates the basic method used to introduce volatile liquid neutral reagents into the ion trap. Helium flows through 1/4 inch outer diameter stainless steel tubing to a tee connection. Within this tee (photograph included in Figure 2.9 (a)), a syringe needle is situated so that the tip is in the center of the helium flow. A septum (9.5 mm diameter, Agilent) creates a seal around the syringe needle to prevent leaking. Helium flow rates through this line are varied (1.0-1.9 L min^{-1}) using a flow controller, and the pressure is kept at a constant value (850 ± 25 Torr) and monitored using an absolute pressure manometer (Baratron). The flow of liquid neutral reagent into the helium line (0.5-5.0 μL min^{-1}) is introduced using a syringe pump (Hamilton). Only volatile liquid neutral reagents are used (b. p. ≤ 175 °C) to ensure efficient sampling of the liquid into the helium flow by vaporization at the syringe tip. Relatively high helium flows are used in this setup due to the practical limitations of the syringe pump itself. It is necessary to use large flows of helium in order to dilute the neutral reagents adequately, while introducing them at a low yet accurate flow rate.[23] A second, more comprehensive diagram of our instrument modification is depicted in Figure 2.10. Here, the possibility of introducing dilute gases (1.00 ± 0.02% in helium) is also shown. These gases can simply be introduced into the helium line, and the increase in line pressure upon their addition (5-95 Torr) is used to quantify their flow. Whether introducing a gaseous or liquid neutral reagent into the helium line, a molar helium:reagent ratio of 10^2-10^4 is established. This mixture of helium and neutral reagent continues to flow through the stainless steel line, which is reduced to 1/8 inch outer diameter for increased line flexibility, for another ~1 m before encountering a second tee connection (photographed in Figure 2.9 (b)). Prior to modification, the helium flow into the mass analyzer was maintained using a pressure regulator and capillary restrictor. This is bypassed and replaced by the second tee shown in Figure 2.9. A small capillary (75 μm ID, 10 cm length) is sealed into the tee with a reducing graphite ferrule (Restek). Approximately 99.9% of the helium/reagent mixture flows past this tee and out the exhaust through the flow controller, and ~1 mL min^{-1} (~0.1%) is sampled into

this capillary line and transferred into the ion trap. Reactions between trapped ions and these introduced neutral reagents may then be examined by isolating and trapping reagent ions of a specific m/z for 1-5000 ms using the "activation time" feature of the LCQ Tune software, while keeping the applied NCE (%) set to 0. The amount of time that the ions are trapped in the presence of neutral reagents is equivalent to the reaction time, allowing kinetic information to be measured with this modification. It is important to note that the ion injection time (discussed in section 2.3.2), the amount of time that ions are allowed to build in the trap prior to being isolated, may impact the reaction time determination. For this reason, the injection time is kept at least an order of magnitude below the reaction time to minimize error. The following section details how kinetic data may be obtained from both the FA-SIFT and modified ion trap instruments.

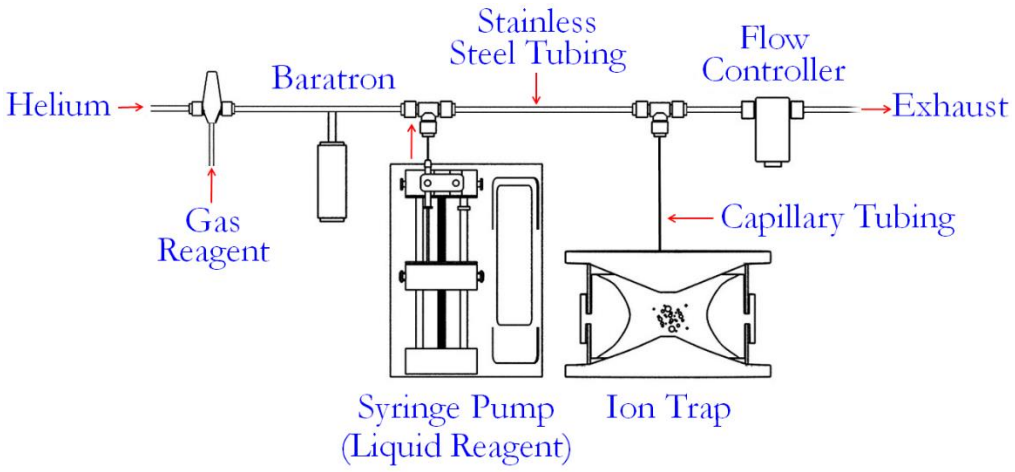

Figure 2.10
Modified LCQ Deca XP Plus Ion Trap. (Image courtesy of Ben Cole, founder of Tidbit Universe LLC).

2.4 Kinetic Measurements

The FA-SIFT and ion trap setups are utilized to obtain the kinetic results presented in this work. Three different neutral introduction techniques, and therefore three different data analysis methods, will be discussed in this section. These include the modified ion trap method, the FA-SIFT seven inlet method, and the FA-SIFT fixed inlet method (for H atom introduction).

2.4.1 Pseudo-First-Order Ion-Neutral Reaction Rate Constants

The bimolecular reaction between an ion ($I^{\pm}$) and a neutral atom or molecule (N) to produce products (including ions, neutrals, and/or electrons) is shown in reaction (2.1) below. The rate constant for this reaction will be represented by k_{exp} throughout this work, as we experimentally determine this quantity.

$$I^{\pm} + N \xrightarrow{k_{exp}} \text{products} \tag{2.1}$$

The change in the concentration of the reactant ion, $[I^{\pm}]$, over time, t, is represented by the second order differential rate law given in equation (2.2). As shown, $d[I^{\pm}]/dt$ is dependent on the concentration of neutral reagent, [N]. Within all instrumental setups described in this work, [N] is higher than $[I^{\pm}]$ by at least two orders of magnitude. Due to these experimental conditions, the second order rate expression may be greatly simplified into what is known as a pseudo-first-order expression. According to the pseudo-first-order rate law, [N] is approximated to be a constant over the course of the reaction. The vast excess of the neutral with respect to the reactant ion leaves its concentration essentially unchanged such that $[N]=[N]_o$, the initial neutral concentration.

$$\frac{d[I^{\pm}]}{dt} = -k_{exp}[I^{\pm}][N] \tag{2.2}$$

The differential rate law in equation (2.2) can then be rearranged and integrated over a given reaction time [0, t], where both k_{exp} and [N] are constant, see equation (2.3).

$$\int_0^t \frac{1}{[I^{\pm}]} d[I^{\pm}] = -k_{exp}[N] \int_0^t dt \tag{2.3}$$

After integration, a new expression dependent on the initial concentration of ion, $[I^{\pm}]_0$, and the concentration of ion at reaction time t, $[I^{\pm}]_t$, is obtained. Reaction (2.4) gives this integrated pseudo-first-order rate law.

$$\ln \frac{[I^{\pm}]_t}{[I^{\pm}]_0} = -k_{exp}[N]t \tag{2.4}$$

This rate law reveals a linear relationship between the dependent variable, $\ln[I^{\pm}]_t$, and the independent variable, t. To clearly show this linearity, we rearrange equation (2.4) to obtain equation (2.5) in the form of a y = mx + b expression. For the ion trap apparatus, equation (2.5) is used to quantitatively determine k_{exp}. The blue data shown in Figure 2.11 provide an example of the reaction rate constant determined with the ion trap apparatus by monitoring the depletion of reactant ion signal during a reaction. The y-axis is the ion intensity on a logarithmic scale (where $\ln[I^{\pm}]_t = 2.303 \log[I^{\pm}]_t$), and the x-axis is the length of time in seconds that the ion is trapped in the presence of the neutral reagent, also known as the reaction time, t. The magnitude of the slope of this line is $k_{exp}[N]t$. Since [N] and t are both known and the slope is experimentally obtained using this plot, the reaction rate constant (k_{exp}) is determined.

$$\ln [I^{\pm}]_t = -k_{exp}[N]\ t + \ln[I^{\pm}]_0 \tag{2.5}$$

$$\ln [I^{\pm}]_z = -\frac{k_{exp}[N]}{v_{ion}}\ z + \ln[I^{\pm}]_0 \tag{2.6}$$

$$y = m x + b$$

In contrast to the ion trap, the FA-SIFT is a constant flow system. The reaction time in the FA-SIFT is consequently dependent upon the reaction distance, z, and the average velocity of ions in the flow,

v_{ion}, as shown in equation (2.6). Therefore, a simple substitution into equation (2.5) of $t = z/v_{ion}$ yields equation (2.6). The same linear relationship between $\ln[I^{\pm}]_z$ and z still holds in an analogous manner, and data for FA-SIFT reaction rate constant determination is shown in Figure 2.11 in red. The y-axis is still the ion intensity on a logarithmic scale ($\ln[I^{\pm}]_z$), but now the x-axis is the distance in cm, z, that the ion is entrained in helium and travelling through the reaction flow tube in the presence of the neutral reagent. The magnitude of the slope of this data is $k_{exp}[N]z/v_{ion}$, where all quantities are known except the reaction rate constant (k_{exp}), which is then quantified.

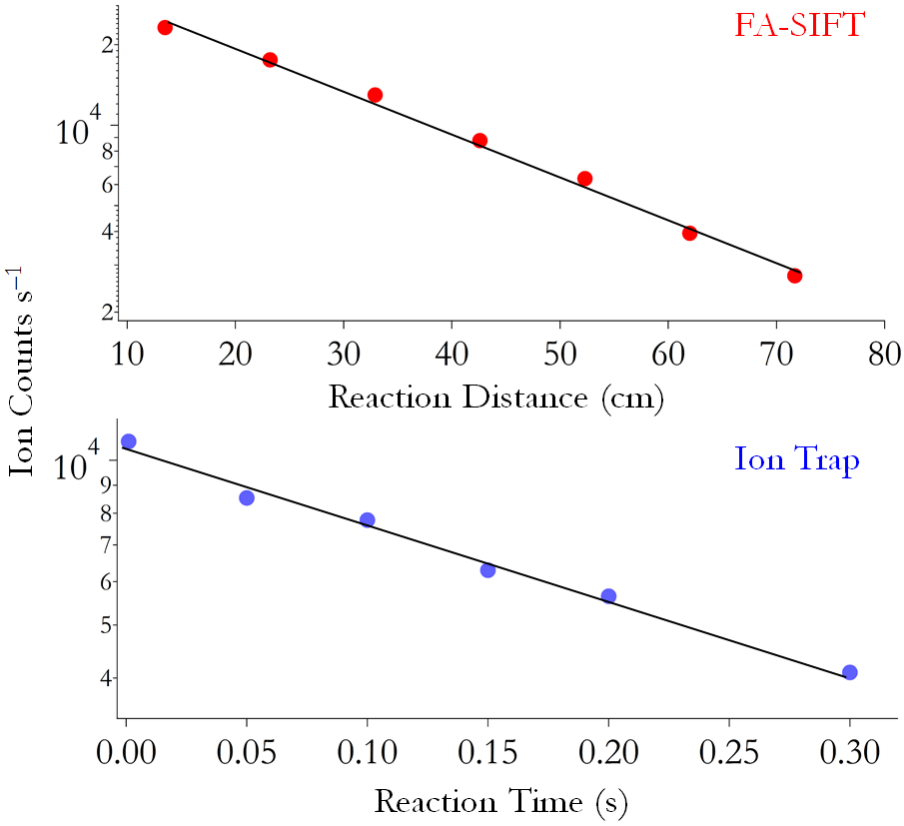

Figure 2.11
Semilogarithmic plots of ion signal versus reaction distance (cm) for the $CH_3OH_2^+$ + HCOOH reaction using the FA-SIFT apparatus (red), and versus reaction time (s) for the $C_3H_2NO^-$ + CS_2 reaction using the modified ion trap apparatus (blue).

As previously discussed, there are several measurable quantities that allow for the determination of k_{exp} from the slope of the reactant ion depletion data (Figure 2.11). For the ion trap, these include t and [N] (equation (2.5)), and for the FA-SIFT, these are z, v_{ion}, and [N] (equation (2.6)). The reaction time, t, is the length of time that the ion is trapped in the presence of neutral reagent, as previously discussed. The reaction distance, z, is simply the measured distance from the solenoid valve through which neutral reagent is introduced to the nose cone orifice used to sample the ions into the detection region (Figure 2.1). The average ion velocity (v_{ion}) is dependent on the average velocity of helium (v_{He}) through the flow tube, such that $v_{ion} = \alpha v_{He}$. The velocity correction factor, α, has been previously measured[2] to be 1.6. This correction factor is necessary for two reasons. First, ions are lost when they come into contact with the flow tube, so a radial ion-density gradient exists, leaving the highest ion density at the center of the flow tube. Similarly, helium interacts with the walls of the flow tube, and the velocity there is decreased by friction. Hence, the v_{He} is greatest in the center of the flow tube, and that is where most of the ion density is also located. This causes v_{ion} to be a factor of 1.6 greater than v_{He}. An expression for v_{He} is provided below.

$$v_{He} = \frac{F_{He}}{A(P_{He})} \frac{T}{273.15K} \tag{2.7}$$

As shown in equation (2.7), the velocity of helium through the FA-SIFT (cm s^{-1}) is determined based on the flow of helium measured with a mass-flow controller (F_{He}, atm cm^3 s^{-1}), the cross-sectional area of the flow tube (A = 41.854 cm^2), the pressure of helium in the flow tube measured by a capacitance manometer (P_{He}, atm), and the temperature (T, K).

The measurable quantity remaining is the concentration of neutral reagents (cm^{-3}) in both the ion trap and FA-SIFT instruments ($[N]_{trap}$ and $[N]_{FA\text{-}SIFT}$, respectively). Within the ion trap apparatus, the $[N]_{trap}$ is based on the pressure within the trap (P_{trap}, calibrated to be 5.1 x 10^{-3} Torr, see section

2.4.2), the ratios of the neutral:helium molar flows and molar masses (F_N:F_{He} and MM_N:MM_{He}), and the density of molecules at 1 Torr (d = 3.24 x 10^{16} cm^{-3} $Torr^{-1}$). The square root of the molar masses of neutral reagent:helium accounts for the differential effusion of the species out of the ion trap. Heavier molecules effuse more slowly than helium, causing their concentration to become higher in the trap over time, relative to the buffer gas.[23] The expression used to derive the concentration of neutral reagents within the ion trap (~10^8-10^{11} cm^{-3}) is shown in equation (2.8) below.

$$[N]_{trap} = P_{trap} \frac{F_N}{F_{He}} \sqrt{\frac{MM_N}{MM_{He}}}\ d \tag{2.8}$$

The concentration of neutral reagents in the reaction flow tube of the FA-SIFT is determined differently. This quantity is dependent on the flow of neutral reagent (F_N, atm cm^3 s^{-1}), the cross sectional area of the flow tube (A = 41.854 cm^2), the velocity of helium (v_{He}, cm s^{-1}), and the density of molecules at 1 Torr (d = 3.24 x 10^{16} cm^{-3} $Torr^{-1}$), as given in equation (2.9). F_N is measured by directing the flow of neutral reagent into one of two glass bulbs of known volume (2401.3 cm^3 or 2423.4 cm^3), where the change in pressure over time is monitored using a capacitance manometer.

$$[N]_{FA\text{-}SIFT} = \frac{F_N}{A(v_{He})} \frac{760\ Torr}{1\ atm}\ d \tag{2.9}$$

In a similar manner to equation (2.6), $[N]_{FA\text{-}SIFT}$ may be varied while z is held constant. This is the method used to obtain kinetic data for reactions with H atom, because this species is introduced into the reaction flow tube at a fixed reaction distance (see section 2.2.3). Equation (2.6) is minimally rearranged to give equation (2.10) where the independent variable is [N], or [H] for our studies, and the dependent variable is $\ln[I^{\pm}]$. Once again, the slope of the linear plot of logarithmic reagent ion loss (Figure 2.11) versus [H] is used to determine the reaction rate constant, k_{exp}. However, [H] is not a

directly measurable quantity. Recall from section 2.2.3 that [H] is varied by applying different voltages across the tungsten filament used to thermally dissociate H_2.

$$\ln[I^{\pm}] = \frac{-k_{exp}\, z}{v_{ion}}[N] + \ln[I^{\pm}]_0 \qquad (2.10)$$

$$y = m\ x + b$$

A calibration reaction, $Cl^- + H \rightarrow HCl + e^-$, is used to quantify k_{exp} without directly measuring [H] in the flow tube. The reaction rate constant of this calibration reaction, k_{cal}, has been experimentally measured several times and found to be 9.6 x 10^{-10} cm^3 s^{-1}.[2,13,14] The slopes of the linear plots of the experiment and the calibration data (m_{exp} and m_{cal}, respectively) are related to the reaction rate constants as shown below:

$$\frac{m_{exp}}{m_{cal}} = \frac{\frac{-k_{exp}\, z}{v_{ion}}[H]}{\frac{-k_{cal}\, z}{v_{ion}}[H]} = \frac{k_{exp}}{k_{cal}} \qquad (2.11)$$

The calibration and experimental data are measured using identical conditions, so many variables ([H], z, and v_{ion}) are eliminated when the ratio of these slopes is taken. When the like variables in the numerator and denominator are removed, a simple expression remains that relates the measurable slopes (m_{exp} and m_{cal}) and known calibration reaction rate constant (k_{cal}) to the unknown k_{exp}.

$$k_{exp} = k_{cal}\frac{m_{exp}}{m_{cal}} \qquad (2.12)$$

The total error associated with the FA-SIFT[9] and ion trap[23] kinetics measurements has been previously analyzed. Briefly, the ion trap measurements have an uncertainty of ±20-30%, which is comparable to that of the FA-SIFT.[23] A major assumption made in the ion trap kinetics measurements is that the sampling of neutral reagents into the flow of helium is perfectly efficient. As is discussed in the next section, the ion trap pressure is calibrated using FA-SIFT data, so the errors associated with the FA-SIFT also impact the ion trap measurements. Several assumptions are made that lead to systematic errors in FA-SIFT data. We assume that the helium flows have a perfectly parabolic velocity profile, the ion velocity is known exactly, axial diffusion of ions does not impact the reaction rate constant, the axial pressure gradient does not impact the reaction rate constant, radial diffusive ion loss is constant over the entire flow tube, and neutral reagents are introduced uniformly. Random errors also occur in the determination of the slope of the semilogarithmic plot, and in the measurements of pressure, temperature, and neutral reagent flow. The total systematic and random errors associated with the FA-SIFT experiment account for an uncertainty of 13.4%, but a more conservative error bar of 20% is typically reported. All kinetic measurements for both the ion trap and the FA-SIFT are reported herein as the average of a minimum of three measurements with error bars reported according to the precision of the experiment (± one standard deviation).

2.4.2 Ion Trap Reaction Rate Constant Calibration

A series of experiments were performed to calibrate the reaction rate constants measured by the ion trap apparatus. First, several reaction rate constants were measured using the FA-SIFT. These are described here in brief. Precursor vapor (2,2,3,3,3-pentafluoro-1-propanol 97% and 2,2,2-trifluoroethanol ≥99%, Sigma-Aldrich; 1,1,1,3,3,3-hexafluoro-2-propanol 99%, Alfa Aesar) is leaked into the FA-SIFT ion production region with helium buffer gas (0.2 Torr, 99.997%, Airgas). An additional 0.05 Torr of ammonia is added to produce amide (NH_2^-) by electron ionization. Amide

anions deprotonate the precursor molecules[30] to form the reagent ions of interest. Neutral reagents are introduced to react with these ions (2-chloro-2-methylpropane 99% and 2-chloropropane 99+%, Sigma-Aldrich; 2-bromo-2-methylpropane 96%, Acros Organics; 2-bromopropane 99%, Alfa Aesar; methyl chloride 99.9%, Matheson). The FA-SIFT results provide the comparative data necessary to verify the results of the modified ion trap experimental setup.

Ion trap rate constants are determined in a similar manner to the FA-SIFT using pseudo-first-order kinetic analyses and measuring the decline in thermalized[31] reagent ion signal at six or more separate reaction times (1-5000 ms), as discussed in the previous section. The neutral reagent concentration in the trap, $[N]_{trap}$, is determined according to the expression shown in equation (2.9).[23]

The only unknown, non-measurable quantity in the calculation of $[N]_{trap}$ is the pressure within the trap itself (P_{trap}). This quantity depends on the pressure in the modified helium line and the dimensions of the silica capillary leading to the ion trap, and is determined to be 5.1×10^{-3} Torr through careful calibration using known reaction rate constants. Table 2.1 presents the data gathered for this purpose. FA-SIFT reaction rate constants varying over two orders of magnitude for six different reactions (two with gaseous neutral reagents and four with liquid neutral reagents) are included in the table. We have gathered new FA-SIFT data in addition to that which has previously been published.[32,33] The same fluorinated alcohols are used for both instruments as ion precursors, but they are diluted to 10^{-4} M in 1:1 $CH_3OH:H_2O$ for the ESI source of the ion trap. All FA-SIFT and ion trap rate constants agree within the expected experimental uncertainties for gas-phase ion kinetics using the calibrated pressure of 5.1×10^{-3} Torr (±20-30%).[23]

Table 2.1
Ion trap rate constant calibration.

Reaction	k_{FA}[a,b]	k_{FA}[a,c]	k_{trap}[a,d]
$(CF_3)_2CHO^- + (CH_3)_2CHBr$	0.042	0.040	0.031
$C_2F_5CH_2O^- + (CH_3)_2CHCl$	0.85	0.55	0.73
$C_2F_5CH_2O^- + CH_3Cl$	1.0	0.96	1.2
$C_2F_5CH_2O^- + (CH_3)_3CCl$	1.7	1.6	1.4
$CF_3CH_2O^- + CH_3Cl$	2.2	2.3	3.0
$C_2F_5CH_2O^- + (CH_3)_3CBr$	12	11	11

[a] All rate constants are reported in units of 10^{-10} cm^3 s^{-1}.
[b] FA-SIFT rate constants previously published.[32,33]
[c] FA-SIFT rate constants measured in the present study (precision ± 10%; total error ± 30%).
[d] Rate constants measured on newly modified ion trap apparatus (precision ± 15%; total error ± 30).

2.4.3 Product Distribution

In some cases, ion-neutral reactions follow multiple pathways leading to more than one ionic product. Below, the reaction of an ion ($I^{\pm}$) and a neutral atom or molecule (N) involving two routes with reaction rate constants k_1 and k_2 is shown. The measurements described in the previous section rely on the depletion of the $I^{\pm}$ signal, and therefore allow the quantification of the total reaction rate constant, k_{tot}, which is the sum of k_1 and k_2. Determining the reaction rate constant for each pathway requires that product distributions, or branching fractions, be measured. Branching fractions express the portion of $I^{\pm}$ that reacts to form a given product.

$$\begin{aligned} I^{\pm} + N &\xrightarrow{k_1} A^{\pm} + C \\ &\xrightarrow{k_2} B^{\pm} + D \end{aligned} \qquad (2.13)$$

The branching fraction (BF) for the $A^{\pm}$ product in reaction (2.13) is shown in equation (2.14). It is the ratio of the concentration of one product ($[A^{\pm}]$) to the concentration of all products ($[A^{\pm}] + [B^{\pm}]$). Equivalently, this is the ratio of one reaction rate constant (k_1) to the total reaction rate constant ($k_{tot} = k_1 + k_2$). Branching fractions are experimentally measured by recording each product ion

concentration at six or more reaction times (ion trap), seven neutral reagent introduction inlets (FA-SIFT), or three or more different neutral reagent concentrations (FA-SIFT, H atom source).

$$BR = \frac{[A^{\pm}]}{[A^{\pm}] + [B^{\pm}]} = \frac{k_1}{k_1 + k_2} \tag{2.14}$$

To eliminate any unwanted contributions from secondary reactions, the fraction of each product ion to the total product ion signal is plotted versus the reaction time (s). The reported branching fractions result from the extrapolation to "zero reaction time." For the FA-SIFT apparatus, this extrapolation is performed to "zero reaction distance" or "zero concentration of H atom" in an analogous fashion.

Errors associated with branching fractions in this work are ± 30% of the reported values due to several factors that impact observed product ion signals. These include differential diffusion (FA-SIFT) and non-uniform detection of all ions. The FA-SIFT apparatus is prone to mass discrimination among product ions due to variant transmission efficiencies of different ion masses. By performing experiments on exothermic reactions that form one product similar in mass to the product of interest, correction factors can be applied to account for the difference between initial reactant ion signal and the sum of reactant and product ion signals, which are ideally equivalent.

2.4.4 Collision Theory and Reaction Efficiency

When an ion and a neutral species interact, dipole moments and polarizabilities play an important role. For different ion-neutral reactions, specific magnitudes of attractive forces (namely dipole-dipole and dipole-induced dipole) govern this interaction. Reaction rate constants can be normalized to account for this variation among ion and neutral properties, allowing for direct comparisons to be made between reactions of very differently structured species. This normalization

results in a calculation of the reaction efficiency, defined as the ratio of the experimentally measured reaction rate constant to the calculated collision rate constant (k_{exp}/k_{col}).

The simplest model of an ion-neutral collision was formulated in 1905 by Paul Langevin. The Langevin model describes an ion as a point charge and a neutral as a polarizable species. The collision between ion and neutral is therefore a result of the point charge inducing a dipole in the polarizable molecule, causing an attraction between the ion and neutral. Equation (2.15) is the expression of the Langevin collision rate constant, k_L.

$$k_L = 2\pi q\sqrt{\frac{\alpha}{\mu}} \tag{2.15}$$

According to this expression, the collision between an ion and a neutral depends on the magnitude of the point charge, q, the polarizability of the neutral, α, and the reduced mass of the collision partners, μ.

Since the inception of Langevin collision theory, models of ion-neutral collisions have continued to increase in accuracy and complexity to include properties of the ion and neutral that were previously unaccounted for.[34] For polarizable ions, the point polarizable ion (PPI) model was developed in 2003 by Eichelberger and coworkers.[35] This collision theory is applied in Chapter 3 of this work to account for the highly polarizable nitrogen-containing carbanions and their collisions with H atoms. Neutral molecules with permanent dipole moments have also been accounted for, using the parametrized trajectory theory (PTT) of collisions, developed by Su and Chesnavich in 1982.[36] All reaction efficiencies involving neutral reagents with permanent dipole moments in this thesis incorporate PTT. The polarizabilities and dipole moments of species studied in this work are taken from one of two sources: the *NIST Chemistry WebBook*[37] or the *CRC Handbook of Chemistry and Physics*.[38]

2.5 Computational Methods

Electronic structure calculations based on *ab initio* methods and on density functional theory (DFT) are employed throughout this work to explore the experimentally-observed processes at a greater depth. The *Gaussian 03* and *09* suites of programs are employed in these endeavors.[39,40] The Cartesian coordinates, optimized ground state geometries, total electronic energies, and zero point corrected electronic energies for all of the major species discussed in this thesis are summarized by chapter and by figure number in Appendices A and B. The Becke-Lee-Yang-Parr exchange-correlation functional (B3LYP),[41] Møller–Plesset perturbation theory (MP2),[42,43] and coupled cluster (CCSD)[44] methods are used with Pople (6-311++G(d,p))[45] and Dunning (cc-pVDZ and cc-pVTZ)[46] basis sets with added diffuse functions, as specified in the following chapters. These methods are applied for single-point energy calculation, structural optimization (minima and transition states), reaction enthalpy and gas-phase acidity determination, and potential energy surface (PES) exploration of reaction and dissociation mechanisms. We would like to express our gratitude to Prof. Zhibo Yang, Prof. Eric Herbst, and Dr. Zhe-Chen Wang for their computational collaborations on the work reported in Chapters 3, 4, and 6-7, respectively.

The optimization of transition state structures is the most challenging and complex computation performed throughout this work. Initial approximations of the transition state structures of interest are obtained by performing relaxed PES scans in a manner similar to that depicted in Figure 2.12. This figure shows an O-H bond length scan for deprotonated cytosine, an ion that is explored in Chapter 6. As the O-H bond is lengthened from 1.0 to 2.4 Å, the energy increases to a maximum (the H is approximately equidistant from the N and the O), and then decreases back to a minimum. The geometry at this maximum may be further optimized to search for the transition state structure, while the intermediates at the minima may also be optimized for an accurate view of the overall PES

of this process. PES scans such as this are utilized in exploring reaction mechanisms as well as dissociation processes. Optimized geometries are further verified using two techniques. First, the vibrational frequencies of stable intermediates and transition states are calculated to confirm that the reaction intermediates have all positive frequencies and that the transition states have only one negative (imaginary) frequency. Secondly, intrinsic reaction coordinate (IRC) analyses are applied to confirm that the transition state connects two local minima in the PES.[47] Further computational details are provided for each study outlined in the following chapters.

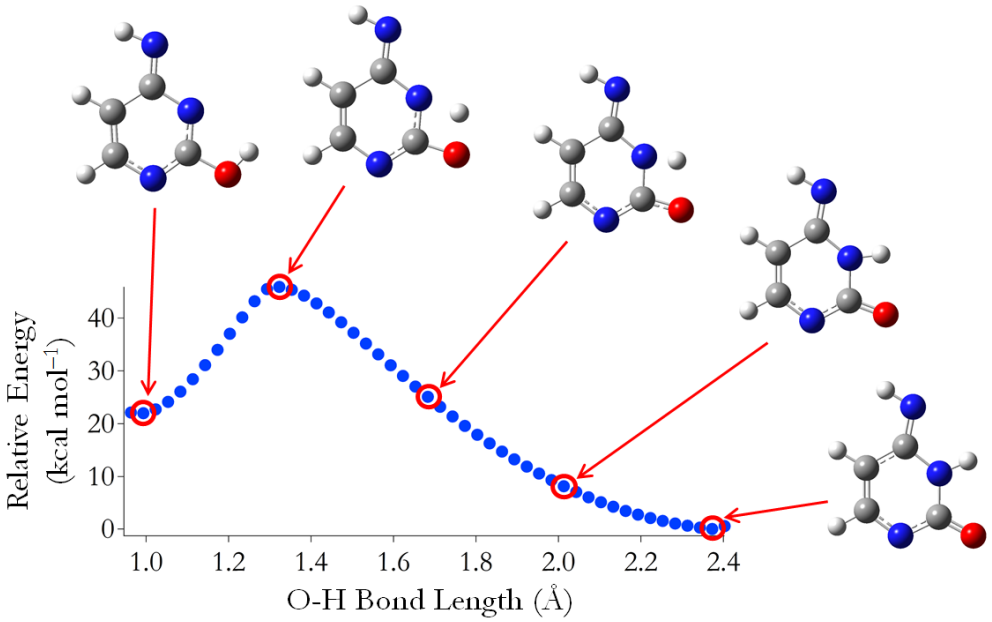

Figure 2.12
The length of an O-H bond of deprotonated cytosine is scanned with step sizes of 0.03 Å using *Gaussian* 09 software. Bond length scans such as this allow for the determination of barriers to different processes, in this case intramolecular proton transfer during CID.

2.6 References

1 V. M. Bierbaum, *Go with the Flow: Fifty Years of Innovation and Ion Chemistry using the Flowing Afterglow*. Int. J. Mass Spectrom. , **2014**, *in press*.

2 E. E. Ferguson; F. C. Fehsenfeld; A. L. Schmeltekopf, *Flowing Afterglow Measurements of Ion-Neutral Reactions*. Academic Press, Inc.: New York, NY, 1969; Vol. 5.

3 S. Gronert, *Mass Spectrometric Studies of Organic Ion/Molecule Reactions*. Chem. Rev., **2001**, *101*, 329-360.

4 K. M. Ervin, *Experimental Techniques in Gas-Phase Ion Thermochemistry*. Chem. Rev., **2001**, *101*, 391-444.

5 D. Smith; P. Španěl, *The SIFT and FALP Techniques; Applications to Ionic and Electronic Reaction Studies and their Evolution to the SIFT-MS and FA-MS Analytical Methods*. Int. J. Mass Spectrom., **2014**, *in press*.

6 I. W. M. Smith, *Laboratory Astrochemistry: Gas-Phase Processes*. In *Ann. Rev. Astron. Astrophys.*, Faber, S. M.; VanDishoeck, E., Eds. 2011; Vol. 49, 29-66.

7 V. M. Bierbaum, *Flow Tubes*. In *Encyclopedia of Mass Spectrometry*, Armentrout, P. B.; Gross, M. L.; Caprioli, R., Eds. Elsevier: Amsterdam, 2003; Vol. 1, 98-109.

8 T. P. Snow; V. M. Bierbaum, *Ion Chemistry in the Interstellar Medium*. Annu. Rev. Anal. Chem., **2008**, *1*, 229-259.

9 J. M. Van Doren; S. E. Barlow; C. H. DePuy; V. M. Bierbaum, *The Tandem Flowing Afterglow-SIFT-DRIFT*. Int. J. Mass Spectrom. Ion Proc., **1987**, *81*, 85-100.

10 N. Adams; D. Smith, *The Selected Ion Flow Tube (SIFT); A Technique for Studying Ion-Neutral Reactions*. Int. J. Mass Spectrom. Ion Proc., **1976**, *21*, 349-359.

11 D. W. Trainor; D. O. Ham; F. Kaufman, *Gas Phase Recombination of Hydrogen and Deuterium Atoms*. J. Chem. Phys., **1973**, *58*, 4599-4609.

12 Y. A. Mankelevich; M. N. Ashfold; H. Umemoto, *Molecular Dissociation and Vibrational Excitation on a Metal Hot Filament Surface*. J. Phys. D: Appl. Phys., **2014**, *47*, 025503.

13 C. J. Howard; F. C. Fehsenfeld; M. McFarland, *Negative Ion-Molecule Reactions with Atomic Hydrogen in the Gas Phase at 296 K*. J. Chem. Phys., **1974**, *60*, 5086-5089.

14 F. C. Fehsenfeld; C. J. Howard; E. E. Ferguson, *Thermal Energy Reactions of Negative Ions with H Atoms in the Gas Phase*. J. Chem. Phys., **1973**, *58*, 5841-5842.

15 W. Paul; H. Steinwedel, *Ein Neues Massenspektrometer Ohne Magnetfeld*. Z. Naturforsch., **1953**, *8*, 448-450.

16 G. Stafford; P. Kelley; J. Syka; W. Reynolds; J. Todd, *Recent Improvements in and Analytical Applications of Advanced Ion Trap Technology*. Int. J. Mass Spectrom. Ion Proc., **1984**, *60*, 85-98.

17 R. E. March; J. F. Todd, *A Historical Review of the Early Development of the Quadrupole Ion Trap*. In *Quadrupole Ion Trap Mass Spectrometry*, 2 ed.; 2005; Vol. 165, 1-33.

18 C. M. Zimmermann; G. P. Jackson, *Gas Chromatography Tandem Mass Spectrometry for Biomarkers of Alcohol Abuse in Human Hair*. Ther. Drug Monit., **2010**, *32*, 216-223.

19 T. Benijts; W. Lambert; A. De Leenheer, *Analysis of Multiple Endocrine Disruptors in Environmental Waters via Wide-Spectrum Solid-Phase Extraction and Dual-Polarity Ionization LC-Ion Trap-MS/MS*. Anal. Chem., **2004**, *76*, 704-711.

20 J. F. J. Todd; S. J. Barber; I. P. Wright; G. H. Morgan; A. D. Morse; S. Sheridan; M. R. Leese; J. Maynard, et al., *Ion Trap Mass Spectrometry on a Comet Nucleus: the Ptolemy Instrument and the Rosetta Space Mission*. J. Mass Spec., **2007**, *42*, 1-10.

21 J. F. Todd, *Ion Trap Mass Spectrometer—Past, Present, and Future (?)*. Mass Spec. Rev., **1991**, *10*, 3-52.

22 R. E. March, *Quadrupole Ion Traps*. Mass Spec. Rev., **2009**, *28*, 961-989.

23 S. Gronert, *Quadrupole Ion Trap Studies of Fundamental Organic Reactions*. Mass Spectrom. Rev., **2005**, *24*, 100-120.

24 Finnigan LCQ Series Hardware Manual 97344-97023 Revision B. *Thermo Electron Corporation*, Technical Publications: San Jose, CA, 2005.

25 J. B. Fenn; M. Mann; C. K. Meng; S. F. Wong; C. M. Whitehouse, *Electrospray Ionization–Principles and Practice*. Mass Spectrom. Rev., **1990**, *9*, 37-70.

26 C. A. Cole; N. J. Demarais; Z. Yang; T. P. Snow; V. M. Bierbaum, *Heterocyclic Anions of Astrobiological Interest*. Astrophys. J., **2013**, *779*, 181-190.

27 O. V. Borisov; M. B. Goshe; T. P. Conrads; V. S. Rakov; T. D. Veenstra; R. D. Smith, *Low-Energy Collision-Induced Dissociation Fragmentation Analysis of Cysteinyl-Modified Peptides*. Anal. Chem., **2002**, *74*, 2284-2292.

28 E. L. Zins; C. Pirim; L. Vettier; M. Chaboud; L. Krim, *May Interstellar Leucine React with NO Radicals Present in Interstellar/Interplanetary Medium? An Ion-Trap Mass Spectrometry Study*. Int. J. Mass Spectrom., **2013**, *348*, 47-52.

29 D. Schroder; M. Engeser; M. Bronstrup; C. Daniel; J. Spandl; H. Hartl, *Ion Chemistry of the Hexanuclear Methoxo-Oxovanadium Cluster $V_6O_7(OCH_3)_{12}$*. Int. J. Mass Spectrom., **2003**, *228*, 743-757.

30 N. J. Demarais; Z. Yang; O. Martinez; N. Wehres; T. P. Snow; V. M. Bierbaum, *Gas-Phase Reactions of Polycyclic Aromatic Hydrocarbon Anions with Molecules of Interstellar Relevance*. Astrophys. J., **2012**, *746*, 32-38.

31 S. Gronert, *Estimation of Effective Ion Temperatures in a Quadrupole Ion Trap*. J. Am. Soc. Mass Spectrom., **1998**, *9*, 845-848.

32 C. H. DePuy; S. Gronert; A. Mullin; V. M. Bierbaum, *Gas-Phase S_N2 and E2 Reactions of Alkyl-Halides*. J. Am. Chem. Soc., **1990**, *112*, 8650-8655.

33 S. Gronert; C. H. DePuy; V. M. Bierbaum, *Deuterium-Isotope Effects in Gas-Phase Reactions of Alkyl-Halides - Distinguishing E2 and S_N2 Pathways*. J. Am. Chem. Soc., **1991**, *113*, 4009-4010.

34 K. M. Ervin, *Capture Collisions of Polyynide Anions with Hydrogen Atoms: Effect of the Ion Dipole, Quadrupole, and Anisotropic Polarizability*. Int. J. Mass Spectrom., **2014**, *in press*.

35 B. R. Eichelberger; T. P. Snow; V. M. Bierbaum, *Collision Rate Constants for Polarizable Ions*. J. Am. Soc. Mass Spectrom., **2003**, *14*, 501-505.

36 T. Su; W. J. Chesnavich, *Parametrization of the Ion-Polar Molecule Collision Rate-Constant by Trajectory Calculations*. J. Chem. Phys., **1982**, *76*, 5183-5185.

37 *NIST Chemistry WebBook, NIST Standard Reference Database Number 69*. National Institute of Standards and Technology, webbook.nist.gov, accessed 2010-2014.

38 W. M. Haynes, *CRC Handbook of Chemistry and Physics*. 93 ed.; Taylor & Francis: 2012.

39 M. J. Frisch; G. W. Trucks; H. B. Schlegel; G. E. Scuseria; M. A. Robb; J. R. Cheeseman; J. A. Montgomery; T. Vreven, et al., Gaussian 03, Revision C.02. Gaussian Inc. Wallingford, CT 2003.

40 M. J. Frisch; G. W. Trucks; H. B. Schlegel; G. E. Scuseria; M. A. Robb; J. R. Cheeseman; G. Scalmani; V. Barone, et al., Gaussian 09 Revision A.02. Gaussian Inc. Wallingford, CT: 2009.

41 C. Lee; W. Yang; R. G. Parr, *Development of the Colle-Salvetti Correlation-Energy Formula into a Functional of the Electron Density*. Phys. Rev. B, **1988**, *37*, 785-789.

42 D. Cremer, Møller–Plesset perturbation theory. *Encyclopedia of Computational Chemistry*, John Wiley and Sons, Ltd.: 2002.

43 C. Møller; M. S. Plesset, *Note on an Approximation Treatment for Many-Electron Systems*. Phys. Rev., **1934**, *46*, 618-622.

44 R. J. Bartlett; M. Musiał, *Coupled-Cluster Theory in Quantum Chemistry*. Rev. Mod. Phys., **2007**, *79*, 291-352.

45 G. Petersson; A. Bennett; T. G. Tensfeldt; M. A. Al-Laham; W. A. Shirley; J. Mantzaris, *A Complete Basis Set Model Chemistry. I. The Total Energies of Closed-Shell Atoms and Hydrides of the First-Row Elements*. J. Chem. Phys., **1988**, *89*, 2193-2218.

46 T. H. Dunning Jr., *Gaussian Basis Sets for use in Correlated Molecular Calculations. I. The Atoms Boron through Neon and Hydrogen*. J. Chem. Phys., **1989**, *90*, 1007-1023.

47 C. Gonzalez; H. B. Schlegel, *An Improved Algorithm for Reaction Path Following*. J. Chem. Phys., **1989**, *90*, 2154-2161.

CHAPTER 3

Reactions of Nitrogen–Containing Carbanions and H Atoms

3.1 Introduction

Although the conditions of the interstellar medium (ISM) may seem unconducive to chemical reactions (due to low particle density and temperature), a diverse array of chemical processes takes place there.[1-3] Approximately 170 molecules have currently been detected,[4] including six anions: HC_x^- (x=4, 6, 8) and C_xN^- (x=1, 3, 5).[5-11] Half of these anions, CN^-, C_3N^-, and C_5N^-, have also been detected in the upper atmosphere of Saturn's moon, Titan.[12] This discovery highlights their importance to the chemistry of planetary atmospheres as well as the ISM. The first step in understanding the chemical role of these anions is to study their reactivity with the most abundant atomic and molecular species in the universe, H and H_2. In this chapter, we report the reaction rate constants of these processes to improve astrochemical models and establish more defined reaction networks among interstellar and atmospheric species.

Anions and H atoms commonly react by associative detachment (AD), whereby the H atom bonds to the anion and an electron is subsequently lost. Previous work in our laboratory has shown that deprotonated nitriles, acetaldehyde, acetone, ethyl acetate, methanol, acetic acid, and glycine all react with H atom according to this mechanism.[13,14] Carbon chain anions including HC_x^- (x=2, 4, 6, 7) and C_x^- (x=2, 4-10) also predominantly react by AD, although some (C_x^-, x=7-10) exhibit association in addition to AD.[15] It is important to understand these reaction mechanisms, because they contribute to the ionization balance between anions and free electrons in the ISM.[1,2,16]

Reaction efficiencies, the ratio of experimental reaction rate constants to calculated collision rate constants, are also notable characteristics of reactions between anions and atoms. Carbanions, including HC_x^- (x=2, 4, 6, 7) and C_x^- (x=2, 4-10), react with H atoms with efficiencies of 0.3-0.4.[15] Interestingly, no discernable trend emerges between these reaction efficiencies and the reaction exothermicities, electronic spin states of reactants, or the size of the anions. This differs from the reactions of typical molecular anions and H atoms, whose reaction efficiencies are largely proportional to their reaction exothermicities. Other factors may also contribute to the reaction efficiencies; for example, the charge density on the reactive site of the anion, potential energy surface characteristics along the approach of the reactants, and the conservation of angular momentum upon the anion-H atom collision are all worthy of exploration. Therefore, further studies of the reactions between anions and H atoms are necessary to elucidate the fundamental properties of these reactions.

In this chapter, both experimental and theoretical explorations were conducted to study three categories of anions that are classified by their number of N atoms. These anions include C_xN^- (x=1-6), $C_xN_2^-$ (x=1, 3-5), and $C_xN_3^-$ (x=2, 4). Figure 3.1 depicts their optimized structures. In addition to our experimental measurements of reaction rate constants and efficiencies, we have carried out theoretical calculations at several levels of theory to explore the underlying reaction mechanisms and factors that influence the reaction efficiencies.

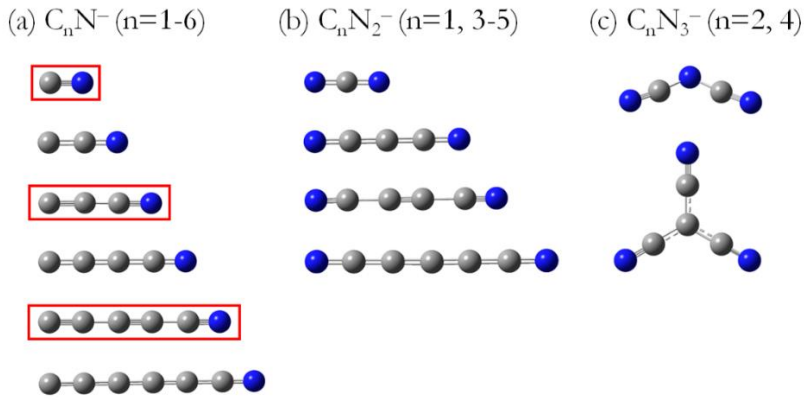

Figure 3.1
The lowest energy structures (CCSD(T)/aug-cc-pVDZ//B3LYP/aug-cc-pVTZ) of the nitrogen-containing carbanions of interest with one (a), two (b), and three (c) nitrogen atoms. The anions outlined in red (CN^-, C_3N^-, and C_5N^-) have been detected in the interstellar medium and in the upper atmosphere of Titan.[5-7,12]

3.2 Methods

3.2.1 Experimental

The experiments outlined in this chapter utilize the flowing afterglow-selected ion flow tube (FA-SIFT) apparatus that has been described in detail in Chapter 2. Nitrogen-containing carbanions are produced via direct current (DC) discharge on graphite.[17] This discharge is accomplished by applying a bias of ~2-3 kV (~10 mA DC) to a graphite rod relative to the source chamber. This rod is suspended within the source chamber by hollow stainless steel supports that allow for the continuous flow of water to conductively cool the rod during discharge. Both helium (the carrier gas) and N_2 (the discharge medium) flow over the graphite discharge apparatus to produce the $C_xN_y^-$ ions in this study. Specific anions are then mass selected using a quadrupole mass filter and injected through a Venturi inlet into the reaction flow tube. Within the flow tube, the selected anions are entrained in helium buffer gas (0.4 Torr, 200 std cm^3 s^{-1}) at 298 K and collisionally thermalized. H atoms are injected into the flow tube, and the remaining reactant ions as well as the product ions are monitored with a quadrupole mass filter coupled to an electron multiplier. These reactions occur under pseudo-

first-order conditions, where the H atom population is about 10^6 greater than that of the reagent anions in the flow tube.

The H atoms are produced by thermal dissociation of H_2, which is described in depth in Chapter 2.[18,19] Hydrogen gas (~9 std cm^3 s^{-1}, Airgas Inc., 99.999%) is passed through a molecular sieve trap cooled by liquid nitrogen to remove impurities, and over a heated tungsten filament to thermally dissociate the molecules. The newly formed H atoms are then transferred to the flow tube through Teflon tubing to minimize recombination. The inlet into the flow tube is positioned such that laminar flow and anion relaxation has been established (35 cm downstream from the Venturi inlet) and adequate reaction time is possible (70 cm upstream from ion sampling orifice). The H atom concentration is measured through an AD reaction of known rate constant with Cl^-.[20-22] All experimental rate constants reported herein are reproducible within ±20% and represent the mean of 2-4 measurements under varied H atom/He concentrations. We estimate that the total error of our measurements is ±50% including the systematic errors and the uncertainty in the measurement of H atom concentration.

3.2.2 Computational

Theoretical calculations are performed using the *Gaussian 03* suite of programs.[23] Geometry optimization and frequency analyses are calculated at the B3LYP/aug-cc-pVTZ level of theory, and the single-point energy calculations are carried out at the CCSD(T)/aug-cc-pVDZ level for the optimized structures to limit computational expense while obtaining reliable energetics. We have found in previous studies involving carbanions that this level of theory is both accurate and efficient.[24] Zero-point energy (ZPE) and thermal-energy (298 K) corrections are applied at the same level of theory as well. The reaction coordinate plots and the reaction enthalpies included in this work were obtained from these computational results.

3.3 Results and Discussion

The following sections detail the experimental and computational results of the reactions between H atoms and three sets of nitrogen-containing carbanions: C_xN^- (x=1-6), $C_xN_2^-$ (x=1, 3-5), and $C_xN_3^-$ (x=2, 4). We did not observe reactions with H_2 for any of these species. Reactions predominantly proceed by AD ($A^- + H \rightarrow AH + e^-$), although some anions also fragment upon reaction with H atom. Table 3.1 and Table 3.2 summarize the rate constants, reaction efficiencies, and products of the reactions studied. In addition, Table 3.1-Table 3.5 include the calculated reaction enthalpies. The reported reaction efficiencies are defined as the ratio of the experimental rate constant (k_{exp}) to the calculated collision rate constant (k_{PPI}), which is determined using point-polarizable-ion (PPI) collision theory.[25] As outlined in Chapter 2, this collision theory incorporates the polarizabilities, dipole moments, and masses of the collision partners, but does not account for the effect of spin conservation. Overall, the C_xN^- (x=1-6) and $C_xN_2^-$ (x=1, 3-5) ions react with H atom with moderate reaction efficiencies (0.18-0.35), but the $C_xN_3^-$ (x=2, 4) ions are unreactive. Detailed computations accompany our experimental data to help explain the mechanisms behind the observed reactions and to uncover potential energy barriers along the reaction coordinate between unreactive species.

3.3.1 Reactions of C_xN^- (x = 1–6)

The reagent ions C_xN^- (x=1-6) primarily react with H atom to produce neutral nitrile species by AD. The energetics of these reagent ion structures, the reaction mechanisms, and the overall exothermicities are calculated at the CCSD(T)/aug-cc-pVDZ//B3LYP/aug-cc-pVTZ level of theory.

Table 3.1
Kinetic data for reactions between C_xN^- (x=1-6) and H atoms.

Anion[a]	k_{exp}[b] (10^{-10} cm^3 s^{-1})	Efficiency[c] (k_{exp}/k_{PPI})	$\Delta H^{a,d}$ {0 K kcal mol^{-1}}[298 K kcal mol^{-1}]
CN^- (S)	6.3[e]	0.28	HCN (S) {-33.3} [-33.2]
			HNC (S) {-19.5} [-19.2]
C_2N^- (T)	7.9	0.35	HC_2N (S) {-20.7} [-20.3]
			HC_2N (T) {-32.5} [-31.9]
			c-CC(H)N (S) {-22.7} [-22.7]
			c-CC(H)N (T) {-31.8} [-31.6]
			CN^- (S) + CH (D) {-12.2} [-10.4]
C_3N^- (S)	5.4[f]	0.23	HC_3N (S) {-30.4} [-30.3]
C_4N^- (T)	8.0	0.34	HC_4N (S) {-11.8} [-11.5]
			HC_4N (T) {-24.5} [-24.0]
			c-CC(H)C_2N (S) {-29.5} [-29.7]
			C_2CHCN (D) {-16.4} [-16.2]
			CN^- (S) + C_3H (D) {-0.8} [0.8]
			C_3^- (D) + HCN (S) {-9.0} [-7.7]
C_5N^- (S)	5.8	0.24	HC_5N (S) {-26.3} [-26.2]
C_6N^- (T)	6.5	0.26	HC_6N (S) {-10.5} [-10.1]
			HC_6N (T) {-24.9} [-24.7]
			$C_4C(H)CN$ (S) {-10.3} [-10.2]
			$C_2C(H)C_3N$ (S) {-10.9} [-10.8]
			CC(H)C_4N (S) {-24.4} [-24.6]
			CN^- (S) + C_5H (D) {-25.4} [-24.2]

[a] The ground state of reactant anions. Calculations were performed at the CCSD(T)/aug-cc-pVDZ//B3LYP/aug-cc-pVTZ level of theory including zero-point energy corrections. Letters in parentheses indicate the spin state of the species, *i.e.*, singlet (S), doublet (D), and triplet (T).
[b] Reproducibility is better than ±20%; total error is ±50%.
[c] k_{PPI} is the point-polarizable ion model theoretical rate constant.[25]
[d] Energies are relative to the corresponding reactants (ground-state anion and the H atom). The letter "*c*" as a prefix for a chemical formula indicates a cyclic structure. Product ions observed in the experiment are in bold font; however, their branching ratios were not measured due to experimental limitations. The numbers in parentheses indicate the calculated reaction enthalpies at 0 and 298 K.
[e] 8 x 10^{-10} cm^3 s^{-1}.[21,26]
[f] In exact agreement with our previous measurement.[27]

Computational resources were conserved by refraining from calculating every structural permutation for all species in this study. Rather, calculations were performed for every possible singlet and triplet isomer structure for the C_xN^- (x=1-4) anions. According to these results, C_xN^- (x=1, 3) have a singlet ground state and C_xN^- (x=2, 4) have a triplet ground state. Additionally, all ground state structures are linear with a terminal nitrogen atom (see Figure 3.1). Previous experimental and theoretical work on C_xN^- (x=2-7) has reported this trend as well.[28,29] For C_5N^- and C_6N^-, only structures with energies close to the ground states were calculated. These are summarized in Table 3.1 and Table 3.3.

Table 3.2
Kinetic data for reactions between $C_xN_2^-$ (x=1, 3-5) and H atoms.

Anion[a]	k_{exp}[b] (10^{-10} cm^3 s^{-1})	Efficiency[c] (k_{exp}/k_{PPI})	ΔH[a,d] {0 K kcal mol^{-1}}[298 K kcal mol^{-1}]
NCN^- (D)	5.5	0.25	HNCN (D) {-25.1} [-24.7]
NC_3N^- (D)	5.1	0.23	NCC(H)CN (D) {-25.5} [-25.3]
NC_4N^- (D)	4.1	0.18	NCC(H)C_2N (D) {-11.9} [-11.9]
			CN^- (S) + HC_3N (S) {-43.5} [-42.7]
			C_3N^- (S) + HNC (S) {-32.5} [-31.5]
			C_3N^- (S) + HCN (S) {-46.4} [-45.5]
NC_5N^- (D)	5.4	0.23	NC_2HC_3N (D) {-18.5} [-18.6]
			C_4N^- (T) + HCN (S) {-6.5} [-5.5]

[a] The ground state of reactant anions. Calculations were performed at the CCSD(T)/aug-cc-pVDZ//B3LYP/aug-cc-pVTZ level of theory including zero-point energy corrections. Letters in parentheses indicate the spin state of the species, *i.e.*, singlet (S), doublet (D), and triplet (T).
[b] Reproducibility is better than ±20%; total error is ±50%.
[c] k_{PPI} is the point-polarizable ion model theoretical rate constant.[25]
[d] Energies are relative to the corresponding reactants (ground-state anion and the H atom). The letter "*c*" as a prefix for a chemical formula indicates a cyclic structure. Product ions observed in the experiment are in bold font; however, their branching ratios were not measured due to experimental limitations. The numbers in parentheses indicate the calculated reaction enthalpies at 0 and 298 K.

Table 3.3
Complete computational results for reactions between C_xN^- (x=1-6) and H atoms.

Anion[a]	ΔE^b {0 K kcal mol^{-1}}[298 K kcal mol^{-1}]	
	AH^-	AH & Fragments
CN^- (S) {0.0}	HCN^- (D) {-17.7}	HCN (S) {-33.3} [-33.2]
CN^- (T) {129.2}	HNC^- (D) {-6.8}	HNC (S) {-19.5} [-19.2]
C_2N^- (S) {23.6}	HC_2N^- (D) {-75.9}	HC_2N (S) {-20.7} [-20.3]
C_2N^- (T) {0.0}	HC_2N^- (Q) {-19.8}	HC_2N (T) {-32.5} [-31.9]
CNC^- (S) {38.2}	$CCNH^-$ (D) {-50.6}	CCNH (S) {2.7} [3.2]
CNC^- (T) {15.9}	$CCNH^-$ (Q) {6.8}	CCNH (T) {1.6} [2.0]
	$CC(H)N^-$ (D) {-24.3}	*c*-CC(H)N (S) {-22.7} [-22.7]
	$CC(H)N^-$ (Q) {-9.6}	*c*-CC(H)N (T) {-31.8} [-31.6]
	c-$CC(H)N^-$ (D) {-27.3}	CN^- (S) + CH (D) {-12.2}[-10.4]
	c-$CC(H)N^-$ (Q) {33.2}	
C_3N^- (S) {0.0}	HC_3N^- (D) {-33.1}	HC_3N (S) {-30.4} [-30.3]
C_3N^- (T) {83.8}	HC_3N^- (Q) {34.6}	HC_3N (T) {58.8} [59.2]
CNC_2^- (S) {31.6}	HNC_3^- (D) {-8.9}	HNC_3 (S) {17.7} [18.3]
CNC_2^- (T) {107.6}	HNC_3^- (Q) {71.4}	HNC_3 (T) {74.9} [75.4]
	$CC(H)CN^-$ (D) {-28.8}	CC(H)CN (S) {12.4} [12.8]
	$CC(H)CN^-$ (Q) {43.0}	CC(H)CN (T) {53.4} [53.5]
	$C_2C(H)N^-$ (D) {-9.7}	$C_2C(H)N$ (S) {59.4} [59.6]
	$C_2C(H)N^-$ (Q) {50.4}	$C_2C(H)N$ (T) {91.4} [91.7]
		CN^- (S) + C_2H (D) {26.7} [28.4]
		C_2^- (D) + HCN (S) {26.0} [27.3]
C_4N^- (S) {4.9}	HC_4N^- (D) {-73.6}	HC_4N (S) {-11.8} [-11.5]
C_4N^- (T) {0.0}	HC_4N^- (Q) {-24.2}	HC_4N (T) {-24.5} [-24.0]
CNC_3^- (S) {25.7}	HNC_4^- (D) {-48.0}	HNC_4 (S) {15.5} [15.9]
CNC_3^- (T) {31.8}	HNC_4^- (Q) {1.5}	HNC_4 (T) {19.8} [20.2]
$C_2NC_2^-$ (S) {53.6}	C_3CHN^- (D) {-19.4}	C_3CHN (S) {17.6} [17.5]
$C_2NC_2^-$ (T) {50.5}	C_3CHN^- (Q) {33.3}	C_3CHN (T) {41.1} [41.4]
	C_2CHCN^- (D) {-80.4}	C_2CHCN (S) {-16.4} [-16.2]
	C_2CHCN^- (Q) {-7.1}	C_2CHCN (T) {8.9} [9.1]
	c-$CC(H)C_2N^-$ (D) {-51.3}	*c*-$CC(H)C_2N$ (S) {-29.5} [-29.7]
	c-$CC(H)C_2N^-$ (Q) {6.6}	*c*-$CC(H)C_2N$ (T) {16.5} [16.7]
		CN^- (S) + C_3H (D) {-0.8} [0.8]
		C_2N^- (S) + C_2H (D) {45.0} [46.4]
		C_3N^- (S) + CH (D) {22.1} [23.5]
		C_3^- (D) + HCN (S) {-9.0} [-7.7]
C_5N^- (S) {0.0}	HC_5N^- (D) {-42.1}	HC_5N (S) {-26.3} [-26.2]
C_5N^- (T) {73.2}	HC_5N^- (Q) {12.4}	HC_5N (T) {42.4} [43.2]

CNC_4^- (S) {31.6}	HNC_5^- (D) {-12.8}	HNC_5 (S) {31.7} [32.4]
$C_2NC_3^-$ (S) {56.6}	HNC_5^- (Q) {34.9}	HNC_5 (T) {75.8} [76.5]
	$C_4C(H)N^-$ (D) {-11.4}	$C_4C(H)N$ (S) {67.3} [67.6]
	$C_4C(H)N^-$ (Q) {38.1}	$C_4C(H)N$ (T) {89.5} [89.8]
	C_3CHCN^- (D) {-42.1}	$C_3C(H)CN$ (S) {17.5} [17.7]
	C_3CHCN^- (Q) {9.9}	$C_3C(H)CN$ (T) {49.8} [49.9]
	$C_2CHC_2N^-$ (D) {-23.9}	$C_2C(H)C_2N$ (S) {43.3} [43.4]
	$C_2CHC_2N^-$ (Q) {17.7}	$C_2C(H)C_2N$ (T) {71.8} [71.9]
	$CC(H)C_3N^-$ (D) {-25.5}	$CC(H)C_3N$ (S) {18.6} [19.1]
	$CC(H)C_3N^-$ (Q) {35.7}	$CC(H)C_3N$ (T) {65.0} [65.3]
		CN^- (S) + C_4H (D) {30.3} [31.8]
		C_2N^- (T) + C_3H (D) {87.6} [89.1]
		C_3N^- (S) + C_2H (D) {32.3} [33.9]
		C_4N^- (S) + CH (D) {92.2} [93.8]
C_6N^- (S) {4.5}	HC_6N^- (D) {-79.5}	HC_6N (S) {-10.5} [-10.1]
C_6N^- (T) {0.0}	HC_6N^- (Q) {-35.3}	HC_6N (T) {-24.9} [-24.7]
	HNC_6^- (D) {-50.1}	HNC_6 (S) {19.1} [19.6]
	HNC_6^- (Q) {-10.7}	HNC_6 (T) {25.7} [26.2]
	$C_5C(H)N^-$ (D) {-17.3}	$C_5C(H)N$ (S) {29.6} [29.6]
	$C_5C(H)N^-$ (Q) {-21.5}	$C_5C(H)N$ (T) {61.4} [61.8]
	$C_4C(H)CN^-$ (D) {-83.2}	$C_4C(H)CN$ (S) {-10.3} [-10.2]
	$C_4C(H)CN^-$ (Q) {-28.0}	$C_4C(H)CN$ (T) {11.2} [11.4]
	$C_3C(H)C_2N^-$ (D) {-40.2}	$C_3C(H)C_2N$ (S) {23.7} [23.9]
	$C_3C(H)C_2N^-$ (Q) {-33.0}	$C_3C(H)C_2N$ (T) {30.0} [30.3]
	$C_2C(H)C_3N^-$ (D) {-76.9}	$C_2C(H)C_3N$ (S) {-10.9} [-10.8]
	$C_2C(H)C_3N^-$ (Q) {-6.9}	$C_2C(H)C_3N$ (T) {15.4} [15.6]
	$CC(H)C_4N^-$ (D) {-58.9}	$CC(H)C_4N$ (S) {-24.4} [-24.6]
	$CC(H)C_4N^-$ (Q) {-29.3}	$CC(H)C_4N$ (T) {17.3} [17.4]
		CN^- (S) + C_5H (D) {-25.4} [-24.2]
		C_2N^- (S) + C_4H (D) {49.8} [50.8]
		C_3N^- (S) + C_3H (D) {6.0} [7.3]
		C_4N^- (S) + C_2H (D) {33.5} [34.9]
		C_5N^- (S) + CH (D) {23.2} [24.6]

[a] Calculated at the CCSD(T)/aug-cc-pVDZ//B3LYP/aug-cc-pVTZ level of theory including zero-point energy corrections. The letter "*c*" as a prefix to the chemical formulas indicates the cyclic structure. Letters in parentheses indicate the spin state of the species, *i.e.*, singlet (S), doublet (D), triplet (T), and quartet (Q). Energies are relative to the ground state anions.

[b] Energies are relative to reactants (ground state anion and the H atom). The numbers in parentheses indicate the calculated reaction enthalpies at 0 and 298 K.

As described above, the C_xN^- (x=1-6) species fall into two categories based on their ground state structures: singlet (x=1, 3, 5) and triplet (x=2, 4, 6). Recall that the former group (x=1, 3, 5) has been detected in the ISM and in Titan's upper atmosphere. Their reactions with H atom, therefore, are very relevant to the field of astrochemistry. Notably, the efficiencies of the reactions between these anions and H atom also are divided along the same lines. The anions with an even number of carbon atoms (C_2N^-, C_4N^-, and C_6N^-) have slightly higher reaction efficiencies than their odd counterparts (CN^-, C_3N^-, and C_5N^-). Moreover, as shown in Table 3.1 and Table 3.3, anions with an even number of carbon atoms can access a greater number of reaction channels. Fragmentation processes are observed for C_xN^- (x=2, 4, 6), although AD channels dominate. All three anions react to produce CN^-, and C_3^- is also produced from C_4N^-. Due to signal intensity limitations in our experiment, we have not reported branching ratios for these different product channels.

As an example of the anions containing an odd number of nitrogen atoms, the potential energy plot of CN^- + H is shown in Figure 3.2. This reaction proceeds through AD, and may involve H atom addition to either the carbon or nitrogen sites on CN^-. Our computational results reveal that H addition at the carbon site is barrierless and produces HCN + e^- via an exothermic process (-33.3 kcal mol^{-1}). The previously reported rate constant for this reaction (8 x 10^{-10} cm^3 s^{-1} ± factor of 2)[21,26] agrees well with our current results reported in Table 3.1 (6.3 x 10^{-10} cm^3 s^{-1}). Previously, this reaction rate constant has been incorrectly cited as 1.3 x 10^{-9} cm^3 s^{-1} in both publications[30,31] and databases (UDFA and KIDA). As opposed to the addition on the carbon site, H atom addition to the nitrogen site on CN^- involves a barrier (1.0 kcal mol^{-1}) that will slow this reaction channel. Therefore, although it is an exothermic channel (-19.5 kcal mol^{-1}), production of HNC is less favorable than HCN:

$$CN^-(S) + H(D) \rightarrow [HCN^-(D)] \rightarrow HCN(S) + e^- \qquad \Delta H_0 = -33.3 \text{ kcal mol}^{-1}$$

$$\rightarrow [HNC^-(D)] \rightarrow HNC(S) + e^- \qquad \Delta H_0 = -19.5 \text{ kcal mol}^{-1}$$

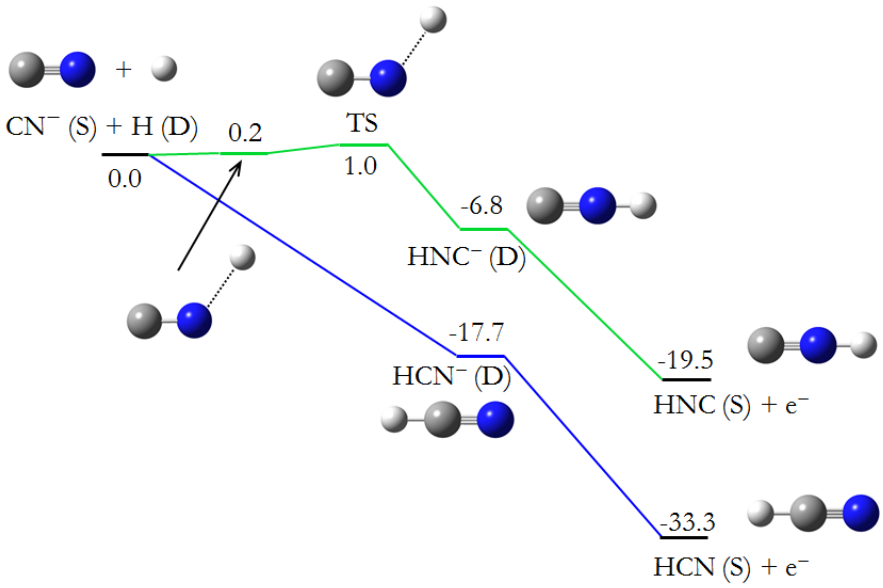

Figure 3.2
The reaction coordinate plot (in kcal mol^{-1}, 0 K) for CN^- + H in which H atom binds to C (blue line) and N (green line) is shown. Calculations were performed at the CCSD(T)/aug-cc-pVDZ//B3LYP/aug-cc-pVTZ level of theory. Letters in parentheses indicate the spin state of the species, *i.e.*, singlet (S) and doublet (D). Some of the species shown are not stable (HCN^- (D) and HNC^- (D)); these are included for comparison with products and other species along the calculated reaction coordinate.

We indicate the spin state of the species in parentheses as follows: singlet (S), doublet (D), triplet (T), and quartet (Q). The intermediate species HCN^-(D) and HNC^-(D) are unstable, and they are shown above to relate the products to other species along the reaction coordinate for clarity. C_3N^- and C_5N^- likely follow similar reaction pathways to CN^-, although the formation of isocyanides HNC_3 and HNC_5 is endothermic and therefore excluded from Table 3.1.

The potential energy surfaces of the reaction pathways of C_2N^- + H (an example of a reagent ion containing an even number of nitrogen atoms) are shown in Figure 3.3. Reactions may proceed through spin-allowed doublet and quartet pathways due to the triplet ground state of the reagent anion and the doublet spin state of H atom. There are three points of attachment for the H atom on C_2N^-, C1, C2, and N3, as shown in Figure 3.3 (a)-(c). The potential energy diagram for the addition of H

atom to the C1 site on the anion, Figure 3.3 (a), involves a spin-allowed quartet transition state (-5.5 kcal mol^{-1}). This leads to two products: a triplet neutral HC_2N and an electron.

$$C_2N^-(T) + H(D) \rightarrow [HC_2N^-(Q)] \rightarrow HC_2N(T) + e^- \qquad \Delta H_0 = -32.5 \text{ kcal mol}^{-1}$$

Doublet-state pathways are also possible for this reaction. Both fragmentation and AD may occur through these routes. The doublet adduct (HC_2N^-) may form CN^- and HC fragment products, or detach an electron to form either the singlet or triplet neutral HC_2N molecules.

$$C_2N^-(T) + H(D) \rightarrow [HC_2N^-(D)] \rightarrow CN^-(S) + HC(D) \qquad \Delta H_0 = -12.2 \text{ kcal mol}^{-1}$$

$$\rightarrow HC_2N(S) + e^- \qquad \Delta H_0 = -20.7 \text{ kcal mol}^{-1}$$

$$\rightarrow HC_2N(T) + e^- \qquad \Delta H_0 = -32.5 \text{ kcal mol}^{-1}$$

All four of the reactions shown above likely contribute to our experimental observations, as both the quartet and doublet pathways are barrierless and exothermic. Based on our previous work,[24,32] we expect spin-conserved reaction pathways to represent the dominant anion-atom interactions. We have found that spin-forbidden reaction pathways, which are limited by the efficiency of spin conversion, cannot compete with barrierless, spin-allowed channels.

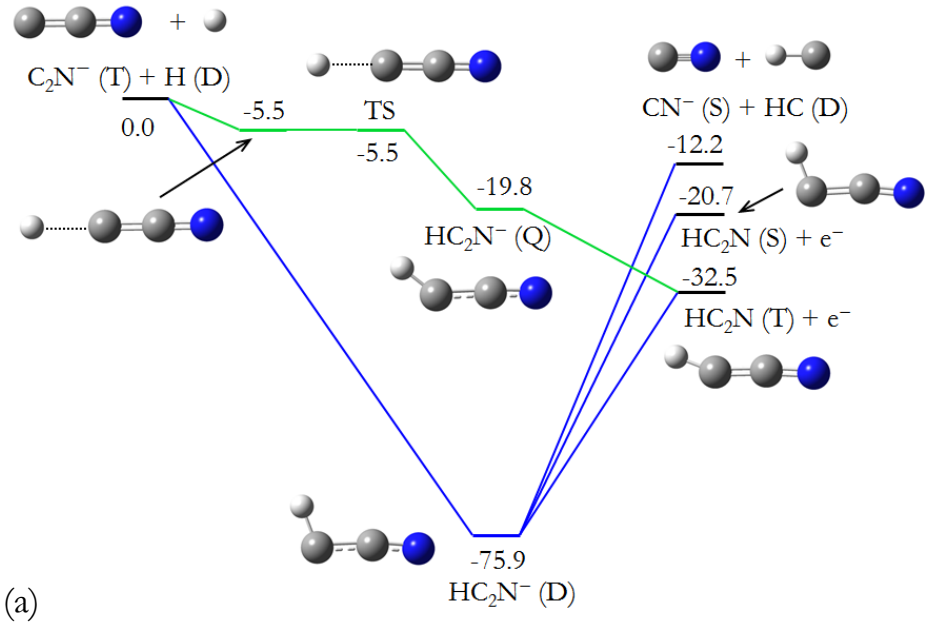
C2N− (T) + H (D)
0.0
-5.5
TS
-5.5
-19.8
HC2N− (Q)
CN− (S) + HC (D)
-12.2
-20.7
HC2N (S) + e−
-32.5
HC2N (T) + e−
-75.9
HC2N− (D)

(a)

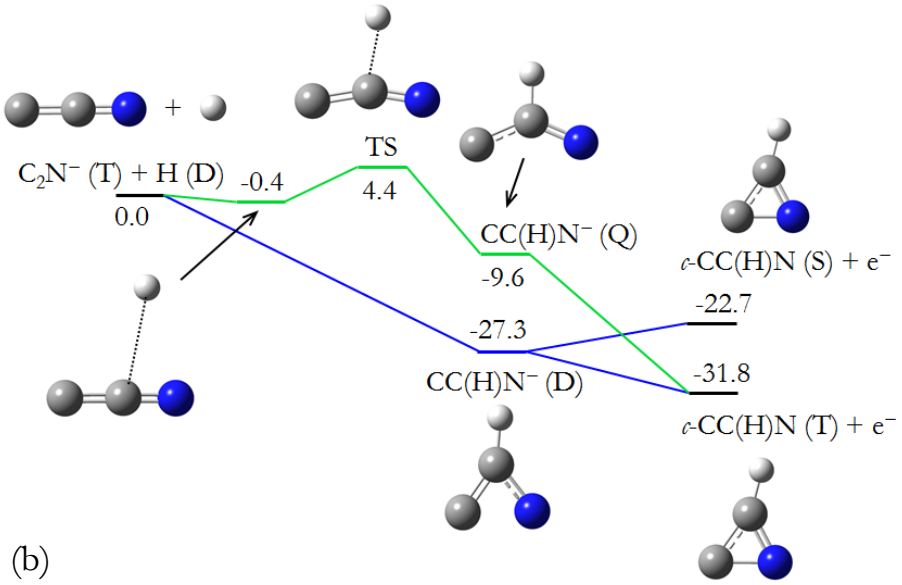
C2N− (T) + H (D)
0.0
-0.4
TS
4.4
CC(H)N− (Q)
-9.6
-27.3
CC(H)N− (D)
c-CC(H)N (S) + e−
-22.7
-31.8
c-CC(H)N (T) + e−

(b)

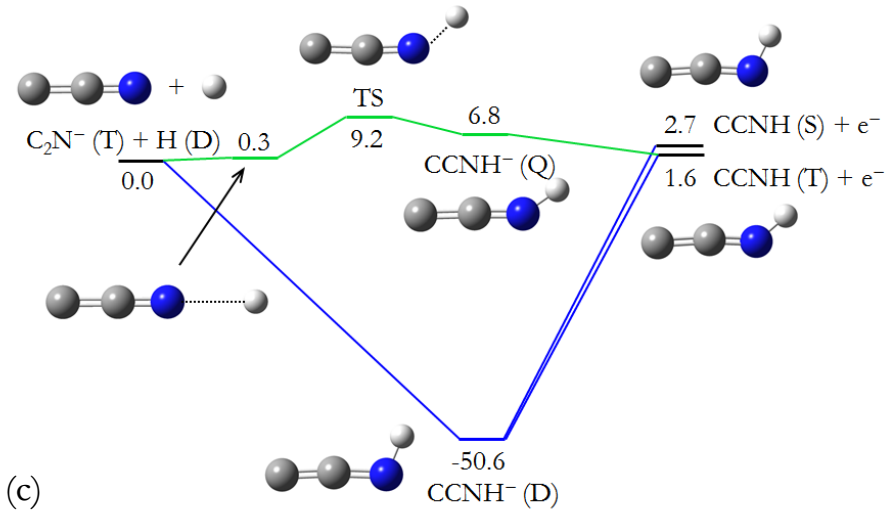

Figure 3.3
The reaction coordinate plot (in kcal mol^{-1}, 0 K) for C_2N^- + H in which H atom binds to (a) C1, (b) C2, and (c) N3 is shown. Calculations were performed at the CCSD(T)/aug-cc-pVDZ//B3LYP/aug-cc-pVTZ level of theory. Letters in parentheses indicate the spin state of the species, *i.e.*, singlet (S), doublet (D), triplet (T), and quartet (Q). Only spin-allowed reactions are investigated, where the green and blue lines indicate the high-spin (quartet) and low-spin (doublet) processes, respectively. Some of the species shown are not stable (HC_2N^- (Q), $CC(H)N^-$ (D), $CC(H)N^-$ (Q), and $CCNH^-$ (Q)); these are included for comparison with products and other species along the calculated reaction coordinate.

Reaction pathways involving the second H attachment site, C2, are shown in Figure 3.3 (b). Due to the thermal energy distribution among the reagent ions in our experimental apparatus, the 4.4 kcal mol^{-1} barrier of the spin-allowed quartet route likely causes its contribution to be insignificant. The spin-allowed doublet pathways, however, produce cyclic neutral *c*-CC(H)N in both the singlet and triplet states by barrierless and exothermic processes. We will use "*c*" to denote the cyclic structure throughout this work.

$$C_2N^-(T) + H(D) \rightarrow [CC(H)N^-(D)] \rightarrow c\text{-}CC(H)N(S) + e^- \qquad \Delta H_0 = -22.7 \text{ kcal mol}^{-1}$$

$$\rightarrow c\text{-}CC(H)N(T) + e^- \qquad \Delta H_0 = -31.8 \text{ kcal mol}^{-1}$$

The final H attachment option is depicted in Figure 3.3 (c). At the N3 site of the anion, the spin-allowed reaction pathways are slightly endothermic. Additionally, a high energy transition state (9.2 kcal mol^{-1}) prevents the quartet route from being feasible under our experimental conditions. Hence, we do not expect either channel to contribute greatly to the observed reaction.

$$C_2N^-(T) + H(D) \rightarrow [CCNH^-(D)] \rightarrow CCNH(S) + e^- \qquad \Delta H_0 = 2.7 \text{ kcal mol}^{-1}$$

$$\rightarrow [CCNH^-(D)] \rightarrow CCNH(T) + e^- \qquad \Delta H_0 = 1.6 \text{ kcal mol}^{-1}$$

When two potential energy curves of different spin states intersect, spin conversion may occur. However, as previously mentioned, the efficiency of this conversion is commonly very low, and spin-forbidden pathways are not generally competitive with their spin-allowed counterparts.[32,33] Although higher energy species may be produced in the DC discharge ion source, we only investigate the ground state reactant anions, because they are likely the most dominant species formed. The ground state species are often much more energetically favorable than other structures. For example, Table 3.3 reveals that the most stable $C_2N^-(T)$ ion is 23.6, 38.2, and 15.9 kcal mol^{-1} more stable than the C_2N^- (S), CNC^- (S), and CNC^- (T), respectively. Therefore, only the ground state structures are investigated, and the exothermic products are shown in Table 3.1. Additional computational results for the C_xN^- (x=1-6) species can be found in Table 3.3.

3.3.2 Reactions of $C_xN_2^-$ (x = 1, 3–5)

For carbanions containing two nitrogen atoms, our computational results are summarized in Table 3.2 and Table 3.4. The reaction efficiencies for all $C_xN_2^-$ (x=1, 3-5) are very similar (0.18-0.25), and we do not observe any discernable trend in their reactivity. These anions all have linear, doublet ground state structures with the nitrogen atoms located at both ends of the carbon chain. Once again, AD is the most exothermic reaction pathway with H atom. The most exothermic binding sites for the

H atoms are the terminal N atom in NCN^- and NC_4N^-, and the middle and second C atoms in NC_3N^- and NC_5N^-, respectively. Fragmentation channels are observed in addition to AD for NC_4N^- and NC_5N^-. The reaction between NC_4N^- and H atom produces CN^- and C_3N^-, and NC_5N^- reacts to form C_4N^-.

Table 3.4
Complete computational results for reactions between $C_xN_2^-$ (x=1, 3-5) and H atoms.

Anion[a]	ΔE^b {0 K kcal mol^{-1}}[298 K kcal mol^{-1}]	
	AH^-	AH & Fragments
NCN^- (D) {0.0}	$HNCN^-$ (S) {-81.2}	HNCN (D) {-25.1} [-24.7]
CN_2^- (D) {45.4}	$HNCN^-$ (T) {-16.1}	HNCN (Q) {46.4} [46.8]
NCN^- (Q) {59.1}	$NC(H)N^-$ (S) {-5.0}	NC(H)N (D) {13.6} [13.8]
CN_2^- (Q) {82.9}	$NC(H)N^-$ (T) {-4.3}	NC(H)N (Q) {91.2} [91.6]
NC_3N^- (D) {0.0}	HNC_3N^- (S) {-58.8}	HNC_3N (D) {5.1} [5.7]
NC_3N^- (Q) {66.9}	HNC_3N^- (T) {-9.7}	HNC_3N (Q) {56.4} [56.8]
CNC_2N^- (D) {27.1}	$NC(H)C_2N^-$ (S) {-16.1}	$NCHC_2N$ (D) {27.3} [27.6]
CNC_2N^- (Q) {88.3}	$NC(H)C_2N^-$ (T) {-13.9}	$NCHC_2N$ (Q) {93.2} [93.5]
C_2NCN^- (D) {41.8}	$NCC(H)CN^-$ (S) {-88.5}	NCC(H)CN (D) {-25.5} [-25.3]
C_2NCN^- (Q) {101.8}	$NCC(H)CN^-$ (T) {-21.0}	NCC(H)CN (Q) {69.0} [69.2]
$C_3N_2^-$ (D) {81.5}		CN^- (S) + HC_2N (S) {4.0} [5.6]
$C_3N_2^-$ (Q) {106.8}		C_2N^- (T) + HCN (S) {26.8} [28.0]
$C_2N_2C^-$ (D) {82.1}		
$C_2N_2C^-$ (Q) {145.3}		
$C_4N_2^-$ (D) {76.0}	HNC_4N^- (S) {-41.9}	HNC_4N (D) {7.5} [7.8]
$C_4N_2^-$ (Q) {121.8}	HNC_4N^- (T) {-26.7}	HNC_4N (Q) {62.1} [62.6]
C_3NCN^- (D) {37.4}	$NC(H)C_3N^-$ (S) {-38.0}	$NC(H)C_3N$ (D) {4.8} [4.7]
C_3NCN^- (Q) {100.8}	$NC(H)C_3N^-$ (T) {-19.8}	$NC(H)C_3N$ (Q) {66.1} [66.2]
$C_2NC_2N^-$ (D) {51.2}	$NCC(H)C_2N^-$ (S) {-11.6}	$NCC(H)C_2N$ (D) {-11.9} [-11.9]
$C_2NC_2N^-$ (Q) {94.1}	$NCC(H)C_2N^-$ (T) {42.2}	$NCC(H)C_2N$ (Q) {41.4} [41.7]
CNC_3N^- (D) {22.9}		CN^- (S) + HC_3N (S) {-43.5} [-42.7]
CNC_3N^- (Q) {83.3}		C_2N^- (S) + HC_2N (T) {55.5} [56.5]
NC_4N^- (D) {0.0}		C_3N^- (S) + HNC (S) {-32.5} [-31.5]
NC_4N^- (Q) {59.3}		C_3N^- (S) + HCN (S) {-46.4} [-45.5]
$C_2N_2C_2^-$ (D) {123.8}		
$C_2N_2C_2^-$ (Q) {147.1}		
c-C_3NCN^- (D) {88.2}		
c-C_3NCN^- (Q) {111.3}		
c-$C_2NC_2N^-$ (D) {107.7}		

c-$C_2NC_2N^-$ (Q) {158.6}		
$CC(CN)_2^-$ (D) {10.2}		
$CC(CN)_2^-$ (Q) {80.3}		
NC_5N^- (D) {0.0}	HNC_5N^- (S) {-58.3}	HNC_5N (D) {11.1} [11.4]
NC_5N^- (Q) {48.6}	HNC_5N^- (T) {-14.7}	HNC_5N (Q) {54.9} [55.3]
$(CN)_2C_3^-$ (D) {2.1}	$NCC(H)C_3N^-$ (S) {-87.2}	$NCC(H)C_3N$ (D) {-18.5} [-18.6]
$(CN)_2C_3^-$ (Q) {77.2}	$NCC(H)C_3N^-$ (T) {-44.9}	$NCC(H)C_3N$ (Q) {47.9} [48.0]
	$NC_2C(H)C_2N^-$ (S) {-33.6}	$NC_2C(H)C_2N$ (D) {35.9} [35.8]
	$NC_2C(H)C_2N^-$ (T) {-26.3}	$NC_2C(H)C_2N$ (Q) {34.2} [34.5]
		CN^- (S) + HC_4N (S) {2.3} [3.6]
		C_2N^- (T) + HC_3N (S) {64.2} [64.9]
		C_3N^- (S) + HC_2N (S) {12.6} [13.7]
		C_4N^- (T) + HCN (S) {-6.5} [-5.5]

[a] Calculated at the CCSD(T)/aug-cc-pVDZ//B3LYP/aug-cc-pVTZ level of theory including zero-point energy corrections. The letter "*c*" as a prefix to the chemical formulas indicates the cyclic structure. Letters in parentheses indicate the spin state of the species, *i.e.*, singlet (S), doublet (D), triplet (T), and quartet (Q). Energies are relative to the ground state anions.
[b] Energies are relative to reactants (ground state anion and the H atom). The numbers in parentheses indicate the calculated reaction enthalpies at 0 and 298 K.

The potential energy diagram for the NCN^- + H reaction is depicted in Figure 3.4. The H atom adds to the nitrogen, and both the spin-allowed singlet and triplet pathways are barrierless and exothermic. The final products are a doublet neutral HNCN molecule and an electron. As shown in Table 3.4, the production of other AD products such as NC(H)N (D and Q) are endothermic. Therefore, these pathways are not included in Figure 3.4.

$$NCN^-(D) + H(D) \rightarrow [HNCN^-(S)] \rightarrow HNCN(D) + e^- \qquad \Delta H_0 = -25.1 \text{ kcal mol}^{-1}$$

$$\rightarrow [HNCN^-(T)] \rightarrow HNCN(D) + e^- \qquad \Delta H_0 = -25.1 \text{ kcal mol}^{-1}$$

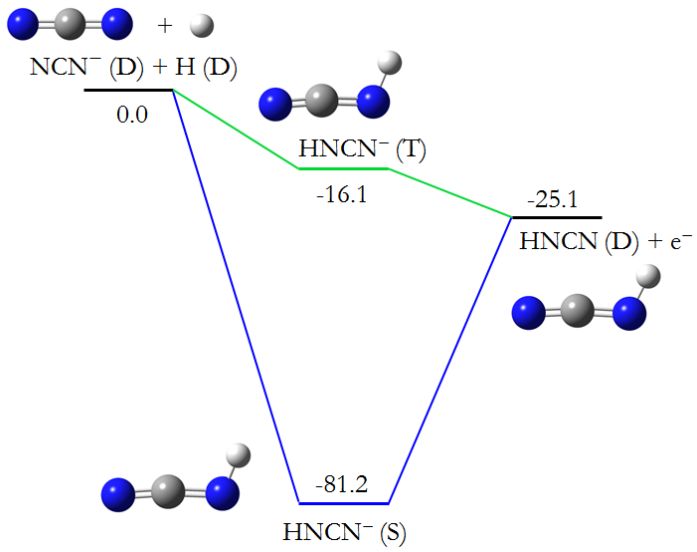

Figure 3.4

The reaction coordinate plot (in kcal mol^{-1}, 0 K) for NCN^- + H is shown. Calculations were performed at the CCSD(T)/aug-cc-pVDZ//B3LYP/aug-cc-pVTZ level of theory. Letters in parentheses indicate the spin state of the species, *i.e.*, singlet (S), doublet (D), and triplet (T). Only spin-allowed reactions are investigated, where the green and blue lines indicate the high-spin (triplet) and low-spin (singlet) processes, respectively. The species $HNCN^-$ (T) is not stable. We include it for comparison with products and other species along the calculated reaction coordinate.

AD processes represent the most exothermic reaction channels, with one exception. NC_4N^- reacts with H atom to form C_3N^- and HCN in a very exothermic process:

$$NC_4N^-(D) + H(D) \rightarrow [NC(H)C_3N^-(S)] \rightarrow C_3N^-(S) + HCN(S) \qquad \Delta H_0 = -46.4 \text{ kcal mol}^{-1}$$

This reaction involves the formation of a singlet adduct upon the addition of H atom to the carbon adjacent to the nitrogen ($NC(H)C_3N^-$, –38.0 kcal mol^{-1}). This adduct then fragments into C_3N^- and HCN following a low energy transition state (–35.4 kcal mol^{-1}). During the dissociation process, HCN can also transfer a proton to C_3N^-, forming CN^- and HC_3N. Alternatively, another transition state may lead to these products, as shown below.

$$NC_4N^-(D) + H(D) \rightarrow [NCC(H)C_2N^-(S)] \rightarrow CN^-(S) + HC_3N(S) \qquad \Delta H_0 = -43.5 \text{ kcal mol}^{-1}$$

Lastly, the only exothermic AD pathway for NC_4N^- involves an H atom addition to the central C atom to form a singlet adduct, $NCC(H)C_2N^-$ (–11.6 kcal mol^{-1}). This adduct ejects an electron leaving the neutral molecule NCC(H)C_2N (D).

$$NC_4N^-(D) + H(D) \rightarrow [NCC(H)C_2N^-(S)] \rightarrow NCC(H)C_2N(D) + e^- \qquad \Delta H_0 = -11.9 \text{ kcal mol}^{-1}$$

3.3.3 Reactions of $C_xN_3^-$ (x = 2, 4)

Neither $C_2N_3^-$ nor $C_4N_3^-$ are reactive with H atom according to our experimental measurements. To better explain this lack of reactivity, we computationally investigated these reactions, and our results are summarized in Figure 3.5. The singlet ground state structure of $C_2N_3^-$ is V-shaped with alternating C and N atoms, as shown in Figure 3.5 (a). An H atom can theoretically attach to three different positions along this structure, but according to our calculations, endothermic transition states (3.4, 3.9, and 8.3 kcal mol^{-1}) prevent such additions. Thermalized reagent ions do not possess adequate energy to overcome these barriers. Furthermore, the overall products are also endo-

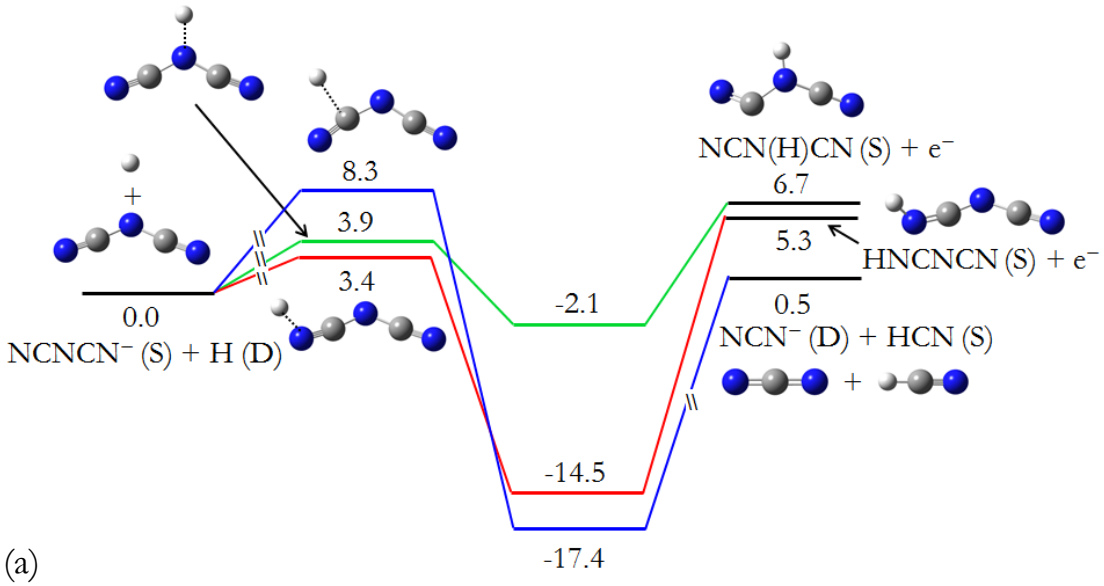

(a)

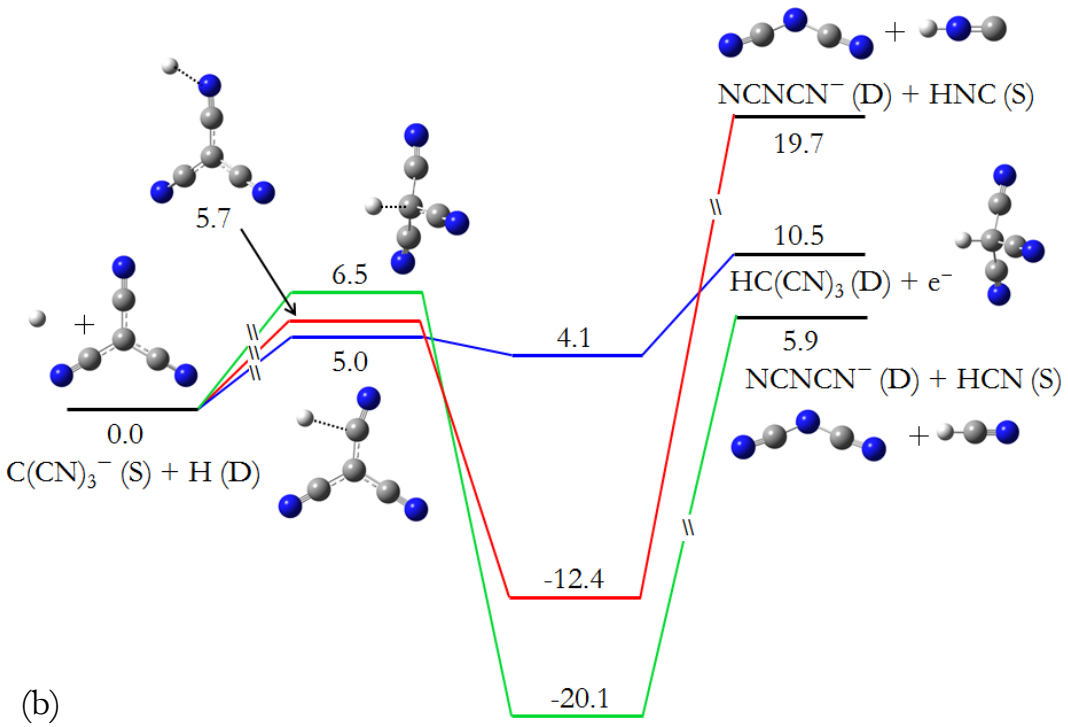

Figure 3.5

The reaction coordinate plot (in kcal mol^{-1}, 0 K) for (a) $NCNCN^-$ + H and (b) $C(CN)_3^-$ + H is shown. Calculations were performed at the CCSD(T)/aug-cc-pVDZ//B3LYP/aug-cc-pVTZ level of theory. Letters in parentheses indicate the spin state of the species, *i.e.*, singlet (S) and doublet (D). Only spin-allowed reactions are investigated, where different reaction pathways are shown in different colors. The loosely-bound ion-neutral complexes prior to the transition states are not shown. The transition states prior to the fragmentation products (7.3 kcal mol^{-1} for HCN formation channel in (a); 10.5 and 22.9 kcal mol^{-1} for HCN and HNC formation channels in (b), respectively) are not shown.

thermic for the AD and the fragmentation processes (0.5, 5.3, and 6.7 kcal mol^{-1}). Although it is not included in Figure 3.5, the fragmentation reaction producing NCN^- and HCN involves a second high energy transition state (7.3 kcal mol^{-1}) solidifying its energetic impracticality. Due to overall endothermic reactions combined with high energy transition state barriers, these computations agree well with our experimental observation that no reaction takes place.

The potential energy diagram for $C_4N_3^-$ + H atom is included in Figure 3.5 (b), and the complete computational results are part of Table 3.5. The ground state structure of this anion is planar

with three equivalent CN branches, in its singlet state. H atoms may once again presumably attach at three different sites on the anion. However, high energy transition states along the approach of the reactants (5.0, 5.7, and 6.5 kcal mol^{-1}) prevent this from occurring. The final product channels are also endothermic (5.9, 10.5, and 19.7 kcal mol^{-1}), and additional high energy barriers exist for the fragmentation processes (10.5 and 22.9 kcal mol^{-1} for HCN and HNC production, respectively), although these are not included in Figure 3.5 (b).

3.3.4 Astrophysical Implications

The reactions outlined in this chapter involve H atoms, which are abundant in diffuse atomic clouds,[1] and organic molecules, which are predicted to be predominantly in their anionic forms in dense interstellar regions.[34,35] These reactions are therefore important to the boundary regions between diffuse and dense clouds in the ISM. Our laboratory studies of these processes provide an understanding of both anion stability and pertinent reaction mechanisms involving interstellar species. Although $C_xN_3^-$ (x=2, 4) are not reactive with H atom, C_xN^- (x=1-6) and $C_xN_2^-$ (x=1, 3-5) react with a moderate efficiency (0.18-0.35). Previous work has revealed similar reaction efficiencies (0.3-0.4) for H atoms with bare, C_x^- (x=2, 4-10), and monohydride, HC_x^- (x=4, 6, 7), carbanions.[15] Barrierless and exothermic reaction pathways likely exist for these reactions, although a systematic computational analysis of these reactions has yet to be performed.

Table 3.5
Complete computational results for reactions between $C_xN_3^-$ (x=2 and 4) and H atoms.

Anion[a]	ΔE^b {0 K kcal mol^{-1}}[298 K kcal mol^{-1}]	
	AH^-	AH
$C_2N_3^-$ (S) {115.5}	$HNCNCN^-$ (D) {-14.5}	HNCNCN (S) {5.3} [5.7]
CN_2CN^- (S) {47.7}	$HNCNCN^-$ (Q) {64.7}	HNCNCN (T) {64.1} [64.5]
$NCNCN^-$ (S) {0.0}	$NC(H)NCN^-$ (D) {-17.4}	NCN(H)CN (S) {6.7} [7.2]
$NCNCN^-$ (T) {75.9}	$NCN(H)CN^-$ (D) {-2.1}	NCN(H)CN (T) {86.6} [87.2]
$NC_2N_2^-$ (S) {86.5}		NC(H)NCN (S) {58.4} [58.6]
$NC_2N_2^-$ (T) {84.2}		NC(H)NCN (T) {56.6} [56.9]
$CNCN_2^-$ (S) {79.1}		NCN^- (D) + HCN (S) {0.5} [1.8]
$CNCN_2^-$ (T) {102.6}		NCN^- (D) + HNC (S) {14.3} [15.8]
CN_3C^- (S) {91.3}		CN^- (S) + HNCN (D) {8.7} [10.2]
CN_3C^- (T) {108.2}		
$C_3N_2CN^-$ (S) {99.3}	$HC(CN)_3^-$ (D) {4.1}	$HC(CN)_3$ (S) {10.5} [10.8]
C_2NCNCN^- (S) {81.8}	$C(CN)_2CNH^-$ (D) {-12.4}	$HC(CN)_3$ (T) {105.7} [106.1]
C_2NCNCN^- (T) {120.6}	$C(CN)_2C(H)N^-$ (D) {-20.1}	$C(CN)_2CNH$ (S) {22.2} [22.4]
$C_2N_2C_2N^-$ (S) {129.0}		$C(CN)_2CNH$ (T) {54.9} [55.3]
$C_2N_2C_2N^-$ (T) {139.8}		$C(CN)_2C(H)N$ (S) {40.7} [40.7]
$C_2N_3C_2^-$ (S) {199.7}		$C(CN)_2C(H)N$ (T) {71.9} [72.2]
$C_2N_3C_2^-$ (T) {201.3}		CN^- (S) + NCC(H)CN (S) {13.7} [15.0]
$C(CN)_3^-$ (S) {0.0}		NC_3N^- (S) + HCN (S) {5.9} [7.1]
$C(CN)_3^-$ (T) {72.0}		NC_3N^- (S) + HNC (S) {19.7} [21.1]
NC_3NCN^- (S) {23.6}		
NC_3NCN^- (T) {79.8}		
$NC_2NC_2N^-$ (S) {56.3}		

[a] Calculated at the CCSD(T)/aug-cc-pVDZ//B3LYP/aug-cc-pVTZ and B3LYP/aug-cc-pVTZ levels of theory for $C_2N_3^-$ and $C_4N_3^-$, respectively. Zero-point energy corrections are included. Letters in parentheses indicate the spin state of the species, *i.e.*, singlet (S), doublet (D), triplet (T), and quartet (Q). Energies are relative to the ground state anions.

[b] Calculated at the CCSD(T)/aug-cc-pVDZ//B3LYP/aug-cc-pVTZ level of theory. Energies are relative to reactants (ground state anion and the H atom). The numbers in parentheses indicate the calculated reaction enthalpies at 0 and 298 K.

Bare carbanions that lack nitrogen are not stable in diffuse interstellar clouds where H atoms are abundant. Either AD or fragmentation reactions with H atoms readily remove them from these environments. Nitrogen-rich carbanions, however, are comparatively very stable and may in fact survive in these regions. Particularly those anions that are unreactive with H atom, $NCNCN^-$ and $C(CN)_3^-$, could persist in diffuse areas such as these. $C(CN)_3^-$ lacks a permanent dipole moment, and therefore is invisible to radio spectroscopy. However, radio astronomy is capable of detecting the V-shaped $NCNCN^-$, whose permanent dipole moment may allow for its future detection.

Even though H atom is often regarded as a very reactive interstellar species, our experiments reveal reaction efficiencies much below unity. These decreased reaction efficiencies should be taken into account in astrophysical models of H atom rich regions. Potentially, angular momentum conservation is responsible for this phenomenon, which appears to impact carbanions[14] and nitrogen-containing carbanions alike. Angular momentum conservation can cause light reactants such as H atom to associate less efficiently due to their rapid rotation about their reacting partners upon collision.[36,37] This constraint on reaction efficiency likely applies to most H atom reactions, and therefore has important astrophysical implications.

3.4 Conclusion

In this chapter, we have characterized reactions between H atoms and 12 nitrogen-containing carbanions: C_xN^- (x=1-6), $C_xN_2^-$ (x=1, 3-5), and $C_xN_3^-$ (x=2, 4). These species are of great interest to astrochemistry, because CN^-, C_3N^-, and C_5N^- have been detected in both the ISM and Titan's upper atmosphere.[5-7,12] The data reported herein provides the groundwork for future investigations of the astrochemical processing of carbanions and predicts possible stable, persistent interstellar species. We predominantly observe AD reactions among these anions, although some additionally undergo

fragmentation. There is no clear trend between reaction efficiencies and reaction exothermicities for the C_xN^- (x=1-6) and $C_xN_2^-$ (x=1, 3-5) anions, and all of the efficiencies are comparable. In contrast, the $C_xN_3^-$ (x=2, 4) anions do not exhibit reactivity with H atoms. Our computational results indicate that this is caused by both overall reaction endothermicity and transition state barriers along the approach of the reactants. The bare and monohydride carbanions,[15] previously explored in our laboratory, likely undergo similar mechanisms. Finally, we propose that angular momentum conservation of anion-H atom collisions leads to a decreased reaction efficiency among these species. This work has combined both experimental and theoretical perspectives to further our knowledge of the astrochemistry of negative ions.

3.5 References

1 T. P. Snow; B. J. McCall, *Diffuse Atomic and Molecular Clouds*. Annu. Rev. Astron. Astrophys., **2006**, *44*, 367-414.

2 T. P. Snow; V. M. Bierbaum, *Ion Chemistry in the Interstellar Medium*. Annu. Rev. Anal. Chem., **2008**, *1*, 229-259.

3 E. Herbst; E. F. van Dishoeck, *Complex Organic Interstellar Molecules*. Annu. Rev. Astron. Astrophys., **2009**, *47*, 427-480.

4 A. G. G. M. Tielens, *The Molecular Universe*. Rev. Mod. Phys., **2013**, *85*, 1021-1081.

5 J. Cernicharo; M. Guelin; M. Agundez; M. C. McCarthy; P. Thaddeus, *Detection of C_5N^- and Vibrationally Excited C_6H in IRC+ 10216* Astrophys. J. Lett., **2008**, *688*, L83-L86.

6 P. Thaddeus; C. A. Gottlieb; H. Gupta; S. Bruenken; M. C. McCarthy; M. Agundez; M. Guelin; J. Cernicharo, *Laboratory and Astronomical Detection of the Negative Molecular Ion C_3N^-*. Astrophys. J., **2008**, *677*, 1132-1139.

7 M. Agundez; J. Cernicharo; M. Guelin; C. Kahane; E. Roueff; J. Klos; F. J. Aoiz; F. Lique, et al., *Astronomical Identification of CN^-, the Smallest Observed Molecular Anion*. Astron. Astrophys., **2010**, *517*, L2-L6.

8 M. McCarthy; C. Gottlieb; H. Gupta; P. Thaddeus, *Laboratory and Astronomical Identification of the Negative Molecular Ion C_6H^-*. Atrophys. J. Lett., **2006**, *652*, L141-L144.

9 S. Brünken; H. Gupta; C. Gottlieb; M. McCarthy; P. Thaddeus, *Detection of the Carbon Chain Negative Ion C_8H^- in TMC-1*. Astrophys. J. Lett., **2007**, *664*, L43-L46.

10 J. Cernicharo; M. Guélin; M. Agúndez; K. Kawaguchi; M. McCarthy; P. Thaddeus, *Astronomical Detection of C_4H^-, the Second Interstellar Anion*. Astron. Astrophys., **2007**, *467*, L37-L40.

11 A. J. Remijan; J. Hollis; F. Lovas; M. Cordiner; T. Millar; A. Markwick-Kemper; P. Jewell, *Detection of C_8H^- and Comparison with C_8H toward IRC+10216*. Astrophys. J. Lett., **2007**, *664*, L47-L50.

12 V. Vuitton; P. Lavvas; R. Yelle; M. Galand; A. Wellbrock; G. Lewis; A. Coates; J.-E. Wahlund, *Negative Ion Chemistry in Titan's Upper Atmosphere*. Planet. Space Sci., **2009**, *57*, 1558-1572.

13 T. P. Snow; M. Stepanovic; N. B. Betts; B. R. Eichelberger; O. Martinez Jr; V. M. Bierbaum, *Formation of Gas-Phase Glycine and Cyanoacetylene via Associative Detachment Reactions*. Astrobiology, **2009**, *9*, 1001-1005.

14 Z. Yang; B. Eichelberger; M. Y. Carpenter; O. Martinez Jr; T. P. Snow; V. M. Bierbaum, *Experimental and Theoretical Studies of Reactions Between H atoms and Carbanions of Interstellar Relevance*. Astrophys. J., **2010**, *723*, 1325-1330.

15 C. Barckholtz; T. P. Snow; V. M. Bierbaum, *Reactions of C_n^- and C_nH^- with Atomic and Molecular Hydrogen*. Astrophys. J. Lett., **2001**, *547*, L171-L174.

16 C. Walsh; N. Harada; E. Herbst; T. Millar, *The Effects of Molecular Anions on the Chemistry of Dark Clouds*. Astrophys. J., **2009**, *700*, 752-761.

17 D. G. Leopold; J. Ho; W. C. Lineberger, *Photoelectron Spectroscopy of Mass-Selected Metal Cluster Anions. I. Cu_n^-, n= 1–10*. J. Chem. Phys., **1987**, *86*, 1715-1726.

18 O. Martinez; Z. Yang; N. B. Betts; T. P. Snow; V. M. Bierbaum, *Experimental Determination of the Rate Constant for the Associative Detachment Reaction $H^- + H \rightarrow H_2 + e^-$ at 300 K*. Astrophys. J. Lett., **2009**, *705*, L172-L175.

19 D. W. Trainor; D. O. Ham; F. Kaufman, *Gas Phase Recombination of Hydrogen and Deuterium Atoms*. J. Chem. Phys., **1973**, *58*, 4599-4609.

20 C. J. Howard; F. C. Fehsenfeld; M. McFarland, *Negative Ion-Molecule Reactions with Atomic Hydrogen in the Gas Phase at 296 K*. J. Chem. Phys., **1974**, *60*, 5086-5089.

21 F. C. Fehsenfeld; C. J. Howard; E. E. Ferguson, *Thermal Energy Reactions of Negative Ions with H Atoms in the Gas Phase*. J. Chem. Phys., **1973**, *58*, 5841-5842.

22 E. E. Ferguson; F. C. Fehsenfeld; A. L. Schmeltekopf, *Flowing Afterglow Measurements of Ion-Neutral Reactions*. Academic Press, Inc.: New York, NY, 1969; Vol. 5.

23 M. J. Frisch; G. W. Trucks; H. B. Schlegel; G. E. Scuseria; M. A. Robb; J. R. Cheeseman; J. A. Montgomery; T. Vreven, et al., Gaussian 03, Revision C.02. Gaussian Inc. Wallingford, CT 2003.

24 Z. Yang; T. P. Snow; V. M. Bierbaum, *Computational Studies of Gas Phase Reactions of Carbon Chain Anions with N and O Atoms*. Phys. Chem. Chem. Phys., **2010**, *12*, 13091-13098.

25 B. R. Eichelberger; T. P. Snow; V. M. Bierbaum, *Collision Rate Constants for Polarizable Ions*. J. Am. Soc. Mass Spectrom., **2003**, *14*, 501-505.

26 E. E. Ferguson; F. C. Fehsenfeld; A. L. Schmeltekopf, *Ion-Molecule Reaction Rates Measured in a Discharge Afterglow*. Adv. Chem. Ser., **1969**, 83-91.

27 T. P. Snow; M. Stepanovic; N. B. Betts; B. R. Eichelberger; O. Martinez, Jr.; V. M. Bierbaum, *Formation of Gas-Phase Glycine and Cyanoacetylene via Associative Detachment Reactions*. Astrobiology, **2009**, *9*, 1001-1005.

28 G. Pascoli; H. Lavendy, *Are C_nN^- clusters really bent?* Chem. Phys. Lett., **1999**, *312*, 333-340.

29 E. Garand; T. I. Yacovitch; D. M. Neumark, *Slow Photoelectron Velocity-Map Imaging Spectroscopy of C_2N^-, C_4N^-, and C_6N^-*. J. Chem. Phys., **2009**, *130*, 64304.

30 F. C. Fehsenfeld, *Interactions between Ions and Molecules*. NATO Advanced Study Institutes Series. Series B, Physics. Plenum Press, New York, **1975**, 387.

31 Y. Ikezoe; S. Matsuoka; M. Takebe, *Gas Phase Ion-Molecule Reaction Rate Constants through 1986*. Tokyo: Maruzan Company, Ltd.: 1987.

32 Z. Yang; B. Eichelberger; O. Martinez Jr; M. Stepanovic; T. P. Snow; V. M. Bierbaum, *The Influence of Spin Effects on the Gas Phase Reactions of Carbanions with N and O Atoms*. J. Am. Chem. Soc., **2010**, *132*, 5812-5819.

33 J. N. Harvey, *Understanding the Kinetics of Spin-Forbidden Chemical Reactions*. Phys. Chem. Chem. Phys., **2007**, *9*, 331-343.

34 E. L. O. Bakes; A. G. G. M. Tielens, *The Photoelectric Heating Mechanism for Very Small Graphitic Grains and Polycyclic Aromatic Hydrocarbons*. Astrophys. J., **1994**, *427*, 822-838.

35 S. Lepp; A. Dalgarno, *Polycyclic Aromatic Hydrocarbons in Interstellar Chemistry*. Astrophys. J., **1988**, *324*, 553-556.

36 H. Koizumi; P. B. Armentrout, *The Kinetic Energy Dependence of Association Reactions. A New Thermokinetic Method for Large Systems*. J. Chem. Phys., **2003**, *119*, 12819-12829.

37 H. Koizumi; F. Muntean; P. B. Armentrout, *Reaction of Cu^+ with Dimethoxyethane: Competition between Association and Multiple Dissociation Channels*. J. Chem. Phys., **2004**, *120*, 756-766.

CHAPTER 4

Formation of Interstellar Propene and Trans-Methyl Formate

4.1 Introduction

At the intersection of observational astronomy detections, astrochemical modelling results, and laboratory astrophysics data, there is often an abundance of disparities. The stories of two particular interstellar species, propene and methyl formate, represent an amalgamation of these inconsistencies among disciplines. This chapter seeks to add a piece to this complex puzzle by increasing the laboratory data available on possible formation pathways to these molecules. Propene (CH_3CHCH_2) has been identified in the interstellar cold core TMC-1,[1] despite its small dipole moment and efficient destruction by atomic oxygen in cold core environments. Its detected abundance suggests that it must be synthesized very efficiently, although the current experimental data suggest that gas phase synthesis routes are slow. More experiments are necessary to bring about agreement between observed interstellar abundances and laboratory data. Methyl formate, similarly, has been detected throughout the ISM, most recently in Sgr B2(N) and Orion KL.[2,3] However, chemical models continue to underpredict its abundance.[4-6] Due to the fact that trans-methyl formate has not been observed on grain surfaces,[7] gas-phase formation routes to this molecule are necessary to improve the accuracy of astrochemical models. Before we describe our findings, a background of interstellar propene and methyl formate is provided below.

By and large, the carbon chains detected in cold cores are unsaturated.[8] This initially came as a surprise to astronomers, due to the vast abundance of H_2 in these environments. However, both experimental and theoretical investigations have revealed that reactions with H_2 that were once thought to be rapid ($A^+ + H_2 \rightarrow AH^+ + H$) are actually much slower for ions with more than a few

H atoms.[9] Hence, unsaturated species dominate in cold cores, and partially saturated species have been detected in small abundances. These include methanol (CH_3OH), acetaldehyde (CH_3CHO), dimethyl ether (CH_3OCH_3), and methyl formate ($HCOOCH_3$).[10] The current hypothesis is that the hydrogenation of these molecules results from a sequential addition of H atoms in the icy mantles of interstellar grains.[11] Methanol, for example, has been proposed to form by the accretion and hydrogenation of CO.[12] Desorption of these species may then occur via non-thermal processes including photodesorption.[13]

After its laboratory examination,[14] one of these partially unsaturated molecules was recently detected in large abundance (2×10^{-9} with respect to total hydrogen) in the cold core TMC-1: propene (shown in Figure 4.1 (a)).[1] This was an unexpected discovery, because propene is known to react rapidly with atomic oxygen at low temperatures, a process by which the molecule should be readily destroyed in cold cores.[15] Propene's weak dipole moment in combination with an efficient cold core sink (via reactions with O atom) leaves its detection in TMC-1 nothing short of remarkable. In comparison to other partially saturated cold core molecules, the synthesis reactions to produce propene would have to be far more efficient. However, the gas phase synthesis by reaction with hydrogen ($A^+ + H_2 \rightarrow AH^+ + H$) does not occur,[9] and although a surface synthesis like that of methanol is possible, there is no evidence suggesting that six H atoms can be efficiently added in this manner.

Radiative association mechanisms are among various other suggestions for propene formation processes.[1] The rate coefficients of two of the ion-molecule association reactions potentially involved in propene formation have been previously investigated.[16] According to these reactions, propargyl ion (H_2CCCH^+) is the precursor to propene. The linear form of this ion is higher in energy than the cyclic form (c-$C_3H_3^+$), both of which are included in Figure 4.1 (b). Despite its relative instability, simulations

predict that both isomers are present in interstellar regions.[16] The first of the two radiative association reactions is shown below:

$$H_2CCCH^+ + H_2 \rightarrow H_3CCCH_2^+ + h\nu \quad (4.1)$$

As long as the product ion is not the lower energy allenic form, $H_2CCHCH_2^+$, but rather the higher energy metastable isomer of $C_3H_5^+$, $H_3CCCH_2^+$ (shown in Figure 4.1 (c)), there is no activation energy barrier to reaction (4.1). This was determined using *ab initio* calculations at the CCSD level using a triple-zeta basis set extended by polarization and diffuse functions.[16] Following this process, a second radiative association reaction may occur:

$$H_3CCCH_2^+ + H_2 \rightarrow H_3CCHCH_3^+ + h\nu \quad (4.2)$$

This reaction forms an isomer of protonated propene, the isopropyl radical cation $H_3CCHCH_3^+$ shown in Figure 4.1 (d), without a reaction barrier. For the lower energy allenic form of $C_3H_5^+$ ($H_2CCHCH_2^+$), however, a significant barrier prevents the reaction from being feasible.[17] At the low temperatures of cold cores (10 K), the calculated rate coefficients for reactions (4.1) and (4.2) are very large. For reaction (4.1), the rate coefficient is 1.2×10^{-9} cm^3 s^{-1}, very near the Langevin collision limit. Reaction (4.2) has a slightly slower rate coefficient, 3.5×10^{-10} cm^3 s^{-1}. Due to the vast abundance of H_2, every propargyl ion (H_2CCCH^+) is essentially converted into protonated propene ($H_3CCHCH_3^+$) according to these processes. Protonated propene is then converted to propene by dissociative recombination with an electron, which has been previously shown to produce a considerable propene branching fraction.[18]

$$H_3CCHCH_3^+ + e^- \rightarrow CH_3CHCH_2 + H \quad (4.3)$$

The work of Herbst et al.[16] concluded that the observed interstellar propene abundance may be explained by reactions (4.1)-(4.3). Early simulation efforts based on estimated rate coefficients indeed showed that propene was produced in sufficient amounts.[19] Unfortunately, these predictions contradict earlier experimental measurements of three-body association processes analogous to reactions (4.1) and (4.2),[9] which found them to be very slow. To build on these experiments and clarify the discrepancies between experiment and simulation, we have carried out detailed experiments as well as more refined calculations to determine the feasibility of forming interstellar propene via reactions (4.1)-(4.3).

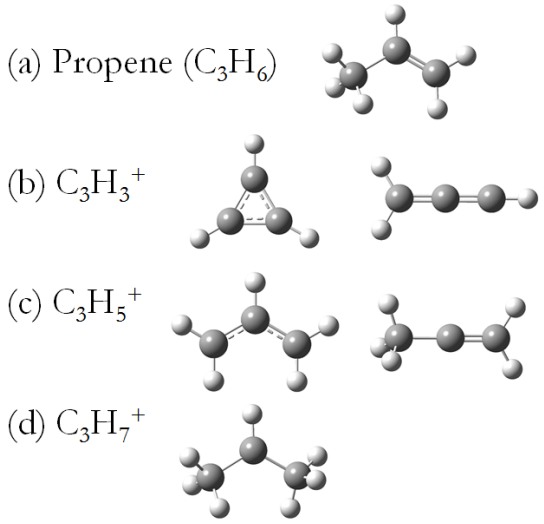

Figure 4.1
Relevant structures for the formation of interstellar propene (a), including cyclic and linear isomers of $C_3H_3^+$ (b), the allenic and metastable isomers of $C_3H_5^+$ (c), and $C_3H_7^+$ (d).

Both propene and methyl formate have been detected in greater abundance than can currently be explained. The abundance of methyl formate in the ISM has previously been underpredicted by chemical models.[4-6] Additionally, grain surface chemistry cannot account for the relative abundance of the cis- and trans-conformers of methyl formate, and the trans-conformer is not even formed at

detectable abundance on these surfaces.[7] This highlights the importance of studying formation pathways to methyl formate in addition to propene.

Methyl formate ($HC(O)OCH_3$) is a well-known interstellar molecule that has been detected in several astronomical environments. These include high mass star-forming regions such as Orion KL[3,20] and Sgr B2(N),[2] low mass star-forming regions including IRAS 16293,[21] prestellar cores,[10] protostars, and protoplanetary disks.[22] Glycolaldehyde ($HCOCH_2OH$),[23] the astrobiologically relevant isomer of methyl formate, contains functional groups characteristic of a sugar. In addition to glycolaldehyde, acetic acid (CH_3COOH) has been detected[24] in the ISM. Both of these isomers, however, have a significantly lower interstellar abundance than methyl formate.[25] There are also two conformers of methyl formate. Observational studies of the lower energy (by 5.72 kcal mol^{-1})[7] cis-conformer have been extensive, as illustrated by the studies cited above. In a recent publication, however, several rotational lines were presented as evidence of the interstellar existence of the trans-conformer as well.[6] The structures of these two conformers are depicted in Figure 4.2 below.

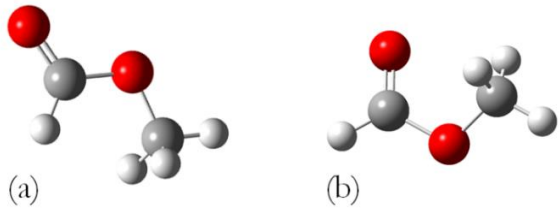

Figure 4.2
The structures of trans- (a) and cis- (b) methyl formate ($HCOOCH_3$).

Although methyl formate has been thoroughly investigated, its interstellar abundance remains incorrectly predicted by several chemical kinetics models,[4-6] and grain surface chemistry provides an incomplete explanation for several observations of this molecule. Trans-methyl formate is not formed at a detectable abundance on grain surfaces,[7] so chemistry on these surfaces cannot lead to the

observed ratio of cis- to trans-methyl formate. Potentially, the discovery of new gas-phase formation routes to methyl formate can help resolve this disagreement between model and observation. Neill et al. computationally explored a route to protonated methyl formate through the methyl cation transfer from protonated methanol to formic acid, shown in reaction (4.4a) below:[6]

$$CH_3OH_2^+ + HCOOH \rightarrow HC(OH)OCH_3^+ + H_2O \quad (4.4a)$$

$$\rightarrow CH_3OH_2^+ – HCOOH \quad (4.4b)$$

$$\rightarrow HCOOH_2^+ + CH_3OH \quad (4.4c)$$

Reactions (4.4a) and (4.4b) were calculated at the M06-2X/6-31+G(d, p) level of theory and found to be exothermic and barrierless. This indicates the potential for reaction (4.4a) to be a previously overlooked gas-phase formation pathway to this molecule.[6] The previous experimental study of this reaction, however, observed only proton-transfer products,[26] shown in reaction (4.4c). In this study, we experimentally revisit reactions (4.4a)-(4.4c) in order to resolve this discrepancy between experiment and computation. Neill and coworkers also explored the reaction between protonated formic acid and methanol as a formation route to protonated methyl formate through acid-catalyzed Fischer esterification:[6]

$$HCOOH_2^+ + CH_3OH \rightarrow HC(OH)OCH_3^+ + H_2O \quad (4.5)$$

The reaction barriers to produce protonated cis- and trans-methyl formate were found to be 4.1 and 5.0 kcal mol^{-1}, respectively. Previous experiments have shown that these reactants undergo only proton transfer and that no protonated trans-methyl formate is produced.[27,28] This result is expected from the relative proton affinities (177.3 and 180.3 kcal mol^{-1} for formic acid and methanol, respectively).[29] We have also studied this reaction, and observed only the proton transfer channel.

Therefore, our experimental results confirm that reaction (4.5) does not likely contribute to the interstellar abundance of trans-methyl formate, and the following discussion will focus on the more probable production route to protonated trans-methyl formate, reaction (4.4a).

For reaction (4.4a) to contribute to the abundance of interstellar methyl formate, a proton must be lost by $HC(OH)OCH_3^+$ in a subsequent reaction. This may occur through dissociative electron recombination,[30] although previous studies of other organic molecules indicate that this process often results in extensive fragmentation.[31-33] Potentially, electron transfer from interstellar anions to protonated methyl formate could decrease the exothermicity of this process, decreasing the fragmentation, and thereby increasing the methyl formate branching fraction. Proton transfer from protonated methyl formate to an interstellar species with a greater proton affinity (>187.0 kcal mol^{-1})[29] is also a possible mechanism to form the detected neutral molecule.

The following sections outline our experimental and theoretical investigations of reactions (4.1)-(4.3) and (4.4a) for the formation of propene and trans-methyl formate, respectively.

4.2 Methods

4.2.1 Experimental

All experiments are carried out using the FA-SIFT (flowing afterglow-selected ion flow tube) apparatus, which has been previously described in Chapter 2. In general, the reagent ion is generated using electron ionization (EI) on a neutral precursor in helium. The ions involved in this study are $C_3H_3^+$, $C_3H_5^+$, protonated methanol ($CH_3OH_2^+$ and $CD_3OH_2^+$), and protonated formic acid ($HCOOH_2^+$). The $C_3H_3^+$ and $C_3H_5^+$ ions are produced from EI (70 eV) on 0.01 Torr propene (Airgas, 99.9%) seeded in 0.25 Torr helium (Airgas, 99.997%). Helium is purified by passage through a molecular sieve trap immersed in liquid N_2. Protonated methanol is produced from EI on neutral

methanol (CH_3OH, Aldrich, >99.9% and CD_3OD, CDN Isotopes, 99.8%) in 0.25 Torr helium, and protonated formic acid is formed from EI on a mixture of 1 mTorr of formic acid vapor (HCOOH, Alfa Aesar, 96.0%) and 25 mTorr of methane (CH_4, Airgas, 99.0%) in 0.25 Torr helium. The reactant ion is then sampled, focused through a series of electrostatic lenses, and isolated from other ions in the source plasma using a quadrupole mass filter at 10^{-6} Torr. The ion is guided into a 300 K reaction flow tube where it is thermalized by 0.53 Torr helium buffer gas (He >99.97%). In the flow tube, neutral reagents are introduced by two methods:

1. Through a series of seven inlets to vary the reaction distance.

2. Through a single inlet, with varied flows of neutral reagent.

By varying either of these parameters and monitoring the decrease in reactant ion intensity, the reaction rate constants are determined according to pseudo-first-order kinetic analysis. For the propene experiments, H_2 gas (Airgas, 99.999%) is purified by passage through a molecular sieve trap immersed in liquid N_2 and added to the flow tube by method 2 above. For the methyl formate experiments, formic acid and methanol are introduced by both method 1 and method 2. After traveling through the flow tube, the product ions and remaining reactant ions are isolated and detected using a second quadrupole mass filter and an electron multiplier detector. Initial branching fractions are determined by correcting the product ion signals using mass discrimination factors, and extrapolating the branching fractions to zero reaction time.

4.2.2 Computational

The *Gaussian 03* and *Gaussian 09* suites of programs[34,35] are used to perform theoretical calculations to complement experimental results in this study. Potential energy surfaces for $C_3H_3^+$ and $C_3H_5^+ + H_2$ were calculated at the CCSD/6-311++G(d,p) and CCSD(T)/6-311++G(3df,2pd) levels

of theory to search for barriers along the approach of the reagents. Geometry optimization and frequency analysis are carried out using the MP2(full)/aug-cc-pVTZ level of theory for the $C_3H_3^+$ isomer and methyl formate results. Energy calculations account for zero-point vibrational energy (ZPVE).

4.3 Results and Discussion

4.3.1 Propene Formation: Reactions of $C_3H_3^+$ and $C_3H_5^+$ with H_2

Before reaction rate constants can be reliably measured for the three-body association reactions shown below (reactions (4.6) and (4.7)), it is necessary to quantify the isomers present in the reagent ion population.

$$C_3H_3^+ + H_2 \rightarrow C_3H_5^+ \quad (4.6)$$

$$C_3H_5^+ + H_2 \rightarrow C_3H_7^+ \quad (4.7)$$

The relative populations of the $C_3H_5^+$ isomers, see Figure 4.1 (c) have previously been determined through collision-induced dissociation experiments to be 65:35 $H_2CCHCH_2^+$:$H_3CCCH_2^+$.[36] We have performed our current measurements under similar experimental conditions as the previous investigators:[36] 70 eV EI on propene. Therefore, we expect to have a similar mixture of isomers in our instrumental setup for this reagent ion.

The relative populations of the two isomers of $C_3H_3^+$, shown in Figure 4.1 (b), can be traced by reaction with benzene (C_6H_6). As shown in Figure 4.3, the ion signal of $C_3H_3^+$ is recorded as a function of reaction distance, which is proportional to reaction time. Benzene is introduced at various inlets along the flow tube to alter this reaction time. The initial steep signal fall-off is indicative of a fast reaction with some of the $C_3H_3^+$ ions. For larger reaction distances, however, the signal plateaus.

This indicates that a portion of the $C_3H_3^+$ ions are unreactive, specifically 1850 of the initial 7300 ion counts s^{-1} in Figure 4.3. After reproducing this experiment, we find that 20-30% of the overall $C_3H_3^+$ ions produced are unreactive.

Calculations reveal that the most stable isomer of $C_3H_3^+$ is the cyclic isomer. The cyclic species is more stable than the linear by 25.1 kcal mol^{-1} according to previous reports,[37] and our own calculations reveal that it is lower in energy by 32.5 kcal mol^{-1}. This more stable ion is not reactive with benzene, while the linear propargyl isomer of $C_3H_3^+$ reacts at nearly the collision rate according to the following mechanism:[38]

$$c\text{-}C_3H_3^+ + C_6H_6 \rightarrow \text{no reaction} \quad (4.8)$$

$$l\text{-}C_3H_3^+ + C_6H_6 \rightarrow C_9H_7^+ + H_2 \quad (4.9a)$$

$$\rightarrow C_7H_7^+ + C_2H_2 \quad (4.9b)$$

Thus, both cyclic and linear isomers of $C_3H_3^+$ are present in our current experiment. Roughly 20-30% are cyclic, and 70-80% are linear according to our analysis.

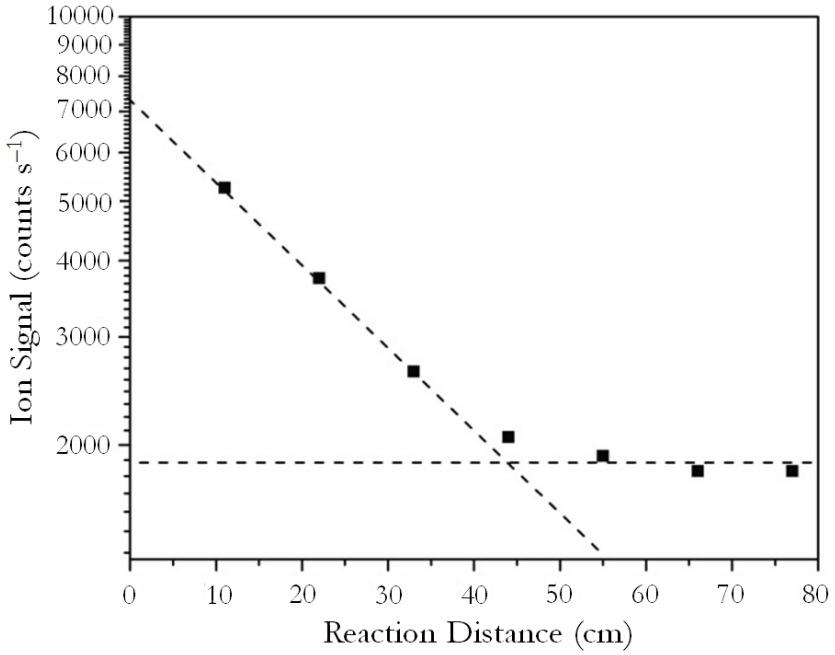

Figure 4.3
Experimental data for the reaction of $C_3H_3^+$ with benzene is shown. This reaction is used as a tracer of the isomeric ratio (cyclic:linear) of $C_3H_3^+$. Our results indicate that the cyclic structure makes up 20-30% of the overall $C_3H_3^+$ signal, depending on the experimental conditions.

Both $C_3H_3^+$ and $C_3H_5^+$ are separately mass-selected and injected into the flow tube to react with H_2 according to reactions (4.6) and (4.7). Our measurements confirm the previously reported experimental results of McEwan et al.:[9] no reaction is observed for either process. Therefore, we report an upper limit, $k_{exp} < 1 \times 10^{-13}$ cm^3 s^{-1}, based on the limit of detection of our experimental apparatus. This upper limit refers to either the ternary or saturated binary regime of association reactions. Typically, reaction rate constants in the radiative regime (applicable to interstellar environments) are even lower. Methods for converting three-body reaction rate constants to estimates in the radiative regime are described in detail in the work of Herbst and colleagues.[16] Although these reaction rates are immeasurably slow in our instrument, they may theoretically produce some interstellar propene. It is therefore prudent to use theory to determine whether or not barriers exist that will decrease the reactivity even more at lower temperatures.

Indeed, activation energy barriers were found for both reaction (4.6) and reaction (4.7): 6.1 kcal mol^{-1} and 5.9 kcal mol^{-1}, respectively. The height of these barriers removes these association reactions from being possible sources of interstellar propene. This stands in contradiction to previous work,[16] which found no high energy transition states in these reactions. The major deviation between the previous calculations[16] and the present one can be found in the version of *Gaussian* software used. Currently, we have used *Gaussian 09*, whereas Herbst et al. employed *Gaussian 03*.[16] Additional default algorithms for longer jobs in the newer version of the software helped facilitate our current transition state search.

4.3.2 Propene Formation: Grain Surface Reactions

Our experimental and theoretical results show that the large abundance of propene observed in the cold core TMC-1 (2×10^{-9} with respect to hydrogen) cannot be accounted for by reactions (4.6) and (4.7). The association of H_2 with $C_3H_3^+$ and $C_3H_5^+$ both involve high energy transition states. Possibly, grain surface reactions in conjunction with non-thermal desorption play a partial role in cold core propene synthesis. Starting from C_3 or C_3H_2, successive surface reactions with H atom may lead to propene, just as methanol is synthesized from CO. Although barriers to these processes are largely unexplored, the barrier for C_3H_4 + H is 1000 K and therefore not excessively large for surface processes.[39] Also, radicals such as C_3H_3 and C_3H_5 may react with H atom favorably. However, if grain surface reactions do not produce sufficient amounts of propene, ethane may be synthesized by a similar H atom addition process. Previous work predicts that an increased ethane abundance could lead to propene in the gas phase.[19,40] Ethane is likely produced efficiently on grain surfaces starting from acetylene (C_2H_2). The necessary reactions, C_2H_2 + H and C_2H_4 + H, possess barriers under 1000 K. Similarly, H atoms are expected to react without barriers with the radicals C_2H_3 and C_2H_5.[8]

4.3.3 Trans-Methyl Formate Formation

Although our investigation of propene formation yielded negative results, a similar analysis is necessary to explain the interstellar abundance of trans-methyl formate. We report the first experimental formation of protonated trans-methyl formate from the reaction between protonated methanol and formic acid. Although we are unable to distinguish conformers within our instrument, previous computational results[6] and the calculations presented in this study indicate that the trans-conformer of protonated methyl formate is a more probable product than the cis-conformer, due to reaction barriers involved in the formation of the latter. In addition to the production of protonated trans-methyl formate (reaction (4.4a)), adduct ion (reaction (4.4b)), and the proton transfer product (reaction (4.4c)) are also observed.

The adduct ion ($CH_3OH_2^+$– HCOOH) comprises most of the product ion signal, but limited secondary complexation ($CH_3OH_2^+$– $(HCOOH)_2$) is also observed. The proton transfer product ($HCOOH_2^+$) is detected, but at a signal level too low to be quantifiable in our experiments (≤50 ion counts s^{-1}). Proton transfer (reaction (4.4c)) is the only channel for this reaction that has been previously observed by experimentalists.[26] This $HCOOH_2^+$ product is detected in trace amounts despite a 3.7 kcal mol^{-1} endothermicity (MP2(full)/aug-cc-pVTZ) due to the Maxwell-Botzmann distribution of molecular energies in the FA-SIFT apparatus.

The associated branching fractions for the two quantifiable primary products, protonated trans-methyl formate ($HC(OH)OCH_3^+$) and adduct ion ($CH_3OH_2^+$– HCOOH), are shown in Table 4.1. Our observations reveal that adduct ion formation is the predominant reaction channel, with a branching fraction of 0.95 ± 0.04. It should be noted that the high pressures of helium in our instrument aid the collisional stabilization of the adduct ion, effectively decreasing the branching fraction of protonated methyl formate. At the much lower pressures of the ISM, these branching fractions will likely change in favor of the protonated methyl formate product. The overall reaction

rate constant for the depletion of $CH_3OH_2^+$ is (3.19 ± 0.39) x 10^{-10} cm^3 s^{-1}. Using the branching fractions and this overall rate constant, the corresponding rate constants and efficiencies for reactions (4.4a) and (4.4b) are also reported in Table 4.1.

Table 4.1
Experimental kinetic data for $CH_3OH_2^+$ + HCOOH.[a]

Product Ion	Branching Fraction	k_{exp}[b] (10^{-10} cm^3 s^{-1})	Efficiency (k_{exp}/k_{col})[c]
$HC(OH)OCH_3^+$	0.05 ± 0.04	0.17 ± 0.13	0.01
$CH_3OH_2^+$ – HCOOH	0.95 ± 0.04	3.02 ± 0.39	0.16

[a] Error bars represent 1σ of the mean of the experimental measurements. There is an estimated total error of ±30%.
[b] All rate constants are corrected for the dissociation of formic acid dimer upon entering the flow tube, as discussed in section 4.4.
[c] k_{col} is the collision rate constant between reactants (1.87 x 10^{-9} cm^3 s^{-1}). This quantity was calculated using parametrized trajectory theory.[41]

4.3.4 Trans-Methyl Formate Formation: Verification of Products

Our detection of protonated trans-methyl formate is based on its mass-to-charge ratio (m/z). Since multiple ions can produce the same m/z, a simple verification experiment is performed using isotope labeling. A deuterated reagent ion $CD_3OH_2^+$ is produced from EI on deuterated methanol to mimic reaction (4.4a):

$$CD_3OH_2^+ + HCOOH \rightarrow HC(OH)OCD_3^+ + H_2O \quad (4.11)$$

If the product is formed by methyl cation transfer, the protonated trans-methyl formate peak from reaction (4.4a) will increase by 3 amu, corresponding to the deuterated counterpart shown in reaction (4.11). However, if protonated acetic acid (a possible impurity in the formic acid reagent) is responsible for the signal, no shift in mass will result. Our experiment definitively supports the formation of protonated trans-methyl formate by methyl cation transfer. We observe a clear mass shift of 3 amu

for the protonated trans-methyl formate peak from m/z 61 to m/z 64. The trace proton transfer product ($HCOOH_2^+$) is also detected, as well as the corresponding adduct ion ($CD_3OH_2^+$– HCOOH).

4.3.5 Trans-Methyl Formate Formation: Ab Initio Calculations

As a complement to our experimental results, computations were performed at the MP2(full)/aug-cc-pVTZ level of theory. The production of the trans conformer of protonated trans methyl formate, reaction (4.4a), is shown in Figure 4.4 to be exothermic (-11.8 kcal mol^{-1}) with a low energy transition state (-3.4 kcal mol^{-1}). This result confirms and expands previous density functional theory calculations (M06-2X/6-31+G(d,p)).[6] Our calculations are therefore in agreement with our experiments in demonstrating that reaction (4.4a) is a feasible route to protonated trans-methyl formate. The optimized ground state geometries, total electronic energies, and zero point corrected electronic energies for the major structures in Figure 4.4 are included in Appendix A.

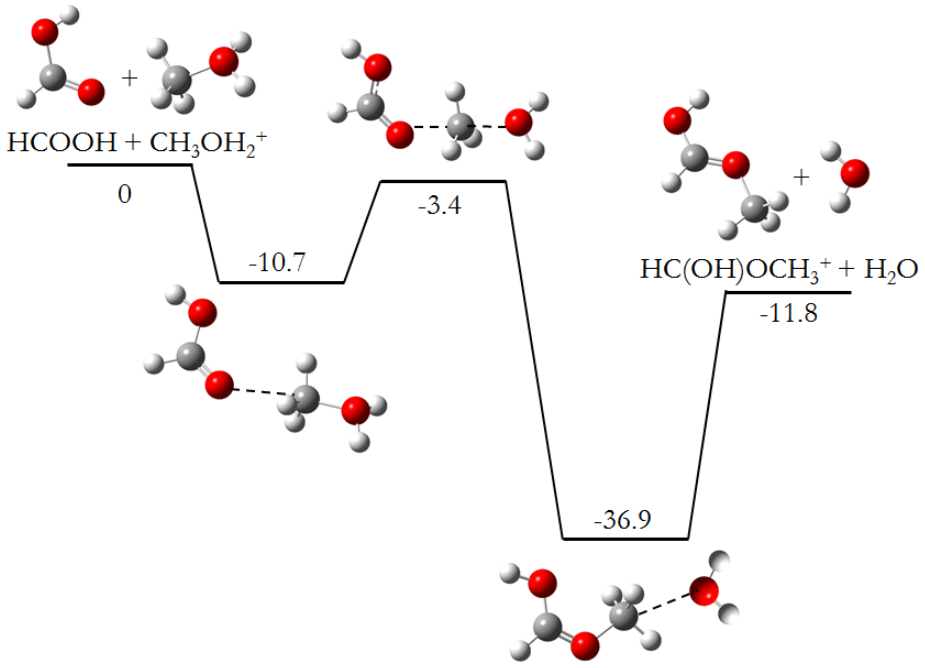

Figure 4.4
The reaction coordinate plot (0 K, ZPVE corrected, kcal mol^{-1}), calculated at the MP2(full)/aug-cc-pVTZ level of theory, for the reaction between formic acid and protonated methanol to produce protonated trans-methyl formate and water.

4.3.6 Trans-Methyl Formate Formation: Formic Acid Dimer Dissociation

Formic acid molecules readily form dimers under ambient laboratory conditions.[42-44] To account for the possibility of dimers in our instrumental setup, the extent of dimer dissociation has been experimentally explored. Our instrument has been modified to allow the formic acid vapor to be heated prior to introduction into the reaction flow tube. The vapor flow is passed through a 30 cm long glass tube with a 2.5 cm internal diameter, wrapped in resistively heated tape. This allows sufficient residence time (approximately 6 s) for heating. Based on the experimental dimerization equilibrium constant expression developed by Buttner & Maurer,[45] 373 K is an adequate temperature to bring the composition of formic acid vapor from approximately 23% dimer (300 K) to <0.4% dimer. Reactions (4.4a)-(4.4c) were studied with heated (373 K) and room temperature (300 K) formic acid vapor using this setup. Reaction rate constants at these temperatures are in agreement within 1%, indicating that the formic acid dimer is destroyed by collisions with helium prior to reaction in the flow tube regardless of the injection temperature. Due to the dissociation of dimers, the total flow of formic acid monomer is a factor of 1.23 higher after injection into the reaction flow tube. This correction factor, therefore, is applied to all data presented in this study.

4.4 Conclusion

A combined experimental and computational study of the formation of propene and trans-methyl formate is reported here. The association reactions for $C_3H_3^+$ and $C_3H_5^+$ with H_2 (reactions (4.6) and (4.7)) were shown to have no influence on the vast abundance of interstellar propene detected in cold core TMC-1 due to immeasurably slow reaction rate constants ($k_{exp} < 1 \times 10^{-13}$ cm^3 s^{-1}) and high transition state barriers (6.1 kcal mol^{-1} and 5.9 kcal mol^{-1}, respectively). However, other reactions involving H atom addition on grain surfaces may play a role in propene's formation. For the reaction between protonated methanol and formic acid (reactions (4.4a)–(4.4c)), our experiments

show an overall reaction rate constant of $(3.19 \pm 0.39) \times 10^{-10}$ cm^3 s^{-1}, a predominant branching fraction of adduct ion (0.95 ± 0.04), a small fraction of protonated trans-methyl formate (0.05 ± 0.04), and only trace detection of proton transfer (in contrast to previous studies).[26] It is likely that at the low pressures of the ISM, the adduct ion will represent a smaller branching fraction due to decreased collisional stabilization. Several measures were taken to verify these results. A deuterated reaction analogous to reaction (4.4a) was studied and confirmed that impurities (such as protonated acetic acid) do not contribute to our data. The formic acid dimer in the reagent vapor was found to dissociate into monomer upon injection into the reaction flow tube, yielding no influence of the formic acid dimer on our kinetic data. Finally, *ab initio* calculations were performed, and in agreement with previous density functional theory results,[6] indicate that there are no reaction barriers above the reactant energies and that an exothermic overall pathway exists for the production of protonated trans-methyl formate. This result motivates further observational efforts to detect trans-methyl formate toward additional astronomical sources outside of the Sgr B2(N) region. In addition, because neither the observed abundances of cis- or trans-methyl formate can be explained by grain surface chemistry only, our study serves to reinvigorate the consideration of gas-phase formation routes to complex organic molecules that have been detected in various regions of the ISM. Although, in the case of propene formation, grain surfaces may still play a key role. In summary, a new laboratory measurement of the branching fractions and reaction rate constant to produce protonated trans-methyl formate has been reported, and a previously disputed set of reactions leading to propene was shown to be unlikely; these results should be included in chemical kinetics models attempting to explain the formation of molecular material in the universe.

4.5 References

1 N. Marcelino; J. Cernicharo; M. Agúndez; E. Roueff; M. Gerin; J. Martín-Pintado; R. Mauersberger; C. Thum, *Discovery of Interstellar Propylene (CH_2CHCH_3): Missing Links in Interstellar Gas-Phase Chemistry*. Astrophys. J. Lett., **2007**, *665*, L127-L130.

2 Y. T. Miao; D. M. Mehringer; Y. J. Kuan; L. E. Snyder, *Complex Molecules in Sagittarius B2(N) - The Importance of Grain Chemistry*. Astrophys. J., **1995**, *445*, L59-L62.

3 B. Tercero; L. Margules; M. Carvajal; R. A. Motiyenko; T. R. Huet; E. A. Alekseev; I. Kleiner; J. C. Guillemin, et al., *Microwave and Submillimeter Spectroscopy and First ISM Detection of ^{18}O-Methyl Formate*. Astron. Astrophys., **2012**, *538*, A119.

4 A. Horn; H. Mollendal; O. Sekiguchi; E. Uggerud; H. Roberts; E. Herbst; A. A. Viggiano; T. D. Fridgen, *The Gas-Phase Formation of Methyl Formate in Hot Molecular Cores*. Astrophys. J., **2004**, *611*, 605-614.

5 R. T. Garrod; E. Herbst, *Formation of Methyl Formate and Other Organic Species in the Warm-Up Phase of Hot Molecular Cores*. Astron. Astrophys., **2006**, *457*, 927-936.

6 J. L. Neill; A. L. Steber; M. T. Muckle; D. P. Zaleski; V. Lattanzi; S. Spezzano; M. C. McCarthy; A. J. Remijan, et al., *Spatial Distributions and Interstellar Reaction Processes*. J. Phys. Chem. A, **2011**, *115*, 6472-6480.

7 J. C. Laas; R. T. Garrod; E. Herbst; S. L. W. Weaver, *Contributions from Grain Surface and Gas Phase Chemistry to the Formation of Methyl Formate and its Structural Isomers*. Astrophys. J., **2011**, *728*, 71-79.

8 Z. Lin; D. Talbi; E. Roueff; E. Herbst; N. Wehres; C. A. Cole; Z. Yang; T. P. Snow, et al., *Can Interstellar Propene (CH_3CHCH_2) be Formed via Gas-Phase Reactions?* Astrophys. J., **2013**, *765*, 80-84.

9 M. J. McEwan; G. B. I. Scott; N. G. Adams; L. M. Babcock; R. Terzieva; E. Herbst, *New H and H_2 Reactions with Small Hydrocarbon Ions and their Roles in Benzene Synthesis in Dense Interstellar Clouds*. Astrophys. J., **1999**, *513*, 287-293.

10 A. Bacmann; V. Taquet; A. Faure; C. Kahane; C. Ceccarelli, *Detection of Complex Organic Molecules in a Prestellar Core: A New Challenge for Astrochemical Models*. Astron. Astrophys., **2012**, *541*, L12-L16.

11 N. G. Petrik; R. J. Monckton; S. P. Koehler; G. A. Kimmel, *Distance-Dependent Radiation Chemistry: Oxidation versus Hydrogenation of CO in Electron-Irradiated H_2O/CO/H_2O Ices*. J. Phys. Chem. C, **2014**, *118*, 27483-27492.

12 N. Watanabe; A. Kouchi, *Measurements of Conversion Rates of CO to CO_2 in Ultraviolet-Induced Reaction of Amorphous $D_2O(H_2O)$/CO Amorphous Ice*. Astrophys. J., **2002**, *567*, 651-655.

13 K. I. Oberg; E. F. van Dishoeck; H. Linnartz, *Photodesorption of Ices I: CO, N_2, and CO_2*. Astron. Astrophys., **2009**, *496*, 281-293.

14 J. C. Pearson; K. Sastry; E. Herbst; F. C. Delucia, *The Millimeter-Wave and Submillimeter-Wave Spectrum of Propylene (CH_3CHCH_2)*. J. Mol. Spectrosc., **1994**, *166*, 120-129.

15 H. Sabbah; L. Biennier; I. R. Sims; Y. Georgievskii; S. J. Klippenstein; I. W. M. Smith, *Understanding Reactivity at Very Low Temperatures: The Reactions of Oxygen Atoms with Alkenes*. Science, **2007**, *317*, 102-105.

16 E. Herbst; E. Roueff; D. Talbi, *Radiative Association and the Formation of Interstellar Propylene*. Molec. Phys., **2010**, *108*, 2171-2177.

17 J. Almlof; G. Hvistendahl; E. Uggerud, *An MC SCF Study of the Reaction $C_3H_7^+$ -> $C_3H_5^+$+H_2*. Chem. Phys., **1984**, *90*, 55-62.

18 A. I. Florescu-Mitchell; J. B. A. Mitchell, *Dissociative Recombination*. Phys. Rep., **2006**, *430*, 277-374.

19 E. Roueff; E. Herbst, Molecular Ions in Astrophysics. *J. Phys. Conf. Ser.*, Van Der Zande, W. J., Ed. 2009; Vol. 192.

20 C. Favre; D. Despois; N. Brouillet; A. Baudry; F. Combes; M. Guelin; A. Wootten; G. Wlodarczak, *$HCOOCH_3$ as a Probe of Temperature and Structure in Orion-KL*. Astron. Astrophys., **2011**, *532*, A32.

21 S. Cazaux; A. G. G. M. Tielens; C. Ceccarelli; A. Castets; V. Wakelam; E. Caux; B. Parise; D. Teyssier, *The Hot Core Around the Low-Mass Protostar IRAS 16293-2422: Scoundrels Rule!* Astrophys. J., **2003**, *593*, L51-L55.

22 E. Herbst; E. F. van Dishoeck, *Complex Organic Interstellar Molecules*. Annu. Rev. Astron. Astrophys., **2009**, *47*, 427-480.

23 J. M. Hollis; F. J. Lovas; P. R. Jewell, *Interstellar Glycolaldehyde: The First Sugar*. Astrophys. J., **2000**, *540*, L107-L110.

24 D. M. Mehringer; L. E. Snyder; Y. T. Miao, *Detection and Confirmation of Interstellar Acetic Acid*. Astrophys. J., **1997**, *480*, L71-L74.

25 J. M. Hollis; S. N. Vogel; L. E. Snyder; P. R. Jewell; F. J. Lovas, *The Spatial Scale of Glycolaldehyde in the Galactic Center*. Astrophys. J., **2001**, *554*, L81-L85.

26 C. G. Freeman; P. W. Harland; M. J. McEwan, *Ion-Molecule Reactions of Formic Acid .1. Proton-Transfer Reactions*. Aust. J. Chem., **1978**, *31*, 2157-2160.

27 P. W. Tiedemann; J. W. Riveros, *Ion-Molecule Reactions of Acids and Esters with Alcohols. Gas Phase Analogs of Acidic Esterification Processes*. J. Am. Chem. Soc., **1974**, *96*, 185-189.

28 W. Y. Feng; C. Lifshitz, *Thermal-Reactions of Protonated Formic Acid Clusters $(HCOOH)_nH^+$ (n=1-3)*. J. Phys. Chem., **1994**, *98*, 3658-3663.

29 *NIST Chemistry WebBook, NIST Standard Reference Database Number 69*. National Institute of Standards and Technology, webbook.nist.gov, accessed 2010-2014.

30 P. A. Lawson; D. S. Osborne, Jr.; N. G. Adams, *Dissociative Electron-Ion Recombination of the Interstellar Species Protonated Glycolaldehyde, Acetic Acid, and Methyl Formate*. J. Phys. Chem. A, **2012**, *116*, 2880-2884.

31 W. D. Geppert; M. Hamberg; R. D. Thomas; F. Osterdahl; F. Hellberg; V. Zhaunerchyk; A. Ehlerding; T. J. Millar, et al., *Dissociative Recombination of Protonated Methanol*. Faraday Disc., **2006**, *133*, 177-190.

32 Y. Osamura; K. Fukuzawa; R. Terzieva; E. Herbst, *A Molecular Orbital Study of the HC_3NH^+ + e^- Dissociative Recombination and Its Role in the Production of Cyanoacetylene Isomers in Interstellar Clouds*. Astrophys. J., **1999**, *519*, 697-704.

33 E. Vigren; M. Hamberg; V. Zhaunerchyk; M. Kaminska; J. Semaniak; M. Larsson; R. D. Thomas; M. af Ugglas, et al., *Dissociative Recombination of Protonated Formic Acid: Implications for Molecular Cloud and Cometary Chemistry*. Astrophys. J., **2010**, *709*, 1429-1434.

34 M. J. Frisch; G. W. Trucks; H. B. Schlegel; G. E. Scuseria; M. A. Robb; J. R. Cheeseman; J. A. Montgomery; T. Vreven, et al., Gaussian 03, Revision C.02. Gaussian Inc. Wallingford, CT 2003.

35 M. J. Frisch; G. W. Trucks; H. B. Schlegel; G. E. Scuseria; M. A. Robb; J. R. Cheeseman; G. Scalmani; V. Barone, et al., Gaussian 09 Revision A.02. Gaussian Inc. Wallingford, CT: 2009.

36 M. T. Bowers; L. Shuying; P. Kemper; R. Stradling; H. Webb; D. H. Aue; J. R. Gilbert; K. R. Jennings, *$C_3H_5^+$ Isomers - Evidence for the Existence of Long-Lived Allyl and 2-Propenyl Cations in the Gas-Phase*. J. Am. Chem. Soc., **1980**, *102*, 4830-4832.

37 F. P. Lossing, *Free Radicals by Mass Spectrometry. XLV. Ionization Potentials and Heats of Formation of C_3H_3, C_3H_5, and C_4H_7 Radicals and Ions*. Can. J. Chem., **1972**, *50*, 3973-3981.

38 P. J. Ausloos; S. G. Lias, *Discrimination of $C_3H_3^+$ Structures on the Basis of Chemical Reactivity*. J. Am. Chem. Soc., **1981**, *103*, 6505-6507.

39 E. Herbst; T. J. Millar, *The Chemistry of Cold Interstellar Cloud Cores*. Smith, I. W. M., Ed. Imperial College Press, World Scientific Publishing Co.: Singapore, 2008; 1-54.

40 A. Canosa; I. R. Sims; D. Travers; I. W. M. Smith; B. R. Rowe, *Reactions of the Methylidine Radical with CH_4, C_2H_2, C_2H_4, C_2H_6, and But-1-ene Studied Between 23 and 295 K with a CRESU Apparatus*. Astron. Astrophys., **1997**, *323*, 644-651.

41 W. J. Chesnavich; T. Su; M. T. Bowers, *Collisions in a Non-Central Field - Variational and Trajectory Investigation of Ion-Dipole Capture*. J. Chem. Phys., **1980**, *72*, 2641-2655.

42 A. S. Coolidge, *The Vapor Density and Some Other Properties of Formic Acid*. J. Am. Chem. Soc., **1928**, *50*, 2166-2178.

43 J. Chao; B. J. Zwolinski, *Ideal Gas Thermodynamic Properties of Methanoic and Ethanoic Acids*. J. Phys. Chem. Ref. Dat., **1978**, *7*, 363-377.

44 J. V. Auwera; K. Didriche; A. Perrin; F. Keller, *Absolute Line Intensities for Formic Acid and Dissociation Constant of the Dimer*. J. Chem. Phys., **2007**, *126*, 124311.

45 R. Buttner; G. Maurer, *Dimerization of Some Organic Acids in the Gas Phase*. Phys. Chem. Chem. Phys., **1983**, *87*, 877-882.

CHAPTER 5

Gas–Phase Chemistry of Deprotonated Azoles

5.1 Introduction

The study of prebiotic, organic molecules is of fundamental importance to both astrochemistry and astrobiology.[1-4] Specifically, cyclic molecules have gained attention in the astrophysical community due to their widespread detections throughout the interstellar medium,[5-10] in Titan's atmosphere,[11] and in meteorites.[12,13] Due to the pervasive presence of ring structures, the existence of more complex interstellar heterocycles such as azoles is very probable in dark clouds, molecular clouds, or hot molecular cores.[14,15] Recent studies indicate that azoles are essential to the syntheses of both DNA and RNA, placing them at the forefront of prebiotic chemistry. Pyrimidine ribonucleotides may be synthesized from 2-aminooxazole, and deoxyribonucleotides may arise from 2-aminothiazole through a similar mechanism.[16-18] In fact, the former ribonucleotide precursor has been spectroscopically studied due to its astrobiological importance.[19] However, both molecules have yet to be detected in an extraterrestrial environment.

Azoles are 5-membered heterocycles containing an N atom and often an additional O, N, or S atom in their ring. Beyond their role as biomolecules, heterocycles containing O, N, and S atoms display a diverse chemistry with a multitude of applications from pharmaceuticals[20-22] and medicinal dyes[23] to explosives,[24] fuels,[25,26] and ionic liquids.[27] These applications have motivated several studies involving their thermochemical properties,[28-30] reactivity,[31-34] and fragmentation.[35] Few studies, however, have examined azoles in an astrochemical context. The characterization of azole acidity, reactivity with interstellar species, and fragmentation will illuminate their potential role in the vast web of astrochemical syntheses.

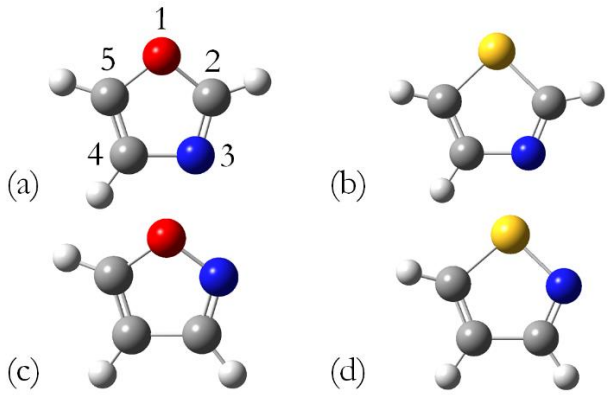

Figure 5.1
Azole structures of interest: (a) oxazole, (b) thiazole, (c) isoxazole, and (d) isothiazole.

Many of the fundamental chemical properties of oxazoles and thiazoles remain to be explored. The goal of this study is to characterize the chemistry of the four azole molecules shown in Figure 5.1: oxazole (a), thiazole (b), isoxazole (c), and isothiazole (d). These molecules are deprotonated at the C5 position and analyzed in an ion trap. Their gas-phase acidities are determined for a deeper understanding of the intrinsic molecular properties of azoles and to better predict their interaction with other potential interstellar species. Bracketing[36] and H/D exchange[37] techniques are used to gain the first experimental insights into these acidities. The reactivity of these anions with several confirmed interstellar molecules (N_2O, O_2, CO, OCS, CO_2, and SO_2) and potential interstellar molecules (CS_2, CH_3Cl, $(CH_3)_3CCl$, and $(CH_3)_3CBr$) is also examined here. We report the reaction rate constants, branching fractions, and efficiencies for these reactions to aid in astrophysical models and elucidate interstellar reaction networks. Lastly, fragmentation routes are studied to investigate the production of other interstellar species through azole destruction in high-energy environments. We will expand the work of previous azole studies[28,35] using a modified Finnigan LCQ Deca XP Plus ion trap apparatus. Through a combination of experimental and computational data, we hope to illuminate the chemical complexity of deprotonated azole anions.

5.2 Methods

5.2.1 Experimental

The instrument used in this study is a modified Finnigan LCQ Deca XP Plus ion trap mass spectrometer with an electrospray ionization (ESI) source. Modifications to the instrument were performed based on the previous studies of Gronert and coworkers,[38,39] and are briefly outlined here (see Chapter 2 for an in depth description). Deprotonated azoles are produced by first electrospraying a 10^{-4} M solution of the carboxylic acid precursor (isothiazole-5-carboxylic acid and thiazole-5-carboxylic acid, Aldrich^{CPR}, Sigma-Aldrich; isoxazole-5-carboxylic acid and oxazole-5-carboxylic acid, 98%, Alfa Aesar) in a solvent mixture of 1:1 CH_3OH:H_2O (HPLC grade, Sigma-Aldrich). ESI conditions include a spray voltage of 4.5 kV, a flow of 3-10 μL min^{-1}, and heated capillary temperatures of 200-250 °C. The deprotonated carboxylic acids formed from electrospray are injected into the ion trap with a 5-10 V potential difference between the skimmer and the first multipole DC offset of the LCQ setup, causing a collision-induced decarboxylation of the anions prior to entering the ion trap (300 K, 5.1 x 10^{-3} Torr helium). This process is shown in Figure 5.2 for oxazole-5-carboxylic acid.

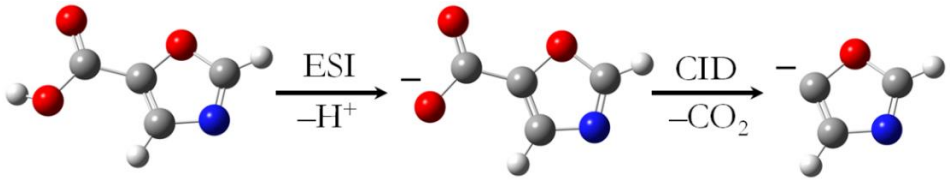

Figure 5.2
Electrospray ionization and decarboxylation via collision induced dissociation (CID) of oxazole-5-carboxylic acid.

Within the ion trap, these C5-deprotonated azoles are isolated for a wide time range (1-5000 ms) during which their reaction with a neutral reagent is monitored. The activation Q, a variable that

controls the q_z of the trapped ion, is maintained at 0.30. The external LCQ helium buffer gas line has been modified for the introduction of both liquid and gaseous neutral reagents into the trap, as described in Chapter 2. In this setup, helium (99.999%, Airgas) flows are varied from 1.0-1.9 L min^{-1} using a flow controller, and pressures are measured with an absolute pressure baratron and maintained at 850 Torr (±3%). Gaseous neutral reagents are purchased as dilute mixtures (1.00 ± 0.02%) in helium (OCS, CO_2, SO_2, CH_3Cl, Airgas) and leaked into the helium line. Their concentrations are quantified using the measurable pressure increase upon addition of gaseous neutral reagents (5-95 Torr). Other gaseous neutral reagents (N_2O, O_2, and CO, 99.5%, Airgas) that showed no preliminary reactivity were not purchased diluted in helium. Liquid neutral reagents are introduced by syringe pump at constant flows (0.5-5.0 μL min^{-1}). These reagents include 2-chloro-2-methylpropane 99%, carbon disulfide >99%, methanol-d4, chlorobenzene 99.8%, fluorobenzene 99%, HPLC Grade methanol, toluene 99+%, n-propanol ≥99.5%, acetonitrile 99.8%, and aniline ≥99.5%, Sigma-Aldrich; 2-bromo-2-methylpropane 96%, Acros Organics; ethanol 99+%, Decon Laboratories; n-butanol 99.4%, Mallinckrodt Chemicals; isobutanol 99% and 3-pentanol 98+%, Alfa Aesar; and acetone 99.7%, Fisher Scientific. The syringe tip is inserted through a septum directly into the flow of helium. For efficient sampling of liquids into the helium flow by vaporization, only highly volatile liquids (b.p. < 175 °C) are introduced by this method. Whether the neutral reagent is a gas or liquid, the range of molar ratios of helium:reagent is approximately 10^2-10^4. Only a small fraction (~1 mL min^{-1}, 0.1%)[40] of this helium-reagent mixture is sampled through fused silica capillary tubing (75 um ID, 10 cm length) into the ion trap itself, while the remainder (~99.9%) is directed to exhaust through a flow controller. All experimental data are the averages of eight data points taken over two days with a minimum of three different helium:reagent ratios to ensure reproducibility over a range of experimental conditions.

5.2.2 Computational

Electronic structure calculations are performed using the *Gaussian 03* and *Gaussian 09* suites of programs[41,42] to complement experiments in this study. Reaction enthalpies are reported at 298 K for the formation of ions within our room temperature instruments and 0 K for all reaction and fragmentation pathways relevant to astrophysical environments. Gas-phase acidities are calculated and reported as the change in the Gibbs free energy for the reaction below at 298 K, where AH represents an azole molecule.[43,44]

$$AH \rightarrow A^- + H^+$$

All geometry optimizations and frequency calculations are performed at either the B3LYP/6-311++G(d,p) or MP2(full)/aug-cc-pVDZ level of theory, as specified. Associated zero point energy (ZPE) and thermal energy (298 K) corrections are applied. Appendix A includes the optimized ground state geometries, total electronic energies, and zero point corrected electronic energies for the major structures described herein, organized by figure number.

5.3 Results and Discussion

5.3.1 Ion Production

Reagent ions are formed in the ion trap by the well-established method of decarboxylation.[45,46] Three of the four acids behave as expected, efficiently decarboxylating to form the deprotonated azole anion at the C5-position, shown in Figure 5.2. Isoxazole, however, favors HCN loss over decarboxylation. The experimental and computational results of this method are presented in Table 5.1. Carbon dioxide is indeed lost for all four acids, but isoxazole-5-carboxylic acid does not produce the resulting fragment ion at sufficient signal for experimentation. Rather, it is the only ion which loses HCN in appreciable quantities. From a computational perspective, the three acids that readily

decarboxylate show significantly higher overall enthalpy changes ($\Delta H°_{298}$ ~20-40 kcal mol^{-1}) for HCN loss than for CO_2 loss, whereas isoxazole-5-carboxylic acid displays similar $\Delta H°_{298}$ for both loss mechanisms. These combined results suggest that a low energy pathway exists for HCN loss from the isoxazole ring structure that is missing for the other three azole molecules. For the purposes of our present study, the chemistry of the three azoles which freely decarboxylate (oxazole, thiazole, and isothiazole) are examined further here.

Table 5.1
Deprotonated carboxylic acid fragmentation.

Deprotonated species	$\Delta H°_{298K}$ CO_2 loss[a]	$\Delta H°_{298K}$ HCN loss[a]	Fragments Observed
Isoxazole-5-carboxylic acid	39.4	42.1	m/z 68 (CO_2 loss)[b]; m/z 85 (HCN loss)
Oxazole-5-carboxylic acid	41.9	63.7	m/z 68 (CO_2 loss) only
Isothiazole-5-carboxylic acid	37.8	73.7	m/z 68 (CO_2 loss) only
Thiazole-5-carboxylic acid	38.1	75.5	m/z 68 (CO_2 loss) only

[a] Reported in units of kcal mol^{-1} and calculated at the MP2(full)/aug-cc-pVDZ level of theory.
[b] Signal too low for efficient isolation and experimentation.

5.3.2 Gas-Phase Acidity

For the first time, the gas-phase acidities of oxazole, thiazole, and isothiazole are experimentally determined using a qualitative bracketing technique. Each deprotonated azole (A^-) is trapped in the presence of the neutral molecules (RH) listed in Table 5.2. This table indicates the positive or negative detection of the R^- proton abstraction product with a Y or N, respectively.

The lines in Table 5.2 indicate our experimental brackets for these acidities. There is a clear distinction between the acidity of oxazole and the thiazoles ($\Delta\Delta G°_{acid}$~7.5 kcal mol^{-1}), whereas the acidities of the thiazole isomers are indistinguishable by our bracketing method. Previous studies have

shown that C-H bonds adjacent to sulfur atoms yield higher acidities (lower $\Delta G°_{acid}$) than those adjacent to oxygen atoms[47] due in part to the considerable charge-holding abilities of sulfur heteroatoms.[48] Our results indicate that azole molecules also follow this trend, as the thiazoles are more acidic than oxazole. The structural difference between the thiazole isomers does not have a measurable impact on the C5 acidity within experimental error (±2.9 kcal mol^{-1}). The C5 acidities of both thiazoles and oxazole are bracketed at 365.7 ± 2.9 kcal mol^{-1} and 373.2 ± 2.3 kcal mol^{-1}, respectively.

Table 5.2
Acidity Bracketing Results.[a]

RH	$\Delta G°_{acid}$(RH) [b,c]	$\Delta H°_{acid}$(RH) [b,c]	Oxazole	Thiazole	Isothiazole
Chlorobenzene	382.8 ± 2.0	391.0 ± 1.9	N	N	N
Fluorobenzene	378.6 ± 2.0	386.8 ± 2.1	N	N	N
Methanol	376.02 ± 0.62	382 ± 1	Y[d]	N	N
Toluene	373.7 ± 2.0	382.33 ± 0.45	N	N	N
Ethanol	372.6 ± 1.1	379.2 ± 1	Y	N	N
n-Propanol	369.2 ± 1.4	375.7 ± 1.3	Y	N	N
n-Butanol	368.7 ± 2.1	375.3 ± 2.0	Y	N	N
Isobutanol	367.9 ± 2.1	374.5 ± 2.0	Y	N	N
3-Pentanol	366.2 ± 2.1	372.8 ± 2.0	Y	N	N
Acetonitrile	365.2 ± 2.0	372.9 ± 2.1	Y	Y	Y
Acetone	361.9 ± 2.0	368.8 ± 2.1	Y	Y	Y
Aniline	359.1 ± 2.0	366.4 ± 2.1	Y	Y	Y

[a] $A^- + RH \rightarrow AH + R^-$; where AH represents oxazole, thiazole, and isothiazole.
[b] Values are expressed in kcal mol^{-1}.
[c] All values are taken from NIST Chemistry WebBook.[49]
[d] Products observed only in trace amounts; likely due to methanol solvent rather than reaction.

In addition to bracketing, H/D exchange reactions are performed in the ion trap with CD_3OD to examine other acidic sites on the C5-deprotonated azole anions. This technique involves the formation of a CD_3OD-anion complex (I), depicted in Figure 5.3 for the oxazole case. Once a deuteron is transferred from the methanol, a second complex (II) is formed between the CD_3O^- and the now singly-deuterated azole molecule. If the overall process is exothermic or thermoneutral, a final complex resulting from the removal of an azole proton may be formed (III), causing our observation of a deuterated azole anion with a mass that is 1 amu greater than our reactant anion (m/z 69).[50] For all three deprotonated azoles, one H/D exchange is observed. This reveals that one of the two remaining sites on the deprotonated azoles is significantly more acidic than the other. Our computational results will further delineate this order of azole site acidity.

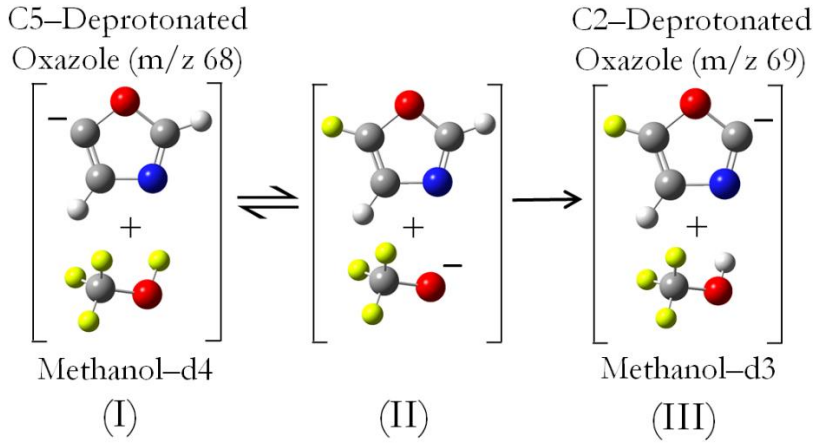

Figure 5.3
H/D exchange experiment between CD_3OD and C5-deprotonated oxazole anion; one exchange is observed. Computational results (Table 5.3) suggest that C2 rather than C4 participates in this exchange.

Calculations are performed for comparison with these experimental results and are summarized in Table 5.3. The C2 position on the oxazole molecule is the most acidic according to these results, indicating its involvement in the one H/D exchange that we experimentally observe (Figure 5.3). Although the C2 and C3 acidities of thiazole and isothiazole, respectively, were not

calculated due to ring-opened product structures,[28] we expect from our H/D exchange experiments that we are indeed deprotonating at these sites due to the endothermicity of the process at C4 for both isomers. Finally, our experimental brackets agree closely with the computational results for the C5 position of each azole, and the calculations shown in Table 5.3 are in excellent agreement with previous theoretical work (B3LYP/6-311++G**//B3LYP/6-31+G* level of theory).[28]

Table 5.3
Experimental and computational gas-phase acidities ($\Delta G°_{acid}$, kcal mol^{-1}).

Species	Deprotonation Site	Experimental	Computational[a]
Oxazole	C2	–	371.7
	C4	–	384.4
	C5	373.2 ± 2.3[b]	373.2
Thiazole	C2	–	–
	C4	–	381.1
	C5	365.7 ± 2.9[c]	368.6
Isothiazole	C3	–	–
	C4	–	375.5
	C5	365.7 ± 2.9[c]	364.8

[a] Calculated at the B3LYP/6–311++G(d,p) level of theory.
[b] Deprotonated oxazole was bracketed between ethanol and toluene (Table 5.2).
[c] Deprotonated thiazole and isothiazole were bracketed between acetonitrile and 3–pentanol (Table 5.2).

5.3.3 Reactivity of Deprotonated Oxazole, Thiazole, and Isothiazole

To further our knowledge of deprotonated azole chemistry, their reactivity is examined with a set of molecules including several detected interstellar species. C5-deprotonated oxazole, thiazole, and isothiazole all show no measureable reaction ($k_{exp} \leq 1 \times 10^{-13}$ cm^3 s^{-1}) with N_2O, O_2, and CO. We find, however, that several other interstellar molecules (OCS, CO_2, and SO_2) as well as CS_2, CH_3Cl, $(CH_3)_3CCl$, and $(CH_3)_3CBr$ react readily with one or more of the azoles in our modified ion trap apparatus. All experimental data, including reaction rate constants (k_{exp}), efficiencies (k_{exp}/k_{col}), and branching fractions are summarized in Table 5.4–Table 5.6 for each azole. Reaction efficiencies are expressed as the ratio of the reaction rate constant and the collision rate constant, which is determined

by parametrized trajectory theory.[51] This collision theory simplifies to the Langevin collision theory[52] for neutral reagents that lack a permanent dipole moment (CS_2 and CO_2). The error reported in these tables represents the precision of each measurement, defined as one standard deviation of the experimental mean. The total error of our modified instrumental setup is ±30%. Lastly, theoretical calculations (MP2(full)aug-cc-pVDZ) are incorporated into these tables to illustrate the overall enthalpy changes for each reaction pathway at 0 K. The reactivity of each azole is discussed in the following section.

Table 5.4
C5 Deprotonated Oxazole Reactivity.

Neutral Reagent	Products	k_{exp} (10^{-10} cm^3 s^{-1})	k_{exp}/k_{col} (%)	Branching Fraction[a]	ΔH_{0K}[b] (kcal mol^{-1})
		Atom abstraction and association			
OCS	$C_4H_2NO_2S^-$	0.98 ± 0.10	8.2	0.95	–50.7
	$C_3H_2NOS^-$ + CO			0.05	–36.7
CS_2	$C_3H_2NOS^-$ + CS	1.5 ± 0.2	13	0.90	–3.6
	$C_3HOS_2^-$ + HCN			0.08	–8.0
	$C_4H_2NOS_2^-$			0.02	–61.8
CO_2	$C_4H_2NO_3^-$	0.12 ± 0.02	1.6	1	–41.3
SO_2	$C_3H_2NO_3S^-$	0.41 ± 0.05	2.6	1	–43.7
		Nucleophilic substitution (S_N2)			
CH_3Cl	$C_4H_5NO + Cl^-$	0.42 ± 0.06	2.1	1	–64.4
		Elimination (E2)			
$(CH_3)_3CCl$	$C_3H_3NO + (CH_3)_2CCH_2 + Cl^-$	0.088 ± 0.013	0.41	1	–26.5
$(CH_3)_3CBr$	$C_3H_3NO + (CH_3)_2CCH_2 + Br^-$	2.2 ± 0.2	11	1	–30.9

[a] Branching fractions are measured with a precision of ±20% of the reported value.
[b] Calculated at the MP2(full)/aug-cc-pVDZ level of theory.

Deprotonated oxazole is the most reactive of the three azoles studied. This anion participates in a diverse array of reaction mechanisms including sulfur atom abstraction (OCS, CS_2), association (OCS, CS_2, CO_2, SO_2), association with HCN loss (CS_2), nucleophilic substitution (CH_3Cl), and elimination ($(CH_3)_3CCl$, $(CH_3)_3CBr$). The experimental and computational data for these reactions are

summarized in Table 5.4. Although only ionic products are detected in our instrument, thermodynamics calculations verify that our inferred neutral products are feasible. The overall enthalpy changes for all reaction pathways are exothermic (ΔH_{0K} = -3.6 to -64.4 kcal mol^{-1}), and our studies are performed under near-thermal conditions,[38] implying an absence of barriers above the reactant energy. The most efficient reaction is observed with CS_2, but the reaction efficiencies vary widely as a whole (0.41-13%). Notably, several of the predicted neutral products (CO, CS, and HCN) are confirmed interstellar species.

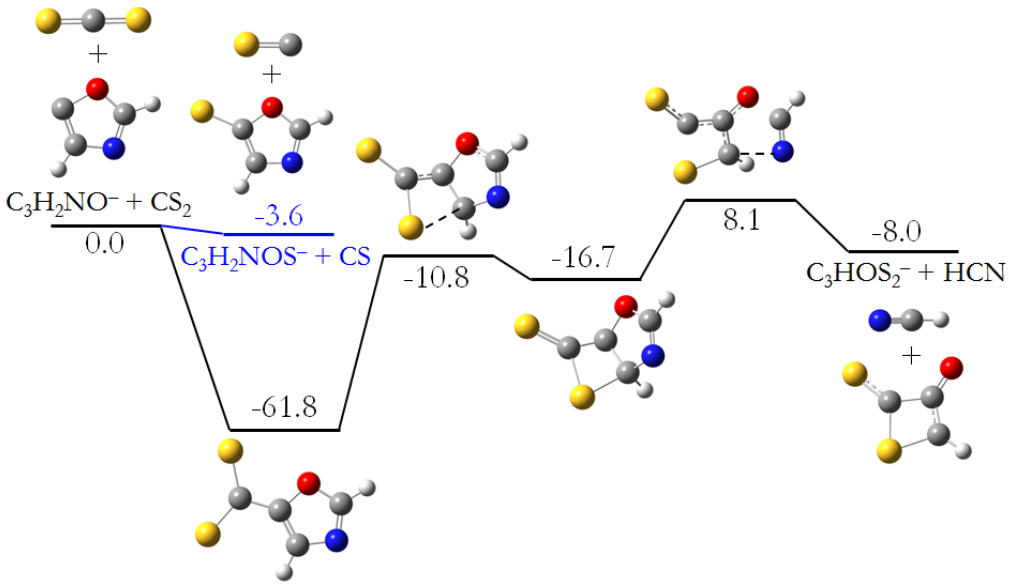

Figure 5.4
Deprotonated oxazole ($C_3H_2NO^-$) + CS_2 reaction pathways involving sulfur atom transfer (blue) and association/HCN loss (black). The ΔH_{0K} are calculated at the MP2(full)/aug-cc-pVDZ level of theory and shown in kcal mol^{-1}.

The reaction between deprotonated oxazole and CS_2 is not only the most efficient reaction observed in this study, it also involves the most reaction pathways, with three distinct ionic products observed. For this reason, we computationally explore them at the MP2(full)/aug-cc-pVDZ level of theory in Figure 5.4. Association and sulfur atom abstraction are both barrierless processes that are exothermic by 61.8 and 3.6 kcal mol^{-1}, respectively. We also observe the loss of HCN from the

association product. According to our calculations, an 8.1 kcal mol^{-1} barrier above the energy of the reactants is involved in this process. Since conditions in the ion trap are near-thermal,[38] it is unreasonable to observe a process with a barrier of this size. Using the B3LYP/6-311++G(d,p) level of theory, the barrier is still present, and the potential follows the same qualitative pathway. Although we have failed to calculate them here, there are likely other low energy pathways and transition states that exist and contribute to the experimental product that we observe here.

Table 5.5
C5 Deprotonated Thiazole Reactivity.

Neutral Reagent	Products	k_{exp} (10^{-10} cm^3 s^{-1})	k_{exp}/k_{col} (%)	Branching Fraction[a]	ΔH_{0K}[b] (kcal mol^{-1})
		Atom abstraction and association			
OCS	$C_4H_2NOS_2^-$	0.58 ± 0.07	5.1	0.98	–46.8
	$C_3H_2NS_2^-$ + CO			0.02	–30.5
CS_2	$C_4H_2NS_3^-$	0.12 ± 0.01	1.1	0.92	–58.2
	$C_3H_2NS_2^-$ + CS			0.08	2.6
CO_2	$C_4H_2NO_2S^-$	0.081 ± 0.009	1.1	1	–37.5
SO_2	$C_3H_2NO_2S_2^-$	0.42 ± 0.03	2.7	1	–40.9
		Nucleophilic substitution (S_N2)			
CH_3Cl	C_4H_5NS + Cl^-	0.18 ± 0.02	1.0	1	–56.6
		Elimination (E2)			
$(CH_3)_3CBr$	C_3H_3NS + $(CH_3)_2CCH_2$ + Br^-	0.43 ± 0.03	2.4	1	–25.0

[a] Branching fractions are measured with a precision of ±20% of the reported value.
[b] Calculated at the MP2(full)/aug-cc-pVDZ level of theory.

The reactivity of deprotonated thiazole and isothiazole are also characterized. Although the reactions of isothiazole are 25-76% less efficient than those of thiazole, their reaction mechanisms are nearly identical. Similar to oxazole, the thiazoles react by sulfur atom abstraction (OCS, CS_2), association (OCS, CS_2, CO_2, and SO_2), nucleophilic substitution (CH_3Cl), and elimination ($(CH_3)_3CBr$). In contrast to the more reactive oxazole, no measureable reaction was observed between the thiazole isomers and $(CH_3)_3CCl$ ($k_{exp} \leq 1 \times 10^{-13}$ cm^3 s^{-1}). Experimental and computational data are shown in

Table 5.5 and Table 5.6. With the exception of one pathway, all reaction enthalpies are exothermic for thiazole (ΔH_{0K} = -25.0 to -58.2 kcal mol^{-1}) and isothiazole (ΔH_{0K} = -23.3 to -58.9 kcal mol^{-1}). The slightly endothermic sulfur atom abstractions from CS_2 have reaction enthalpies of 2.6 and 1.6 kcal mol^{-1} for thiazole and isothiazole, respectively. These pathways are essentially thermoneutral within computational uncertainty. The only other sulfur atom abstraction that we observe is from OCS to both thiazoles. This reaction provides a viable, exothermic formation route to CO, one of the most abundant interstellar molecules.

Table 5.6
C5 Deprotonated Isothiazole Reactivity.

Neutral Reagent	Products	k_{exp} (10^{-10} cm^3 s^{-1})	k_{exp}/k_{col} (%)	Branching Fraction[a]	ΔH_{0K}[b] (kcal mol^{-1})
		Atom abstraction and association			
OCS	$C_4H_2NOS_2^-$	0.43 ± 0.05	3.8	0.99	–46.8
	$C_3H_2NS_2^-$ + CO			0.01	–31.5
CS_2	$C_4H_2NS_3^-$	0.076 ± 0.007	0.70	0.90	–58.9
	$C_3H_2NS_2^-$ + CS			0.10	1.6
CO_2	$C_4H_2NO_2S^-$	0.040 ± 0.004	0.54	1	–37.2
SO_2	$C_3H_2NO_2S_2^-$	0.31 ± 0.04	2.0	1	–40.5
		Nucleophilic substitution (S_N2)			
CH_3Cl	C_4H_5NS + Cl^-	0.065 ± 0.005	0.34	1	–41.3
		Elimination (E2)			
$(CH_3)_3CBr$	C_3H_3NS + $(CH_3)_2CCH_2$ + Br^-	0.11 ± 0.01	0.58	1	–23.3

[a] Branching fractions are measured with a precision of ±20% of the reported value.
[b] Calculated at the MP2(full)/aug-cc-pVDZ level of theory.

In summary, deprotonated oxazole, thiazole, and isothiazole react with an array of interstellar molecules, providing important mechanistic and kinetic data to improve astrochemical models. Overall trends in our data show that reactivity is directly correlated to azole anion basicity. The order of greatest to least reactive deprotonated azoles (determined by the reaction efficiencies) is oxazole > thiazole > isothiazole. The same progression in anion basicities is reported in Table 5.3. This trend is

also observed for a variety of other systems.[53] Associations and atom abstractions are common among small (triatomic) neutral molecules in our study, providing evidence for the efficient growth of heterocyclic prebiotic anions into larger molecules of astrobiological interest. Understanding this growth from small, prebiotic species to more complex biomolecules is a central goal of astrobiology.[54] Lastly, the formation of detected interstellar molecules (CO,[55] CS,[56] and HCN[57]) through these azole reactions lends insights into the web of astrochemical syntheses.

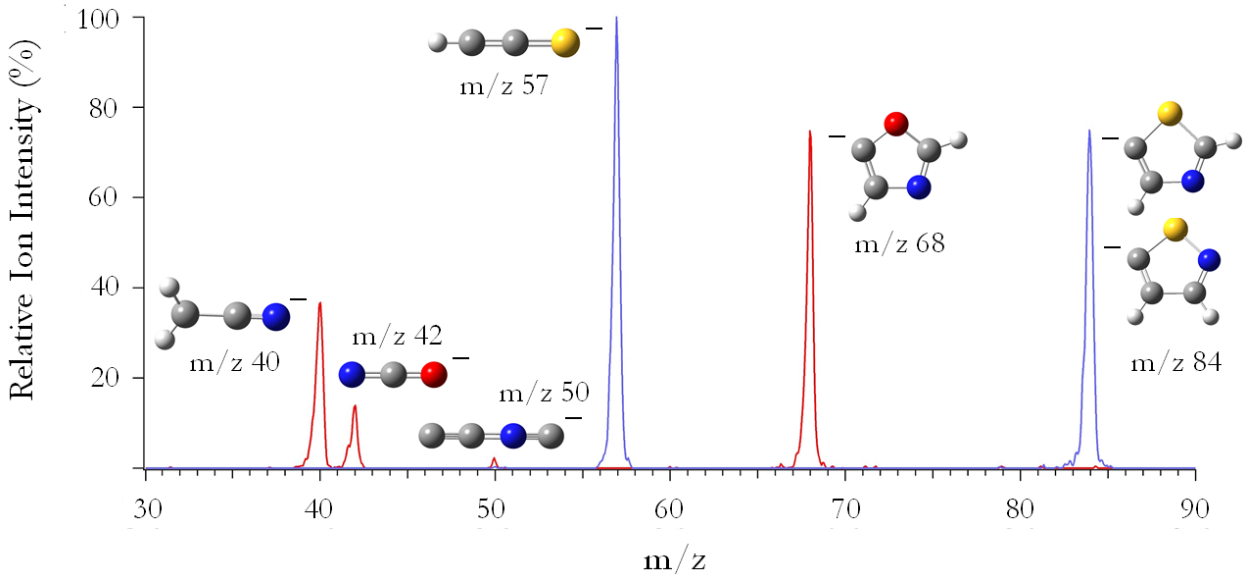

Figure 5.5
Deprotonated azole fragmentation mass spectra. Deprotonated oxazole (red), thiazole, and isothiazole (blue) are shown.

5.3.4 Fragmentation

Our final investigation of deprotonated azole chemistry focuses on their fragmentation within the ion trap apparatus. We trap each anion and apply an excitation voltage to the end caps of the ion trap until extensive molecular dissociation occurs through collision with helium atoms. The normalized collision energy (NCE; %) of the LCQ software is directly proportional to this excitation voltage.[58] For this study, we apply 45% NCE over a 100 ms activation time to dissociate the ions. All

fragments reported here are also observed in a previous study.[35] We have expanded this work by including computational results alongside our experimental observations. The experimental mass spectrum and optimized ion structures at the B3LYP/6-311++G(d,p) level of theory for this process are presented in Figure 5.5. Both thiazole and isothiazole form one abundant fragment ion, HC_2S^-, by HCN loss. Through the losses of CO, C_2H_2, and H_2O, deprotonated oxazole forms three fragment ions ($H_2C_2N^-$, OCN^-, and C_3N^-). All of the neutral molecules lost in these fragmentation processes have been detected in interstellar regions (HCN,[57] CO,[55] H_2O,[59] and C_2H_2[60]). Additionally, one of the six detected interstellar anions, C_3N^-,[61] is an isomer of the oxazole fragment that we observe here. Possible pathways to these observed fragments are calculated at the B3LYP/6-311++G(d,p) level of theory, and illustrated in Figure 5.6 and Figure 5.7.

C5-deprotonated oxazole exhibits more complex fragmentation pathways than the thiazoles. The barrier heights along each fragmentation pathway shown in Figure 5.6 correspond to the experimental ion intensities observed. The most abundant ion fragment, $H_2C_2N^-$, involves barriers ≤ 26.7 kcal mol^{-1}, whereas barriers over twice as large (≤ 66.5 kcal mol^{-1}) lead to the least intense fragment (C_3N^-). The remaining fragment, OCN^-, falls between the others in both experimental intensity and computational barrier heights (≤ 36.8 kcal mol^{-1}). Therefore, although many pathways are possible for high-energy processes such as these, our experimental observations corroborate these calculated routes.

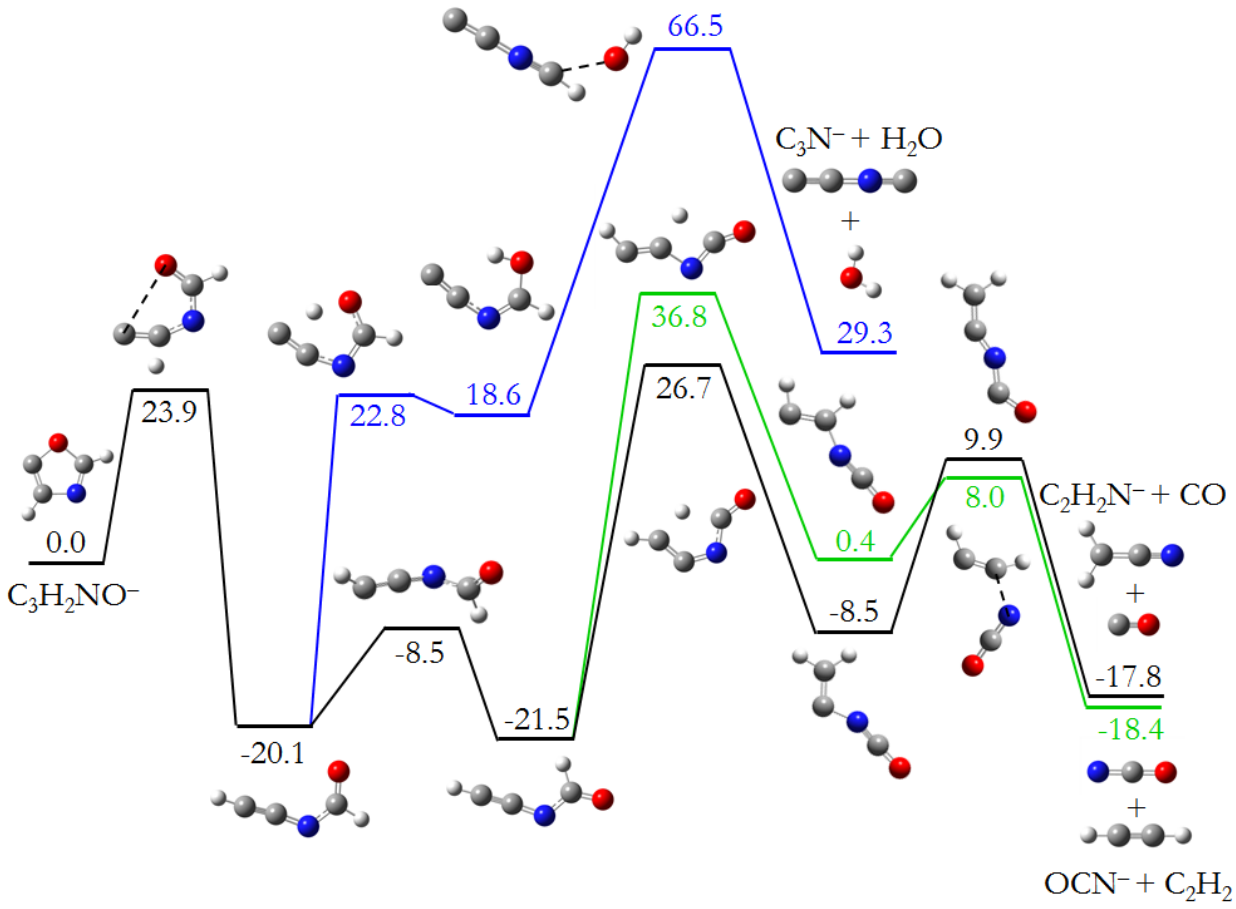

Figure 5.6
Deprotonated oxazole ($C_3H_2NO^-$) fragmentation pathways calculated at the B3LYP/6-311++G(d,p) level of theory and shown in kcal mol^{-1}.

Both C5-deprotonated thiazoles follow similar fragmentation routes to form HCN and HC_2S^-, depicted in Figure 5.7. Isothiazole is 0.3 kcal mol^{-1} higher in energy than its isomer due to the repulsion between its sulfur and nitrogen atoms.[28] This repulsive interaction also lowers the barrier to isothiazole fragmentation to ~10 kcal mol^{-1} less than that of thiazole. As expected, the difference in these barriers leads to a greater intensity of ion fragment formed from isothiazole than thiazole under identical conditions. Due to this simple fragmentation route with only one comparatively low-energy barrier, the HC_2S^- fragment is produced in high abundance (Figure 5.5).

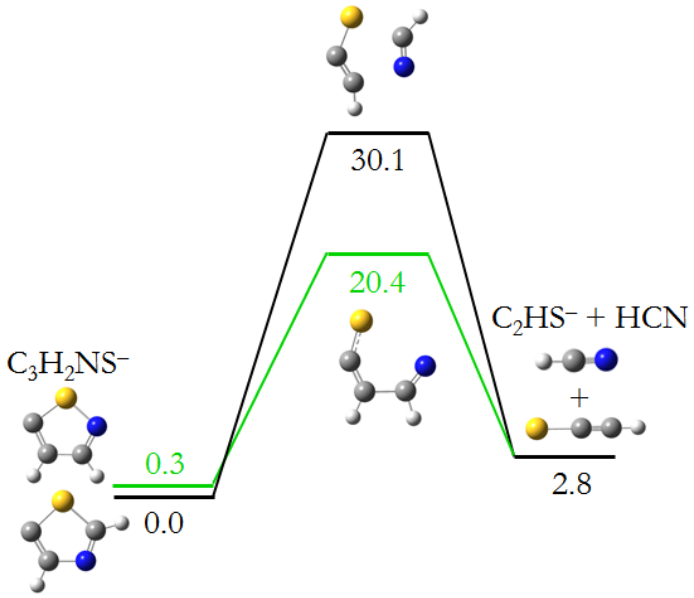

Figure 5.7
Deprotonated thiazole ($C_3H_2NS^-$; black) and isothiazole (green) fragmentation pathways calculated at the B3LYP/6-311++G(d,p) level of theory and shown in kcal mol^{-1}.

5.4 Conclusion

Azole molecules are important to both astrobiology and astrochemistry. Their prebiotic significance was recently highlighted when 2-aminooxazole and 2-aminothiazole were found to be critical intermediates in the synthesis of ribo- and deoxyribonucleotides.[16-18] Although azoles have not yet been detected in interstellar regions, these studies have motivated chemists to spectroscopically examine 2-aminooxazole.[19] Several cyclic molecules and anions have been detected,[3,62] lending legitimacy to the astronomical search for azoles in their neutral and deprotonated forms. Based on previous observations, we expect dark clouds and molecular clouds to be potential sources of these species.[14,15]

In an effort to understand the chemistry of these azole molecules, we have employed instrumental modifications, ESI, and CID techniques. Data are gathered using a modified commercial Finnigan LCQ Deca XP Plus mass spectrometer[39] that is successfully calibrated with previous[53,63] and current FA-SIFT reaction rate constants for both liquid and gaseous neutral reagents, as described in

Chapter 2. C5-deprotonated azoles are formed by collision-induced decarboxylation of deprotonated azole-5-carboxylic acid precursors, formed by ESI. Deprotonated oxazole, thiazole, and isothiazole are efficiently formed by this process. Deprotonated isoxazole-5-carboxylic acid, however, preferentially loses HCN rather than CO_2.

Several novel experimental and computational measurements are reported here for oxazole, thiazole, and isothiazole. Our study has focused on three chemical properties of these azoles: their gas-phase acidities, reactivity, and fragmentation. The first experimental measurements of their gas-phase acidities ($\Delta G°_{acid}$) at the C5 site are measured by bracketing (373.2 ± 2.3 and 365.7 ± 2.9 kcal mol^{-1} for oxazole and the thiazoles, respectively) and agree well with computations at the B3LYP/6-311++G(d,p) level of theory (373.2, 368.6, and 364.8 kcal mol^{-1} for oxazole, thiazole, and isothiazole) and previous studies.[28] Additionally, experiments and corroborating computations indicate that one site on all three deprotonated azolate anions is accessible for H/D exchange upon reaction with CD_3OD. Azole reactivity was characterized with several interstellar molecules (OCS, CO_2, and SO_2) and CS_2, CH_3Cl, $(CH_3)_3CCl$, and $(CH_3)_3CBr$. A direct correlation was observed between anion reaction efficiencies and basicities, and many reaction mechanisms were observed including association, atom abstraction, nucleophilic substitution, and elimination. Notably, several of the observed products have been detected in the interstellar medium (CO, CS, and HCN). As an extension of previous studies,[35] each deprotonated azole molecule was also fragmented by CID within the ion trap. Deprotonated oxazole fragments by the loss of CO, C_2H_2, and H_2O, and the deprotonated thiazole molecules fragment exclusively by HCN loss. All of the neutral molecules produced by fragmentation are detected interstellar species. Each pathway has been calculated at the B3LYP/6-311++G(d,p) level of theory, and the reaction barrier heights correspond well to the relative ion fragment intensities observed.

Overall, we have illuminated the acidities, reactivity, and fragmentation patterns of a set of azole molecules to better understand their potential role in the chemistry of the interstellar medium. Many stable interstellar molecules have been observed as both reactants and products in this study, validating the role of these yet undetected species in extraterrestrial chemical processes. Our results highlight the relevance of azole molecules to astrobiology and astrochemistry, and we hope they help motivate continued astronomical searches for heterocyclic, prebiotic molecules.

5.5 References

1 E. Herbst; E. F. van Dishoeck, *Complex Organic Interstellar Molecules*. Annu. Rev. Astron. Astrophys., **2009**, *47*, 427-480.

2 P. Ehrenfreund; M. A. Sephton, *Carbon Molecules in Space: from Astrochemistry to Astrobiology*. Faraday Disc., **2006**, *133*, 277-288.

3 T. P. Snow; V. M. Bierbaum, *Ion Chemistry in the Interstellar Medium*. Annu. Rev. Anal. Chem., **2008**, *1*, 229-259.

4 C. F. Chyba; K. P. Hand, *Astrobiology: The Study of the Living Universe*. Annu. Rev. Astron. Astrophys., **2005**, *43*, 31-74.

5 P. Thaddeus; J. M. Vrtilek; C. A. Gottlieb, *Laboratory and Astronomical Identification of Cyclopropenylidene, C_3H_2*. Astrophys. J., **1985**, *299*, L63-L66.

6 S. Yamamoto; S. Saito; M. Ohishi; H. Suzuki; S. Ishikawa; N. Kaifu; A. Murakami, *Laboratory and Astronomical Detection of the Cyclic C_3H Radical*. Astrophys. J., **1987**, *322*, L55-L58.

7 J. E. Dickens; W. M. Irvine; M. Ohishi; M. Ikeda; S. Ishikawa; A. Nummelin; A. Hjalmarson, *Detection of Interstellar Ethylene Oxide (c-C_2H_4O)*. Astrophys. J., **1997**, *489*, 753-757.

8 J. Cernicharo; A. M. Heras; A. G. G. M. Tielens; J. R. Pardo; F. Herpin; M. Guelin; L. Waters, *Infrared Space Observatory's discovery of C_4H_2, C_6H_2, and benzene in CRL 618*. Astrophys. J., **2001**, *546*, L123-L126.

9 Y. J. Kuan; S. B. Charnley; H. C. Huang; Z. Kisiel; P. Ehrenfreund; W. L. Tseng; C. H. Yan, *Searches for Interstellar Molecules of Potential Prebiotic Importance*. Adv. Space. Res., **2004**, *33*, 31-39.

10 J. M. Hollis; A. J. Remijan; P. R. Jewell; F. J. Lovas, *Cyclopropenone (c-H_2C_3O): A New Interstellar Ring Molecule*. Astrophys. J., **2006**, *642*, 933-939.

11 A. Coustenis; A. Salama; B. Schulz; S. Ott; E. Lellouch; T. Encrenaz; D. Gautier; H. Feuchtgruber, *Titan's Atmosphere from ISO Mid-Infrared Spectroscopy*. Icarus, **2003**, *161*, 383-403.

12 P. G. Stoks; A. W. Schwartz, *Nitrogen-Heterocyclic Compounds in Meteorites – Significance and Mechanisms of Formation*. Geochim. Cosmochim. Ac., **1981**, *45*, 563-569.

13 P. G. Stoks; A. W. Schwartz, *Basic Nitrogen-Heterocyclic Compounds in the Murchison Meteorite*. Geochim. Cosmochim. Ac., **1982**, *46*, 309-315.

14 W. M. Irvine; J. Ellder; A. Hjalmarson; E. Kollberg; O. E. H. Rydbeck; G. O. Sorensen; B. Bak; H. Svanholt, *Searches for Inter-Stellar Imidazole and Cyanoform*. Astron. Astrophys., **1981**, *97*, 192-194.

15 Y. J. Kuan; C. H. Yan; S. B. Charnley; Z. Kisiel; P. Ehrenfreund; H. C. Huang, *A Search for Interstellar Pyrimidine*. Mon. Not. Roy. Astron. Soc., **2003**, *345*, 650-656.

16 M. W. Powner; B. Gerland; J. D. Sutherland, *Synthesis of Activated Pyrimidine Ribonucleotides in Prebiotically Plausible Conditions*. Nature, **2009**, *459*, 239-242.

17 J. E. Sponer; J. Sponer; M. Fuentes-Cabrera, *Prebiotic Routes to Nucleosides: A Quantum Chemical Insight into the Energetics of the Multistep Reaction Pathways*. Chem. Euro. J., **2011**, *17*, 847-854.

18 M. W. Powner; S. L. Zheng; J. W. Szostak, *Multicomponent Assembly of Proposed DNA Precursors in Water*. J. Am. Chem. Soc., **2012**, *134*, 13889-13895.

19 H. Mollendal; A. Konovalov, *Microwave Spectrum of 2-Aminooxazole, a Compound of Potential Prebiotic and Astrochemical Interest*. J. Phys. Chem. A, **2010**, *114*, 2151-2156.

20 B. Moriyama; S. A. Henning; J. Leung; O. Falade-Nwulia; P. Jarosinski; S. R. Penzak; T. J. Walsh, *Adverse Interactions Between Antifungal Azoles and Vincristine: Review and Analysis of Cases*. Mycoses, **2012**, *55*, 290-297.

21 E. El Hammi; E. Warkentin; U. Demmer; F. Limam; N. M. Marzouki; U. Ermler; L. Baciou, *Structure of Ralstonia eutropha Flavohemoglobin in Complex with Three Antibiotic Azole Compounds*. Biochem., **2011**, *50*, 1255-1264.

22 A. Milano; M. R. Pasca; R. Provvedi; A. P. Lucarelli; G. Manina; A. Ribeiro; R. Manganelli; G. Riccardi, *Azole Resistance in Mycobacterium Tuberculosis is Mediated by the MmpS5-MmpL5 Efflux System*. Tuberculosis, **2009**, *89*, 84-90.

23 L. P. Jameson; S. V. Dzyuba, *Aza-BODIPY: Improved Synthesis and Interaction with Soluble A Beta 1-42 Oligomers*. Bioorg. Med. Chem. Lett., **2013**, *23*, 1732-1735.

24 V. P. Sinditskii; V. Y. Egorshev; V. V. Serushkin; S. A. Filatov, *Combustion of Energetic Materials Controlled by Condensed-Phase Reactions*. Combust. Explo. Shock Wave., **2012**, *48*, 81-99.

25 Y. Okumura; Y. Sugiyama; K. Okazaki, *Evolution Prediction of Coal-Nitrogen in High Pressure Pyrolysis Processes*. Fuel, **2002**, *81*, 2317-2324.

26 H. Knicker; P. G. Hatcher; A. W. Scaroni, *Solid-State N-15 NMR-Spectroscopy of Coal*. Energy & Fuels, **1995**, *9*, 999-1002.

27 R. L. Thompson; K. Damodaran; D. Luebke; H. Nulwala, *Aprotic Heterocyclic Anion Triazolide Ionic Liquids - A New Class of Ionic Liquid Anion Accessed by the Huisgen Cycloaddition Reaction*. Synlett, **2013**, 1093-1096.

28 D. Kaur; S. Khanna; R. P. Kaur, *The Role of Conjugative Interactions in Acidic and Basic Character of Five Membered Aromatic Heterocyclics*. J. Molec. Struc.-Theochem., **2010**, *949*, 14-22.

29 S. M. Villano; A. J. Gianola; N. Eyet; T. Ichino; S. Kato; V. M. Bierbaum; W. C. Lineberger, *Thermochemical Studies of N-methylpyrazole and N-methylimidazole*. J. Phys. Chem. A, **2007**, *111*, 8579-8587.

30 A. J. Gianola; T. Ichino; S. Kato; V. M. Bierbaum; W. C. Lineberger, *Thermochemical Studies of Pyrazolide*. J. Phys. Chem. A, **2006**, *110*, 8457-8466.

31 N. Otero; L. Estevez; M. Mandado; R. A. Mosquera, *An Electron-Density-Based Study on the Ionic Reactivity of 1,3-Azoles*. Eur. J. Org. Chem., **2012**, 2403-2413.

32 L. Dalila Fondren; J. McLain; D. M. Jackson; N. G. Adams; L. M. Babcock, *Studies of Reactions of a Series of Ions with Nitrogen Containing Heterocyclic Molecules Using a Selected Ion Flow Tube*. Int. J. Mass Spectrom., **2007**, *265*, 60-67.

33 J. M. Garver; Z. Yang; S. Kato; S. W. Wren; K. M. Vogelhuber; W. C. Lineberger; V. M. Bierbaum, *Gas Phase Reactions of 1,3,5-Triazine: Proton Transfer, Hydride Transfer, and Anionic sigma-Adduct Formation*. J. Am. Soc. Mass Spectrom., **2011**, *22*, 1260-1272.

34 R. Flammang; M. Plisnier; G. Bouchoux; Y. Hoppilliard; S. Humbert; C. Wentrup, *Unimolecular Chemistry of Oxazole and Isoxazole Radical Cations in the Gas-Phase - Combined Experimental and Molecular-Orbital Study*. Org. Mass Spectrom., **1992**, *27*, 317-325.

35 G. W. Adams; J. H. Bowie; R. N. Hayes, *Negative-Ion Fragmentations of Deprotonated Heterocycles - the Isothiazole, Thiazole, Isoxazole, and Oxazole Ring-Systems*. Int. J. Mass Spectrom. Ion Proc., **1992**, *114*, 163-182.

36 E. P. L. Hunter; S. G. Lias, *Evaluated Gas Phase Basicities and Proton Affinities of Molecules: An Update*. J. Phys. Chem. Ref. Data, **1998**, *27*, 413-656.

37 C. H. DePuy; V. M. Bierbaum; G. K. King; R. H. Shapiro, *Hydrogen-Deuterium Exchange-Reactions of Carbanions with Deuterated Alcohols in the Gas-Phase*. J. Am. Chem. Soc., **1978**, *100*, 2921-2922.

38 S. Gronert, *Estimation of Effective Ion Temperatures in a Quadrupole Ion Trap*. J. Am. Soc. Mass Spectrom., **1998**, *9*, 845-848.

39 S. Gronert, *Quadrupole Ion Trap Studies of Fundamental Organic Reactions*. Mass Spectrom. Rev., **2005**, *24*, 100-120.

40 G. E. Reid; R. A. J. O'Hair; M. L. Styles; W. D. McFadyen; R. J. Simpson, *Gas Phase Ion-Molecule Reactions in a Modified Ion Trap: H/D Exchange of Non-Covalent Complexes and Coordinatively Unsaturated Platinum Complexes*. Rapid Commun. Mass Spectrom., **1998**, *12*, 1701-1708.

41 M. J. Frisch; G. W. Trucks; H. B. Schlegel; G. E. Scuseria; M. A. Robb; J. R. Cheeseman; J. A. Montgomery; T. Vreven, et al., Gaussian 03, Revision C.02. Gaussian Inc. Wallingford, CT 2003.

42 M. J. Frisch; G. W. Trucks; H. B. Schlegel; G. E. Scuseria; M. A. Robb; J. R. Cheeseman; G. Scalmani; V. Barone, et al., Gaussian 09 Revision A.02. Gaussian Inc. Wallingford, CT: 2009.

43 G. Bouchoux, *Gas Phase Acidity of Substituted Benzenes*. Chem. Phys. Lett., **2011**, *506*, 167-174.

44 A. Moser; K. Range; D. M. York, *Accurate Proton Affinity and Gas-Phase Basicity Values for Molecules Important in Biocatalysis*. J. Phys. Chem. B, **2010**, *114*, 13911-13921.

45 T.-Y. Huang; J. F. Emory; R. A. J. O'Hair; S. A. McLuckey, *Electron-Transfer Reagent Anion Formation via Electrospray Ionization and Collision-Induced Dissociation*. Anal. Chem., **2006**, *78*, 7387-7391.

46 S. K. Koehn; N. L. Tran; S. Gronert; W. M. Wu, *The Stability of Aryl Carbanions Derived from Pyridine N-Oxide: The Role of Resonance in Stabilizing Aryl Anions*. J. Am. Chem. Soc., **2010**, *132*, 390-395.

47 N. D. Epiotis; R. L. Yates; F. Bernardi; S. Wolfe, *Theoretical-Analysis of Factors Determining Conformations and Stabilities of Oxycarbanions and Thiocarbanions*. J. Am. Chem. Soc., **1976**, *98*, 5435-5439.

48 K. Shen; Y. Fu; J.-N. Li; L. Liu; Q.-X. Guo, *What are the pKa Values of C-H Bonds in Aromatic Heterocyclic Compounds in DMSO?* Tetrahedron, **2007**, *63*, 1568-1576.

49 *NIST Chemistry WebBook, NIST Standard Reference Database Number 69*. National Institute of Standards and Technology, webbook.nist.gov, accessed 2010-2014.

50 C. H. DePuy; S. Kato, *H/D Exchange Reactions*. In *Encyclopedia of Mass Spectrometry*, Armentrout, P. B.; Gross, M. L.; Caprioli, R., Eds. Elsevier: Ansterdam, 2003; Vol. 1, 670-674.

51 T. Su; W. J. Chesnavich, *Parametrization of the Ion-Polar Molecule Collision Rate-Constant by Trajectory Calculations*. J. Chem. Phys., **1982**, *76*, 5183-5185.

52 G. Gioumousis; D. P. Stevenson, *Reactions of Gaseous Molecule Ions with Gaseous Molecules. 5. Theory*. J. Chem. Phys., **1958**, *29*, 294-299.

53 C. H. DePuy; S. Gronert; A. Mullin; V. M. Bierbaum, *Gas-Phase S_N2 and E2 Reactions of Alkyl-Halides*. J. Am. Chem. Soc., **1990**, *112*, 8650-8655.

54 D. J. D. Marais; J. A. Nuth, III; L. J. Allamandola; A. P. Boss; J. D. Farmer; T. M. Hoehler; B. M. Jakosky; V. S. Meadows, et al., *The NASA Astrobiology Roadmap*. Astrobiology, **2008**, *8*, 715-730.

55 R. W. Wilson; K. B. Jefferts; A. A. Penzias, *Carbon Monoxide in Orion Nebula*. Astrophys. J., **1970**, *161*, L43-L44.

56 A. A. Penzias; P. M. Solomon; R. W. Wilson; K. B. Jefferts, *Interstellar Carbon Monosulfide*. Astrophys. J., **1971**, *168*, L53-L58.

57 L. E. Snyder; D. Buhl, *Observations of Radio Emission from Interstellar Hydrogen Cyanide*. Astrophys. J., **1971**, *163*, L47-L52.

58 O. V. Borisov; M. B. Goshe; T. P. Conrads; V. S. Rakov; T. D. Veenstra; R. D. Smith, *Low-Energy Collision-Induced Dissociation Fragmentation Analysis of Cysteinyl-Modified Peptides*. Anal. Chem., **2002**, *74*, 2284-2292.

59 A. C. Cheung; D. M. Rank; C. H. Townes; D. D. Thornton; W. J. Welch, *Detection of Water in Interstellar Regions by its Microwave Radiation*. Nature, **1969**, *221*, 626-628.

60 S. T. Ridgway; D. N. B. Hall; S. G. Kleinmann; D. A. Weinberger; R. S. Wojslaw, *Circumstellar Acetylene in Infrared-Spectrum of IRC +10° 216*. Nature, **1976**, *264*, 345-346.

61 P. Thaddeus; C. A. Gottlieb; H. Gupta; S. Bruenken; M. C. McCarthy; M. Agundez; M. Guelin; J. Cernicharo, *Laboratory and Astronomical Detection of the Negative Molecular Ion C_3N^-*. Astrophys. J., **2008**, *677*, 1132-1139.

62 M. A. Cordiner; J. V. Buckle; E. S. Wirstrom; A. O. H. Olofsson; S. B. Charnley, *On the Ubiquity of Molecular Anions in the Dense Interstellar Medium*. Astrophys. J., **2013**, *770*, 48-56.

63 S. Gronert; C. H. DePuy; V. M. Bierbaum, *Deuterium-Isotope Effects in Gas-Phase Reactions of Alkyl-Halides - Distinguishing E2 and S_N2 Pathways*. J. Am. Chem. Soc., **1991**, *113*, 4009-4010.

CHAPTER 6

Gas–Phase Chemistry of Deprotonated Pyrimidines

6.1 Introduction

Research in astrobiology and the origin of life is contingent upon an understanding of the chemistry of nucleobases. Uracil is a pyrimidine nucleobase that makes up ribonucleic acid (RNA), theorized to be the predecessor of deoxyribonucleic acid (DNA) and key to the RNA World hypothesis.[1] The two remaining pyrimidine nucleobases, thymine and cytosine, also make up genetic material. According to one theory for the origin of life, prebiotic organics were delivered to the early earth by comets or meteorites.[2-4] This theory suggests that the first biomolecules were exogenously synthesized, motivating extensive research on the prebiotic formation of biomolecules such as pyrimidines in three interstellar nurseries for complex organic molecules: the gas-phase, grain surfaces, and ice mantles.[5] Many different formation routes to uracil, thymine, and cytosine including the reactions of cyano molecules[6-8] and the ultraviolet photochemistry induced in water and ices mixtures[9-12] have been proposed. The tentatively-detected interstellar molecule urea[13] has also been suggested as a precursor to all three molecules.[14,15] Recent astrochemical interest in small N-containing neutral molecules and ions has increased due to their potential to form more complex biomolecules such as the pyrimidines.[16,17] Although the studies in this field on neutral and cationic species are exhaustive, the anionic chemistry of pyrimidine molecules remains largely missing from proposed syntheses. Our previous research has shown, however, that the chemistry of negative ions can be remarkably important in the interstellar medium (ISM).[18,19]

Uracil is the only pyrimidine nucleobase that has been detected in all three of the Murchison, Murray, and Orgueil carbonaceous meteorites,[12,20-22] providing an important piece of evidence for the

theory of exogenous synthesis and delivery to early Earth. Although cytosine and thymine have not been verified in meteorites, their presence should not be ruled out.[12,23-25] Motivated by these detections, the abundance of interstellar nitrogen, and the known predominance of interstellar aromatic molecules,[26] astronomical searches for nucleobases have been extensive.[27-32] In spite of these efforts, no N-heterocycles including nucleobases have been conclusively detected in the ISM to date.[26] Currently, an upper limit has been placed on the column density of pyrimidine, and the astronomical search continues.[33]

Biomolecule dissociation is vital to the prediction of prebiotic formation routes.[34,35] The reactivity of biomolecule fragments is also essential to this end. In this study, we expand our previous work on the interstellar formation pathways,[36,37] reactivity,[38] and fragmentation[39] of complex interstellar organics through an analysis of deprotonated uracil, thymine, cytosine, and related anions. Former fragmentation studies on these species involve primarily cations, ranging from protonated species[40,41] to metal cation complexes.[42,43] Ionization and fragmentation have been accomplished by energetic interactions of photons,[44,45] electrons,[46] protons,[47] and ions[48,49] with pyrimidine molecules. Anionic species derived from nucleobase fragmentation remain largely unexplored. In a recently-modified Finnigan LCQ Deca XP Plus ion trap apparatus, we examine several anions produced by the ionization and subsequent fragmentation of uracil, thymine, cytosine, and related compounds. The basic pyrimidine structures of interest are shown in Figure 6.1 below.

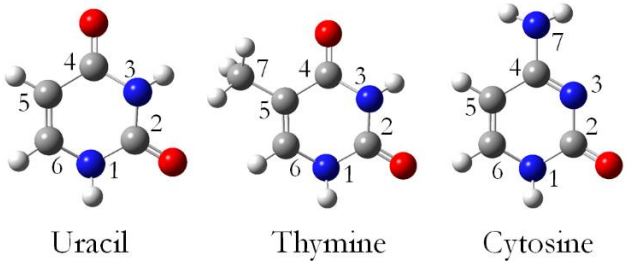

Figure 6.1
Structures of pyrimidine molecules.

The structures of the ions and their fragments are determined by consecutive collision induced dissociation (CID), acidity bracketing, and theoretical calculations. In this study we produce OCN^-, a known substituent of interstellar ices,[50] directly from all three deprotonated pyrimidine nucleobases. Imidoylketene (HN=CH–CH=C=O), a molecule of cosmological interest that has been largely overlooked for decades,[51] is another key fragment that arises from deprotonated uracil. Imidoylketene has been computationally shown to react to form cyclic, aromatic structures similar to uracil,[52] yet no reports to date have suggested this molecule as a precursor to uracil itself. The positive interstellar detection of its isomer, oxiranecarbonitrile, provides encouraging evidence for the future discovery of imidoylketene.[53,54] The two fragments that are derived from deprotonated uracil, therefore, are both likely interstellar species and may be involved in larger biomolecule formation in ice mantles, or other environments where complex organics are predicted to survive. In addition to fragmentation, we report the rate constants and reaction efficiencies of deprotonated imidoylketene with several detected and potential interstellar species (SO_2, OCS, CS_2, NO, N_2O, CO, NH_3, O_2, and C_2H_4). Our overall goal is to explore the role of anion dissociation and reactivity in the formation of more complex biomolecules of astrobiological relevance.

6.2 Methods

6.2.1 Experimental

Experimental data are gathered using a modified Finnigan LCQ Deca XP Plus ion trap. This instrument has been described in our previous work[39] and in Chapter 2. Ions are generated from an electrospray ionization (ESI) source with a spray voltage of 4.5 kV, a flow of 5-10 μL min^{-1}, and heated capillary temperatures of 200-250 °C. The electrospray solutions consist of 10^{-4} M uracil-5-carboxylic acid (97+%, Alfa Aesar), uracil (99%, Sigma Aldrich), thymine (99%, Sigma Aldrich), or cytosine (99%, Sigma Aldrich) in solvent mixtures of 1:1 CH_3OH:H_2O (HPLC grade, Sigma-Aldrich). Sodium

hydroxide (99.1%, Fischer Scientific) was also added to the solutions of uracil, thymine, and cytosine to raise the pH to the 8-9 range. The ions formed from the ESI source are injected into the ion trap where they are collisionally thermalized by helium at 5.1 x 10^{-3} Torr.[55] The activation Q, a variable that controls the q_z of the precursor ion, is maintained at 0.30. Multiple CID events (MS^n) are then possible by applying appropriate resonance excitation RF voltages to the endcap electrodes of the trap. For all dissociations performed in this study, we apply a normalized collision energy (NCE) of 40-70% for a duration of 20-50 ms to optimize fragment ion signal. Figure 6.2 outlines the formation of deprotonated uracil-5-carboxylic acid from the solution containing uracil-5-carboxylic acid by ESI. Our previous work[39] and that of others[56,57] often involve molecules whose most acidic site is on the carboxylic acid group itself. Here, the N_1 site is actually the most acidic, yielding parent anions that are predominantly deprotonated there rather than on the carboxylic acid group. CID on this ion involves several processes including decarboxylation, which are examined in depth in the following sections. The most acidic site on uracil, thymine, and cytosine is also the N_1 site. Therefore, we expect an analogous ionization process for these anions.

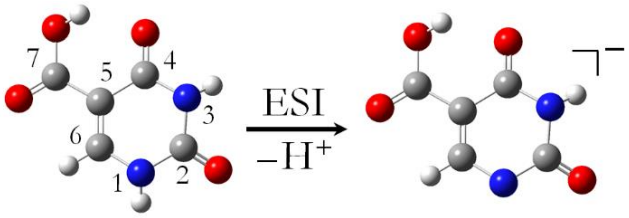

Figure 6.2
Uracil-5-carboxylic acid is deprotonated upon ESI predominantly at the most acidic site, N_1.

The parent or fragment ions may be isolated within the ion trap between 1 and 5000 ms. Over this time range, we are able to monitor reactions between these ions and neutral reagents that are introduced through the pre-existing helium buffer gas line. The modifications required to introduce these reagents are based on those of Gronert and coworkers.[58] Helium (UHP, 99.999%, Airgas) is

maintained at a constant flow between 1.0-1.9 L min^{-1} using a flow controller through a line external to the ion trap. Within this line, the pressure is maintained at 850 Torr (± 3%). Only a small fraction (0.1%)[59] of this helium-reagent mixture is sampled through fused silica capillary tubing into the ion trap itself. Gaseous neutral reagents are purchased as dilute mixtures (1.00 ± 0.02%) in helium (OCS, SO_2, Airgas) and added into the helium line. Other gases that showed no reactivity were not purchased diluted in helium (N_2O, O_2, C_2H_4, and CO, 99.5%; NO and HCl, 5% in helium; and NH_3, 99.9995%, Airgas). Volatile liquid neutral reagents are introduced into the helium line by syringe pump (0.5-5.0 μL min^{-1}). The liquid reagents used in this study include carbon disulfide >99%, pyrrole 98%, 2,2,3,3,3-pentafluoro-1-propanol 97%, liquefied phenol >85%, propionic acid >99.5%, thiophenol >99%, aniline ≥99.5%, and aqueous HBr 48% purchased from Sigma-Aldrich, acetone 99.7% from Fisher Scientific, and acetone-d6 99.5% from Cambridge Isotope Laboratories, Inc.

Reaction kinetics data are determined using pseudo-first-order kinetic analyses and by measuring the decline in reagent ion signal at six or more separate reaction times (1-5000 ms). Ion trap rate constants are calibrated against flowing afterglow-selected ion flow tube (FA-SIFT) measurements[60,61] and agree within the expected experimental uncertainties for gas-phase ion kinetics (±20-30%).[58] Lastly, all experimental data reported herein are the averages of six data points taken over two days with a minimum of three different helium:reagent ratios to ensure reproducibility over a range of experimental conditions.

6.2.2 Computational

Experiments in this study are complemented by *ab initio* calculations performed using the *Gaussian 03* and *Gaussian 09* suites of programs.[62,63] Enthalpies are reported at 0 K for all reaction and fragmentation pathways. All transition states (TS) reported within these pathways are verified by forward and reverse intrinsic reaction coordinate analyses. Gas-phase enthalpies of deprotonation

($\Delta H°_{acid}$) are calculated and reported as the change in the enthalpy for the reaction below at 298 K, where AH represents the molecule of interest.

$$AH \rightarrow A^- + H^+$$

The B3LYP/6-311++G(d,p) level of theory is used for all geometry optimizations and frequency calculations. Associated zero point energy (ZPE) and thermal energy (298 K) corrections are applied as specified.

6.3 Results and Discussion

6.3.1 Deprotonated Uracil-5-Carboxylic Acid and Uracil

Decarboxylation is not the exclusive CID pathway for deprotonated heterocyclic carboxylic acids. For example, our recent study on deprotonated isoxazole-5-carboxylic acid revealed that HCN loss and CO_2 loss occur together.[39] Analogous to this process, deprotonated uracil-5-carboxylic acid involves two competing fragmentation channels: decarboxylation and isocyanic acid (HNCO) loss, which result in three fragment ions (structures II-IV, Figure 6.3).

The overall breakdown of deprotonated uracil-5-carboxylic acid (I, $C_5H_3N_2O_4^-$) is summarized in the series of collision events shown in Figure 6.3 (MS^1–MS^3). The initial CID process involves decarboxylation to form deprotonated uracil (II, $C_4H_3N_2O_2^-$), isocyanic acid (HNCO) loss to form deprotonated imidoylketene carboxylic acid (III, $C_4H_2NO_3^-$), and losses of both CO_2 and HNCO yielding deprotonated imidoylketene (IV, $C_3H_2NO^-$). The following sections detail our structural identification of each of these fragments. The second (MS^2) and third (MS^3) CID processes provide evidence for specific parent ion structures. Briefly, $C_4H_3N_2O_2^-$ (II) yields OCN^-, suggesting an N-deprotonated rather than a C-deprotonated parent ion. $C_4H_2NO_3^-$ (III) produces IV, indicating a decarboxylation process and likely a carboxylic acid parent ion. Finally, $C_3H_2NO^-$ (IV) fragments to

form HC_2O^- in both cases, strongly indicating that the $C_3H_2NO^-$ (IV) species from both CID sequences are identical. Further computational and experimental analyses are given in the following discussion to verify the fragment structures shown here.

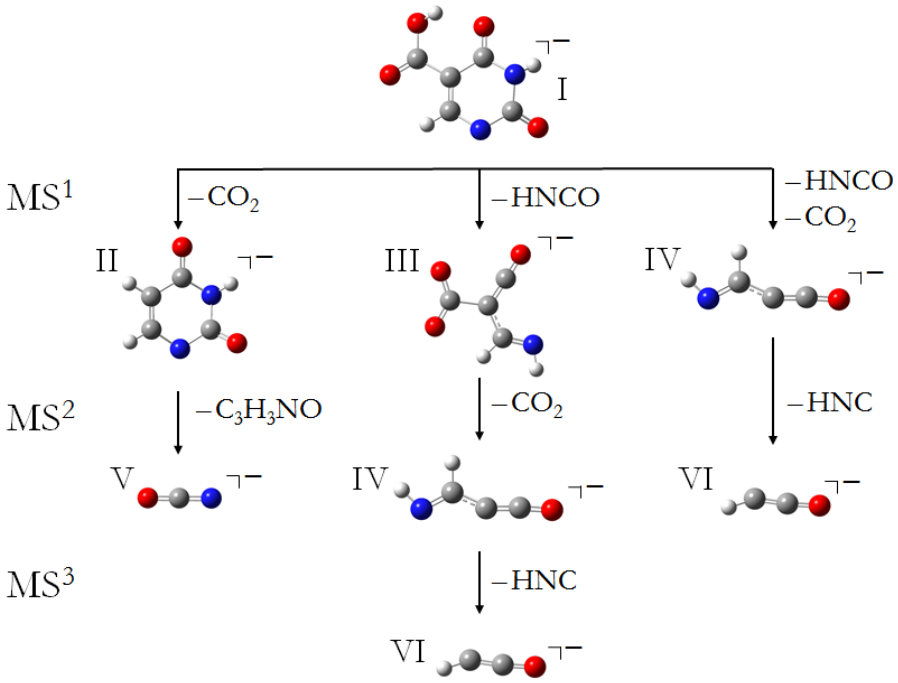

Figure 6.3
Proposed structures that arise from the fragmentation of deprotonated uracil-5-carboxylic acid (I) are summarized by collision event (MS^1–MS^3). Deprotonated uracil (II), deprotonated imidoylketene carboxylic acid (III), deprotonated imidoylketene (IV), OCN^- (V) and HC_2O^- (VI) are all derived from these fragmentation processes.

Parent and fragment ions in this study may tautomerize and isomerize under CID conditions, increasing the number of possible fragmentation pathways and structures. Therefore, it is prudent to verify the expected structures for each experimentally-observed mass-to-charge ratio. An approach comprised of theoretical calculations, experimental acidity bracketing, and consecutive fragmentation is used to determine the most viable structure of each ion.

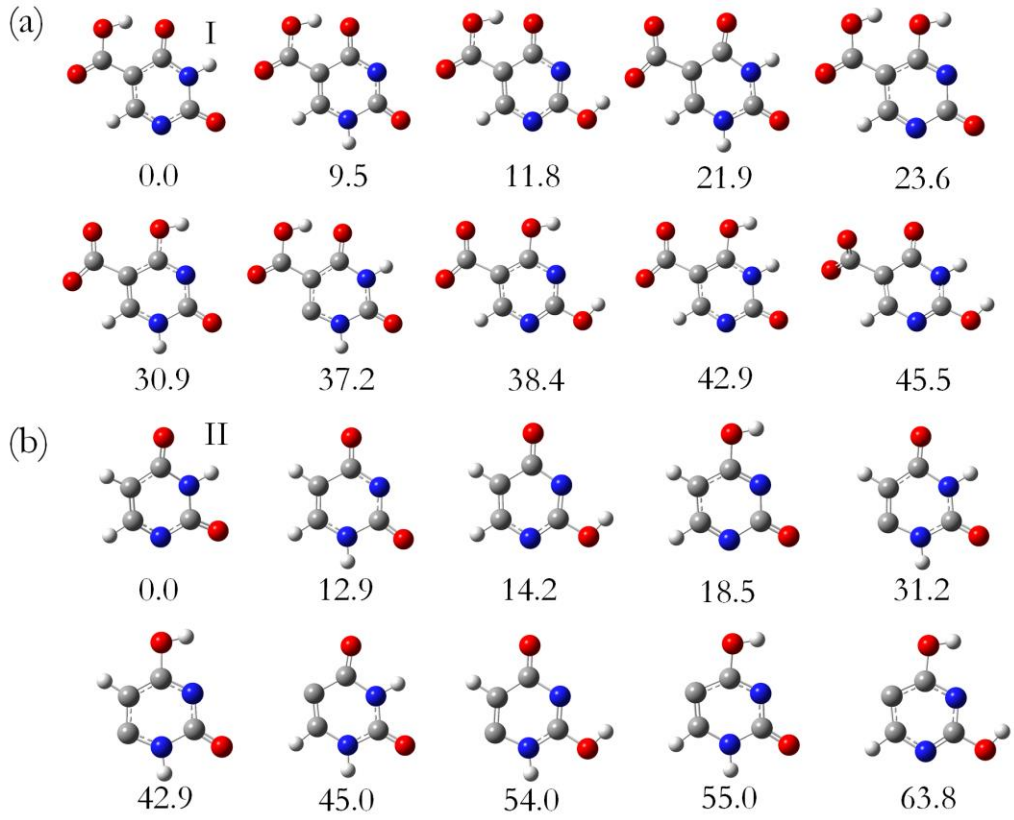

Figure 6.4
Several possible isomeric structures of $C_5H_3N_2O_4^-$ (a) and $C_4H_3N_2O_2^-$ (b) are listed in order of increasing ZPE corrected electronic energies relative to the most stable isomer. These energies (kcal mol^{-1}) are calculated at the B3LYP/6-311++G(d,p) level of theory and shown beneath each structure. N_1 deprotonated uracil-5-carboxylic acid (I) and N_1 deprotonated uracil (II) are the most stable structures.

The mechanism of ESI has been shown to deprotonate large biomolecules at multiple sites,[64] although the most acidic site is energetically favored.[65] At the B3LYP/6-311++G(d,p) level of theory, we have calculated the ZPE corrected electronic energies of 10 isomers of deprotonated uracil-5-carboxylic acid, shown in Figure 6.4 (a). Additionally, we have calculated the acidity of each viable deprotonation site. The most stable anion is the N_1 deprotonated structure (I; $\Delta H°_{acid}$=315.5 kcal mol^{-1}). Approximately 9 kcal mol^{-1} higher in energy is the N_3 deprotonated species ($\Delta H°_{acid}$=325.0 kcal mol^{-1}). Interestingly, deprotonating uracil-5-carboxylic acid at the carboxylic acid group produces a structure 22 kcal mol^{-1} less stable and this group is much less acidic than the N_1 site ($\Delta H°_{acid}$=337.4 kcal mol^{-1}). This is in part due to intramolecular hydrogen bonding between the carboxylic acid

hydrogen and the oxygen of the adjacent carbonyl group of the parent molecule (Figure 6.2). Many tautomers and isomers, as Figure 6.4 (a) illustrates, are accessible within 50 kcal mol^{-1} of the most stable species (I). For this reason, we have experimentally bracketed the acidity of this ion to validate our assertion that ESI of a solution of uracil-5-carboxylic acid preferentially produces the N_1 deprotonated anion.

Table 6.1
Acidity bracketing results.[a]

			A^-		
RH	$\Delta G°_{acid}(RH)$[b]	$\Delta H°_{acid}(RH)$[b]	$C_5H_3N_2O_4^-$	$C_4H_3N_2O_2^-$	$C_3H_2NO^-$
Acetone[c]	361.9 ± 2.0	368.8 ± 2.1	N	N	N
Aniline	359.1 ± 2.0	366.4 ± 2.1	N	N	N
Pyrrole	350.9 ± 2.0	359.54 ± 0.25	N	N	N
2,2,3,3,3-Pentafluoro-1-propanol	348.8 ± 6.0	355.4 ± 6.1	N	N	Y
Phenol	342.3 ± 2.0	349 ± 2	N	N	Y
Propionic Acid	340.4 ± 2.0	347.4 ± 2.2	N	N	Y
Thiophenol	333.4 ± 2.1	340.4 ± 2.1	N	N	Y
Hydrochloric Acid	328.10 ± 0.10	333.40[d]	N	Y	Y
Hydrobromic Acid	318.30 ± 0.15	323.540 ± 0.050	N	Y	Y

[a] $A^- + RH \rightarrow AH + R^-$; where AH represents the fragment ions $C_5H_3N_2O_4^-$, $C_4H_3N_2O_2^-$, and $C_3H_2NO^-$.
[b] All values are given in kcal mol^{-1} and obtained from the NIST WebBook.[66]
[c] Acetone-d6 was also studied, and no reactions were observed.
[d] Error bars are not specified in the NIST WebBook.

Using the known experimental acidities of several reagents,[66] we observed the reactivity of $C_5H_3N_2O_4^-$ with an array of neutral molecules in our modified ion trap apparatus. The acidity bracketing data are summarized in Table 6.1 for $C_5H_3N_2O_4^-$, $C_4H_3N_2O_2^-$, and $C_3H_2NO^-$ (the latter two are outlined in the following discussion). This experiment involves trapping each ion (A^-) in the presence of the neutral molecules (RH) listed in Table 6.1. This table indicates the positive or negative detection of the R^- proton abstraction product (with a Y or N, respectively). Had the structure of $C_5H_3N_2O_4^-$ contained a mixture of isomers such as those listed in Figure 6.4 (a), we would expect to observe reactivity with one or more of these neutral reagents. Rather, we do not observe the formation

of any product ions (R^-). Our calculated acidity of the N_1 site of uracil-5-carboxylic acid is $\Delta H°_{acid}$ =315.5 kcal mol^{-1}, whereas alternative deprotonation sites on uracil-5-carboxylic acid are much less acidic ($\Delta H°_{acid} \geq 325.0$ kcal mol^{-1}). Our results (Table 6.1) indicate that the protonated neutral parent of $C_5H_3N_2O_4^-$ is in fact more acidic than hydrobromic acid, generating an experimental upper limit of $\Delta H°_{acid} < 323.540 \pm 0.050$ kcal mol^{-1}, in agreement with our theoretical value for the N_1 deprotonated species (I).

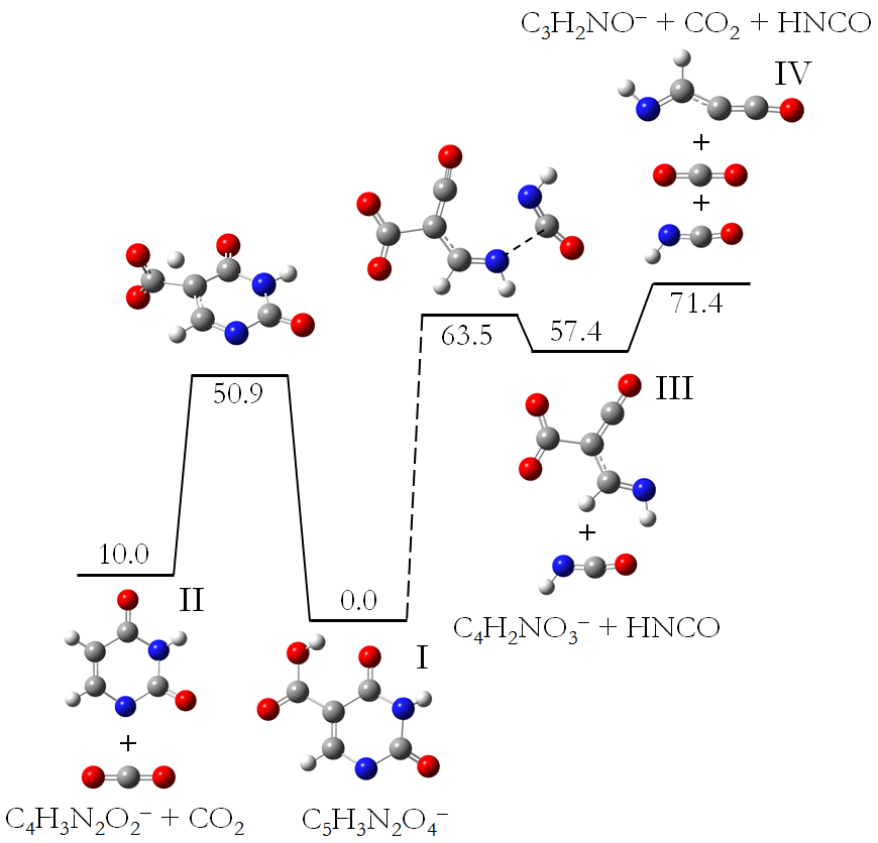

Figure 6.5
Possible pathways (kcal mol^{-1}) calculated at the B3LYP/6-311++G(d,p) level of theory are shown for the CID of N_1 deprotonated uracil-5-carboxylic acid (I) to produce anions II-IV. The dashed line indicates the isomerization of I prior to further fragmentation. A potential energy surface of the low energy isomerization processes of I is included in Appendix B.

The CID pathways accessible to uracil molecules are often defined by their ease of tautomerization and isomerization.[41] Many of the structures listed in Figure 6.4 (a) are accessible by

pathways with barriers readily overcome under CID conditions (≤ 50 kcal mol^{-1}; Appendix B). Figure 6.5 includes a potential CID process to form fragments II-IV from I. Decarboxylation occurs directly from structure I, yielding II by way of a 50.9 kcal mol^{-1} transition state. In contrast to this direct process, we propose that I isomerizes into a species deprotonated at the carboxylic acid site (+22.0 kcal mol^{-1}, Figure 6.4 (a)) prior to fragmenting into III and IV. This isomerization process is represented by a dashed line in the figure, and is included in Appendix B. Considering the barriers of isomerization are lower than the barriers to isocyanic acid (HNCO) loss (63.5 kcal mol^{-1}), these rearrangements likely occur prior to this fragmentation process.

As Figure 6.5 demonstrates, deprotonated uracil ($C_4H_3N_2O_2^-$) is produced by decarboxylation of deprotonated uracil-5-carboxylic acid ($C_5H_3N_2O_4^-$) upon CID. Similar to its parent, however, deprotonated uracil has many tautomers and isomers which may be accessible through CID. Ten of these structures are shown in Figure 6.4 (b). Due to the direct CID pathway from the parent ion (I) to N_1 deprotonated uracil (II) as well as its overall stability, this structure is reasonably in highest abundance. Next higher in energy is its N_3 deprotonated counterpart (+12.9 kcal mol^{-1}), followed by two N_1 deprotonated tautomers (+14.2 and +18.5 kcal mol^{-1}, respectively). Even less stable are the C_6 (+31.2 kcal mol^{-1}) and C_5 (+45.0 kcal mol^{-1}) deprotonated ions and their associated tautomers. To clearly delineate which structure is produced from CID, we have performed another series of bracketing experiments, included in Table 6.1 under $C_4H_3N_2O_2^-$.

Our experimental results suggest that the most stable ion, N_1 deprotonated uracil (II), is formed in our apparatus. The acidities ($\Delta H°_{acid}$) of different sites on uracil have previously been calculated by the Kenttämaa research group to be 332.8 ± 2.2, 345.1 ± 2.2, 380.2 ± 0.5, and 366.2 ± 0.5 kcal mol^{-1} for the N_1, N_3, C_5, and C_6 sites, respectively.[67] Using these data and the known experimental acidities of the aforementioned reagents,[66] we observed the reactivity of $C_4H_3N_2O_2^-$

(Table 6.1). Hydrochloric and hydrobromic acids reacted with this ion to produce Cl^- and Br^- products, but no products were observed for the less acidic reagents. Therefore, the acidity of the neutral parent is 336.9 ± 2.1 kcal mol^{-1} according to our bracket, in agreement with the N_1 results of the Kenttämaa group (332.8 ± 2.2 kcal mol^{-1}).

A further verification of these results is required, due to a process previously observed in our research[68] involving the isomerization of anions upon reaction with an acid. Briefly, the anions that we are bracketing may originate as a more basic structure (shown in Figure 6.4). For example, C_5 deprotonated uracil would readily abstract a proton from an acid RH to form an ion-neutral complex of uracil and R^- as shown in the equation below; however, before separation of the complex, R^- can abstract a proton from the most acidic site of uracil to form N_1 deprotonated uracil (II). This isomerization produces no change in the mass of the ion, making the ion appear to be unreactive.

$$C_5 \text{ deprotonated uracil} + RH \rightarrow [\text{Uracil} + R^-] \rightarrow II + RH$$

If the parent ion is deprotonated at the carboxylic acid site (+22.0 kcal mol^{-1}, Figure 6.4 (a)), it would readily decarboxylate under CID to form C_5 deprotonated uracil (+45.0 kcal mol^{-1}, Figure 6.4 (b)). To test whether an acid-catalyzed isomerization is taking place, we use acetone-d6 as an additional bracketing reagent (Table 6.1). If C_5 deprotonated uracil is present in our apparatus, the acetone would deuterate the C_5 site before abstracting a proton from the N_1 site, producing an ion with 1 amu higher mass. We did not observe a deuterated product from the reaction of acetone-d6 with $C_4H_3N_2O_2^-$. This provides additional support that our structural identifications of I and II are correct, and no acid-catalyzed isomerization is taking place.

Lastly, II forms a single ionic product when fragmented: OCN^-. We have inferred the neutral product, imidoylketene, and the potential energy diagram of this dissociation process is provided in Figure 6.6. Analogous to the fragmentation of I in Figure 6.5, the lowest energy CID pathway for II involves isomerization. The initial conversion of N_1 to N_3 deprotonated uracil prior to fragmentation

allows a low energy transition state (32.6 kcal mol^{-1}) for dissociation of the N_1-C_2 bond leading to OCN^- and imidoylketene, a total of 53.3 kcal mol^{-1} higher in energy than II. We expand on the astrochemical relevance of these products in an upcoming section.

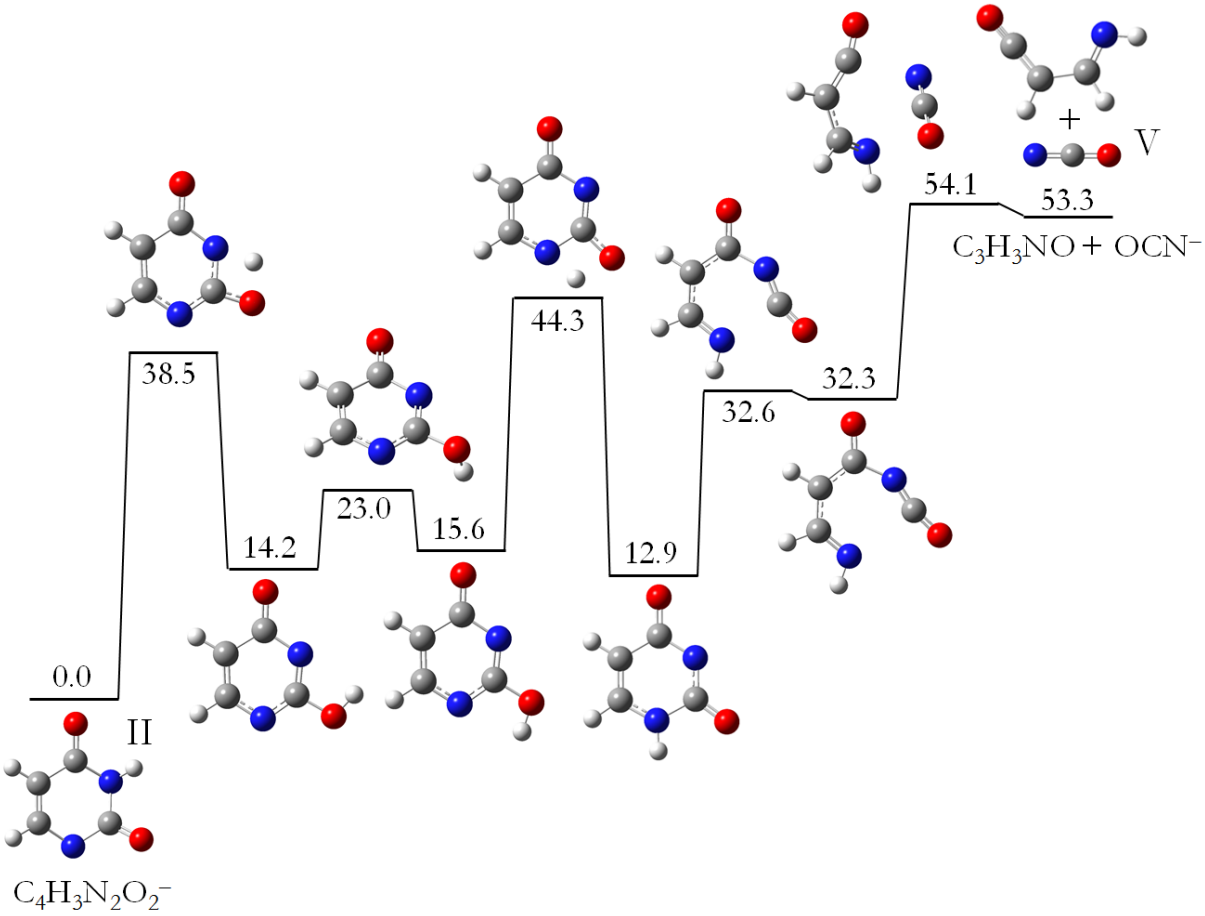

Figure 6.6
A pathway (kcal mol^{-1}) calculated at the B3LYP/6-311++G(d,p) level of theory is shown for the CID of N_1 deprotonated uracil (II). OCN^- and imidoylketene (C_3H_3NO) are produced.

6.3.2 Deprotonated Imidoylketene

The remaining two fragments of deprotonated uracil-5-carboxylic acid, III and IV, are formed by means of isocyanic acid (HNCO) loss. As shown in Figure 6.3, structure III leads to IV and will therefore be implicit in our discussion of the formation and structure of IV. We began with an overall examination of several ring-closed and ring-opened candidates for $C_3H_2NO^-$. Although ring

structures have been proposed in previous investigations of protonated uracil fragments,[41] we do not expect that the analogous deprotonated ring species will be formed here due to their instability (≥47.3 kcal mol^{-1}) relative to IV. Although more stable isomers of IV do exist, they cannot be formed directly from I without significant rearrangements.

Experimental bracketing results similarly indicate that IV is a reasonable structure. As Table 6.1 demonstrates, our experimental bracket of $C_3H_2NO^-$ gives an acidity ($\Delta H°_{acid}$) of the parent molecule of 357.5 ± 6.1 kcal mol^{-1}. The calculated acidity at the B3LYP/6-311++G(d,p) level of theory is 349.5 kcal mol^{-1}. Although this result is slightly lower than our experimental bracket, these values are in reasonable agreement due to the known underestimation of thermochemical values by density functional theory,[69] and the large error bar on the available experimental value. The fragmentation processes leading to and from $C_3H_2NO^-$ provide deeper insights into the feasibility of structure IV. Only one daughter ion, HC_2O^-, is formed from the CID of $C_3H_2NO^-$ (Figure 6.3). The formation of this ion from IV involves one H transfer, which is minimal rearrangement by comparison to other $C_3H_2NO^-$ isomers. Furthermore, the CID channel from I to IV (Figure 6.5) reveals a concurrent dissociation of both the N_1–C_2 and N_3–C_4 bonds, the most likely cleaved bonds in the uracil cation according to recent computational data.[70] This retro Diels Alder reaction results in the production of HNCO and deprotonated imidoylketene carboxylic acid (III). From III, only 14.0 additional kcal mol^{-1} are required to produce IV by decarboxylation. The reactivity of the anion, discussed in the following section, solidifies our identification of structure IV. However, the acidity and fragmentation processes discussed here clearly indicate that deprotonated imidoylketene (IV) is the dominant structure of $C_3H_2NO^-$.

Of the three major fragments derived from I, IV is the most reactive. We therefore focus our study on the reactivity of this ion. Reactivity is characterized with several detected and potential interstellar species. Although no measurable reactions ($k_{exp} \leq 1 \times 10^{-13}$ cm^3 s^{-1}) occurred between II,

III, or IV with many of these molecules (NO, N_2O, CO, NH_3, O_2, and C_2H_4), reactions were observed for several sulfur-containing triatomic molecules (SO_2, OCS, and CS_2). The reactions examined with IV are measured quantitatively and discussed in detail below.

Table 6.2
Deprotonated imidoylketene (IV) reactivity.

Neutral Reagent	Products	k_{exp} (10^{-11} cm^3 s^{-1})	k_{exp}/k_{col} (%)	TS[a]	ΔH_{0K}[a]
SO_2	$C_2H_2NOS^- + CO_2$[b]	89 ± 14	56	-14.0	-26.1
OCS	$C_3H_2NS^- + CO_2$[c]	0.59 ± 0.06	0.50	-6.3	-15.2
CS_2	$C_3H_2NS^- + OCS$[d]	≤ 0.01	–	+1.2	-15.9

[a] All calculations are performed at the B3LYP/6-311++G(d,p) level of theory and results are reported in kcal mol^{-1}.
[b] A secondary product ($C_2H_2NOS^-$–SO_2 adduct ion) is also observed. Only primary products are included in our analysis.
[c] Adduct ions ($C_3H_2NO^-$– OCS) are observed in trace amounts (<10^3 ion counts s^{-1}).
[d] $C_3H_2NS^-$ is observed in trace amounts (<10^3 ion counts s^{-1}).

The observed ionic products, reaction rate constants (k_{exp}) and reaction efficiencies (k_{exp}/k_{col}) for IV with SO_2, OCS, and CS_2 are summarized in Table 6.2. Reaction efficiencies are expressed as the ratio of the reaction rate constant and the collision rate constant, determined by parametrized trajectory theory[71] for polar and by Langevin theory[72] for nonpolar neutral reagents. The error reported in this table represents the precision of each measurement, defined as one standard deviation of the experimental mean. Additional systematic errors of our modified instrumental setup are approximately ±30%. Also, theoretical calculations (B3LYP/6-311++G(d,p)) illustrate the largest TS barriers (TS in Table 6.2) and overall enthalpy changes for each reaction pathway at 0 K. Even though ionic products are observed in all three cases, only the reactivities with SO_2 and OCS were experimentally measureable, resulting in an upper limit for the reaction rate constant with CS_2.

From Table 6.2, a number of interesting observations can be made regarding the overall kinetics and thermodynamics of these reactions. As the largest TS barrier increases in energy from -14.0 to -6.3 kcal mol^{-1}, the overall reaction efficiency expectedly decreases dramatically, from 0.56 to

0.0050. Barriers even slightly above the energy of the reactants (+1.2 kcal mol^{-1}) give rise to only trace observable ion products and no measurable reaction rate constant. This verifies that ions in the modified ion trap apparatus are near-thermal.[55] Finally, the sulfur-centered reagent (SO_2) displays a significantly higher reaction efficiency than either of the carbon-centered reagents (OCS and CS_2), likely due to the bent geometry and increased molecular polarity of SO_2.

A more in depth look at these reactions is provided by potential energy diagrams. A direct comparison between the SO_2 (a) and OCS (b) reactions is shown in Figure 6.7. These reactions are similar in that they both involve the formation of an adduct ion and the subsequent transfer of an O atom from the neutral reagent molecule to the terminal CO on IV. This results in the eventual production of CO_2 from the adduct ion complex. Important differences in these diagrams are the increased barrier heights and the decreased overall exothermicity of the reaction with OCS, leading to a reaction efficiency two orders of magnitude below that of SO_2 (Table 6.2). Adding to this inefficiency, the OCS molecule forms a stable reactant complex rotated 180° with respect to its reactive geometry to produce CO_2. The first barrier shown in Figure 6.7 (b) (-6.6 kcal mol^{-1}) in fact represents two TS structures and an optimized geometry all within 0.1 kcal mol^{-1} of one another. This flat section of the potential energy surface certainly contributes to the overall inefficiency of this reaction. Notably, the more common reaction observed with OCS reagents, sulfur atom transfer,[73] is not observed here. Our calculations show that this process is in fact 8.1 kcal mol^{-1} endothermic (ΔH_{0K}) and therefore not feasible within our ion trap apparatus.

The reaction rate constant is immeasurably slow ($k_{exp} \leq 1 \times 10^{-13}$ cm^3 s^{-1}) between IV and CS_2, although trace ($<10^3$ ion counts s^{-1}) product ions are visible in the mass spectrum. The barrier (+1.2 kcal mol^{-1}) resulting from the approach of CS_2 to the negatively charged C atom of IV is high enough to slow down the reaction significantly. The calculated potential energy diagram for this reaction is presented in Figure 6.7 (c). Following the initial barrier, a mechanism analogous to the other sulfur-

containing reagents (Figure 6.7 (a) and (b)) is shown, producing OCS rather than CO_2 through a sulfur atom transfer to the terminal CO of the ion.

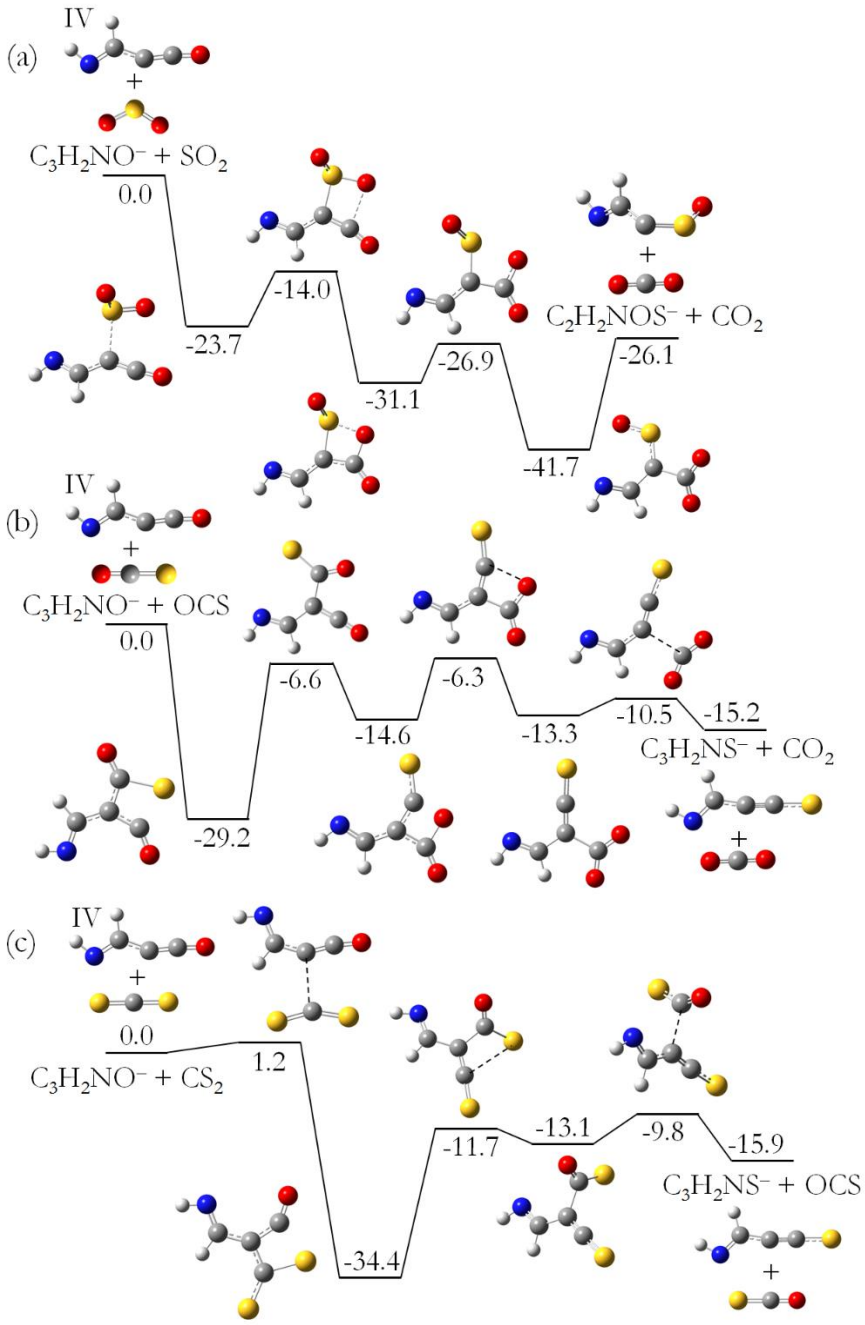

Figure 6.7
Deprotonated imidoylketene (IV) reacts similarly with SO_2 (a) and OCS (b) to produce CO_2. IV and CS_2 (c) do not react with a measurable rate constant to produce OCS and $C_3H_2NS^-$ due to a small barrier (+1.2 kcal mol^{-1}). Units are in kcal mol^{-1} and all species are calculated at the B3LYP/6-311++G(d,p) level of theory (ΔH_{0K}).

6.3.3 Deprotonated Thymine and Cytosine

In addition to uracil and its related anions, we consider next the structures and fragmentation patterns of deprotonated thymine and cytosine. The purpose of this section is to compare the previously discussed deprotonated uracil data with that of these two pyrimidine nucleobases. In terms of fragmentation, we observe striking similarities among all three molecules. Our experimental mass spectra at several different NCEs (40-60%) are shown in Figure 6.8. As is expected due to the similarities in the structures of these three molecules, the same amount of collision energy is required to bring the parent ion signal to a negligible intensity in all cases (60% NCE). Furthermore, OCN^- is produced by all three fragmentation processes. Previous anion studies involving these molecules have also observed cyanate ion production.[74] In the case of deprotonated cytosine, HNCO loss accompanies OCN^- formation. This undoubtedly results from the additional H atoms available for proton transfer from the amino group on cytosine (Figure 6.1). The fragmentation mechanisms are computationally examined and described later in this section. Before exploring the potential energy diagrams of these processes, an investigation of the lowest energy tautomers of each pyrimidine will help facilitate our discussion.

Comparative studies of deprotonated pyrimidine structures are severely lacking. We find that previous works have primarily analyzed the chemistry of pyrimidine neutrals and cations.[75,76] Our results have much in common with these reported data, but there are a few key dissimilarities. Figure 6.9 (a)-(c) summarizes the four lowest energy isomers of deprotonated uracil (a), thymine (b), and cytosine (c) for comparison. We find that the most energetically preferential structures for uracil and thymine are dioxo tautomers, in agreement with those of their neutral counterparts.[77] However, our results indicate that the amino-oxo tautomer of cytosine is not in fact the most stable structure (0.0 kcal mol^{-1}, Figure 6.9 (c)), in contrast to previous results.[77] Rather, the imino-oxo structure is more stable by over 5 kcal mol^{-1} for deprotonated cytosine. It has long been established that the order of

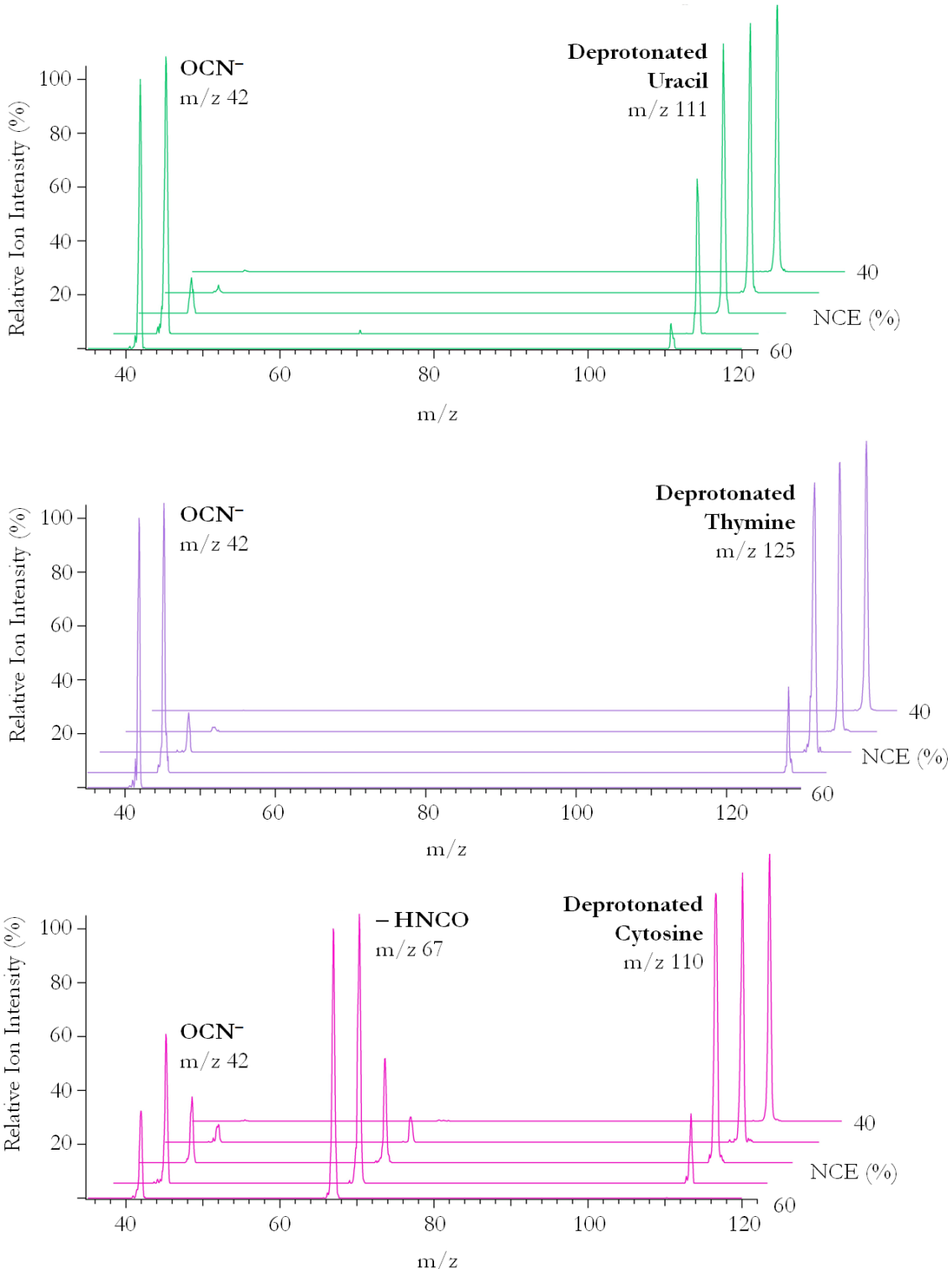

Figure 6.8

The experimental CID mass spectra of deprotonated uracil, thymine, and cytosine are shown. OCN^- is a primary fragment of all three ions. Deprotonated cytosine additionally fragments by HNCO loss. The applied NCE increases in increments of 5% and can be found to the right of the spectra.

tautomer stabilities does not change with the addition of a group to the C_5 position of neutral uracil, whether that group is a methyl or even fluorine.[75] We find the same principle applies to the deprotonated anions. When Figure 6.9 (a) and Figure 6.9 (b) are compared, the order of tautomer stabilities and the relative energies of the structures are analogous. Finally, as previously described and depicted in Figure 6.6, the tautomerization and isomerization of these anions often involve low energy barriers compared to their ring opening and fragmentation. Therefore, although these barriers are not computed for thymine and cytosine, the calculated fragmentation mechanisms begin with slightly higher energy structures which are accessible during CID.

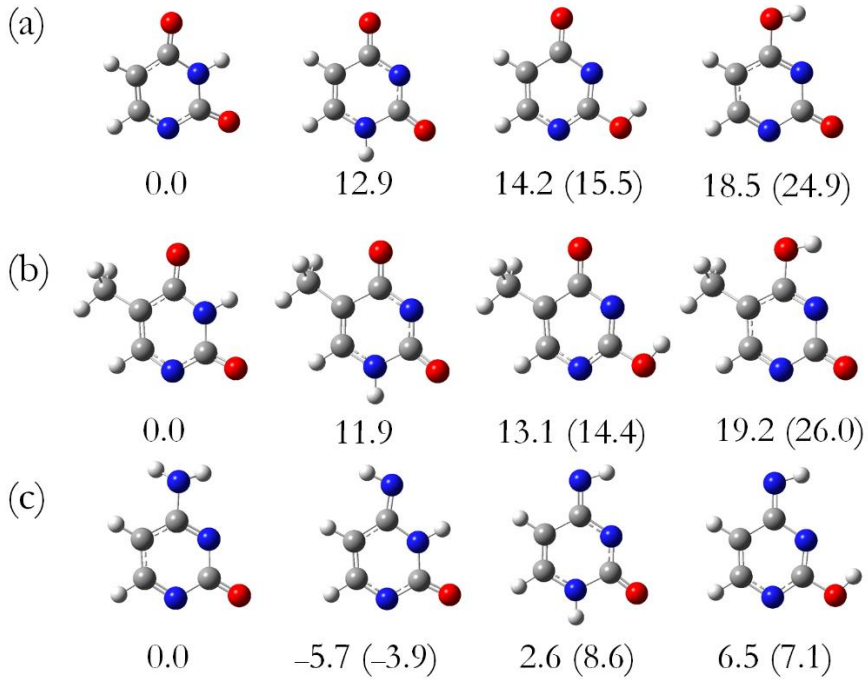

Figure 6.9
Several possible isomeric structures of deprotonated uracil (a), deprotonated thymine (b), and deprotonated cytosine (c), are listed with ZPE corrected electronic energies relative to the N_1 deprotonated isomer. Energies in parentheses represent those of the associated rotamers. These energies (kcal mol^{-1}) are calculated at the B3LYP/6-311++G(d,p) level of theory and shown beneath each structure. N_1 deprotonated species are the most stable structures.

The chemistry of uracil and thymine is similar not only in isomerization, but fragmentation as well. Figure 6.10 depicts potential fragmentation processes for these deprotonated pyrimidines side by side, beginning with their N_3 deprotonated structures. Both molecules ring open through a N_1-C_2 bond cleavage, which has been reported as a likely initiation process for ring opening in dissociative electron attachment studies.[78] An OCN group protrudes from each molecule, and is subsequently lost when the N_3-C_4 bond is broken. Thymine favorably splays open prior to dissociation, whereas uracil does not. However, the final bond breaking processes in both cases require similar amounts of energy (~20 kcal mol^{-1}). Imidoylketene and methyl-substituted imidoylketene are produced with the cyanate ion for uracil and thymine, respectively. Notably, the reverse reactions of these CID mechanisms have barriers that are < 1 kcal mol^{-1} higher in energy than the products.

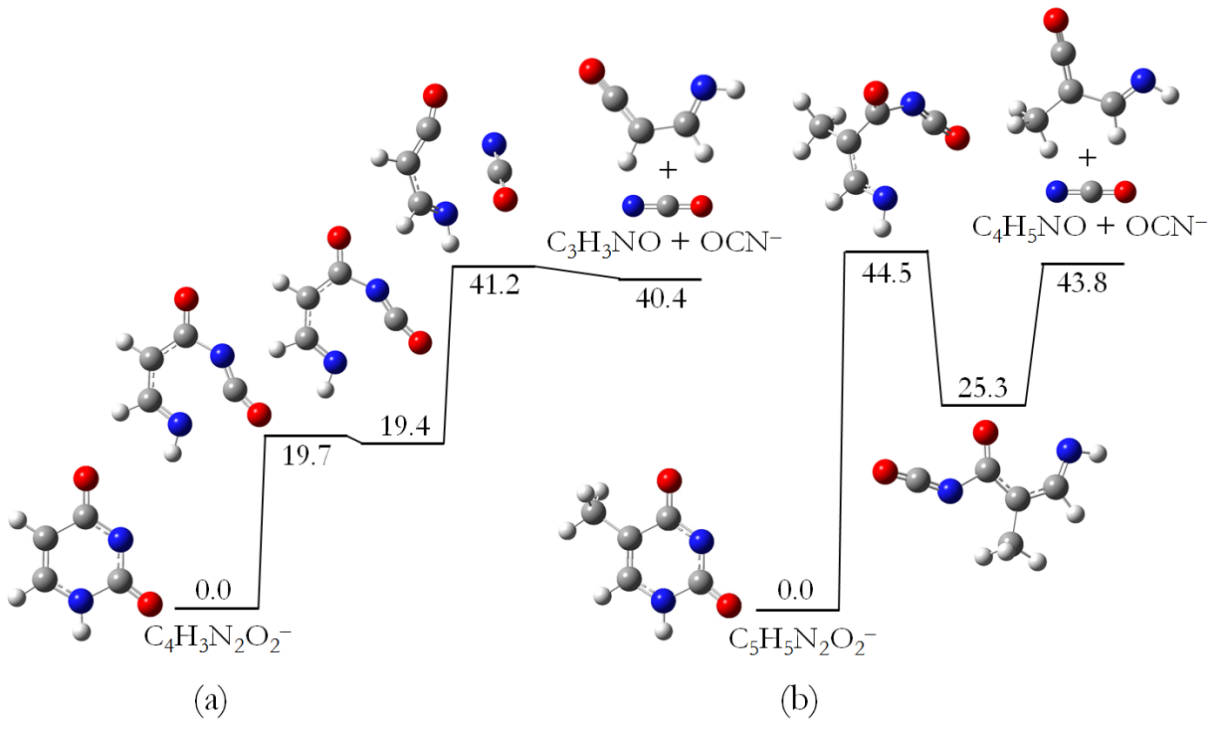

Figure 6.10
A pathway (kcal mol^{-1}) calculated at the B3LYP/6-311++G(d,p) level of theory is shown for the CID of N_3 deprotonated uracil (a) and N_3 deprotonated thymine (b). OCN^- is produced in both reactions. The predicted neutral products include imidoylketene (C_3H_3NO) and methylimidoylketene (C_4H_5NO) from deprotonated uracil and deprotonated thymine, respectively.

Cytosine, although similar in structure to its pyrimidine counterparts, displays slightly different dissociation patterns. Our proposed fragmentation pathway is shown in Figure 6.11. Starting with its N_3 deprotonated imine tautomer, the pyrimidine ring opens through N_1-C_2 bond cleavage, analogous to uracil and thymine. A stable, splayed-open structure (12.6 kcal mol^{-1}) results from this ring-opening, similar to that of thymine. When OCN^- is liberated upon the severance of the N_3-C_4 bond, the anion and neutral may separate, or a low energy product complex may arise (0.8 kcal mol^{-1}). This product complex facilitates a proton transfer to OCN^-, forming isocyanic acid and $C_3H_3N_2^-$. According to our experimental observations (Figure 6.8), HNCO loss is favored over OCN^- formation. These computations support our experiments, showing the latter process to be 13.6 kcal mol^{-1} higher in energy than the former.

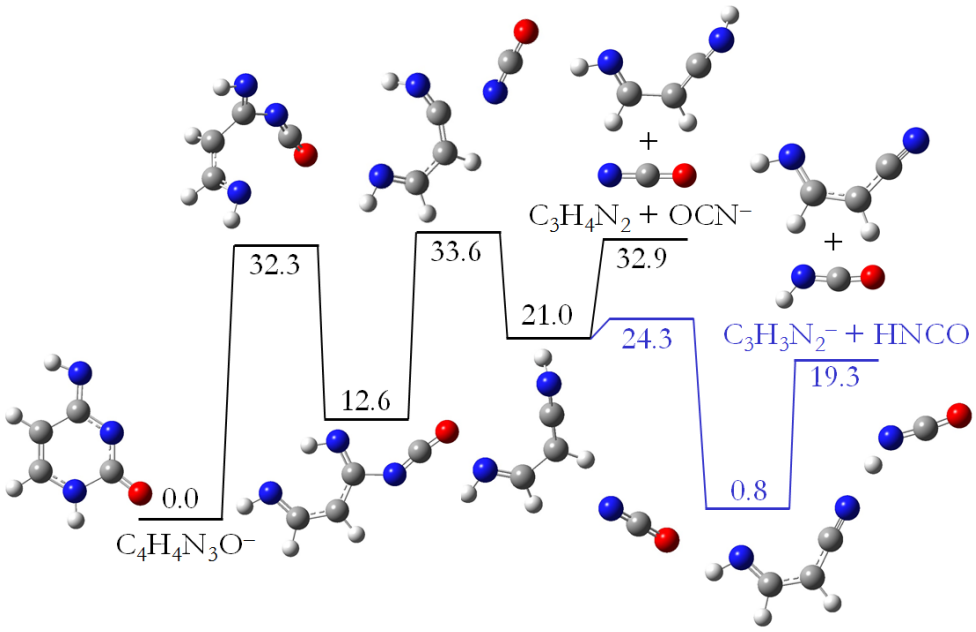

Figure 6.11
Two pathways (kcal mol^{-1}) calculated at the B3LYP/6-311++G(d,p) level of theory are shown for the CID of N_3 deprotonated cytosine. The most abundant experimentally observed product, $C_3H_3N_2^-$, corresponds to HNCO loss (blue). The second product channel forms OCN^- and $C_3H_4N_2$ (black).

6.3.4 Astrochemical Relevance

In certain situations, fragmentation can be considered the reverse of synthesis. Therefore, the products of a fragmentation process lend insights into possible precursors. In considering Figure 6.3, Figure 6.10, and Figure 6.11, many of the neutral fragments that are formed have been detected in the ISM: CO_2, HNCO, and HNC. HNCO (isocyanic acid) has been detected in many areas of the ISM and for this reason is used as an environmental diagnostic for different interstellar regions.[79,80] We observe HNCO loss from uracil-5-carboxylic acid as well as cytosine. The ionic CID products observed in this study involve one detected (OCN^-)[50,81] and several potential (II, III, IV, HC_2O^-, and $C_3H_3N_2^-$) interstellar species. The fragmentation of uracil, thymine, and cytosine all yield OCN^-. The OCN^- anion is present in interstellar ices,[50] supporting the prospect of pyrimidine formation in ice mantles. Additionally, cyanate is predicted to exist in the presence of H_2O in Titan's atmosphere.[82] This highlights the importance of further extraterrestrial searches for pyrimidine molecules, particularly in dense clouds and atmospheres where N-heterocycles and larger organics are predicted to be stable.[83]

Deprotonated imidoylketene reactivity is also astrochemically relevant. This molecule can isomerize into many different heterocyclic structures including azoles,[84,85] and has been long recognized as a molecule of cosmochemical interest.[51] The ability of imidoylketene to form ring structures suggests its involvement in N-heterocycle synthesis.[41] Additionally, the future interstellar detection of imidoylketene is promising due to the detection of its isomer, oxiranecarbonitrile.[53,54] Our study unveils interesting reactions for deprotonated imidoylketene (IV) with interstellar triatomic sulfur-containing molecules (OCS and SO_2) involving association and subsequent CO_2 loss. These reactions provide important suggestions for gas-phase sulfur incorporation into larger organic species.

6.4 Conclusion

According to NASA, the origin of terrestrial life is among the three basic topics addressed by the field of astrobiology.[86] The study of nucleobases, from their reactivity and fragmentation to their prebiotic synthesis routes, is essential in this effort. For the Murchison, Murray, and Orgueil carbonaceous meteorites, uracil was the only pyrimidine nucleobase detected in all three,[10] supporting the theory of its exogenous synthesis and delivery to early Earth.[3] Although neither thymine nor cytosine have yet been detected in meteorites, the possibility of their presence has not been eliminated.[12] Interstellar detections of nucleobases remain inconclusive, although the abundance of interstellar nitrogen and aromatic organics is well known.[26] These data have motivated the proposal of many prebiotic formation pathways to the pyrimidines,[6-12,14,15] but anions are commonly missing reagents in these endeavors.

Recent studies have used fragmentation to reveal possible biomolecule synthesis routes.[34,35] Our investigation similarly examines the dissociation of deprotonated uracil-5-carboxylic acid ($C_5H_3N_2O_4^-$), and deprotonated uracil, thymine, and cytosine to decipher the chemistry of important pyrimidine precursors. Through decarboxylation and/or HNCO loss from $C_5H_3N_2O_4^-$, N_1 deprotonated uracil ($C_4H_3N_2O_2^-$), deprotonated imidoylketene carboxylic acid ($C_4H_2NO_3^-$), and deprotonated imidoylketene ($C_3H_2NO^-$) are produced in a modified Finnigan LCQ Deca XP Plus ion trap. The structures of these ions are verified through theoretical calculations, experimental acidity bracketing, and further fragmentation. Our experimental acidity brackets of $C_5H_3N_2O_4^-$, $C_4H_3N_2O_2^-$, and $C_3H_2NO^-$ ($\Delta H°_{acid}$), $< 323.540 \pm 0.050$, 336.9 ± 2.1 kcal mol^{-1}, and 357.5 ± 6.1 kcal mol^{-1} respectively, agree well with calculated values for our predicted structures of these ions. Further fragmentation results also support our structural identifications. Deprotonated imidoylketene further dissociates into HNC and HC_2O^-. Previous studies have reported comparable fragments for positive

ion studies of uracil,[41] and computational explorations of uracil bond strengths predict that our fragments are reasonable.[70] Notably, imidoylketene itself is a molecule of cosmochemical interest[51] that has been proposed to react to form larger cyclic species, supporting its potential as an N-heterocycle precursor.[52] N_1 deprotonated uracil fragments to form OCN^- and imidoylketene, two possible uracil precursors. Thymine both isomerizes and fragments in a similar fashion, producing OCN^- and methyl-substituted imidoylketene upon CID. Cytosine dissociation allows for proton transfer from $C_3H_4N_2$ to OCN^-, forming HNCO in a more energetically favorable process than cyanate formation. Ice mantles may provide favorable conditions for complex organic molecule formation,[5] and the presence of OCN^- in interstellar ices provides an essential ingredient for pyrimidine synthesis there.

The reactivity of deprotonated imidoylketene ($C_3H_2NO^-$) is examined with a set of neutral reagents including several detected interstellar molecules (SO_2, OCS, CS_2, NO, N_2O, CO, NH_3, O_2, and C_2H_4). An interesting pattern of reactivity is observed for the sulfur-containing triatomic reagents. Deprotonated imidoylketene reveals a mechanism involving association and CO_2 production. SO_2 reacts very efficiently (k_{exp}/k_{col} = 0.56), and the largest calculated barrier to its reaction is 14.0 kcal mol^{-1} below the energy of the reactants. The potential energy surface for the analogous OCS reaction is much flatter and involves higher overall barriers (≥ 6.3 kcal mol^{-1} below the reactant energy), leading to a lower overall reaction efficiency (0.0050). Product ions were visible in trace amounts for the reaction with CS_2, but the reaction rate constant was immeasurably small ($k_{exp} \leq 1 \times 10^{-13}$ cm^3 s^{-1}). The calculated barrier of +1.2 kcal mol^{-1} along the potential energy surface of this reaction is sufficient to prevent the reaction of the near-thermal ions in our ion trap apparatus.

In summary, we have outlined a comprehensive examination of the deprotonated pyrimidine nucelobases and related anions. Our data support the involvement of anions in more complex

biomolecule formation, although they are often overlooked as reagents in prebiotic syntheses. The fragmentation and reaction processes reported herein yield many interstellar ions and neutral molecules, providing important connections among these species. Along with the continued search for nucleobases and other N-heterocycles, these data motivate the further inclusion of anions in proposed prebiotic formation routes to nucleobases.

6.5 References

1 L. E. Orgel, *Prebiotic Chemistry and the Origin of the RNA World*. Crit. Rev. Biochem. Mol. Biol., **2004**, *39*, 99-123.

2 K. Kobayashi; Y. Takano; H. Masuda; H. Tonishi; T. Kaneko; H. Hashimoto; T. Saito, *Possible Cometary Organic Compounds as Sources of Planetary Biospheres*. In *Space Life Sciences: Search for Signatures of Life, and Space Flight Environmental Effects on the Nervous System*, Horneck, G.; Levasseur Regourd, A. C.; Rabin, B. M.; Slenzka, K. B., Eds. 2004; Vol. 33, 1277-1281.

3 C. Chyba; C. Sagan, *Endogenous Production, Exogenous Delivery, and Impact-Shock Synthesis of Organic Molecules - An Inventory for the Origins of Life*. Nature, **1992**, *355*, 125-132.

4 J. Oro, *Comets and Formation of Biochemical Compounds on Primitive Earth*. Nature, **1961**, *190*, 389-390.

5 E. Herbst, *Three Milieux for Interstellar Chemistry: Gas, Dust, and Ice*. Phys. Chem. Chem. Phys., **2014**, *16*, 3344-3359.

6 V. P. Gupta; P. Tandon; P. Mishra, *Some New Reaction Pathways for the Formation of Cytosine in Interstellar Space - A Quantum Chemical Study*. Adv. Space Res., **2013**, *51*, 797-811.

7 A. Horn; H. Mollendal; J.-C. Guillemin, *A Quantum Chemical Study of the Generation of a Potential Prebiotic Compound, Cyanoacetaldehyde, and Related Sulfur Containing Species*. J. Phys. Chem. A, **2008**, *112*, 11009-11016.

8 P. P. Bera; T. J. Lee; H. F. Schaefer, *Are Isomers of the Vinyl Cyanide Ion Missing Links for Interstellar Pyrimidine Formation?* J. Chem. Phys., **2009**, *131*, 074303.

9 P. P. Bera; M. Nuevo; S. N. Milam; S. A. Sandford; T. J. Lee, *Mechanism for the Abiotic Synthesis of Uracil via UV-Induced Oxidation of Pyrimidine in Pure H_2O Ices Under Astrophysical Conditions*. J. Chem. Phys., **2010**, *133*, 104303.

10 M. Nuevo; S. N. Milam; S. A. Sandford; J. E. Elsila; J. P. Dworkin, *Formation of Uracil from the Ultraviolet Photo-Irradiation of Pyrimidine in Pure H_2O Ices*. Astrobiology, **2009**, *9*, 683-695.

11 C. K. Materese; M. Nuevo; P. P. Bera; T. J. Lee; S. A. Sandford, *Thymine and Other Prebiotic Molecules Produced from the Ultraviolet Photo-Irradiation of Pyrimidine in Simple Astrophysical Ice Analogs*. Astrobiology, **2013**, *13*, 948-962.

12 S. A. Sandford; M. Nuevo; C. K. Materese, Formation of Nucleobases from the UV Irradiation of Pyrimidine in Astrophysical Ice Analogs. *Lunar and Planetary Science Conference* Houston, TX, 2014.

13 A. J. Remijan; L. E. Snyder; B. A. McGuire; H.-L. Kuo; L. W. Looney; D. N. Friedel; G. Y. Golubiatnikov; F. J. Lovas, et al., *Observational Results of a Multi-telescope Campaign in Search of Interstellar Urea [$(NH_2)_2CO$]*. Astrophys. J., **2014**, *783*, 77-92.

14 T. Wang; J. H. Bowie, *Can Cytosine, Thymine and Uracil be Formed in Interstellar Regions? A Theoretical Study*. Org. Biomolec. Chem., **2012**, *10*, 652-662.

15 M. P. Robertson; S. L. Miller, *An Efficient Prebiotic Synthesis of Cytosine and Uracil*. Nature, **1995**, *375*, 772-774.

16 H. Gupta; C. A. Gottlieb; V. Lattanzi; J. C. Pearson; M. C. McCarthy, *Laboratory Measurements and Tentative Astronomical Identification of H_2NCO^+*. Astrophys. J. Lett., **2013**, *778*, L1-L5.

17 G. Danger; F. Duvernay; P. Theule; F. Borget; J. C. Guillemin; T. Chiavassa, *Hydroxyacetonitrile ($HOCH_2CN$) as a Precursor for Formylcyanide (CHOCN), Ketenimine (CH_2CNH), and Cyanogen (NCCN) in Astrophysical Conditions*. Astron. Astrophys., **2013**, *549*, A93.

18 C. Barckholtz; T. P. Snow; V. M. Bierbaum, *Reactions of C_n^- and C_nH^- with Atomic and Molecular Hydrogen*. Astrophys. J. Lett., **2001**, *547*, L171-L174.

19 B. Eichelberger; T. P. Snow; C. Barckholtz; V. M. Bierbaum, *Reactions of H, N, and O Atoms with Carbon Chain Anions of Interstellar Interest: An Experimental Study*. Astrophys. J., **2007**, *667*, 1283-1289.

20 R. Hayatsu, *Orgueil Meteorite - Organic Nitrogen Contents*. Science, **1964**, *146*, 1291-1293.

21 C. E. Folsome; J. Lawless; M. Romiez; C. Ponnampe, *Heterocyclic Compounds Indigenous to Murchison Meteorite*. Nature, **1971**, *232*, 108-109.

22 P. G. Stoks; A. W. Schwartz, *Uracil in Carbonaceous Meteorites*. Nature, **1979**, *282*, 709-710.

23 R. Shapiro, *Prebiotic Cytosine Synthesis: A Critical Analysis and Implications for the Origin of Life*. Proc. Nat. Acad. Sci. U. S. A., **1999**, *96*, 4396-4401.

24 K. E. Nelson; M. P. Robertson; M. Levy; S. L. Miller, *Concentration by Evaporation and the Prebiotic Synthesis of Cytosine*. Origin Life Evol. Bio., **2001**, *31*, 221-229.

25 M. P. Callahan; K. E. Smith; H. J. Cleaves, II; J. Ruzicka; J. C. Stern; D. P. Glavin; C. H. House; J. P. Dworkin, *Carbonaceous Meteorites Contain a Wide Range of Extraterrestrial Nucleobases*. Proc. Natl. Acad. Sci. U. S. A., **2011**, *108*, 13995-13998.

26 Z. Peeters; O. Botta; S. B. Charnley; R. Ruiterkamp; P. Ehrenfreund, *The Astrobiology of Nucleobases*. Astrophys. J., **2003**, *593*, L129-L132.

27 S. Brünken; M. C. McCarthy; P. Thaddeus; P. D. Godfrey; R. D. Brown, *Improved Line Frequencies for the Nucleic Acid Base Uracil for a Radioastronomical Search*. Astron. Astrophys., **2006**, *459*, 317-320.

28 E. Herbst; E. F. van Dishoeck, *Complex Organic Interstellar Molecules*. Annu. Rev. Astron. Astrophys., **2009**, *47*, 427-480.

29 Y. J. Kuan; S. B. Charnley; H. C. Huang; W. L. Tseng; Z. Kisiel, *Interstellar Glycine*. Astrophys. J., **2003**, *593*, 848-867.

30 Y. J. Kuan; S. B. Charnley; H. C. Huang; Z. Kisiel; P. Ehrenfreund; W. L. Tseng; C. H. Yan, *Searches for Interstellar Molecules of Potential Prebiotic Importance*. Adv. Space. Res., **2004**, *33*, 31-39.

31 Y. J. Kuan; H. C. Huang; S. B. Charnley; W. L. Tseng; L. E. Snyder; P. Ehrenfreund; Z. Kisiel; S. Thorwirth, et al., *Prebiologically Important Interstellar Molecules*. Bioastronomy 2002: Life among the Stars, **2004**, 185-188.

32 S. B. Charnley; Y. J. Kuan; H. C. Huang; O. Botta; H. M. Butner; N. Cox; D. Despois; P. Ehrenfreund, et al., *Astronomical Searches for Nitrogen Heterocycles*. In *Space Life Sciences: Astrobiology: Steps toward Origin of Life and Titan before Cassini*, 2005; Vol. 36, 137-145.

33 Y. J. Kuan; C. H. Yan; S. B. Charnley; Z. Kisiel; P. Ehrenfreund; H. C. Huang, *A Search for Interstellar Pyrimidine*. Mon. Not. Roy. Astron. Soc., **2003**, *345*, 650-656.

34 A. Simakov; G. B. S. Miller; A. J. C. Bunkan; M. R. Hoffmann; E. Uggerud, *The Dissociation of Glycolate – Astrochemical and Prebiotic Relevance*. Phys. Chem. Chem. Phys., **2013**, *15*, 16615-16625.

35 E. L. Zins; C. Pirim; L. Vettier; M. Chaboud; L. Krim, *May Interstellar Leucine React with NO Radicals Present in Interstellar/Interplanetary Medium? An Ion-Trap Mass Spectrometry Study*. Int. J. Mass Spectrom., **2013**, *348*, 47-52.

36 Z. Lin; D. Talbi; E. Roueff; E. Herbst; N. Wehres; C. A. Cole; Z. Yang; T. P. Snow, et al., *Can Interstellar Propene (CH_3CHCH_2) be Formed via Gas-Phase Reactions?* Astrophys. J., **2013**, *765*, 80-84.

37 C. A. Cole; N. Wehres; Z. Yang; D. L. Thomsen; T. P. Snow; V. M. Bierbaum, *A Gas-Phase Formation Route to Interstellar Trans-Methyl Formate*. Astrophys. J. Lett., **2012**, *754*, L5-L8.

38 Z. Yang; C. A. Cole; O. Martinez, Jr.; M. Y. Carpenter; T. P. Snow; V. M. Bierbaum, *Experimental and Theoretical Studies of Reactions Between H atoms and Nitrogen-Containing Carbanions*. Astrophys. J., **2011**, *739*, 19-29.

39 C. A. Cole; N. J. Demarais; Z. Yang; T. P. Snow; V. M. Bierbaum, *Heterocyclic Anions of Astrobiological Interest*. Astrophys. J., **2013**, *779*, 181-190.

40 C. C. Nelson; J. A. McCloskey, *Collision-Induced Dissociation of Uracil and its Derivatives*. J. Am. Soc. Mass Spectrom., **1994**, *5*, 339-349.

41 D. G. Beach; W. Gabryelski, *Revisiting the Reactivity of Uracil During Collision Induced Dissociation: Tautomerism and Charge-Directed Processes*. J. Am. Soc. Mass Spectrom., **2012**, *23*, 858-868.

42 R. Rodriguez-Fernandez; S. A. Vazquez; E. Martinez-Nunez, *Collision-Induced Dissociation Mechanisms of Li(uracil)$^+$*. Phys. Chem. Chem. Phys., **2013**, *15*, 7628-7637.

43 Z. Yang; M. T. Rodgers, *Tautomerization in the formation and collision-induced dissociation of alkali metal cation-cytosine complexes*. Physical Chemistry Chemical Physics, **2012**, *14*, 4517-4526.

44 B. Barc; M. Ryszka; J. Spurrell; M. Dampc; P. Limao-Vieira; R. Parajuli; N. J. Mason; S. Eden, *Multi-Photon Ionization and Fragmentation of Uracil: Neutral Excited-State Ring Opening and Hydration Effects*. J. Chem. Phys., **2013**, *139*, 244311.

45 B. Yang; R. Wu; G. Berden; J. Oomens; M. Rodgers, *Infrared Multiple Photon Dissociation Action Spectroscopy of Proton-Bound Dimers of Cytosine and Modified Cytosines: Effects of Modifications on Gas-Phase Conformations*. J. Phys. Chem. B, **2013**, *117*, 14191-14201.

46 F. F. da Silva; C. Matias; D. Almeida; G. Garcia; O. Ingolfsson; H. D. Flosadottir; B. Omarsson; S. Ptasinska, et al., *NCO^-, a Key Fragment Upon Dissociative Electron Attachment and Electron Transfer to Pyrimidine Bases: Site Selectivity for a Slow Decay Process*. J. Am. Soc. Mass Spectrom., **2013**, *24*, 1787-1797.

47 J. Tabet; S. Eden; S. Feil; H. Abdoul-Carime; B. Farizon; M. Farizon; S. Ouaskit; T. D. Mark, *20-150 keV Proton Impact-Induced Ionization of Uracil: Fragmentation Ratios and Branching Ratios for Electron Capture and Direct Ionization*. Phys. Rev. A: At., Mol., Opt. Phys., **2010**, *81*, 012711.

48 J. de Vries; R. Hoekstra; R. Morgenstern; T. Schlathoelter, *Ionization and Fragmentation Modes of Nucleobases after Collisions with Multiply Charged Ions*. Phys. Scr., **2004**, *T110*, 336-339.

49 J. d. Vries; R. Hoekstra; R. Morgenstern; T. Schlathölter, *Multiple Ionization and Fragmentation of the DNA Base Thymine by Interaction with C^{q+} ions*. Euro Phys. J. D, **2003**, *24*, 161-164.

50 B. T. Soifer; R. C. Puetter; R. W. Russell; S. P. Willner; P. M. Harvey; F. C. Gillett, *4–8 Micron Spectrum of the Infrared Source W33-A*. Astrophys. J., **1979**, *232*, L53-L57.

51 C. Wentrup; H. Briehl; P. Lorencak; U. J. Vogelbacher; H. W. Winter; A. Maquestiau; R. Flammang, *Primary Ethynamines ($HC{\equiv}CNH_2$, $PhC{\equiv}CNH_2$), Aminopropadienone ($H_2NCH{=}C{=}C{=}O$), and Imidoylketene ($HN{=}CHCH{=}C{=}O$) - Preparation and Identification of Molecules of Cosmochemical Interest*. J. Am. Chem. Soc., **1988**, *110*, 1337-1343.

52 A. Pena-Gallego; J. Rodriguez-Oteroa; E. M. Cabaleiro-Lago, *A DFT Study of the 4+2 Cycloadditions of Conjugated Ketenes (Vinylketene, Imidoylketene and Formylketene) with Formaldimine. The Pericyclic or Pseudopericyclic Character from Magnetic Properties*. Tetrahedron, **2007**, *63*, 4937-4943.

53 J. E. Dickens; W. M. Irvine; M. Ohishi; G. Arrhenius; S. Pitsch; A. Bauder; F. Muller; A. Eschenmoser, *A Search for Interstellar Oxiranecarbonitrile (C_3H_3NO)*. Origins Life Evol. Biospheres, **1996**, *26*, 97-110.

54 M. Behnke; I. Medvedev; M. Winnewisser; F. C. De Lucia; E. Herbst, *The Millimeter- and Submillimeter-Wave Spectrum of Oxiranecarbonitrile*. Astrophys. J. Suppl. Ser., **2004**, *152*, 97-101.

55 S. Gronert, *Estimation of Effective Ion Temperatures in a Quadrupole Ion Trap*. J. Am. Soc. Mass Spectrom., **1998**, *9*, 845-848.

56 S. K. Koehn; N. L. Tran; S. Gronert; W. M. Wu, *The Stability of Aryl Carbanions Derived from Pyridine N-Oxide: The Role of Resonance in Stabilizing Aryl Anions*. J. Am. Chem. Soc., **2010**, *132*, 390-395.

57 N. A. Senger; C. E. Bliss; J. R. Keeffe; S. Gronert; W. Wu, *Stabilities of Uracil and Pyridone-based Carbanions: a Systematic Study in the Gas Phase and Solution and Implications for the Mechanism of Orotidine-5 '-Monophosphate Decarboxylase*. Tetrahedron, **2013**, *69*, 5287-5292.

58 S. Gronert, *Quadrupole Ion Trap Studies of Fundamental Organic Reactions*. Mass Spectrom. Rev., **2005**, *24*, 100-120.

59 G. E. Reid; R. A. J. O'Hair; M. L. Styles; W. D. McFadyen; R. J. Simpson, *Gas Phase Ion-Molecule Reactions in a Modified Ion Trap: H/D Exchange of Non-Covalent Complexes and Coordinatively Unsaturated Platinum Complexes*. Rapid Commun. Mass Spectrom., **1998**, *12*, 1701-1708.

60 S. Gronert; C. H. DePuy; V. M. Bierbaum, *Deuterium-Isotope Effects in Gas-Phase Reactions of Alkyl-Halides - Distinguishing E2 and S_N2 Pathways*. J. Am. Chem. Soc., **1991**, *113*, 4009-4010.

61 C. H. DePuy; S. Gronert; A. Mullin; V. M. Bierbaum, *Gas-Phase S_N2 and E2 Reactions of Alkyl-Halides*. J. Am. Chem. Soc., **1990**, *112*, 8650-8655.

62 M. J. Frisch; G. W. Trucks; H. B. Schlegel; G. E. Scuseria; M. A. Robb; J. R. Cheeseman; J. A. Montgomery; T. Vreven, et al., Gaussian 03, Revision C.02. Gaussian Inc. Wallingford, CT 2003.

63 M. J. Frisch; G. W. Trucks; H. B. Schlegel; G. E. Scuseria; M. A. Robb; J. R. Cheeseman; G. Scalmani; V. Barone, et al., Gaussian 09 Revision A.02. Gaussian Inc. Wallingford, CT: 2009.

64 S. S. Bokatzian-Johnson; M. L. Stover; D. A. Dixon; C. J. Cassady, *Gas-Phase Deprotonation of the Peptide Backbone for Tripeptides and Their Methyl Esters with Hydrogen and Methyl Side Chains*. J. Phys. Chem. B, **2012**, *116*, 14844-14858.

65 S. Kumari; C. L. Devi; S. Prabhakar; K. Bhanuprakash; M. Vairaman, *Estimation of Gas-Phase Acidities of Deoxyribonucleosides: An Experimental and Theoretical Study*. J. Am. Soc. Mass Spectrom., **2010**, *21*, 136-143.

66 *NIST Chemistry WebBook, NIST Standard Reference Database Number 69*. National Institute of Standards and Technology, webbook.nist.gov, accessed 2010-2014.

67 Y. Q. Huang; H. I. Kenttämaa, *Theoretical Estimations of the 298 K Gas-Phase Acidities of the Pyrimidine-Based Nucleobases Uracil, Thymine, and Cytosine*. J. Phys. Chem. A, **2003**, *107*, 4893-4897.

68 C. H. DePuy; V. M. Bierbaum; R. Damrauer; J. A. Soderquist, *Gas-Phase Reactions of the Acetyl Anion*. J. Am. Chem. Soc., **1985**, *107*, 3385-3386.

69 A. J. Cohen; P. Mori-Sanchez; W. Yang, *Insights into Current Limitations of Density Functional Theory*. Science, **2008**, *321*, 792-794.

70 L. S. Arani; P. Mignon; H. Abdoul-Carime; B. Farizon; M. Farizon; H. Chermette, *DFT Study of the Fragmentation Mechanism of Uracil RNA Base*. Phys. Chem. Chem. Phys., **2012**, *14*, 9855-9870.

71 T. Su; W. J. Chesnavich, *Parametrization of the Ion-Polar Molecule Collision Rate-Constant by Trajectory Calculations*. J. Chem. Phys., **1982**, *76*, 5183-5185.

72 G. Gioumousis; D. P. Stevenson, *Reactions of Gaseous Molecule Ions with Gaseous Molecules. 5. Theory*. J. Chem. Phys., **1958**, *29*, 294-299.

73 C. H. DePuy; V. M. Bierbaum, *Gas Phase Sulfur Anions: Synthesis and Reactions of H_2NS^- and Related Ions*. Tetrahedron Lett., **1981**, *22*, 5129-5130.

74 S. Feil; K. Gluch; S. Matt-Leubner; P. Scheier; J. Limtrakul; M. Probst; H. Deutsch; K. Becker, et al., *Partial Cross Sections for Positive and Negative Ion Formation Following Electron Impact on Uracil*. J. Phys. B, **2004**, *37*, 3013-3020.

75 M. J. Scanlan; I. H. Hillier, *An Ab Initio Study of Tautomerism of Uracil, Thymine, 5-Fluorouracil, and Cytosine*. J. Am. Chem. Soc., **1984**, *106*, 3737-3745.

76 J. Y. Salpin; S. Guillaumont; J. Tortajada; L. MacAleese; J. Lemaire; P. Maitre, *Infrared Spectra of Protonated Uracil, Thymine and Cytosine*. ChemPhysChem, **2007**, *8*, 2235-2244.

77 P. Ü. Civcir, *A Theoretical Study of Tautomerism of Cytosine, Thymine, Uracil and their 1-Methyl Analogues in the Gas and Aqueous Phases using AM1 and PM3*. J. Mol. Struc. - Theo. Chem., **2000**, *532*, 157-169.

78 F. A. Gianturco; F. Sebastianelli; R. Lucchese; I. Baccarelli; N. Sanna, *Ring-Breaking Electron Attachment to Uracil: Following Bond Dissociations via Evolving Resonances*. J. Chem. Phys., **2008**, *128*, 174302.

79 D. Quan; E. Herbst; Y. Osamura; E. Roueff, *Gas-Grain Modeling of Isocyanic Acid (HNCO), Cyanic Acid (HOCN), Fulminic Acid (HCNO), and Isofulminic Acid (HONC) in Assorted Interstellar Environments*. Astrophys. J., **2010**, *725*, 2101-2109.

80 D. M. Tideswell; G. A. Fuller; T. J. Millar; A. J. Markwick, *The Abundance of HNCO and Its Use as a Diagnostic of Environment*. Astron. Astrophys., **2010**, *510*, A85.

81 V. Lattanzi; C. A. Gottlieb; P. Thaddeus; S. Thorwirth; M. C. McCarthy, *The Rotational Spectrum of the NCO^- Anion*. Astrophys. J., **2010**, *720*, 1717-1720.

82 R. Hudson; M. Moore, *Reactions of Nitriles in Ices Relevant to Titan, Comets, and the Interstellar Medium: Formation of Cyanate Ion, Ketenimines, and Isonitriles*. Icarus, **2004**, *172*, 466-478.

83 Z. Peeters; O. Botta; S. B. Charnley; Z. Kisiel; Y. J. Kuan; P. Ehrenfreund, *Formation and Photostability of N-Heterocycles in Space - I. The Effect of Nitrogen on the Photostability of Small Aromatic Molecules*. Astron. Astrophys., **2005**, *433*, 583-590.

84 M. T. Nguyen; T. K. Ha; R. A. M. Oferrall, *An Ab Initio Study of the Cyclization and Rearrangement of Vinylketene, Imidoylketene, and Formylketene*. J. Org. Chem., **1990**, *55*, 3251-3256.

85 S. Vijayakumar; P. Kolandaivel, *Isomerization of C_3H_3NO Isomers: Ab Initio Study*. Mol. Phys., **2006**, *104*, 1401-1411.

86 D. J. D. Marais; J. A. Nuth, III; L. J. Allamandola; A. P. Boss; J. D. Farmer; T. M. Hoehler; B. M. Jakosky; V. S. Meadows, et al., *The NASA Astrobiology Roadmap*. Astrobiology, **2008**, *8*, 715-730.

CHAPTER 7

Gas–Phase Chemistry of Deprotonated Purines

7.1 Introduction

Purines are among the most abundant nitrogen-containing heterocyclic molecules in nature.[1] Included among these heterocycles is a diverse array of biomolecules. Two important purines, guanine and adenine, are essential subunits of deoxyribonucleic and ribonucleic acid (DNA and RNA) and therefore carry the genetic information of terrestrial life. Knowledge of their structure and dissociation mechanisms provides a deeper understanding of their probable formation beyond the terrestrial sphere. Key questions in astrobiology regarding the origin of life and the existence of extraterrestrial life depend on the syntheses of molecules such as these in interstellar and planetary environments. Since the well-known experiments of Miller and Urey,[2] the origin of complex organic molecules has been extensively studied. Even so, the process by which purine nucleobases came into being is still a topic of debate. To frame this chapter, an overview of previous purine detections, syntheses, and dissociation studies is provided below.

Purines have been found in several environments within our solar system, but have yet to be detected in the interstellar medium (ISM). The discovery of adenine and guanine in comets[3] and meteorites[4-8] combined with their extraterrestrial isotopic abundances[9] lends support to the theory of their exogenous formation and delivery to early Earth. Saturn's largest satellite also may be home to these purines; two missions to Titan (Voyager I and Cassini-Huygens) revealed the presence of complex carbon and nitrogen-containing molecules in Titan's atmosphere.[10-12] In addition, adenine has been experimentally shown to form in a simulated Titan atmosphere under irradiation.[13] Although neither guanine nor adenine have been detected in the ISM, their molecular substituents and potential

synthetic precursors are in abundance, particularly in dense molecular clouds. These species may include CO,[14] NH_3,[15] HCN, HNC,[16] HNCO,[17] NH_2CHO,[18] NH_2CN, and HNCNH.[19] Lastly, purines are predicted to form upon molecular cloud collapse[20] and are often extremely stable under interstellar conditions. Adenine stands out among the nucleobases as the molecule with the largest stabilizing resonance energy[21] as well as an increased stability in the presence of ionizing radiation compared to its counterparts.[22] This array of data suggests that both guanine and adenine are feasible interstellar species.

The likelihood of purine persistence in the ISM has motivated a multitude of studies on the abiotic syntheses of these molecules. Adenine is an HCN pentamer ($C_5H_5N_5$). It reasonably follows that the central question of adenine synthesis has been: can five HCN molecules favorably come together to form a pentamer in an abiotic environment?[23] The overall free energy change of the pentamerization process ($\Delta G_{298} = -53.7$ kcal mol^{-1})[23] is highly favorable, but large intermediate barriers and kinetic obstacles also play an important role. Two 2007 studies[23,24] focused on the last step of HCN pentamerization, involving the addition of HCN to 4-aminoimidazole-5-carbonitrile (AICN). Both groups reported kinetic barriers to the neutral-neutral reaction, and suggest ways to overcome this barrier through photoactivation, ammonia catalysis, or water catalysis. Doubt has been cast on the formation of HCN oligomers, however. Computational studies reveal that a 71 kcal mol^{-1} barrier prevents the efficient dimerization of two HCN molecules in the gas phase, and even proton catalysis does not improve the efficiency of the reaction.[25,26] Since the first abiotic synthesis of adenine in an aqueous solution of ammonium cyanide (NH_4CN) and hydrogen cyanide (HCN),[27,28] HCN has been central to proposed adenine formation pathways. The most recent studies have deviated from this pattern, suggesting other precursors such as radicals (HCCN)[29] and retrosynthetic precursors (C_3NH, HNCNH, and NH_2CN).[30] Unlike adenine, whose synthesis has been extensively studied independent of its purine counterpart, guanine synthesis is more frequently examined in conjunction with that of

adenine. Both purine nucleobases were formed through a polymerization process in concentrated solutions of NH_4CN[31] and through irradiation of formamide solutions[32] and ices.[33] Furthermore, free radical reactions involving formamide lead to purines,[34] and formamide is more reactive in addition reactions than HCN,[35] highlighting its potential as a nucleobase precursor.[36,37] To build on these proposed mechanisms, ion-neutral synthesis reactions are important to consider, because they often do not experience the thermodynamic or kinetic barriers that plague neutral-neutral reactions.[38]

Another strategy to illuminate biomolecule formation is to analyze the reverse process. Tandem mass spectrometry involving collision-induced dissociation (CID) paired with theoretical calculations can reveal underlying mechanisms and important precursor molecules to specific syntheses.[39,40] The CID processes of protonated purines[41-43] and purine cations[44] have been thoroughly explored. Other purine fragmentation experiments have focused on electron,[45,46] photon,[47] ion,[48,49] and atom[50] bombardment to achieve molecular dissociation. Several of these studies report the sequential loss of HCN molecules from adenine species, lending support to an HCN precursor.[51] Ammonia and cyanamide are common reported losses from guanine species.[43] In contrast to neutral, cationic, and protonated purines, CID studies on deprotonated purine anions are rare, and those that exist lack computational support for their experimental observations. These studies report the primary losses of NH_3, CH_2N_2, and HNCO[52,53] from deprotonated guanine and HCN and CH_2N_2 loss from deprotonated adenine.[52] Tandem mass spectrometry and theoretical calculations are necessary to conclusively delineate fragment structures in these processes.

The goal of this chapter is to experimentally and computationally explore the CID of the deprotonated purine nucleobases adenine and guanine in an astrobiological context. Building on previous CID work,[52-54] we report novel computational analyses and tandem mass spectrometry results. Experimental product branching fractions and computational energies of reactants,

intermediates, transition states, and products for these CID processes are provided. Fragment structures are verified by acidity bracketing experiments, and include primarily imidazoles and carbonitriles. The combined techniques presented in this work advance the chemical understanding of these systems, and delineate possible anionic precursors to interstellar purines.

7.2 Methods

7.2.1 Experimental

The experimental data are obtained using a modified Finnigan LCQ Deca XP Plus ion trap. This instrument has been outlined in Chapter 2. Here, a brief overview of the instrumental aspects relevant to the current chapter are provided. Guanine and adenine, depicted in Figure 7.1 are deprotonated by electrospray ionization (ESI). A potential difference of 4.5 kV is applied between the spray nozzle and the heated ion transfer tube (250°C), and a sample flow is maintained at 5 μL min^{-1}. Dilute samples (10^{-4} M) of guanine and adenine are prepared in aqueous sodium hydroxide solution with a pH of 8-9 (98% guanine, 99% adenine, HPLC Grade H_2O, Sigma Aldrich; 99.1% NaOH, Fischer Scientific). This sample preparation method is simpler than that described previously.[53] It is well known that the N_9 site on both guanine and adenine is the most acidic.[55-57] Therefore, we expect ESI to readily deprotonate this most favored site.[53]

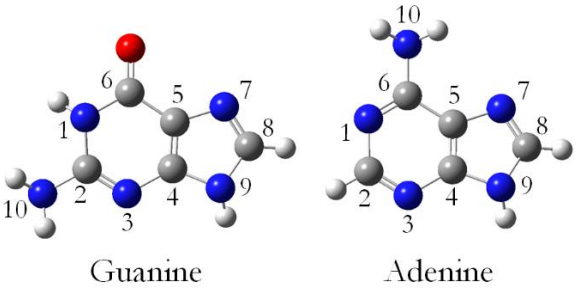

Figure 7.1
Structures of purine molecules.

The deprotonated purine ions travel from the ESI source into the ion trap where they are thermalized by helium at a pressure of ~5.1 x 10^{-3} Torr. This pressure was determined through a calibration process that is characterized in our previous work.[58] Within the ion trap, tandem mass spectrometry (MS^n) experiments are performed by varying the radio frequency amplitudes applied to the end caps, causing higher energy collisions between the trapped ions and the surrounding helium buffer gas. The activation Q, a variable that controls the q_z of the precursor ion, is maintained at 0.30. This normalized collision energy (NCE) is applied for a duration of 30 ms to the end caps prior to scanning the ion abundances, and it ranges from 35-75% depending on the stability of the ion being fragmented. This corresponds to an applied end cap potential of approximately 1.20-1.65 V based on the instrumental calibration used here. Parent and daughter ions are isolated and trapped for up to 5000 ms without significant signal loss. During this time, the reactions between these ions and neutral reagents are monitored. The introduction of neutral reagents is made possible by a modification outlined by Gronert,[59] which utilizes the pre-existing helium buffer gas line to transport these species into the ion trap. Ultra high purity helium (99.999%, Airgas) flows through a line external to the instrument at 1.0 L min^{-1}. A constant pressure of 850 Torr (± 3%) is maintained in this helium line and measured by an absolute pressure gauge. Volatile neutral reagents are introduced into this flow by a syringe pump at flow rates low enough to ensure complete sampling into the gas phase (0.5-5.0 μL min^{-1}), and a very small fraction (~0.1%) of this helium-reagent mixture is sampled into the ion trap itself through a narrow silica capillary. The neutral reagents used in this study include liquefied phenol >85%, propionic acid >99.5%, thiophenol >99%, and aqueous HBr 48% purchased from Sigma-Aldrich, as well as aqueous, ACS grade HCl from Thomas Scientific.

7.2.2 Computational

The *Gaussian 09* suite of programs[60] is implemented to further examine CID processes with the aid of density functional theory (DFT). At the B3LYP/6-311++G(d,p) level of theory, a series of potential energy surface (PES) scans provide data on the energetics of fragmentation. The relative zero-point corrected energies (ΔH_{0K}) of reactants, intermediates, transition states, and products are determined through geometry optimizations and frequency calculations of the local minima and maxima of each PES. Transition state structures are additionally verified using intrinsic reaction coordinate (IRC) analysis.[61,62] Lastly, the gas-phase acidities (ΔH_{298K}) are calculated at the B3LYP/6-311++G(d,p) level of theory with the addition of thermal energy corrections.

7.3 Results and Discussion

7.3.1 Proton Transfer

Intramolecular proton transfer defines nucleobase CID mechanisms.[63] These processes may precede fragmentation due to their comparatively low energy barriers, and the resulting geometry changes from proton transfer[64] may dictate the fragmentation process. The ease of proton transfer displayed by nucleobases also increases the complexity of CID due to the array of accessible starting structures. The proton transfer processes leading to several guanine and adenine isomers are shown in Figure 7.2 and Figure 7.3 and are discussed below.

Previous studies of neutral guanine show that four of the most stable isomers lie within 1 kcal mol^{-1} of each other,[65] providing several interchangeable low energy species. Similarly, Figure 7.2 depicts our calculation of the tautomers and rotamers of deprotonated guanine, revealing ten stable structures (G1-G10) within ~10 kcal mol^{-1} of one another. All energies are shown with respect to N_9 deprotonated guanine (G3). For each set of rotamers indicated by arrows (G4, G5, and G9), the most

stable structure is pictured. Notably, two structures (G1 and G2) are lower in energy than G3, whose structure results from deprotonating the most acidic site on the molecule. Many of the stable structures shown may be accessible during the ESI process.

Several structural changes occur along the surface shown in Figure 7.2. The conversion between imine and amine causes the C_2-N_{10} bond to have the most variable geometry change among all the structures. G3, an abundant anion produced directly from ESI, has the longest C_2-N_{10} bond (1.42 Å), increasing the likelihood of dissociation at that site upon CID. Similarly, the N_1-C_2 bond distance varies among the structures. G7 has the longest N_1-C_2 bond distance (1.43 Å) of all isomers, suggesting this structure may precede a pyrimidine ring opening at that site. Moreover, the N_1-C_6 and C_2-N_3 bonds are important to the structural integrity of deprotonated guanine.[53] Both G1 and G8 have elongated N_1-C_6 and C_2-N_3 bonds compared to their isomeric counterparts, although G1 has slightly longer bonds than G8 (1.44 and 1.37 Å, respectively). A concurrent dissociation of the pyrimidine ring at these two sites may lead to the loss of HNCNH and NH_2CN from G1 and G8, respectively. These geometry changes are therefore critical to the CID results that will be discussed in a later section.

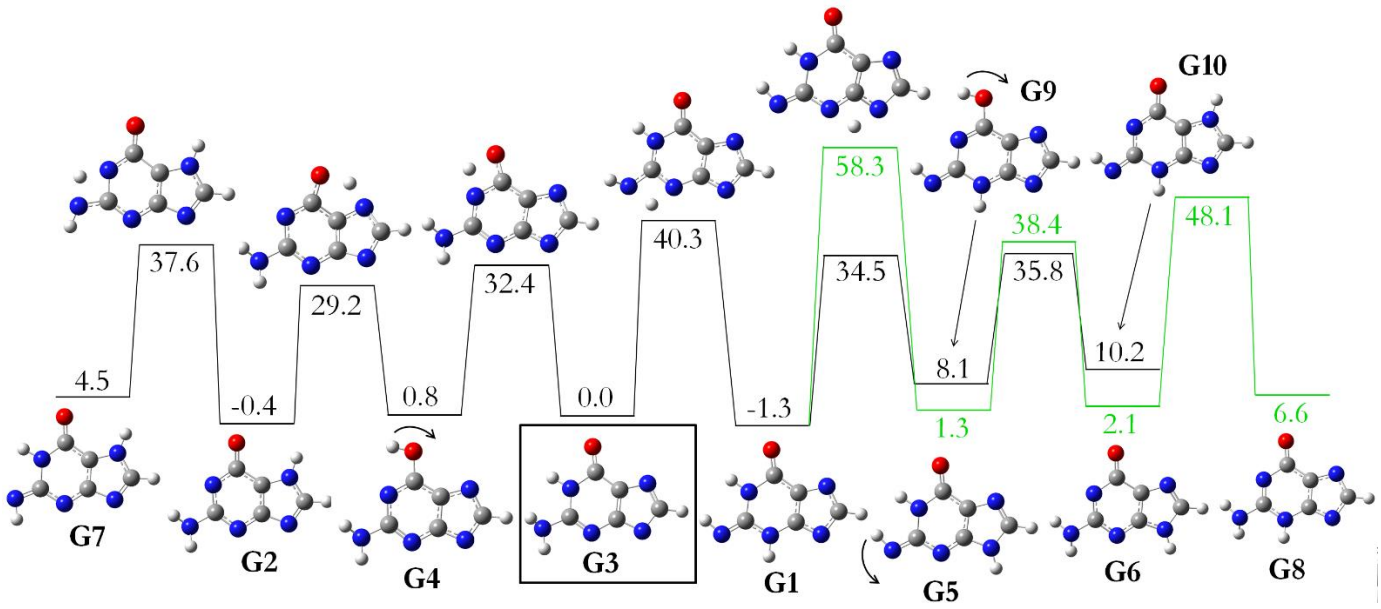

Figure 7.2
Structures involved in the intramolecular proton transfers of N_9 deprotonated guanine (G3) are numbered from lowest to highest zero point corrected energies (G1-G10, kcal mol^{-1}) and are calculated at the B3LYP/6-311++G(d,p) level of theory. Not all transition state structures are shown.

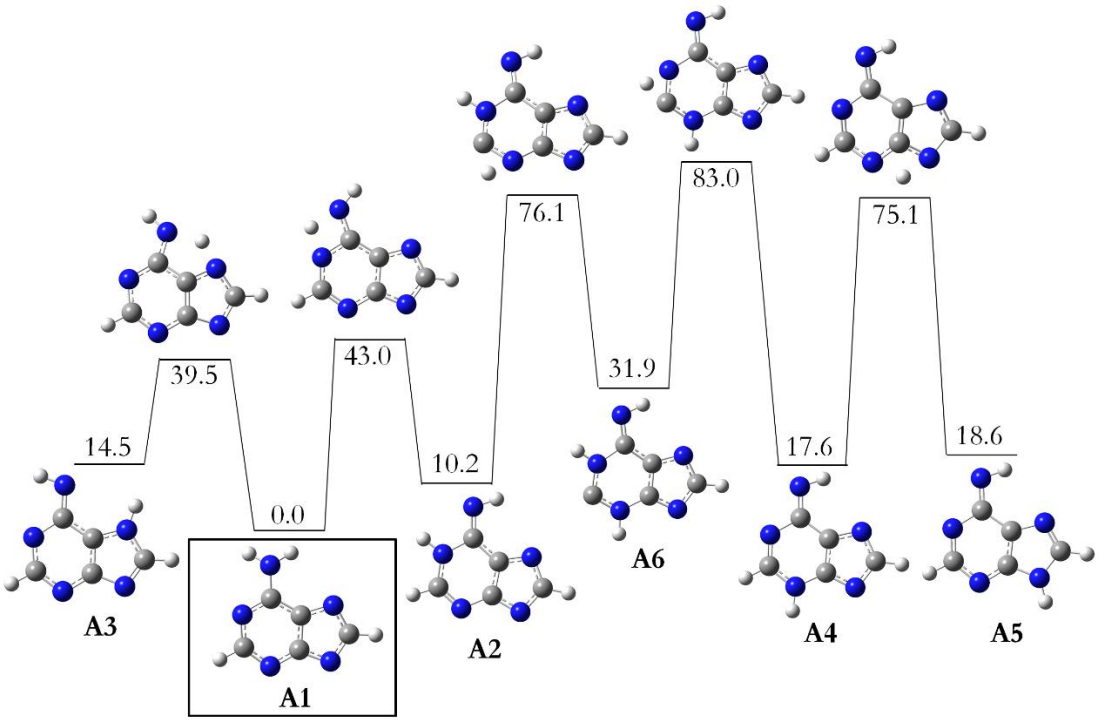

Figure 7.3
Intramolecular proton transfers of N_9 deprotonated adenine (A1) are numbered from lowest to highest zero point corrected energies (A1-A6, kcal mol^{-1}) and are calculated at the B3LYP/6-311++G(d,p) level of theory.

The proton transfer processes of deprotonated adenine differ significantly from those of deprotonated guanine. Figure 7.3 shows the conversion of A1, the N_9 deprotonated ion produced by ESI, into several other isomers (A2-A6). Unlike guanine, whose tautomers and rotamers have very similar low energies, the tautomer closest to A1 is higher in energy by 10.2 kcal mol^{-1} (A2). The height of barriers to proton transfer also greatly increase from deprotonated guanine to adenine, with a maximum barrier to proton transfer of 58.3 kcal mol^{-1} in guanine compared to 83.0 kcal mol^{-1} in adenine. These high barriers have led previous researchers to propose the role of tunneling in the proton transfer of adenine.[64] Two adenine tautomers, A6 and A4, have structures that are particularly conducive to dissociation of the pyrimidine ring structure. A4 has the longest C_6-N_1 and C_2-N_3 combined bond lengths, 1.42 and 1.37 Å, respectively. Similarly, A6 has the longest combined bond lengths for the C_6-N_1 (1.43 Å) and N_3-C_4 (1.39 Å) bonds. The bond strengths between the N_1, C_2, N_3, C_4, and C_6 atoms play a very important role in the structural stability of adenine. These proton transfer-induced geometry changes will aid our further discussion of deprotonated adenine CID.

7.3.2 Experimental Dissociation Results

Experimental data reveal distinctly different dissociation processes for guanine and adenine, despite their structural similarities. As shown in Figure 7.4, we observe three primary fragments (GF1-3) from the CID of deprotonated guanine (G3), and two primary fragments (AF1-2) of deprotonated adenine (A1). These data are in agreement with previous experimental studies.[52,53] G3 dissociates predominantly by deammoniation (GF1). The two additional, low-intensity products (GF2 and GF3) correspond to the losses of CH_2N_2 and HNCO, respectively. By contrast, A1 dissociates primarily by HNC/HCN loss (AF1), and CH_2N_2 loss (AF2) is a minor pathway. The NCE applied to achieve complete dissociation of A1 is also significantly higher than that required for G3 (75% and 60%, respectively). This increased NCE for adenine dissociation is expected based on the high resonance

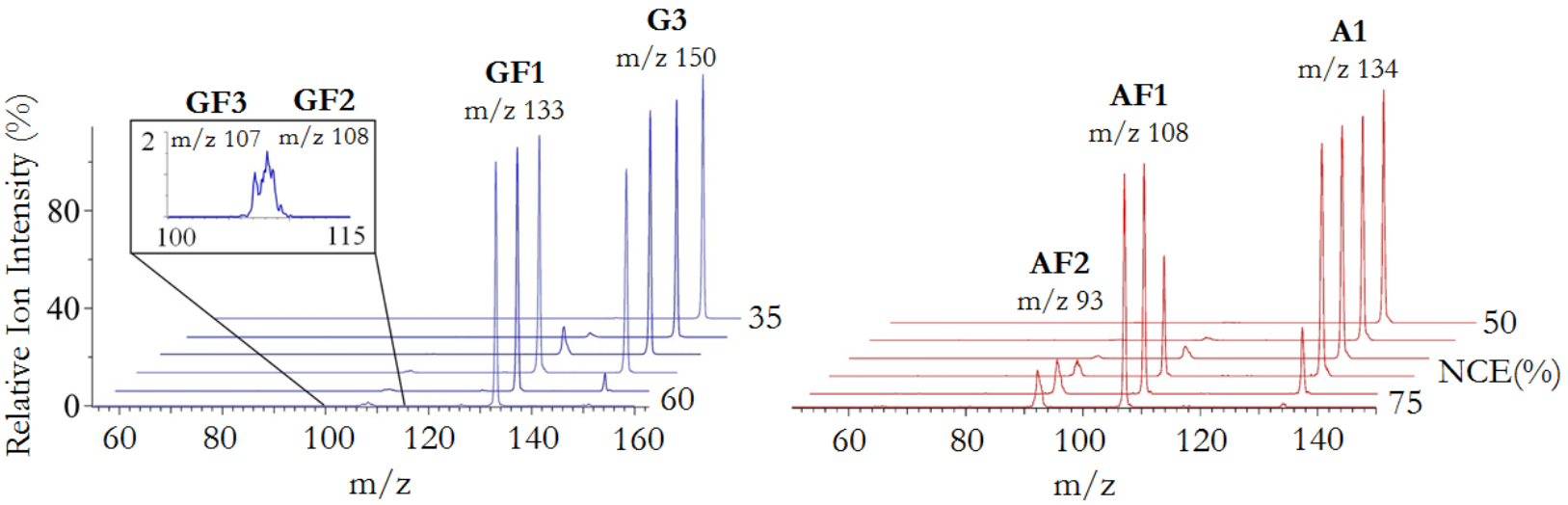

Figure 7.4
The experimental CID spectra of deprotonated guanine (predominantly G3) and deprotonated adenine (predominantly A1) are shown. Primary fragments of G3 are denoted GF1-3, and those of A1 are labeled AF1-2. The applied NCE increases in increments of 5% and can be found to the right of the spectra.

stability of the molecule[21] and the previously discussed barriers to intramolecular proton transfers. Similar observations have been made regarding the structural integrity of adenine under high energy irradiation.[22]

In addition to primary dissociation (MS^1), we performed a second stage of tandem mass spectrometry (MS^2). All experimental purine dissociation data, as well as the overall endothermicities (ΔH_{0K}), are summarized in Table 7.1. The deammoniation channel from G3 constitutes 97% of the overall product ion signal, compared to 2% for CH_2N_2 loss and 1% for HNCO loss. This product distribution is predicted by the endothermicity of the three processes (36.6, 60.7, and 73.1 kcal mol^{-1}, respectively) which are inversely correlated to the observed branching fractions of products. GF1 can be further fragmented with CO (70%) and HCN (30%) loss. These pathways have similar endothermicities (59.7 and 59.3 kcal mol^{-1}), suggesting the involvement of more complex chemical dynamics, which will be discussed in the next section. The last dissociation channel observed for deprotonated guanine is the decarbonylation of GF2. Although the primary fragments of deprotonated guanine have been reported by previous studies,[52,53] tandem mass spectrometry data are not emphasized and do not entirely agree with our results. For example, Kamel et al. (2004) report fragments m/z 106 and m/z 66 from GF1, whereas decarbonylation (m/z 105) is the primary process that we observe.[52] Variations in instrumental parameters may be responsible for these differing fragmentation patterns.

Table 7.1
Fragmentation of N_9 Deprotonated Purines.

MS^n	Guanine	Branching Fraction (%)[a]	ΔH_{0K}[b]	Adenine	Branching Fraction (%)[a]	ΔH_{0K}[b]
MS^1	G3 → GF1 + NH_3	97	36.6	A1 → AF1 + HNC	90	67.8
	G3 → GF2 + HNCNH	2	60.7	A1 → AF1 + HCN		53.8
	G3 → GF2 + NH_2CN			A1 → AF2 + HNCNH	10	82.3
	G3 → GF3 + HNCO	1	73.1			
MS^2	GF1 → GF4 + CO	70	59.7	AF1 → AF3 + HCN	80	53.1
	GF1 → GF5 + HCN	30	59.3	AF1 → AF4 + $H_2C_2N_2$	20	80.0
	GF2 → GF6 + CO	100	50.8	AF2 → AF5 + HNC	100	11.3

[a] These data are collected at sufficient NCE to render the parent ion intensity negligible (60 and 75% NCE for guanine and adenine, respectively). These values are precise within ± 5% of their reported value.
[b] Calculated at the B3LYP/6-311++G(d,p) level of theory (kcal mol^{-1}).

The dissociation of deprotonated adenine is briefly discussed in a previous study,[52] but no further fragmentation or analyses have been published to our knowledge. The primary channels involve 90% HCN/HNC loss and 10% CH_2N_2 loss. The production of HCN is 14 kcal mol^{-1} lower in energy than its isomer, and is therefore likely the favored process. Once again, in comparing the branching fractions with the endothermicity of fragmentation in Table 7.1, we observe an inverse correlation. For example, the loss of HCN dimer is much more endothermic (80.0 kcal mol^{-1}) than the loss of the monomer (53.1 kcal mol^{-1}) from AF1, and 80% of the product results from monomer loss. We observe deprotonated adenine (an HCN pentamer) lose HCN or HNC in series, becoming first the tetramer (AF1), then the trimer (AF3), and finally the dimer (AF4). Based on these data, we predict that the monomer (CN^-) is the final CID product from A1, although its low m/z prevented our observation of this species. Sequential HCN/HNC loss has also been previously observed for adenine cation, supporting the theory of adenine formation by HCN/HNC oligomerization.[51]

7.3.3 Computational Dissociation Mechanisms

Computations are performed to provide a more thorough understanding of the experimental dissociation data. The optimized ground state geometries, total electronic energies, and zero point corrected electronic energies for all of the major structures outlined in this chapter are included in Appendix B. Figure 7.5 outlines the proposed structures for all deprotonated guanine (GF1-6) and adenine (AF1-5) fragments observed in this study. Interestingly, all of the primary fragments and two of the secondary fragments maintain the five-membered purine ring structure, whereas none of these ions retain their pyrimidine ring structure. Isotope labeling experiments corroborate this prediction. For example, when the nitrogen and carbon atoms of the five-membered ring are labeled in the parent ion, the observed fragment ions retain the labeled atoms.[53] Previous work has suggested that the location of the charge contributes to the dissociation mechanisms of these ions,[66] and it is possible for

the charge site on N_9 deprotonated purines to relocate to the pyrimidine ring,[53] decreasing the ring's stability. As discussed in the previous section, geometry distortions resulting from intramolecular proton transfers also contribute to the weakening of the pyrimidine ring. During the dissociation process, this six-membered ring has been shown to open and close causing isomerization in both adenine and guanine. For example, isotope labeling studies reveal that ring opening at the C_6-N_1 bond in guanine and the N_1-C_2 bond in adenine, followed by internal rotation and ring closure, can cause a scrambling of the N_1 and N_{10} nitrogen atoms in each purine.[41,53]

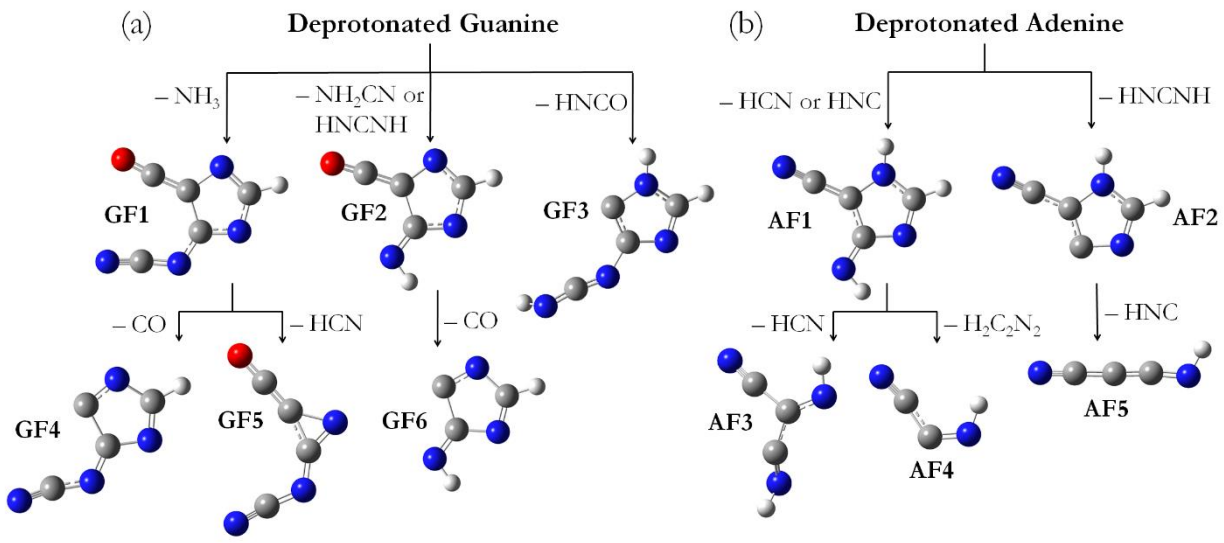

Figure 7.5
Proposed structures that arise from the fragmentation of deprotonated guanine (a) and adenine (b). Primary and secondary deprotonated guanine fragments are denoted GF1-3 and GF4-6, and those of adenine are labeled AF1-2 and AF3-5, respectively. All neutral fragments (NH_3, NH_2CN/HNCNH, HNCO, CO, and HCN/HNC) have been detected in the ISM

The two most abundant fragments that are observed, GF1 and AF1, have great potential to be anionic precursors of the purines. All of the primary fragment structures arising from deprotonated guanine match those of previous predictions[53] with the exception of GF1. Sultan predicted a stable ring-closed carbanion, whereas our calculations show that a ring-opened structure is more probable. GF1, also known as deprotonated 5-cyanoimino-4-oxomethylene-4,5-dihydroimidazole, is a viable guanine precursor that has been studied in conjunction with guanine deamination.[67] Although this molecule has not been a focus of previous guanine syntheses, it may hold the key to the final step of guanine formation. The fragment AF1 is formally known as deprotonated 4-aminoimidazole-5-carbonitrile (AICN), whose neutral counterpart is an essential precursor of adenine according to previous work.[23,24,35] The last, and arguably most crucial, stage of adenine formation may be the conversion of AICN to adenine through HCN addition and subsequent cyclization according to these studies. Barriers to this process may be decreased for anion-neutral reactions, supporting the continued consideration of anion involvement in purine synthesis. Of the remaining fragment structures shown in Figure 7.5, few have been explored. The dimer, trimer, and tetramer of HCN have long been recognized adenine precursors,[68] but their corresponding deprotonated anions (AF4, AF3, and AF1) have not been examined. Furthermore, several of the fragments are isomers of one another (i.e., GF3/AF1 and GF6/AF3) supporting the probable overlap of adenine and guanine synthesis pathways.

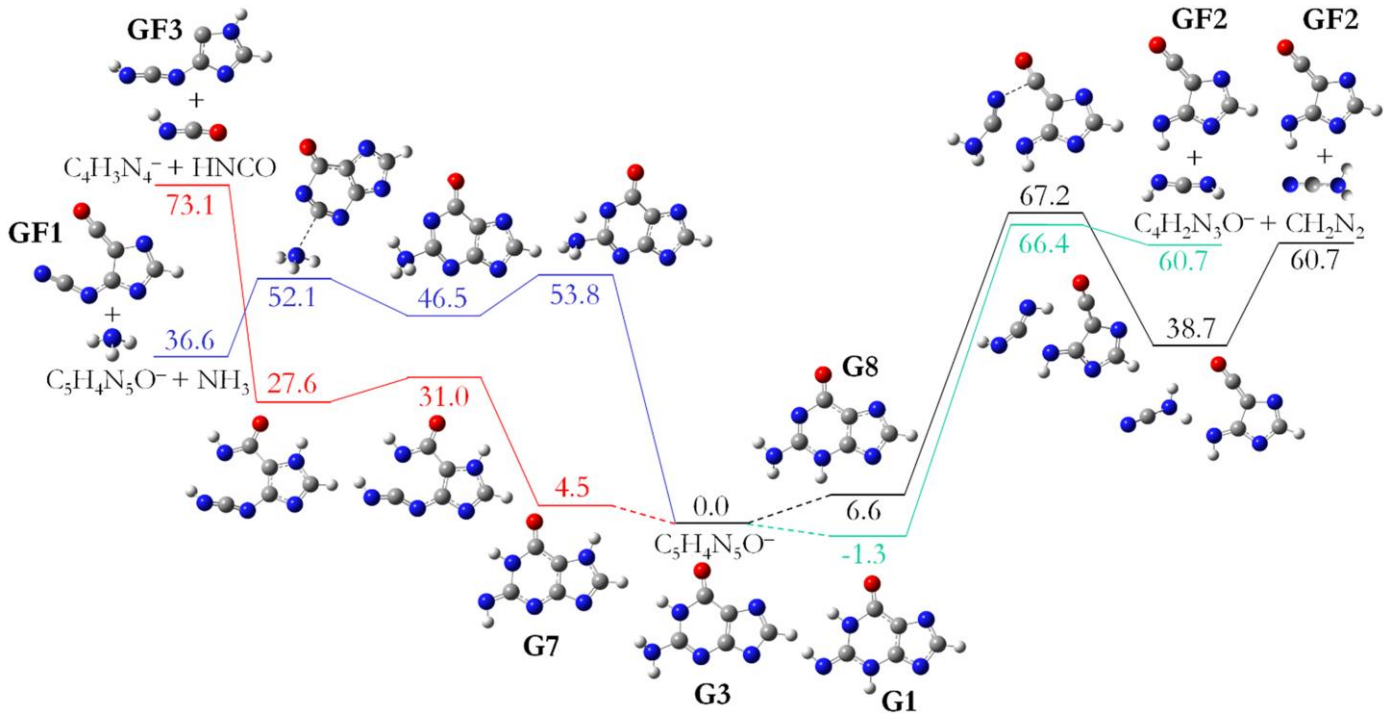

Figure 7.6
The primary CID mechanisms of N_9 deprotonated guanine (G3) involving the loss of NH_3 (blue), HNCO (red), and the isomers HNCNH and NH_2CN (green and black, respectively) are calculated at the B3LYP/6-311++G(d,p) level of theory. Zero point corrected energies are reported in kcal mol^{-1}. For barriers to interconversion of G1, G3, G7 and G8 see Figure 7.2.

The PESs of the primary dissociation processes of deprotonated guanine are overlaid in Figure 7.6. The most energetically favored pathway involves the loss of NH_3 directly from G3, leading to GF1 (shown in blue). The ease of deammoniation at this site is in part due to the C_2-N_{10} bond elongation in G3, as is discussed in a previous section. A proton is simply passed from N_1 to N_{10}, increasing the C_2-N_{10} bond length even further, resulting in dissociation at that site concurrent with the pyrimidine ring opening between C_6 and N_1. Although we do not show the process in Figure 7.6, previous isotope labeling experiments[53] have revealed that the N_1 and N_{10} atoms can be scrambled during dissociation, so either atom may be lost in the deammoniation process. Here, we have shown the loss of N_{10} for simplicity. As discussed above, nearly all of the ion signal observed is attributed to GF1 (97%, Table 7.1). The remaining two fragments involve higher energy pathways, and are consequently lower in intensity. In black and green, the channels to NH_2CN and HNCNH loss and GF2 formation, are shown. These routes are very similar in energy, although HNCNH loss has a slightly lower barrier (66.4 compared to 67.2 kcal mol^{-1}). Again, the geometry distortions accompanying intramolecular proton transfers to form G1 and G8 elongate the N_1-C_6 and C_2-N_3 bonds, and lead to dissociation at these sites. The last pathway in red accounts for only 1% of the observed fragment ion signal (Table 7.1), and is also the highest energy process according to our calculations. Analogous to previous discussions, the structure of G7 facilitates HNCO loss through the elongation and subsequent dissociation of the N_1-C_2 bond. Our understanding of the formation process of guanine may benefit greatly from studying the reverse of these processes in different astrochemical environments.

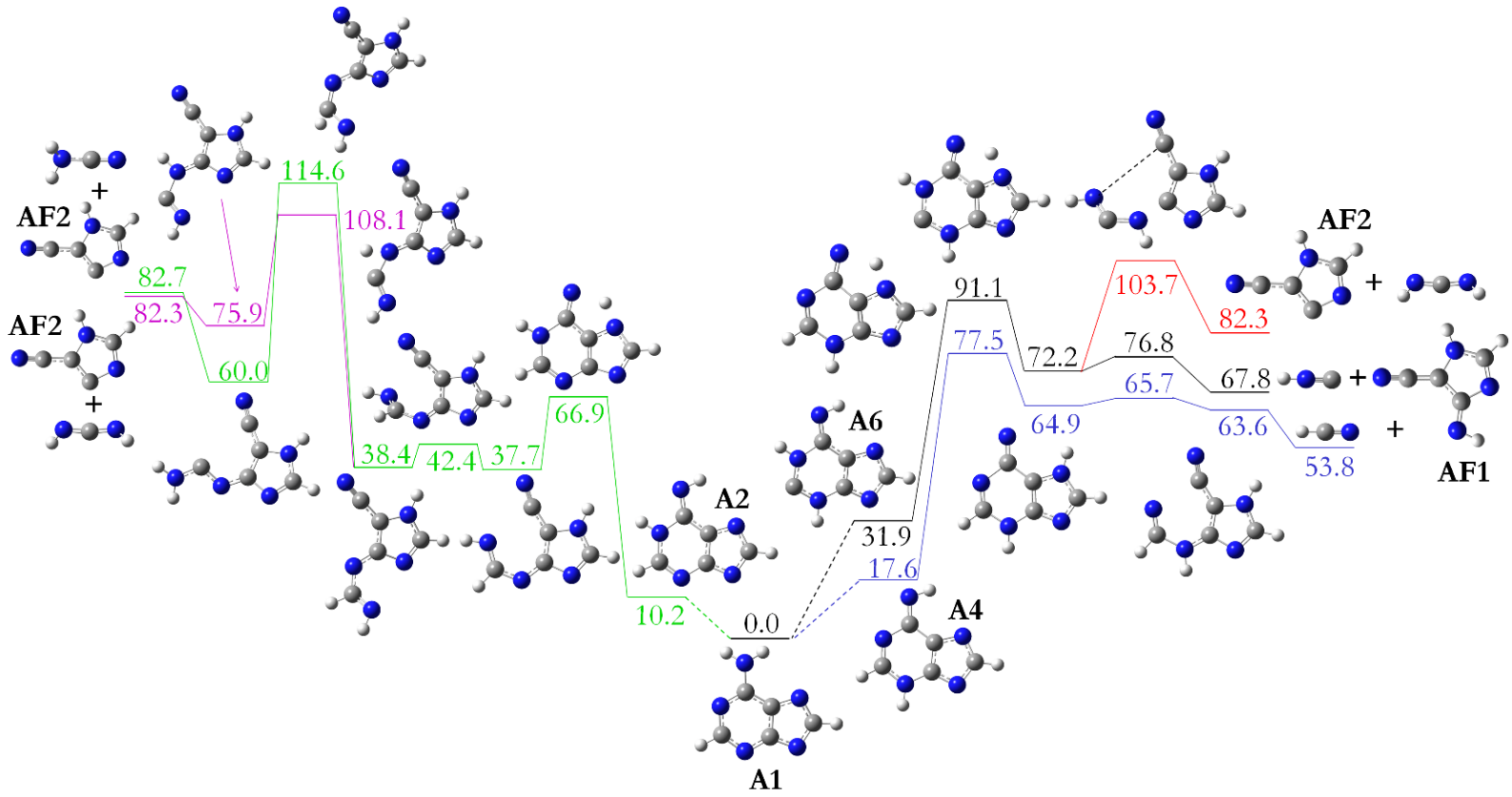

Figure 7.7
The primary CID mechanisms of N_9 deprotonated adenine (A1) involving the loss of CH_2N_2 (red, green, and purple), and the isomers HCN and HNC (blue and black, respectively) are calculated at the B3LYP/6-311++G(d,p) level of theory. Zero point corrected energies are reported in kcal mol^{-1}. The losses of HCN and HNC are analogous processes, so not all structures are shown. For barriers to interconversion of A1, A2, A4 and A6 see Figure 7.3. The lowest energy pathways (blue, black, and red) involve isomers A4 and A6. The higher energy pathways (green and purple) involving isomer A2 are included for comparison.

Our computational results for the CID of deprotonated adenine, presented in Figure 7.7, reveal the reverse of several proposed syntheses.[23,24] For example, the final bond to form adenine in these studies, C_6-N_1, is also the initial bond to break according to our results. Similarly, the most recent investigation of adenine formation involves the initial formation of the pyrimidine ring, and the subsequent fusion of the 5-membered ring;[30] these dissociation mechanisms reveal ring opening in the reverse order. As we reported for the intramolecular proton transfers of adenine, the A4 and A6 tautomers have extended bonds that increase their likelihood to fragment at the locations depicted. Figure 7.7 shows analogous fragmentation of both tautomers, beginning with a proton transfer from N_{10} to N_7, followed by ring opening between C_6 and N_1. A6 gives rise to HNC and A4 leads to HCN, shown in black and blue, respectively. Although both pathways are possible, HCN loss will predominate due to its overall lower barriers. The loss of either isomer leads to the same ion, the deprotonated HCN tetramer, AICN. The last step of HCN loss, shown in blue, involves a plateau in which a structure and TS are within ± 0.1 kcal mol^{-1} of one another. In Figure 7.7, this is shown as one structure with energy 63.6 kcal mol^{-1} for simplicity. The last fragmentation pathway of A1 may lose multiple neutral isomers including HNCNH, NH_2CN, or HNCHN. We have shown the loss of HNCNH in red and purple, and the loss of NH_2CN in green. Compared to our previous work on nucleobase dissociation [69] and the guanine results reported here, deprotonated adenine fragmentation involves much higher energy barriers. This agrees with previous reports of the higher stability of adenine compared to the other nucleobases.[21,22] Lastly, products and pathways involving isomer A2 are provided for comparison, but are much higher in energy and therefore less feasible than those of isomers A4 and A6.

7.3.4 Gas-Phase Acidity

Experimental verification of the proposed fragment structures is possible through acidity bracketing. The three most abundant ion fragments observed, GF1, AF1, and AF2, are characterized using this technique. The experiment involves trapping each ion (A^-) in the presence of the neutral molecules (RH) listed in Table 7.2. This table indicates the positive or negative detection of the R^- proton abstraction product (with a Y or N, respectively), and allows for the determination of the neutral parent molecule (AH) acidity. GF1 is unreactive with even the most acidic reagent, so an upper limit is placed on the acidity of its neutral parent ($\Delta H°_{acid} < 323.5$ kcal mol^{-1}). For comparison, we calculated the acidity of the proposed structure for GF1 protonated at the site corresponding to N_9 of the parent ion, and obtained 320.3 kcal mol^{-1}, in excellent agreement with the experimental data. Similarly, fragments AF1 and AF2 are bracketed between the acidities of thiophenol and hydrochloric acid, giving their neutral parent molecules an experimental acidity of 336.9 ± 2.1 kcal mol^{-1}. The calculated acidity of AF1 protonated at the site corresponding to N_9 of deprotonated adenine, 336.7 kcal mol^{-1}, agrees well with the experimental results. The reactions with AF2 likely involve acid catalyzed isomerization due to the high basicity of the carbon site. We expect our reference acids (RH) to initially transfer a proton to this carbon, and subsequently deprotonate the remaining nitrogen (corresponding to the N7 nitrogen on adenine). We have therefore calculated the acidity of the neutral parent at this site to be 326.8 kcal mol^{-1}. Although this calculated result is smaller than our experimental bracket, it is similar in acidity to HCl, where trace products were observed (Table 7.2). These data are in reasonable agreement within experimental and computational uncertainty. Acidity brackets add additional support to the structures proposed in the previous section.

Table 7.2
Acidity bracketing results.[a]

RH	$\Delta G°_{acid}$(RH)[b]	$\Delta H°_{acid}$(RH)[b]	A^-		
			GF1	AF1	AF2
Phenol	342.3 ± 2.0	349 ± 2	N	N	N
Propionic Acid	340.4 ± 2.0	347.4 ± 2.2	N	N	N
Thiophenol	333.4 ± 2.1	340.4 ± 2.1	N	N	N
Hydrochloric Acid	328.10 ± 0.10	333.40[c]	N	Y[d]	Y[d]
Hydrobromic Acid	318.30 ± 0.15	323.540 ± 0.050	N	Y	Y

[a] $A^- + RH \rightarrow AH + R^-$, where A^- represents GF1, AF1, and AF2.
[b] All values are given in kcal mol^{-1} and obtained from the NIST WebBook.[70]
[c] Error bars are not specified in the NIST WebBook.
[d] Trace Cl^- observed.

7.3.5 Astrobiological Relevance

The anionic fragments of purine nucleobases outlined in this study are pertinent to the field of astrobiology. A combination of experimental and computational results reveal several good candidates, some of which have already been suggested as precursors in their neutral forms. For example, seven of the eleven fragment ions proposed here are deprotonated imidazoles (GF1-4, GF6, AF1-2), and the analogous neutral imidazole molecules have often been proposed intermediates to purine synthesis.[71] The two most abundant deprotonated imidazoles produced in this investigation, GF1 and AF1, differ in this respect. Deprotonated 5-cyanoimino-4-oxomethylene-4,5-dihydroimidazole (GF1) has been studied in the process of nitrosative guanine deamination, but remains largely absent from currently-proposed prebiotic syntheses of this purine.[32-34] According to our results, this molecule deserves greater consideration in future guanine synthesis schemes. Deprotonated AICN (AF1), by contrast, is the prevailing adenine precursor in its neutral form according to several publications.[23,24] Lastly, a neutral radical similar in structure to GF6 is the central imidazole precursor to nucleobase formation in the current work of Jeilani et al..[72] Although no imidazoles have currently been detected in the ISM, the abundance of nitrogen-containing and cyclic species[73] supports their interstellar presence, and our data encourage their continued astronomical pursuit.

In addition to imidazoles, HCN oligomers, nitrogen-containing carbanions, and several abundant interstellar neutral molecules are observed during deprotonated purine dissociation. We report the formation of the deprotonated HCN dimer (AF4), trimer (AF3), and tetramer (AF1) from CID of the pentamer, A1. Although the deprotonated monomer (CN^-) is not observed here, we anticipate that this is the smallest anionic fragment of A1. The observation of this series of HCN oligomers is important to theories of adenine formation, because it suggests HCN plays a crucial role,

despite recent questions about its involvement.[30] The detection of interstellar nitrogen-containing carbanions[74-76] motivated our previous studies of their reactions with H atoms.[77] Here, monohydrogenated carbanions with very similar structures to the neutral associative detachment products of our previous work, $HC_2N_2^-$ (AF4) and $HC_3N_2^-$ (AF5), are produced from deprotonated adenine. These results help bridge the gap between small nitrogen-containing carbanions and larger biomolecules. Finally, all neutral molecules lost from both G1 and A1 including NH_3, NH_2CN/HNCNH, HNCO, CO, and HNC/HCN have been detected in the ISM, adding to the known interstellar ingredients available for purine synthesis.

7.4 Conclusion

The aim of this work is to explore the role of anions in prebiotic purine formation through the examination of deprotonated adenine and guanine dissociation. Extending previous experimental studies,[52,53] we utilize tandem mass spectrometry, computational analyses, and gas-phase acidity bracketing to delineate structures and energies of the reactants, intermediates, transition states, and products of these processes. ESI is expected to readily deprotonate adenine and guanine at the most acidic site, previously shown to be N_9 in both molecules.[55-57] Prior to dissociation, however, these deprotonated purines may undergo intramolecular proton transfers that alter the original geometry of the parent ion. These geometric changes elongate bonds that can predispose the newly formed tautomers to fragmentation at specific sites. Our calculations reveal that G3 will undergo low energy (< 58.3 kcal mol^{-1}) proton migrations among the N_1, N_3, N_7, N_9, N_{10}, and O positions. By contrast, the proton transfer processes of deprotonated adenine are much higher in energy (< 83.0 kcal mol^{-1}) among the N_1, N_3, N_7, N_9, and N_{10} positions. Analogous to these intramolecular proton transfers, deprotonated guanine completely dissociates at a significantly lower energy (60% NCE) than adenine (75% NCE) due in part to the increased resonance stability of the latter.[21] Experimentally, we observe

fragment structures from both purines that include primarily imidazole and carbonitrile structures. Deprotonated guanine primarily fragments by NH_3 loss (97%), and secondarily by elimination of CH_2N_2 (2%) and HNCO (1%). Deprotonated adenine loses HCN/HNC (90%) as well as CH_2N_2 (10%). Further dissociation yields CO and HCN loss from guanine fragments and elimination of HNC and HCN from adenine fragments. Computational analyses reveal the inverse relationship between the experimental branching fractions and the barrier heights along the PES of each dissociation process. They also predict the structures of the ions, none of which maintain their six-membered pyrimidine structure. Rather, both purines dissociate through pyrimidine ring opening, leaving mostly deprotonated imizadole products in a reverse mechanism of many recently-proposed syntheses.[23,24,30,71] Due to barriers along the PESs, we find the solely gas phase interstellar syntheses of purines to be unlikely, and expect surface environments to provide more favorable synthetic conditions. Surfaces can concentrate and orient reactants, as well as provide an energy sink for highly exothermic processes which decreases the fragmentation of products. Higher energy radical species may also replace the stable neutral reactants reported here, resulting in lower overall barriers to gas phase reactions. Regardless, the anion precursor structures reported herein are important to consider for formation routes in any environment through reactions with an array of neutral reactants. For structural verification, the acidity of the neutral parents of the most abundant guanine fragment (GF1) and the two highest intensity adenine fragments (AF1-2) are determined experimentally ($\Delta H°_{acid} < 323.5$ for GF1 and 336.9 ± 2.1 kcal mol^{-1} for AF1-2) and found to agree reasonably well with computational values (320.3, 336.7, and 326.8 kcal mol^{-1} for GF1, AF1, and AF2, respectively). Overall, these results represent a comprehensive study of deprotonated purine dissociation. Products observed herein may be involved in purine synthesis, and therefore deserve further examination. In addition to the continued search for imidazoles and purines, these data support the involvement of anions in adenine and guanine formation.

7.5 References

1 H. Rosemeyer, *The Chemodiversity of Purine as a Constituent of Natural Products*. Chem. Biodivers., **2004**, *1*, 361-401.

2 S. L. Miller; H. C. Urey, *Organic Compound Synthesis on the Primitive Earth*. Science, **1959**, *130*, 245-251.

3 J. Kissel; F. R. Krueger, *The Organic-Component in Dust from Comet Halley as measured by the Puma Mass-Spectrometer onboard Vega-1*. Nature, **1987**, *326*, 755-760.

4 R. Hayatsu; M. H. Studier; L. P. Moore; E. Anders, *Purines and Triazines in Murchison Meteorite*. Geochim. Cosmochim. Ac., **1975**, *39*, 471-488.

5 C. E. Folsome; J. Lawless; M. Romiez; C. Ponnampe, *Heterocyclic Compounds Indigenous to Murchison Meteorite*. Nature, **1971**, *232*, 108-109.

6 P. G. Stoks; A. W. Schwartz, *Nitrogen-Heterocyclic Compounds in Meteorites – Significance and Mechanisms of Formation*. Geochim. Cosmochim. Ac., **1981**, *45*, 563-569.

7 M. P. Callahan; K. E. Smith; H. J. Cleaves, II; J. Ruzicka; J. C. Stern; D. P. Glavin; C. H. House; J. P. Dworkin, *Carbonaceous Meteorites Contain a Wide Range of Extraterrestrial Nucleobases*. Proc. Natl. Acad. Sci. U. S. A., **2011**, *108*, 13995-13998.

8 W. Van Der Velden; A. W. Schwartz, *Search for Purines and Pyrimidines in the Murchison Meteorite*. Geochim. Cosmochim. Ac., **1977**, *41*, 961-968.

9 Z. Martins; O. Botta; M. L. Fogel; M. A. Sephton; D. P. Glavin; J. S. Watson; J. P. Dworkin; A. W. Schwartz, et al., *Extraterrestrial Nucleobases in the Murchison Meteorite*. Earth Planet. Sci. Lett., **2008**, *270*, 130-136.

10 V. G. Kunde; A. C. Aikin; R. A. Hanel; D. E. Jennings; W. C. Maguire; R. E. Samuelson, *C_4H_2, HC_3N and C_2N_2 in Titan's Atmosphere*. Nature, **1981**, *292*, 686-688.

11 A. Coustenis; R. K. Achterberg; B. J. Conrath; D. E. Jennings; A. Marten; D. Gautier; C. A. Nixon; F. M. Flasar, et al., *The Composition of Titan's Stratosphere from Cassini/CIRS Mid-Infrared Spectra*. Icarus, **2007**, *189*, 35-62.

12 J. Cui; R. V. Yelle; V. Vuitton; J. H. Waite; W. T. Kasprzak; D. A. Gell; H. B. Niemann; I. C. F. Muller-Wodarg, et al., *Analysis of Titan's Neutral Upper Atmosphere from Cassini Ion Neutral Mass Spectrometer Measurements*. Icarus, **2009**, *200*, 581-615.

13 S. Pilling; D. P. P. Andrade; A. C. Neto; R. Rittner; A. N. de Brito, *DNA Nucleobase Synthesis at Titan Atmosphere Analog by Soft X-rays*. J. Phys. Chem. A, **2009**, *113*, 11161-11166.

14 R. W. Wilson; K. B. Jefferts; A. A. Penzias, *Carbon Monoxide in Orion Nebula*. Astrophys. J., **1970**, *161*, L43-L44.

15 A. C. Cheung; D. M. Rank; C. H. Townes; D. D. Thornton; W. J. Welch, *Detection of NH_3 Molecules in Interstellar Medium by their Microwave Emission*. Phys. Rev. Lett., **1968**, *21*, 1701-1705.

16 K. Ishii; A. Tajima; T. Taketsugu; K. Yamashita, *Theoretical Elucidation of the Unusually High HNC/HCN Abundance Ratio in Interstellar Space: Two-Dimensional and Two-State Quantum Wave Packet Dynamics Study on the Branching Ratio of the Dissociative Recombination Reaction $HCNH^+ + e^- \rightarrow HNC/HCN + H$*. Astrophys. J., **2006**, *636*, 927-931.

17 L. E. Snyder; D. Buhl, *Interstellar Isocyanic Acid*. Astrophys. J., **1972**, *177*, 619-623.

18 G. R. Adande; N. J. Woolf; L. M. Ziurys, *Observations of Interstellar Formamide: Availability of a Prebiotic Precursor in the Galactic Habitable Zone*. Astrobiology, **2013**, *13*, 439-453.

19 F. Duvernay; T. Chiavassa; F. Borget; J. P. Aycard, *Experimental Study of Water-Ice Catalyzed Thermal Isomerization of Cyanamide into Carbodiimide: Implication for Prebiotic Chemistry*. J. Am. Chem. Soc., **2004**, *126*, 7772-7773.

20 S. Chakrabarti; S. K. Chakrabarti, *Can DNA Bases be Produced During Molecular Cloud Collapse?* Astron. Astrophys., **2000**, *354*, L6-L8.

21 B. Pullman; A. Pullman, *Electronic Delocalization and Biochemical Evolution*. Nature, **1962**, *196*, 1137-1142.

22 S. Pilling; D. P. P. Andrade; E. M. do Nascimento; R. R. T. Marinho; H. M. Boechat-Roberty; L. H. de Coutinho; G. G. B. de Souza; R. B. de Castilho, et al., *Photostability of Gas- and Solid-Phase Biomolecules within Dense Molecular Clouds due to Soft X-rays*. Month. Not. Royal Astron. Soc., **2011**, *411*, 2214-2222.

23 D. Roy; K. Najafian; P. v. R. Schleyer, *Chemical Evolution: The Mechanism of the Formation of Adenine under Prebiotic Conditions*. Proc. Natl. Acad. Sci. U. S. A., **2007**, *104*, 17272-17277.

24 R. Glaser; B. Hodgen; D. Farrelly; E. McKee, *Adenine Synthesis in Interstellar Space: Mechanisms of Prebiotic Pyrimidine-Ring Formation of Monocyclic HCN-Pentamers*. Astrobiology, **2007**, *7*, 455-470.

25 I. W. M. Smith; D. Talbi; E. Herbst, *The Production of HCN Dimer and more Complex Oligomers in Dense Interstellar Clouds*. Astron. Astrophys., **2001**, *369*, 611-615.

26 M. K. Yim; J. C. Choe, *Dimerization of HCN in the Gas Phase: A Theoretical Mechanistic Study*. Chem. Phys. Lett., **2012**, *538*, 24-28.

27 J. Oro, *Mechanism of Synthesis of Adenine from Hydrogen Cyanide Under Possible Primitive Earth Conditions*. Nature, **1961**, *191*, 1193-1194.

28 J. Oro, *Synthesis of Adenine from Ammonium Cyanide*. Biochem. Biophys. Res. Commun., **1960**, *2*, 407-412.

29 V. P. Gupta; P. Tandon; P. Rawat; R. N. Singh; A. Singh, *Quantum Chemical Study of a New Reaction Pathway for the Adenine Formation in the Interstellar Space*. Astron. Astrophys., **2011**, *528*, A129.

30 K. M. Merz; E. C. Aguiar; J. B. P. da Silva, *Adenine Formation without HCN*. J. Phys. Chem. A, **2014**, *118*, 3637-3644.

31 M. Levy; S. L. Miller; J. Oro, *Production of Guanine from NH_4CN Polymerizations*. J. Molec. Evol., **1999**, *49*, 165-168.

32 H. L. Barks; R. Buckley; G. A. Grieves; E. Di Mauro; N. V. Hud; T. M. Orlando, *Guanine, Adenine, and Hypoxanthine Production in UV-Irradiated Formamide Solutions: Relaxation of the Requirements for Prebiotic Purine Nucleobase Formation*. ChemBioChem, **2010**, *11*, 1240-1243.

33 M. Ferus; R. Michalcikova; V. Shestivska; J. Sponer; J. E. Sponer; S. Civis, *High-Energy Chemistry of Formamide: A Simpler Way for Nucleobase Formation*. J. Phys. Chem. A, **2014**, *118*, 719-736.

34 Y. A. Jeilani; N. Huyen Thi; D. Newallo; J.-M. D. Dimandja; N. Minh Tho, *Free Radical Routes for Prebiotic Formation of DNA Nucleobases from Formamide*. Phys. Chem. Chem. Phys., **2013**, *15*, 21084-21093.

35 J. Wang; J. Gu; N. Minh Tho; G. Springsteen; J. Leszczynski, *From Formamide to Adenine: A Self-Catalytic Mechanism for an Abiotic Approach*. J. Phys. Chem. B, **2013**, *117*, 14039-14045.

36 R. Saladino; C. Crestini; S. Pino; G. Costanzo; E. Di Mauro, *Formamide and the Origin of Life*. Phys. Life Rev., **2012**, *9*, 84-104.

37 J. E. Sponer; A. Mladek; J. Sponer; M. Fuentes-Cabrera, *Formamide-Based Prebiotic Synthesis of Nucleobases: A Kinetically Accessible Reaction Route*. J. Phys. Chem. A, **2012**, *116*, 720-726.

38 I. W. M. Smith, *Laboratory Astrochemistry: Gas-Phase Processes*. In *Ann. Rev. Astron. Astrophys.*, Faber, S. M.; VanDishoeck, E., Eds. 2011; Vol. 49, 29-66.

39 A. Simakov; G. B. S. Miller; A. J. C. Bunkan; M. R. Hoffmann; E. Uggerud, *The Dissociation of Glycolate – Astrochemical and Prebiotic Relevance*. Phys. Chem. Chem. Phys., **2013**, *15*, 16615-16625.

40 E. L. Zins; C. Pirim; L. Vettier; M. Chaboud; L. Krim, *May Interstellar Leucine React with NO Radicals Present in Interstellar/Interplanetary Medium? An Ion-Trap Mass Spectrometry Study*. Int. J. Mass Spectrom., **2013**, *348*, 47-52.

41 F. Turecek; X. H. Chen, *Protonated Adenine: Tautomers, Solvated Clusters, and Dissociation Mechanisms*. J. Am. Soc. Mass Spectrom., **2005**, *16*, 1713-1726.

42 C. C. Nelson; J. A. McCloskey, *Collision-Induced Dissociation of Adenine*. J. Am. Chem. Soc., **1992**, *114*, 3661-3668.

43 J. M. Gregson; J. A. McCloskey, *Collision-Induced Dissociation of Protonated Guanine*. Int. J. Mass Spectrom., **1997**, *165*, 475-485.

44 P. Cheng; Y. Li; S. Li; M. Zhang; Z. Zhou, *Collision-Induced Dissociation (CID) of Guanine Radical Cation in the Gas Phase: an Experimental and Computational Study*. Phys. Chem. Chem. Phys., **2010**, *12*, 4667-4677.

45 J. M. Rice; G. O. Dudek, *Mass Spectra of Nucleic Acid Derivatives. 2. Guanine, Adenine and Related Compounds*. J. Am. Chem. Soc., **1967**, *89*, 2719-2725.

46 B. F. Minaev; M. I. Shafranyosh; Y. Y. Svida; M. I. Sukhoviya; I. I. Shafranyosh; G. V. Baryshnikov; V. A. Minaeva, *Fragmentation of the Adenine and Guanine Molecules Induced by Electron Collisions*. J. Chem. Phys., **2014**, *140*, 175101.

47 S. Pilling; A. F. Lago; L. H. Coutinho; R. B. de Castilho; G. G. B. de Souza; A. Naves de Brito, *Dissociative Photoionization of Adenine following Valence Excitation*. Rapid Commun. Mass Spectrom., **2007**, *21*, 3646-3652.

48 V. V. Afrosimov; A. A. Basalaev; Y. G. Morozov; M. N. Panov; O. V. Smirnov; E. A. Tropp, *Fragmentation of Adenine and Uracil Molecules through Electron Captures in Collisions with Ions*. Tech. Phys., **2012**, *57*, 594-602.

49 R. Bredy; J. Bernard; L. Chen; G. Montagne; B. Li; S. Martin, *Fragmentation of Adenine Under Energy Control*. J. Chem. Phys., **2009**, *130*, 114305.

50 F. Alvarado; S. Bari; R. Hoekstra; T. Schlatholter, *Interactions of Neutral and Singly Charged keV Atomic Particles with Gas-Phase Adenine Molecules*. J. Chem. Phys., **2007**, *127*, 034301.

51 L. Chen; R. Bredy; J. Bernard; G. Montagne; A. R. Allouche; S. Martin, *Fragmentation of Singly Charged Adenine Induced by Neutral Fluorine Beam Impact at 3 keV*. J. Chem. Phys., **2011**, *135*, 114309.

52 A. M. Kamel; B. Munson, *Collision-Induced Dissociation of Purine Antiviral Agents: Mechanisms of Ion Formation using Gas-Phase Hydrogen/Deuterium Exchange and Electrospray Ionization Tandem Mass Spectrometry*. Eur. J. Mass Spectrom., **2004**, *10*, 239-257.

53 J. Sultan, *Collision Induced Dissociation of Deprotonated Guanine: Fragmentation of Pyrimidine Ring and Water Adduct Formation*. Int. J. Mass Spectrom., **2008**, *273*, 58-68.

54 B. Tercero; L. Margules; M. Carvajal; R. A. Motiyenko; T. R. Huet; E. A. Alekseev; I. Kleiner; J. C. Guillemin, et al., *Microwave and Submillimeter Spectroscopy and First ISM Detection of ^{18}O-Methyl Formate*. Astron. Astrophys., **2012**, *538*, A119.

55 Y. Q. Huang; H. Kenttamaa, *Theoretical Estimations of the 298 K Gas-Phase Acidities of the Purine-Based Nucleobases Adenine and Guanine*. J. Phys. Chem. A, **2004**, *108*, 4485-4490.

56 E. C. M. Chen; C. Herder; E. S. Chen, *The Experimental and Theoretical Gas Phase Acidities of Adenine, Guanine, Cytosine, Uracil, Thymine and Halouracils*. J. Molec. Struc., **2006**, *798*, 126-133.

57 A. Zhachkina; M. Liu; X. Sun; F. S. Amegayibor; J. K. Lee, *Gas-Phase Thermochemical Properties of the Damaged Base O(6)-Methylguanine versus Adenine and Guanine*. J. Org. Chem., **2009**, *74*, 7429-7440.

58 C. A. Cole; N. J. Demarais; Z. Yang; T. P. Snow; V. M. Bierbaum, *Heterocyclic Anions of Astrobiological Interest*. Astrophys. J., **2013**, *779*, 181-190.

59 S. Gronert, *Quadrupole Ion Trap Studies of Fundamental Organic Reactions*. Mass Spectrom. Rev., **2005**, *24*, 100-120.

60 M. J. Frisch; G. W. Trucks; H. B. Schlegel; G. E. Scuseria; M. A. Robb; J. R. Cheeseman; G. Scalmani; V. Barone, et al., Gaussian 09 Revision A.02. Gaussian Inc. Wallingford, CT: 2009.

61 C. Gonzalez; H. B. Schlegel, *An Improved Algorithm for Reaction Path Following*. J. Chem. Phys., **1989**, *90*, 2154-2161.

62 C. Gonzalez; H. B. Schlegel, *Reaction Path Following in Mass-Weighted Internal Coordinates*. J. Phys. Chem., **1990**, *94*, 5523-5527.

63 A. Bacmann; V. Taquet; A. Faure; C. Kahane; C. Ceccarelli, *Detection of Complex Organic Molecules in a Prestellar Core: A New Challenge for Astrochemical Models*. Astron. Astrophys., **2012**, *541*, L12-L16.

64 J. D. Gu; J. Leszczynski, *A DFT Study of the Water-Assisted Intramolecular Proton Transfer in the Tautomers of Adenine*. J. Phys. Chem. A, **1999**, *103*, 2744-2750.

65 L. Gorb; A. Kaczmarek; A. Gorb; A. J. Sadlej; J. Leszczynski, *Thermodynamics and Kinetics of Intramolecular Proton Transfer in Guanine. Post Hartree-Fock Study*. J. Phys. Chem. B, **2005**, *109*, 13770-13776.

66 M. T. Rodgers; S. Campbell; E. M. Marzluff; J. L. Beauchamp, *Low-Energy Collision-Induced Dissociation of Deprotonated Dinucleotides - Determination of the Energetically Favored Dissociation Pathways and the Relative Acidities of the Nucleic-Acid Bases*. Int. J. Mass Spectrom. Ion Proc., **1994**, *137*, 121-149.

67 S. Rayat; R. Glaser, *5-cyanoimino-4-oxomethylene-4,5-dihydroimidazole and Nitrosative Guanine Deamination. A Theoretical Study of Geometries, Electronic Structures, and N-protonation*. J. Org. Chem., **2003**, *68*, 9882-9892.

68 O. Kikuchi; T. Watanabe; Y. Satoh; Y. Inadomi, *Ab Initio GB Study of Prebiotic Synthesis of Purine Precursors from Aqueous Hydrogen Cyanide: Dimerization Reaction of HCN in Aqueous Solution*. J. Mol. Struc.-Theo. Chem., **2000**, *507*, 53-62.

69 C. A. Cole; Z.-C. Wang; T. P. Snow; V. M. Bierbaum, *Anionic Derivatives of Uracil: Fragmentation and Reactivity*. Phys. Chem. Chem. Phys., **2014**, *16*, 17835-17844.

70 *NIST Chemistry WebBook, NIST Standard Reference Database Number 69*. National Institute of Standards and Technology, webbook.nist.gov, accessed 2010-2014.

71 E. Boulanger; A. Anoop; D. Nachtigallova; W. Thiel; M. Barbatti, *Photochemical Steps in the Prebiotic Synthesis of Purine Precursors from HCN*. Angewandte Chem.-Int. Ed., **2013**, *52*, 8000-8003.

72 Y. A. Jeilani; H. T. Nguyen; B. H. Cardelino; M. T. Nguyen, *Free Radical Pathways for the Prebiotic Formation of Xanthine and Isoguanine from Formamide*. Chem. Phys. Lett., **2014**, *598*, 58-64.

73 Z. Peeters; O. Botta; S. B. Charnley; R. Ruiterkamp; P. Ehrenfreund, *The Astrobiology of Nucleobases*. Astrophys. J., **2003**, *593*, L129-L132.

74 M. Agundez; J. Cernicharo; M. Guelin; C. Kahane; E. Roueff; J. Klos; F. J. Aoiz; F. Lique, et al., *Astronomical Identification of CN^-, the Smallest Observed Molecular Anion*. Astron. Astrophys., **2010**, *517*, L2-L6.

75 J. Cernicharo; M. Guelin; M. Agundez; M. C. McCarthy; P. Thaddeus, *Detection of C_5N^- and Vibrationally Excited C_6H in IRC+ 10216* Astrophys. J. Lett., **2008**, *688*, L83-L86.

76 P. Thaddeus; C. A. Gottlieb; H. Gupta; S. Bruenken; M. C. McCarthy; M. Agundez; M. Guelin; J. Cernicharo, *Laboratory and Astronomical Detection of the Negative Molecular Ion C_3N^-*. Astrophys. J., **2008**, *677*, 1132-1139.

77 Z. Yang; C. A. Cole; O. Martinez, Jr.; M. Y. Carpenter; T. P. Snow; V. M. Bierbaum, *Experimental and Theoretical Studies of Reactions Between H atoms and Nitrogen-Containing Carbanions*. Astrophys. J., **2011**, *739*, 19-29.

CHAPTER 8

Conclusion

This thesis work has illuminated the chemistry of nitrogen-containing carbanions, propene and trans-methyl formate precursors, azoles, pyrimidines, and purines. Many extraterrestrial molecules have been detected in our galaxy, yet the question still remains: How were they formed? This research has taken us closer to the answer, but there is more progress to be made in the future. Our results revealed that $C_2N_3^-$ and $C_4N_3^-$ are unreactive with H_2 and with H atoms. This raises the possibility that these stable anions are persistent in many interstellar regions, and astronomical observations should include these anions (particularly $C_2N_3^-$, due to its dipole moment) in their future searches. Two previously-suggested formation reactions leading to propene from $C_3H_3^+$ and $C_3H_5^+$ were shown to be improbable according to our measurements. Future laboratory experiments and modelling studies are therefore required to explain the unprecedented abundance of propene in cold prestellar cores such as TMC-1. We have verified one gas-phase reaction pathway to trans-methyl formate, yet more are necessary to account for its abundance in dense molecular clouds, prestellar cores, and protoplanetary disks. Models consistently underpredict the observed amount of this molecule, and this discrepancy between models and observations continues to be unresolved. Lastly, nitrogen-containing heterocyclic species from azoles to nucleobases have not been discovered in the ISM to date. However, their detection in cometary dust and meteorites lends support for their extraterrestrial formation. These molecules are essential to the origin of life on Earth, so the processes that govern their formation and destruction are of central importance to astrobiology. Our results provide insight into the acidity, reactivity, and possible precursors of these species. In particular, cyanate (OCN^-) is the only anion currently known to exist in interstellar ice mantles, and we have observed this anion

arise directly from the dissociation of all three deprotonated pyrimidines: uracil, thymine, and cytosine. Adenine, a purine nucleobase, dissociates through the sequential loss of HCN and HNC, likely forming cyanide (CN^-) as its simplest fragment according to our data. This brings us full circle to the nitrogen-containing carbanions that began this research. Could interstellar anions as simple as cyanate and cyanide be involved in the abiotic synthesis of nucleobases? Our research has taken the first step in providing connections among these species, but future astrochemical investigations must continue to explore similar questions to complete our understanding of abiotic biomolecule formation.

The fields of astrochemistry and astrobiology are young, yet the years following the discovery of NH_3 (the first interstellar polyatomic molecule) have been immensely productive. An array of radio telescopes (ALMA) now covers the vast Atacama desert plateau in Chile and possesses the spectral resolution necessary to detect species in much lower abundance than were previously observable. In the fall of 2014, the European Space Agency's Rosetta spacecraft successfully landed a probe on the surface of a comet for the first time, greatly benefitting the progress of cometary astrochemistry. On the astrobiology front, NASA's Kepler spacecraft continues to add to the list of known Earth-like planets that may possess liquid water on their surfaces. Conditions on these planets may promote the development of life forms much like those on Earth. Finally, the complex atmospheric chemistry of Titan intrigues astrochemists and astrobiologists alike. Recent results indicate that nitrogen-containing organic molecules present on Titan may arrange into membrane structures analogous to terrestrial cellular membranes. The formation of structures such as these have enormous implications for both the origin of terrestrial life and the development of extraterrestrial life. Through a continued collaboration among laboratory astrochemists, chemical modelers, and observational astronomers, our understanding of the ionic building blocks of life will continue to grow for years to come.

APPENDIX A

Cartesian coordinates (Å) and energies (Hartree) for optimized geometries in Chapters 4 & 5

Figure 4.4 – MP2(full)/aug-cc-pVTZ

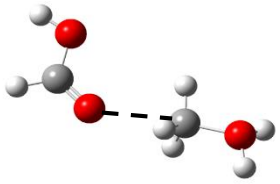

Intermediate 1 (-10.7 kcal mol^{-1})

Atom	X	Y	Z
C	-1.55690300	-0.06157800	-0.00545200
H	-1.38749700	-0.63038300	0.89443700
H	-1.36946500	-0.62013300	-0.90752400
H	-1.07136400	0.90060100	-0.00949100
O	-3.04384800	0.27091300	-0.07667000
H	-3.34757200	0.81674600	0.66800800
H	-3.60593200	-0.52009300	-0.13405800
C	2.04516800	-0.41025500	0.00667700
H	2.89984100	-1.08767100	-0.00138000
O	0.90122100	-0.78670700	0.03783500
O	2.34840300	0.88652300	-0.02028800
H	3.30618600	1.00609700	-0.04435200

ZPE (Zero Point Energy) Corrected Energy: -305.311550

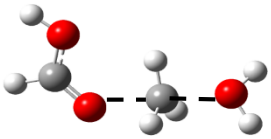

Transition State 1 (-3.4 kcal mol^{-1})

Atom	X	Y	Z
C	0.98824900	-0.26769700	-0.01575100
H	1.16288000	-0.92338100	-0.84502900
H	1.06207800	-0.64079700	0.98654700
H	0.64628300	0.73559300	-0.17625200
O	2.78224000	0.34505300	0.07088500
H	3.11400500	0.79862600	-0.71481900
H	3.43907300	-0.32781800	0.29273100
C	-1.85249500	-0.29248200	-0.00038300
H	-2.84657600	-0.73420500	0.00760700
O	-0.85292700	-0.98769400	-0.02720000
O	-1.77205700	1.02103200	0.01940200
H	-2.65032100	1.42592800	0.04131800

ZPE Corrected Energy: -305.718598

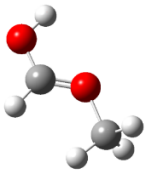

$HC(OH)OCH_3^+$ (Product)

Atom	X	Y	Z
C	-0.57145200	0.37809000	-0.00003400
H	-0.42696900	1.45184900	0.00001500
O	0.38529600	-0.43342700	-0.00002400
H	-1.86404200	-0.98765800	0.00002900
C	1.77562500	0.06397200	0.00001800
H	2.22518600	-0.33930700	-0.89589100
H	1.76916100	1.14724100	-0.00005200
H	2.22510200	-0.33919700	0.89602000
O	-1.77948000	-0.01473500	0.00002100

ZPE Corrected Energy: -228.990708

Figure 5.4 – B3LYP/6-311++G(d,p)

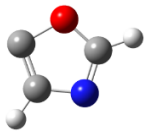

$C_3H_2NO^-$ (Reactant)

Atom	X	Y	Z
C	1.13402100	-0.19744100	-0.00036100
C	0.66651800	1.10209500	-0.00002700
O	-0.76152000	0.86904000	0.00009500
C	-0.96000400	-0.46736900	-0.00032500
N	0.12241500	-1.17733400	0.00058600
H	-1.98022600	-0.82997100	-0.00021100
H	2.17227300	-0.50471600	-0.00037600

ZPE Corrected Energy: -245.477884

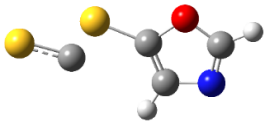

Intermediate 1 (-5.7 kcal mol^{-1})

Atom	X	Y	Z
C	-1.71102400	1.02245200	-0.50251100
C	-0.97443800	-0.11085900	-0.30860400
H	-1.41340600	1.91215300	-1.03132900
C	1.72713900	0.47922400	0.55678800
N	-2.95878300	0.89951600	0.09721600
C	-2.93582500	-0.28119000	0.62699100
H	-3.71603700	-0.77586900	1.18476300
S	3.33546900	0.19989300	0.31865900
S	0.63265700	-0.59855400	-0.73198700
O	-1.78552500	-0.96401000	0.44291500

ZPE Corrected Energy: -1080.032582

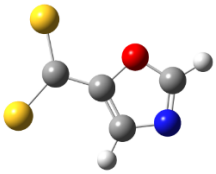

Intermediate 2 (-54.2 kcal mol^{-1})

Atom	X	Y	Z
C	1.38678200	1.15496800	0.00011500
C	0.51585000	0.09823900	0.00000400
H	1.13506800	2.20074200	0.00022300
C	-0.95466000	-0.01104600	0.00000000
N	2.69650600	0.70018500	0.00009300
C	2.57308500	-0.59124500	-0.00006000
H	3.35511000	-1.33501100	-0.00013900
S	-1.64367900	-1.56153300	0.00001100
S	-1.79050900	1.47629100	-0.00001900
O	1.30686900	-1.03858200	-0.00012100

ZPE Corrected Energy: -1080.109955

Intermediate 3 (-8.1 kcal mol^{-1})

Atom	X	Y	Z
C	1.17565100	0.77803100	0.42824500
C	0.30735200	-0.39852200	0.71768500
H	1.67888400	1.33162700	1.22807000
C	-0.92602100	-0.05259300	0.20234900
N	2.18657600	0.24440400	-0.50942600
C	2.04108800	-1.02509600	-0.43272400
H	2.68137100	-1.74686900	-0.93035100
S	-2.38717800	-0.76289400	-0.17998200
S	-0.34628800	1.73005700	-0.12181500
O	1.06009300	-1.57263900	0.32546100

ZPE Corrected Energy: -1080.036375

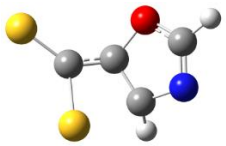

Transition State 1 (-4.9 kcal mol^{-1})

Atom	X	Y	Z
C	1.22253800	0.78262700	0.46635200
C	0.36037500	-0.37853300	0.59550600
H	1.44862400	1.48824100	1.26176900
C	-0.92156600	-0.05489900	0.16270400
N	2.37264200	0.35749900	-0.27436800
C	2.21811700	-0.92076800	-0.38413600
H	2.93911600	-1.59647300	-0.82862300
S	-2.34281000	-0.90602800	-0.09287600
S	-0.61088300	1.72207700	-0.19140200
O	1.12325900	-1.50270200	0.12416600

ZPE Corrected Energy: -1080.031383

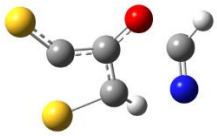

Transition State 2 (15.3 kcal mol^{-1})

Atom	X	Y	Z
C	0.80173100	1.05545900	0.45101200
C	0.37433500	-0.26909800	0.51300400
H	1.55108100	1.61333400	0.98810900
C	-0.95609600	-0.17103300	0.06999800
N	2.62287600	0.25426500	-0.68411400
C	2.43401400	-0.88985400	-0.29906800
H	2.99378100	-1.81907900	-0.41455000
S	-2.27171800	-1.10839300	-0.20072600
S	-0.76416100	1.77074200	-0.08654800
O	1.21814500	-1.31556700	0.55024300

ZPE Corrected Energy: -1079.999169

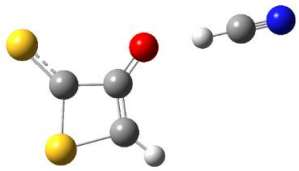

Intermediate 4 (-23.9 kcal mol^{-1})

Atom	X	Y	Z
C	0.09898500	-1.52909800	0.00027100
C	-0.15624400	-0.17639500	0.00038000
H	-0.50172300	-2.42626200	0.00072000
C	1.30919800	0.26864100	-0.00003400
N	-5.09257000	0.08902500	-0.00052800
C	-3.94500300	0.20634800	-0.00010000
H	-2.83138300	0.30301900	0.00034300
S	2.07503000	1.69972600	-0.00014500
S	1.95755800	-1.42910700	-0.00024800
O	-1.17274200	0.56914900	0.00072600

ZPE Corrected Energy: -1080.061597

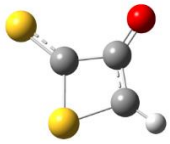

$C_3HOS_2^-$ (Product)

Atom	X	Y	Z
C	1.77823800	-0.08731900	-0.00034600
C	0.73227900	-0.99734500	-0.00013200
H	2.85648300	-0.14925700	0.00147600
C	-0.39379300	0.07307100	-0.00044800
S	-2.02175000	0.03271800	0.00008700
S	0.74998000	1.47301800	0.00009100
O	0.59893600	-2.23412000	0.00015300

ZPE Corrected Energy: -986.594045

Figure 5.6 – B3LYP/6-311++G(d,p)

Intermediate 1 (-20.1 kcal mol^{-1})

Atom	X	Y	Z
C	1.06336300	-0.17196100	-0.00008900
C	2.16093300	0.36429500	0.00002400
O	-1.57080200	0.89055000	-0.00001500
C	-1.25066300	-0.30896100	0.00003300
N	-0.04137900	-0.89354500	0.00000400
H	-2.05790000	-1.07392900	0.00010900
H	3.07216300	0.90410700	0.00017700

ZPE Corrected Energy: -245.509880

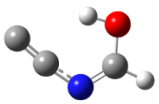

Intermediate 2 (18.6 kcal mol^{-1})

Atom	X	Y	Z
C	-1.09397000	-0.27908500	-0.00002600
C	-2.03028000	0.54762300	0.00005800
O	1.18657200	0.96678300	0.00005400
C	1.12173500	-0.38618800	-0.00009400
N	0.02833700	-1.05800800	0.00000200
H	2.09395800	-0.86707400	0.00036200
H	0.23019500	1.24476400	-0.00043700

ZPE Corrected Energy: -245.448226

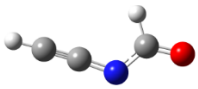

Intermediate 3 (-21.5 kcal mol^{-1})

Atom	X	Y	Z
C	-1.21378200	-0.14294500	0.00003800
C	-2.39139800	0.18874300	-0.00006200
O	2.24358800	0.02825200	-0.00012200
C	1.03516600	0.29535100	0.00007300
N	0.02246700	-0.58694400	0.00008500
H	0.72833900	1.37243000	0.00033800
H	-3.41423200	0.46325800	-0.00025000

ZPE Corrected Energy: -245.512147

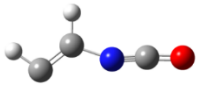

Intermediate 4 (0.4 kcal mol^{-1})

Atom	X	Y	Z
C	-1.38589400	0.40108700	-0.00005100
C	-1.95346200	-0.81309100	-0.00000700
O	2.23620600	-0.34958900	-0.00010700
C	1.11620700	0.06305200	-0.00001100
N	0.05138300	0.59401900	0.00006200
H	-3.05135400	-0.65809000	0.00045400
H	-1.85908100	1.39038400	0.00038400

ZPE Corrected Energy: -245.477860

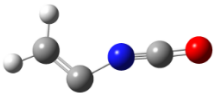

Intermediate 5 (-8.5 kcal mol^{-1})

Atom	X	Y	Z
C	1.27065000	-0.62352400	0.00007100
C	2.27458800	0.28384700	0.00009000
O	-2.41138500	0.09080300	0.00019500
C	-1.20806700	0.01336900	-0.00002200
N	-0.02484200	-0.01139500	-0.00041600
H	3.30566700	-0.06377700	0.00054300
H	2.13627500	1.37497200	-0.00002000

ZPE Corrected Energy: -245.491486

Figure 5.7 – B3LYP/6-311++G(d,p)

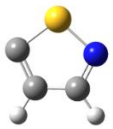

$C_3H_2NS^-$ (Isothiazole)

Atom	X	Y	Z
C	-1.18861900	0.76937900	0.00015400
C	0.07649100	1.36347700	-0.00021300
S	1.13600300	0.00548800	0.00008100
C	-1.18751600	-0.66149900	-0.00012400
N	-0.02450500	-1.28313900	-0.00010800
H	-2.09068200	-1.27307800	0.00045700
H	-2.11596800	1.33909300	0.00010400

ZPE Corrected Energy: -568.468597

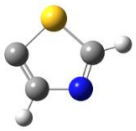

$C_3H_2NS^-$ (Thiazole)

Atom	X	Y	Z
C	-1.23021800	-0.66509900	-0.00007200
C	-0.03596100	-1.36918300	-0.00018400
C	-0.04228500	1.20242800	-0.00026100
N	-1.25667100	0.73217000	0.00001900
S	1.16583900	-0.07737600	0.00008800
H	0.19391800	2.26123100	0.00056000
H	-2.19985400	-1.15728500	0.00101100

ZPE Corrected Energy: -568.469117

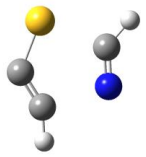

Transition State 1

Atom	X	Y	Z
C	0.78052500	1.41615000	0.00000000
C	-0.46731100	1.20109700	0.00000000
C	0.71577000	-1.24412300	0.00000000
N	1.65735700	-0.48901100	0.00000000
S	-1.24793800	-0.28610600	0.00000000
H	0.57289400	-2.31828100	0.00000000
H	1.61871300	2.08030400	-0.00000100

ZPE Corrected Energy: -568.421161

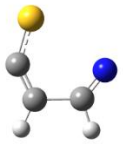

Transition State 2

Atom	X	Y	Z
C	-0.73646100	1.19364000	0.00008900
C	0.55387200	0.95771500	-0.00005500
S	1.51529400	-0.33089900	-0.00017000
C	-1.65510700	-0.13242600	0.00018200
N	-1.32070500	-1.31123800	0.00013800
H	-2.70256100	0.22644700	0.00030000
H	-1.27103500	2.13302300	0.00015300

ZPE Corrected Energy: -568.436533

APPENDIX B

Additional Computational Results for Chapters 6 & 7

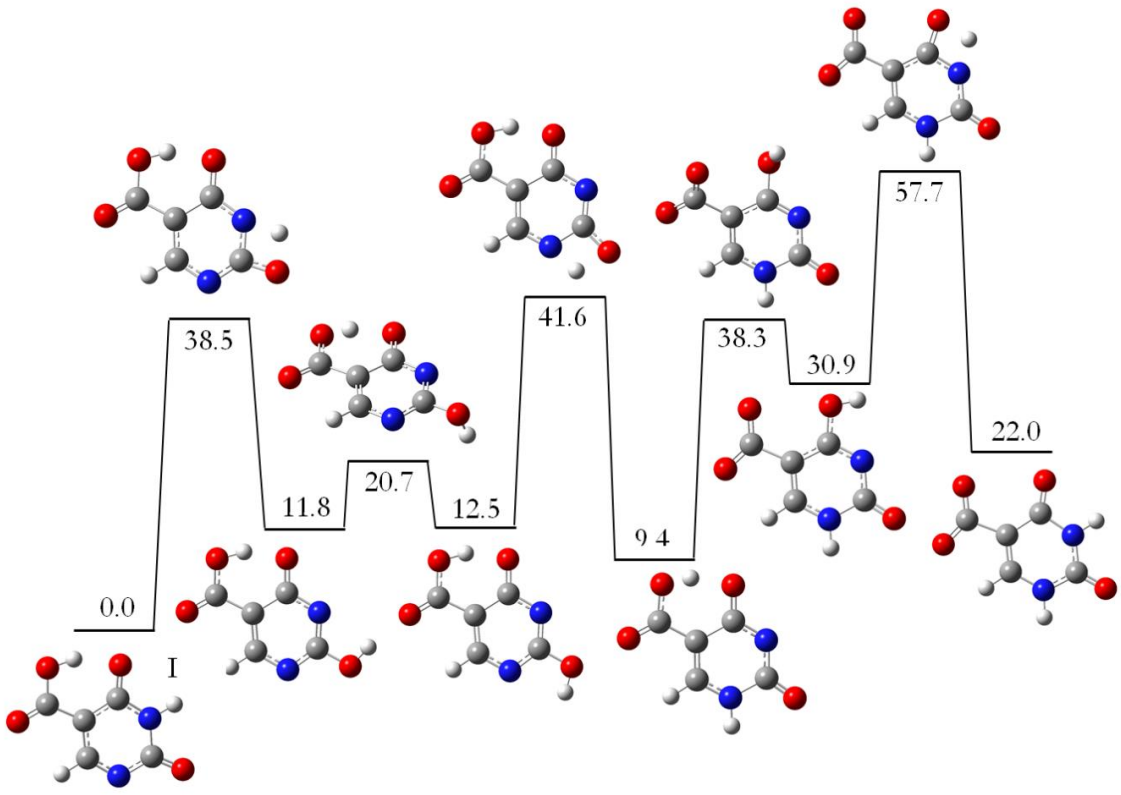

Tautomerization of $C_5H_3N_2O_4^-$ involves many low energy H transfers throughout the ion. This potential energy surface (kcal mol^{-1}) is calculated at the B3LYP/6-311++G(d,p) level of theory and displays the barriers to the conversion between several $C_5H_3N_2O_4^-$ structures.

Cartesian coordinates (Å) and energies (Hartree) for optimized geometries in Chapters 6 & 7

Figures 6.3 and 6.5 – B3LYP/6-311++G(d,p)

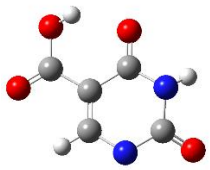

I ($C_5H_3N_2O_4^-$)

Atom	X	Y	Z
C	0.04617500	1.00637400	-0.00006000
O	-0.52984200	2.12022600	-0.00004900
N	1.42610200	0.94647200	-0.00005400
C	2.22715700	-0.21942300	-0.00012000
N	1.56882200	-1.42551300	0.00006100
C	-0.58922000	-0.27656500	0.00000000
C	0.24594700	-1.40323000	0.00007400
O	3.44730900	-0.08582000	0.00006500
C	-2.05344000	-0.42041400	0.00001800
O	-2.75195300	0.74009100	-0.00008000
O	-2.64060300	-1.48822600	0.00013400
H	-0.24794500	-2.37309800	0.00014700
H	1.92140500	1.82818700	-0.00006300
H	-2.09694100	1.48758100	-0.00017500

ZPE (Zero Point Energy) Corrected Energy: -602.981746

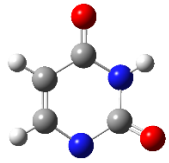

II ($C_4H_3N_2O_2^-$)

Atom	X	Y	Z
N	-0.00659100	-0.93387800	0.00025000
H	0.00671100	-1.94477200	0.00009000
C	1.25709900	-0.30078500	0.00017200
N	1.26762200	1.06509800	0.00004600
C	-1.17660000	1.10051000	0.00000800
C	0.07881600	1.68159400	-0.00010600
O	2.26452000	-1.01760700	-0.00026800
H	-2.08472600	1.68809100	-0.00021600
C	-1.26761400	-0.32772400	0.00052000
O	-2.29398400	-1.02689600	-0.00037200
H	0.13630300	2.77260100	-0.00038000

ZPE Corrected Energy: -414.330551

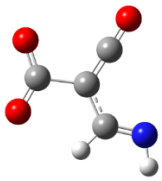

III ($C_4H_2NO_3^-$)

Atom	X	Y	Z
C	-0.55042600	1.23686400	0.00007500
O	-0.84480100	2.36162700	0.00006100
N	-2.42205200	-0.99127600	-0.00005100
C	-0.18048300	-0.02932800	0.00001200
C	-1.13809500	-1.11424700	-0.00005000
H	-2.84839100	-1.91840900	-0.00008800
H	-0.61883100	-2.07940600	-0.00009800
C	1.38226800	-0.31557600	-0.00000300
O	2.10155600	0.69935000	-0.00016800
O	1.66099500	-1.52716900	0.00015000

ZPE Corrected Energy: -434.172845

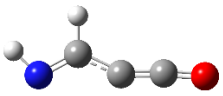

IV ($C_3H_2NO^-$)

Atom	X	Y	Z
C	-1.30872300	-0.02944300	0.00000000
O	-2.52174000	-0.01794100	0.00000100
N	2.34819100	-0.36526200	0.00000100
C	-0.06065500	-0.14852100	-0.00000100
C	1.24623300	0.34021200	-0.00000100
H	3.14025100	0.28094800	0.00000200
H	1.33520300	1.44592200	0.00000100

ZPE Corrected Energy: -245.515298

Figure 6.7 – B3LYP/6-311++G(d,p)

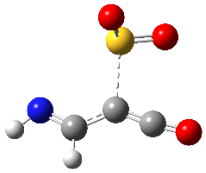

Intermediate 1a

Atom	X	Y	Z
C	-2.05850800	0.35303500	-0.01186200
C	-0.60064400	-1.65798000	0.11555500
C	-0.85295400	-0.40599000	-0.04346100
H	-2.95668100	-0.22042300	0.27156000
H	-3.11452300	1.91296600	-0.17713600
O	-0.21220000	-2.76868000	0.22679600
N	-2.14619400	1.61208600	-0.28668500
S	1.06564300	0.76057700	-0.23166800
O	1.32310500	1.16593900	1.17960400
O	2.02870900	-0.25735400	-0.74919200

ZPE Corrected Energy: -794.211163

Intermediate 2a

Atom	X	Y	Z
C	1.81941200	0.62984600	0.08993000
C	-0.72064400	1.18674400	0.06469500
C	0.43731200	0.35840400	0.05428100
H	2.02922700	1.68674900	0.31818600
H	3.67595000	0.24397400	-0.03043500
O	-0.97283600	2.36660100	0.19520100
N	2.77625200	-0.22654600	-0.11675500
S	-0.49058500	-1.08503900	-0.39380600
O	-0.61788000	-2.09130800	0.70559500
O	-1.72254200	0.22042700	-0.20367000

ZPE Corrected Energy: -794.223070

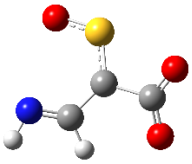

Intermediate 3a

Atom	X	Y	Z
C	0.31236200	1.57839600	-0.03971200
C	-1.65110300	-0.13037300	0.02891600
C	-0.10697300	0.18399100	0.03200500
H	-0.44747800	2.20218100	-0.52126800
H	1.43750400	3.04763000	0.30206600
O	-2.30897900	0.73590800	-0.58281500
N	1.40437800	2.03700400	0.45456000
S	0.85049600	-1.15187000	-0.06453300
O	2.33148800	-0.91548500	-0.27332700
O	-1.99179900	-1.17929800	0.59896200

ZPE Corrected Energy: -794.239892

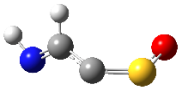

$C_2H_2NOS^-$ (Product)

Atom	X	Y	Z
C	-1.48825600	-0.05082900	0.36970600
C	-0.33206000	-0.79805200	0.03232600
H	-1.55430900	0.13783100	1.45864500
H	-3.16518000	0.79598000	0.13507000
N	-2.45127200	0.32227000	-0.42000700
S	1.21306900	-0.41137600	-0.08648600
O	1.67389700	1.06069900	0.03974000

ZPE Corrected Energy: -605.579781

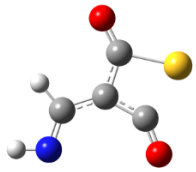

Intermediate 1b

Atom	X	Y	Z
C	1.86141200	0.64673700	0.00002700
C	-0.65853600	1.03342800	-0.00000800
C	0.50619100	0.19623300	-0.00000500
H	1.92516500	1.74587400	-0.00010100
H	3.74895200	0.51404900	-0.00010500
O	-0.87044500	2.22505700	0.00003500
N	2.92655200	-0.09029400	-0.00001400
O	0.21705000	-2.25477600	0.00002300
C	-0.10269100	-1.09993900	0.00002800
S	-1.91069300	-0.37805400	-0.00002600

ZPE Corrected Energy: -757.152824

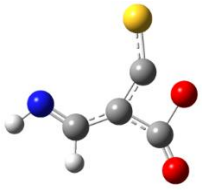

Intermediate 2b

Atom	X	Y	Z
C	1.11898700	1.60693200	0.00029500
C	1.18737400	-0.99862800	0.00017000
C	0.55979900	0.30081600	0.00100400
H	2.22039200	1.57958900	0.00050700
H	1.14674800	3.49873400	-0.00070600
O	2.25754400	-1.54657400	-0.00076800
N	0.47532100	2.73036100	-0.00039000
O	-0.09199200	-1.67439800	0.00026300
C	-0.69387500	-0.36680200	0.00043200
S	-2.31578200	-0.10481200	-0.00027700

ZPE Corrected Energy: -757.129496

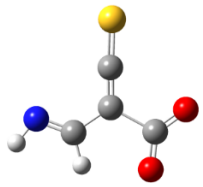

Intermediate 3b

Atom	X	Y	Z
C	-0.82284000	1.60249000	0.00002600
C	-1.37300000	-0.98542500	-0.00001200
C	-0.29019000	0.24481000	0.00026400
H	-1.91787100	1.58756100	-0.00014100
H	-0.75143000	3.48538700	-0.00007700
O	-2.54154700	-0.56724100	-0.00004600
N	-0.12151700	2.68128300	0.00006600
O	-0.88747100	-2.11896500	-0.00021000
C	0.98240700	-0.04214800	0.00036900
S	2.49836300	-0.45441500	-0.00013000

ZPE Corrected Energy: -757.127459

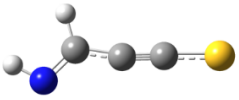

$C_3H_2NS^-$ (Product)

Atom	X	Y	Z
C	-1.92490300	0.37213500	0.00014200
C	-0.55981400	0.07690600	-0.00283000
H	-2.15440700	1.45365200	0.00248300
H	-3.78660100	0.02929300	0.00325800
N	-2.90458500	-0.48706000	0.00057300
C	0.67627300	0.03270400	-0.00067700
S	2.32023600	-0.06025000	0.00065200

ZPE Corrected Energy: -568.495339

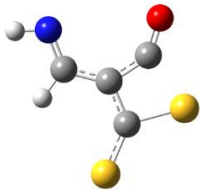

Intermediate 1c

Atom	X	Y	Z
C	1.28655100	-1.52289800	-0.00010700
C	0.96472200	1.07977900	0.00038300
C	0.54849300	-0.29548600	-0.00009300
H	0.62292700	-2.39888500	-0.00018900
H	2.82163200	-2.62627400	-0.00008300
O	1.95573200	1.74623200	0.00012400
N	2.57427100	-1.63596900	-0.00006400
C	-0.86260800	-0.13948900	-0.00016800
S	-0.90042200	1.68181600	-0.00015900
S	-2.14540700	-1.19583900	0.00013600

ZPE Corrected Energy: -1080.115705

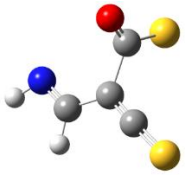

Intermediate 2c

Atom	X	Y	Z
C	0.31320800	1.89260100	-0.29985000
C	0.97367100	-0.55233100	0.51763600
C	-0.11896100	0.53813000	0.01196300
H	-0.49724300	2.54542300	-0.65194400
H	1.57248700	3.28588500	-0.46803700
O	1.20096700	-0.50843500	1.71064200
N	1.51959900	2.30706000	-0.18379100
C	-1.36503100	0.16817000	-0.01824700
S	1.59441300	-1.52146400	-0.73734500
S	-2.85300600	-0.36557800	-0.04688200

ZPE Corrected Energy: -1080.081869

Figure 6.10 – B3LYP/6-311++G(d,p)

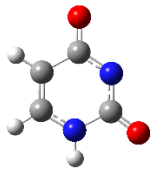

$C_4H_3N_2O_2^-$

Atom	X	Y	Z
C	-1.22266100	-0.41235400	0.00001500
O	-2.32682200	-0.98636500	-0.00001000
N	-0.03775900	-1.10051400	0.00000500
C	1.15097700	-0.47846300	-0.00000800
N	1.15986700	0.95715100	-0.00000300
C	-1.18402500	1.06908900	0.00000200
C	0.00938500	1.69499800	0.00000100
O	2.26990300	-1.01530100	0.00000100
H	0.12461300	2.77539600	-0.00000100
H	-2.11737200	1.61641200	0.00000000
H	2.07129600	1.38545100	-0.00000400

ZPE Corrected Energy: -414.309924

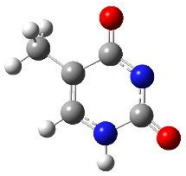

$C_5H_5N_2O_2^-$

Atom	X	Y	Z
N	0.74441600	1.14677100	-0.00005900
H	1.84007200	-1.91723100	0.00002600
C	1.64083500	0.14663000	-0.00022300
N	1.14119400	-1.19209000	-0.00002600
C	-1.10945800	-0.48418100	-0.00002100
C	-0.19864500	-1.47832500	0.00001500
O	2.87735500	0.26007600	0.00016800
C	-0.60248700	0.91887500	-0.00004400
O	-1.43610600	1.84494800	0.00006200
H	-0.46777800	-2.53206800	0.00009200
C	-2.58974800	-0.72649700	0.00002700
H	-3.06315500	-0.26674000	0.87422000
H	-3.06320600	-0.26676700	-0.87415200
H	-2.81817800	-1.79915600	0.00005100

ZPE Corrected Energy: -453.610956

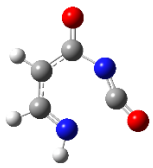

Uracil Transition State 1

Atom	X	Y	Z
N	0.03513100	-1.11445500	0.00038100
H	1.77972800	2.18331300	-0.00008000
C	1.22651400	-0.82408300	0.00008000
N	1.11212500	1.41793800	0.00009900
C	-1.25748900	0.97283000	-0.00031900
C	-0.13983400	1.81592900	0.00012500
O	2.39154900	-1.03711600	-0.00027400
H	-2.24495500	1.41819500	-0.00049600
C	-1.23368100	-0.45136200	-0.00000200
O	-2.23750600	-1.17520800	-0.00003600
H	-0.37096400	2.89282000	0.00039500

ZPE Corrected Energy: -414.278523

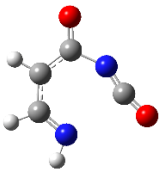

Uracil Intermediate 1

Atom	X	Y	Z
N	-0.15163500	-1.10027400	0.00034100
H	-1.41497600	2.61412400	0.00020800
C	-1.33235800	-0.87561200	-0.00003300
N	-0.95344900	1.70696800	0.00043800
C	1.33715100	0.84756800	-0.00022300
C	0.34680900	1.85581600	-0.00014200
O	-2.51184500	-0.92681400	-0.00032200
H	2.37132800	1.17397800	-0.00061500
C	1.18888600	-0.55909100	0.00004500
O	2.10659600	-1.38808200	0.00003300
H	0.77830600	2.87211700	-0.00061300

ZPE Corrected Energy: -414.279086

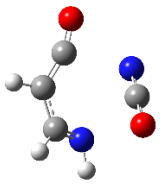

Uracil Transition State 2

Atom	X	Y	Z
N	0.89210700	1.22836500	-0.53191000
H	0.20862500	-2.78487500	-0.96339100
C	1.82466700	0.66301600	-0.05086800
N	-0.35631400	-1.93612500	-0.92715400
C	-1.32588600	-0.46138500	0.72608600
C	-0.60815100	-1.63762200	0.29443300
O	2.77647000	0.08701600	0.44336800
H	-1.80481400	-0.46987400	1.70169000
C	-1.42515500	0.73025300	0.11657100
O	-1.85648100	1.75493700	-0.21434200
H	-0.30712900	-2.29211900	1.12560400

ZPE Corrected Energy: -414.244268

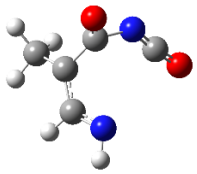

Thymine Transition State 1

Atom	X	Y	Z
N	-1.19705300	-0.83097400	0.21699100
H	1.18316600	2.87170700	0.97682100
C	-1.96811800	0.00485000	-0.17433900
N	0.85705500	1.90825400	1.01148100
C	1.13167200	-0.10388600	-0.32591500
C	1.32608700	1.24566600	-0.03623500
O	-2.81471100	0.73202500	-0.55597200
C	0.26353700	-0.88509900	0.56265100
O	0.53915800	-1.61393600	1.47654200
H	1.93455600	1.76697000	-0.79887000
C	1.40954200	-0.69398300	-1.68454500
H	1.91976800	-1.66838800	-1.64095900
H	0.50622900	-0.84619500	-2.30760800
H	2.06436400	-0.01505200	-2.24295400

ZPE Corrected Energy: -453.540022

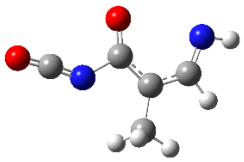

Thymine Intermediate 1

Atom	X	Y	Z
N	-1.36852500	0.33088200	-0.00023600
H	3.92287000	-1.04848500	-0.00060200
C	-2.51949300	0.00154300	-0.00006700
N	2.90442300	-1.11849900	0.00021400
C	1.04486400	0.51307600	0.00004900
C	2.41162800	0.08785300	-0.00013200
O	-3.68210600	-0.23418500	0.00004800
C	-0.02002700	-0.40410300	0.00002600
O	-0.07550500	-1.62218900	0.00006700
H	3.10428400	0.94967800	-0.00113600
C	0.77366400	2.00586200	0.00017200
H	0.20699700	2.34229400	-0.87772000
H	0.20849700	2.34237700	0.87902700
H	1.72313100	2.55307200	-0.00062800

ZPE Corrected Energy: -453.570579

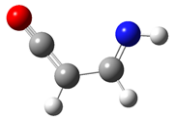

C_3H_3NO (Uracil Product)

Atom	X	Y	Z
H	-2.55196200	-1.07958000	0.00000000
N	-1.55061900	-0.89292700	0.00000000
C	0.03361800	0.91556200	0.00000000
C	-1.31593000	0.36222200	0.00000000
H	0.20586900	1.98397400	-0.00000100
C	1.10520500	0.13518000	0.00000000
O	2.04568000	-0.53219900	0.00000000
H	-2.10237500	1.12590300	0.00000100

ZPE Corrected Energy: -246.069836

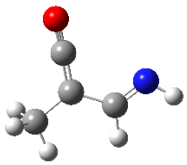

C_4H_5NO (Thymine Product)

Atom	X	Y	Z
H	-2.94169500	-0.63144100	0.00017800
N	-1.93386800	-0.77576800	0.00000300
C	0.15082700	0.44906400	-0.00001700
C	-1.30765100	0.33764300	-0.00011200
C	0.85373000	-0.67641300	-0.00002800
O	1.48604300	-1.64395100	-0.00003500
H	-1.81173900	1.31356300	0.00006100
C	0.85918200	1.79569200	0.00009800
H	1.48204500	1.94090500	0.88618800
H	1.48220700	1.94096100	-0.88586800
H	0.10137600	2.58208300	0.00005300

ZPE Corrected Energy: -285.365389

Figure 6.11 – B3LYP/6-311++G(d,p)

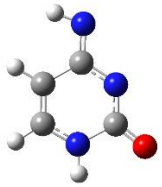

$C_4H_4N_3O^-$

Atom	X	Y	Z
N	-0.02612800	-1.10149900	-0.00751000
C	1.16002000	-0.49280900	0.00279900
N	1.18529700	0.95004500	0.06385500
C	-1.15708500	1.07528300	-0.03753800
C	0.04063100	1.69272500	-0.00701000
O	2.27997700	-1.03117300	-0.02749100
H	-2.07352700	1.65297700	-0.07848100
C	-1.20912200	-0.40209300	-0.00227500
H	0.15646800	2.77296000	-0.02308200
N	-2.34806800	-1.05098500	0.02532000
H	-3.10585500	-0.36626100	0.01862200
H	2.09872000	1.36814500	-0.00464100

ZPE Corrected Energy: -394.392593

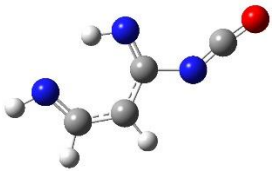

Intermediate 1

Atom	X	Y	Z
N	-1.37517400	0.48525200	0.31669900
C	-2.30668800	-0.19020200	-0.00411400
N	3.13545900	-0.13871400	-0.20250300
C	0.74691900	-0.64323400	0.17794700
C	2.12888700	-0.93542900	0.04021000
O	-3.29894100	-0.78547900	-0.26455100
H	0.11466500	-1.49800400	0.38691400
C	0.09107900	0.60807600	0.09694800
H	2.31542700	-2.01904900	0.16779600
N	0.55663700	1.79587200	-0.11260400
H	-0.20668300	2.46790200	-0.08439900
H	3.98848200	-0.69915700	-0.23098500

ZPE Corrected Energy: -394.354501

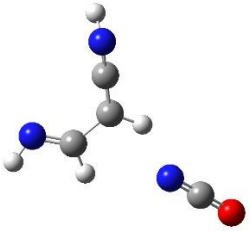

Intermediate 2

Atom	X	Y	Z
N	1.98680400	0.05170100	-0.07247200
C	3.15753500	-0.15566800	-0.00188200
N	-2.17593100	1.93128500	0.06705100
C	-1.04327400	-0.21704000	-0.05780300
C	-1.09620000	1.24269200	-0.03238300
O	4.35613000	-0.36313500	0.07046100
H	-0.02829400	-0.62993000	-0.08693500
C	-2.09914000	-0.99627300	-0.01207800
H	-0.09391500	1.67596200	-0.10093100
N	-3.07294100	-1.73544100	-0.08320500
H	-3.46136300	-2.04138300	0.81001700
H	-1.94451500	2.92534000	0.05942800

ZPE Corrected Energy: -394.359193

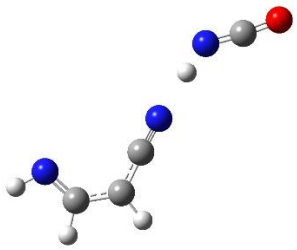

Intermediate 3

Atom	X	Y	Z
N	-2.60818500	0.69030500	-0.00003200
C	-3.66793700	0.14447600	-0.00000800
N	3.69180800	1.10461400	-0.00002200
C	2.39155100	-0.96422000	-0.00004100
C	3.58194500	-0.19668600	0.00021000
O	-4.76861300	-0.29682300	0.00026400
H	2.47215100	-2.04479000	-0.00014500
C	1.10692900	-0.44206700	-0.00019300
H	4.48552600	-0.83143100	0.00090900
N	0.00447200	-0.04863600	-0.00038500
H	-1.57884100	0.41861100	-0.00027600
H	4.67846500	1.35919900	0.00066000

ZPE Corrected Energy: -394.391346

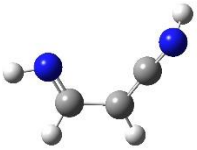

$C_3H_4N_2$ (Product 1)

Atom	X	Y	Z
N	-1.57135600	-0.91745800	0.01779700
C	-0.00895500	0.91901400	0.02690700
C	-1.35015300	0.34031700	-0.01266900
H	0.10403100	1.99545000	0.07918200
C	1.09063500	0.18304200	0.01303100
H	-2.15164700	1.08690100	-0.07079400
N	2.09519800	-0.47669500	-0.13522700
H	2.56212900	-0.86582500	0.68247200
H	-2.57056600	-1.11169000	-0.03246800

ZPE Corrected Energy: -226.164372

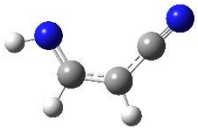

$C_3H_3N_2^-$ (Product 2)

Atom	X	Y	Z
N	-1.66540100	-0.86969200	-0.00002100
C	0.08231000	0.85038700	-0.00000700
C	-1.24488500	0.37374700	-0.00002700
H	0.23681500	1.92385500	-0.00020400
C	1.23660800	0.05985500	0.00017300
H	-1.97843600	1.20099600	0.00003500
N	2.23428500	-0.55234200	-0.00008700
H	-2.68476400	-0.87455700	0.00008900

ZPE Corrected Energy: -225.644365

Figures 7.5 & 7.6 – B3LYP/6-311++G(d,p)

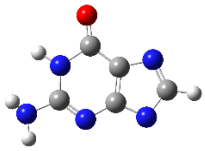

G3

Atom	X	Y	Z
C	0.13613300	1.44941400	-0.00292000
O	0.10955800	2.68160300	0.01171500
N	1.42270100	0.81002500	0.00286800
C	1.64263000	-0.54631200	0.01085800
N	0.71005900	-1.43823400	-0.00114300
C	-0.89394400	0.46547700	-0.01567400
C	-0.57332900	-0.91999900	0.00573000
H	2.19870200	1.44345600	0.13488800
N	3.00278800	-0.93091600	0.07452700
H	3.56896400	-0.49365900	-0.64523600
H	3.05420100	-1.93918500	-0.01108000
N	-2.26040800	0.60126100	-0.02029300
C	-2.66673400	-0.67131200	-0.00422400
N	-1.71031200	-1.64177700	0.01106700
H	-3.72065600	-0.92956600	-0.00409500

ZPE Corrected Energy: -542.062097

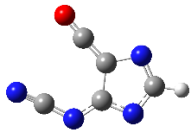

GF1

Atom	X	Y	Z
C	0.41225800	1.55698800	0.00021300
O	1.18102400	2.42642100	-0.00033100
N	2.97131200	-0.68553600	-0.00000100
C	1.87072000	-1.09385400	-0.00003300
N	0.68565600	-1.63859100	0.00004100
C	-0.52344000	0.61586300	0.00021100
C	-0.40245900	-0.86880500	0.00031400
N	-1.89915300	0.95913400	0.00028600
C	-2.45572600	-0.23442900	-0.00017500
N	-1.66063800	-1.33925000	-0.00034500
H	-3.53655400	-0.33625200	-0.00040500

ZPE Corrected Energy: -485.455325

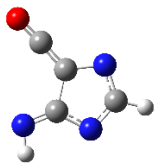

GF2

Atom	X	Y	Z
C	1.65150100	-0.27551700	0.00007700
O	2.81865300	-0.16070300	0.00001900
N	-0.21458800	2.07249400	-0.00005400
C	0.33825800	-0.35772800	-0.00012300
C	-0.58936700	0.82741700	-0.00000700
N	-0.42645500	-1.55419600	-0.00001300
C	-1.65480300	-1.05898600	-0.00000200
N	-1.85318400	0.27654300	0.00024900
H	-2.50539400	-1.73766700	-0.00067800
H	-1.05777400	2.64828700	-0.00041600

ZPE Corrected Energy: -393.164447

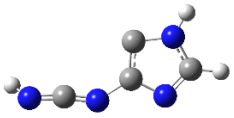

GF3

Atom	X	Y	Z
C	2.19638500	-0.09615500	0.00873100
N	1.10747200	-0.60332400	0.03567000
C	-0.67917100	1.15287200	0.00984100
C	-0.22771000	-0.17522400	0.01065600
N	3.37819400	0.28328500	-0.14478400
H	3.82870300	0.58150900	0.71768800
N	-2.05246600	0.90140300	-0.00668200
C	-2.33146700	-0.44873000	-0.01129100
N	-1.21815900	-1.14554200	0.00284800
H	-3.33378400	-0.85811500	-0.02399300
H	-2.74843400	1.62926800	-0.01068900

ZPE Corrected Energy: -373.228095

GF4

Atom	X	Y	Z
N	-3.21230200	0.42506500	-0.00008900
C	-2.14591700	-0.04433600	-0.00001800
N	-1.05834200	-0.80813200	0.00006300
C	0.56508400	1.20586000	0.00023100
C	0.13154000	-0.30901200	0.00003600
N	1.88822200	1.11080000	-0.00013300
C	2.21729500	-0.26649300	-0.00008000
N	1.25797900	-1.14813500	0.00000700
H	3.26309300	-0.57330000	0.00005600

ZPE Corrected Energy: -372.016101

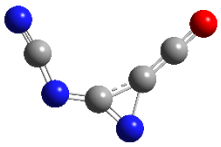

GF5

Atom	X	Y	Z
C	1.96741400	-0.45116300	0.00008100
O	2.86710200	-1.23570100	0.00011400
N	-2.67608300	-1.50393400	-0.00014900
C	-2.11969200	-0.47602200	0.00005500
N	-1.62494400	0.74254600	0.00027900
C	0.99735600	0.37271400	-0.00038000
C	-0.33019600	0.94034700	0.00000300
N	0.58301000	1.84286700	-0.00005300

ZPE Corrected Energy: -391.922741

GF6

Atom	X	Y	Z
N	-2.01469600	-0.17323400	-0.00013000
C	0.25565300	-1.29465100	0.00058600
C	-0.73913100	-0.10058100	-0.00019900
N	1.44425800	-0.69111200	-0.00054200
C	1.21200900	0.70814800	0.00037800
N	-0.00845300	1.14174100	0.00015300
H	2.06108300	1.39420700	-0.00070800
H	-2.38002700	0.78653100	-0.00024500

ZPE Corrected Energy: -279.739460

Figures 7.5 & 7.7 – B3LYP/6-311++G(d,p)

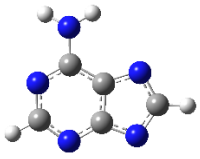

A1

Atom	X	Y	Z
C	-1.17525200	-0.60843900	-0.01912900
N	-1.92708600	0.49953500	0.00291200
C	-1.27678300	1.68665400	0.00706200
N	0.02653200	1.92435900	0.00145100
C	0.21747600	-0.50912200	-0.02061400
C	0.78257800	0.79716400	-0.00687000
N	1.22044400	-1.44652600	-0.00649900
C	2.31230100	-0.65986500	0.01095000
N	2.13792000	0.68296900	0.01036400
H	3.30908500	-1.08994500	0.02597300
H	-1.92674000	2.56038900	0.02229100
N	-1.82135800	-1.84198500	-0.07056000
H	-1.24563400	-2.61187200	0.24168200
H	-2.75380000	-1.82539200	0.31798500

ZPE Corrected Energy: -466.804529

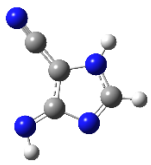

AF1

Atom	X	Y	Z
C	1.81874200	-0.05832500	0.00000000
N	-0.51789500	2.12140700	0.00000000
C	0.43896000	-0.15950100	0.00000000
C	-0.62138000	0.81765500	0.00000000
N	-0.20974400	-1.42576900	-0.00000100
C	-1.54044900	-1.18517700	0.00000000
N	-1.84887500	0.08546300	0.00000000
H	-2.25707700	-1.99847700	0.00000100
N	2.99035700	-0.01995300	0.00000000
H	0.24838700	-2.32017700	0.00000100
H	-1.46344800	2.50270300	0.00000000

ZPE Corrected Energy: -373.281064

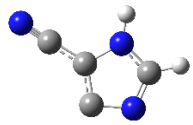

AF2

Atom	X	Y	Z
C	1.72208000	-0.07296000	0.00002100
C	0.31824200	-0.16353300	0.00013700
C	-0.52735800	-1.28408500	0.00009000
N	-0.45491900	1.01909400	-0.00031000
C	-1.74460200	0.58941000	-0.00000200
N	-1.84224200	-0.72267800	-0.00002800
H	-2.56942200	1.29575000	-0.00009600
N	2.88198700	0.03438600	-0.00008000
H	-0.13452600	1.97564800	0.00154700

ZPE Corrected Energy: -317.871764

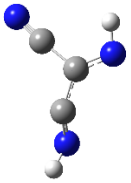

AF3

Atom	X	Y	Z
C	-1.18960900	-0.42674700	0.03078100
N	2.15530900	-0.65000700	-0.28898100
C	-0.03478400	0.45293800	0.03796400
C	1.15290500	-0.23432600	0.37107300
N	-0.18296200	1.77099900	-0.07180500
N	-2.14953300	-1.07429300	-0.06263200
H	2.84381100	-1.07936700	0.34044600
H	-1.17458200	2.00127400	-0.01543000

ZPE Corrected Energy: -279.757886

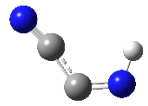

AF4

Atom	X	Y	Z
C	-0.69175500	-0.05351100	0.00000000
C	0.64990600	-0.58915100	0.00000200
N	1.67831300	0.21224700	-0.00000200
N	-1.84314000	0.16485600	0.00000000
H	1.40488900	1.21625600	0.00000800

ZPE Corrected Energy: -186.299160

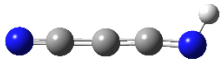

AF5

Atom	X	Y	Z
C	-1.41541700	-0.00037100	-0.00208400
C	-0.07329400	-0.02500500	-0.01484900
C	1.17493400	-0.00332100	-0.00253100
N	2.44388000	-0.10979300	0.00791100
N	-2.59350500	0.02247200	0.00831900
H	2.93003800	0.78343000	0.00317600

ZPE Corrected Energy: -224.437823

BIBLIOGRAPHY

G. W. Adams; J. H. Bowie; R. N. Hayes, *Negative-Ion Fragmentations of Deprotonated Heterocycles - the Isothiazole, Thiazole, Isoxazole, and Oxazole Ring-Systems*. Int. J. Mass Spectrom. Ion Proc., **1992**, *114*, 163-182.

N. Adams; D. Smith, *The Selected Ion Flow Tube (SIFT); A Technique for Studying Ion-Neutral Reactions*. Int. J. Mass Spectrom. Ion Proc., **1976**, *21*, 349-359.

G. R. Adande; N. J. Woolf; L. M. Ziurys, *Observations of Interstellar Formamide: Availability of a Prebiotic Precursor in the Galactic Habitable Zone*. Astrobiology, **2013**, *13*, 439-453.

V. V. Afrosimov; A. A. Basalaev; Y. G. Morozov; M. N. Panov; O. V. Smirnov; E. A. Tropp, *Fragmentation of Adenine and Uracil Molecules through Electron Captures in Collisions with Ions*. Tech. Phys., **2012**, *57*, 594-602.

M. Agundez; J. Cernicharo; M. Guelin; C. Kahane; E. Roueff; J. Klos; F. J. Aoiz; F. Lique; N. Marcelino; J. R. Goicoechea; M. G. Garcia; C. A. Gottlieb; M. C. McCarthy; P. Thaddeus, *Astronomical Identification of CN^-, the Smallest Observed Molecular Anion*. Astron. Astrophys., **2010**, *517*, L2-L6.

J. Almlof; G. Hvistendahl; E. Uggerud, *An MC SCF Study of the Reaction $C_3H_7^+$ -> $C_3H_5^+$+H_2*. Chem. Phys., **1984**, *90*, 55-62.

F. Alvarado; S. Bari; R. Hoekstra; T. Schlatholter, *Interactions of Neutral and Singly Charged keV Atomic Particles with Gas-Phase Adenine Molecules*. J. Chem. Phys., **2007**, *127*, 034301.

L. S. Arani; P. Mignon; H. Abdoul-Carime; B. Farizon; M. Farizon; H. Chermette, *DFT Study of the Fragmentation Mechanism of Uracil RNA Base*. Phys. Chem. Chem. Phys., **2012**, *14*, 9855-9870.

P. J. Ausloos; S. G. Lias, *Discrimination of $C_3H_3^+$ Structures on the Basis of Chemical Reactivity*. J. Am. Chem. Soc., **1981**, *103*, 6505-6507.

J. V. Auwera; K. Didriche; A. Perrin; F. Keller, *Absolute Line Intensities for Formic Acid and Dissociation Constant of the Dimer*. J. Chem. Phys., **2007**, *126*, 124311.

A. Bacmann; V. Taquet; A. Faure; C. Kahane; C. Ceccarelli, *Detection of Complex Organic Molecules in a Prestellar Core: A New Challenge for Astrochemical Models*. Astron. Astrophys., **2012**, *541*, L12-L16.

E. L. O. Bakes; A. G. G. M. Tielens, *The Photoelectric Heating Mechanism for Very Small Graphitic Grains and Polycyclic Aromatic Hydrocarbons*. Astrophys. J., **1994**, *427*, 822-838.

B. Barc; M. Ryszka; J. Spurrell; M. Dampc; P. Limao-Vieira; R. Parajuli; N. J. Mason; S. Eden, *Multi-Photon Ionization and Fragmentation of Uracil: Neutral Excited-State Ring Opening and Hydration Effects*. J. Chem. Phys., **2013**, *139*, 244311.

C. Barckholtz; T. P. Snow; V. M. Bierbaum, *Reactions of C_n^- and C_nH^- with Atomic and Molecular Hydrogen*. Astrophys. J. Lett., **2001**, *547*, L171-L174.

H. L. Barks; R. Buckley; G. A. Grieves; E. Di Mauro; N. V. Hud; T. M. Orlando, *Guanine, Adenine, and Hypoxanthine Production in UV-Irradiated Formamide Solutions: Relaxation of the Requirements for Prebiotic Purine Nucleobase Formation*. ChemBioChem, **2010**, *11*, 1240-1243.

R. J. Bartlett; M. Musiał, *Coupled-Cluster Theory in Quantum Chemistry*. Rev. Mod. Phys., **2007**, *79*, 291-352.

D. G. Beach; W. Gabryelski, *Revisiting the Reactivity of Uracil During Collision Induced Dissociation: Tautomerism and Charge-Directed Processes*. J. Am. Soc. Mass Spectrom., **2012**, *23*, 858-868.

M. Behnke; I. Medvedev; M. Winnewisser; F. C. De Lucia; E. Herbst, *The Millimeter- and Submillimeter-Wave Spectrum of Oxiranecarbonitrile*. Astrophys. J. Suppl. Ser., **2004**, *152*, 97-101.

T. Benijts; W. Lambert; A. De Leenheer, *Analysis of Multiple Endocrine Disruptors in Environmental Waters via Wide-Spectrum Solid-Phase Extraction and Dual-Polarity Ionization LC-Ion Trap-MS/MS*. Anal. Chem., **2004**, *76*, 704-711.

P. P. Bera; T. J. Lee; H. F. Schaefer, *Are Isomers of the Vinyl Cyanide Ion Missing Links for Interstellar Pyrimidine Formation?* J. Chem. Phys., **2009**, *131*, 074303.

P. P. Bera; M. Nuevo; S. N. Milam; S. A. Sandford; T. J. Lee, *Mechanism for the Abiotic Synthesis of Uracil via UV-Induced Oxidation of Pyrimidine in Pure H_2O Ices Under Astrophysical Conditions*. J. Chem. Phys., **2010**, *133*, 104303.

E. A. Bergin In *Astrobiology: An Astronomer's Perspective*, AIP Conference Proceedings, National Observatory of Rio de Janeiro, 2013.

V. M. Bierbaum, *Flow Tubes*. In *Encyclopedia of Mass Spectrometry*, Armentrout, P. B.; Gross, M. L.; Caprioli, R., Eds. Elsevier: Amsterdam, 2003; Vol. 1, 98-109.

V. M. Bierbaum, *Astrochemistry: From the Laboratory to the Stars*. Distinguished Research Lecture, **2012**.

V. M. Bierbaum, *Go with the Flow: Fifty Years of Innovation and Ion Chemistry using the Flowing Afterglow*. Int. J. Mass Spectrom. , **2014**, *in press*.

B. S. Blumberg, *The NASA Astrobiology Institute: Early History and Organization*. Astrobiology, **2003**, *3*, 463-470.

S. S. Bokatzian-Johnson; M. L. Stover; D. A. Dixon; C. J. Cassady, *Gas-Phase Deprotonation of the Peptide Backbone for Tripeptides and Their Methyl Esters with Hydrogen and Methyl Side Chains*. J. Phys. Chem. B, **2012**, *116*, 14844-14858.

O. V. Borisov; M. B. Goshe; T. P. Conrads; V. S. Rakov; T. D. Veenstra; R. D. Smith, *Low-Energy Collision-Induced Dissociation Fragmentation Analysis of Cysteinyl-Modified Peptides*. Anal. Chem., **2002**, *74*, 2284-2292.

G. Bouchoux, *Gas Phase Acidity of Substituted Benzenes*. Chem. Phys. Lett., **2011**, *506*, 167-174.

E. Boulanger; A. Anoop; D. Nachtigallova; W. Thiel; M. Barbatti, *Photochemical Steps in the Prebiotic Synthesis of Purine Precursors from HCN*. Angewandte Chem.-Int. Ed., **2013**, *52*, 8000-8003.

M. T. Bowers; L. Shuying; P. Kemper; R. Stradling; H. Webb; D. H. Aue; J. R. Gilbert; K. R. Jennings, *$C_3H_5^+$ Isomers - Evidence for the Existence of Long-Lived Allyl and 2-Propenyl Cations in the Gas-Phase*. J. Am. Chem. Soc., **1980**, *102*, 4830-4832.

R. Bredy; J. Bernard; L. Chen; G. Montagne; B. Li; S. Martin, *Fragmentation of Adenine Under Energy Control*. J. Chem. Phys., **2009**, *130*, 114305.

R. L. Brown; W. Wild; C. Cunningham, *ALMA–the Atacama Large Millimeter Array*. Adv. Space Res., **2004**, *34*, 555-559.

S. Brünken; M. C. McCarthy; P. Thaddeus; P. D. Godfrey; R. D. Brown, *Improved Line Frequencies for the Nucleic Acid Base Uracil for a Radioastronomical Search*. Astron. Astrophys., **2006**, *459*, 317-320.

S. Brünken; H. Gupta; C. Gottlieb; M. McCarthy; P. Thaddeus, *Detection of the Carbon Chain Negative Ion C_8H^- in TMC-1*. Astrophys. J. Lett., **2007**, *664*, L43-L46.

E. Buenzli; D. Saumon; M. S. Marley; D. Apai; J. Radigan; L. R. Bedin; I. N. Reid; C. V. Morley, *Cloud Structure of the Nearest Brown Dwarfs: Spectroscopic Variability of Luhman 16AB from the Hubble Space Telescope*. Astrophys. J., **2015**, *798*, 127-140.

R. Buttner; G. Maurer, *Dimerization of Some Organic Acids in the Gas Phase*. Phys. Chem. Chem. Phys., **1983**, *87*, 877-882.

M. P. Callahan; K. E. Smith; H. J. Cleaves, II; J. Ruzicka; J. C. Stern; D. P. Glavin; C. H. House; J. P. Dworkin, *Carbonaceous Meteorites Contain a Wide Range of Extraterrestrial Nucleobases*. Proc. Natl. Acad. Sci. U. S. A., **2011**, *108*, 13995-13998.

A. Canosa; I. R. Sims; D. Travers; I. W. M. Smith; B. R. Rowe, *Reactions of the Methylidine Radical with CH_4, C_2H_2, C_2H_4, C_2H_6, and But-1-ene Studied Between 23 and 295 K with a CRESU Apparatus*. Astron. Astrophys., **1997**, *323*, 644-651.

S. Cazaux; A. G. G. M. Tielens; C. Ceccarelli; A. Castets; V. Wakelam; E. Caux; B. Parise; D. Teyssier, *The Hot Core Around the Low-Mass Protostar IRAS 16293-2422: Scoundrels Rule!* Astrophys. J., **2003**, *593*, L51-L55.

J. Cernicharo; A. M. Heras; A. G. G. M. Tielens; J. R. Pardo; F. Herpin; M. Guelin; L. Waters, *Infrared Space Observatory's discovery of C_4H_2, C_6H_2, and benzene in CRL 618*. Astrophys. J., **2001**, *546*, L123-L126.

J. Cernicharo; M. Guélin; M. Agúndez; K. Kawaguchi; M. McCarthy; P. Thaddeus, *Astronomical Detection of C_4H^-, the Second Interstellar Anion*. Astron. Astrophys., **2007**, *467*, L37-L40.

J. Cernicharo; M. Guelin; M. Agundez; M. C. McCarthy; P. Thaddeus, *Detection of C_5N^- and Vibrationally Excited C_6H in IRC+ 10216* Astrophys. J. Lett., **2008**, *688*, L83-L86.

S. Chakrabarti; S. K. Chakrabarti, *Can DNA Bases be Produced During Molecular Cloud Collapse?* Astron. Astrophys., **2000**, *354*, L6-L8.

J. Chao; B. J. Zwolinski, *Ideal Gas Thermodynamic Properties of Methanoic and Ethanoic Acids*. J. Phys. Chem. Ref. Dat., **1978**, *7*, 363-377.

S. B. Charnley; Y. J. Kuan; H. C. Huang; O. Botta; H. M. Butner; N. Cox; D. Despois; P. Ehrenfreund; Z. Kisiel; Y. Y. Lee; A. J. Markwick; Z. Peeters; S. D. Rodgers, *Astronomical Searches for Nitrogen Heterocycles*. In *Space Life Sciences: Astrobiology: Steps toward Origin of Life and Titan before Cassini*, 2005; Vol. 36, 137-145.

E. C. M. Chen; C. Herder; E. S. Chen, *The Experimental and Theoretical Gas Phase Acidities of Adenine, Guanine, Cytosine, Uracil, Thymine and Halouracils*. J. Molec. Struc., **2006**, *798*, 126-133.

L. Chen; R. Bredy; J. Bernard; G. Montagne; A. R. Allouche; S. Martin, *Fragmentation of Singly Charged Adenine Induced by Neutral Fluorine Beam Impact at 3 keV*. J. Chem. Phys., **2011**, *135*, 114309.

P. Cheng; Y. Li; S. Li; M. Zhang; Z. Zhou, *Collision-Induced Dissociation (CID) of Guanine Radical Cation in the Gas Phase: an Experimental and Computational Study*. Phys. Chem. Chem. Phys., **2010**, *12*, 4667-4677.

W. J. Chesnavich; T. Su; M. T. Bowers, *Collisions in a Non-Central Field - Variational and Trajectory Investigation of Ion-Dipole Capture*. J. Chem. Phys., **1980**, *72*, 2641-2655.

A. C. Cheung; D. M. Rank; C. H. Townes; D. D. Thornton; W. J. Welch, *Detection of NH_3 Molecules in Interstellar Medium by their Microwave Emission*. Phys. Rev. Lett., **1968**, *21*, 1701-1705.

A. C. Cheung; D. M. Rank; C. H. Townes; D. D. Thornton; W. J. Welch, *Detection of Water in Interstellar Regions by its Microwave Radiation*. Nature, **1969**, *221*, 626-628.

C. Chyba; C. Sagan, *Endogenous Production, Exogenous Delivery, and Impact-Shock Synthesis of Organic Molecules - An Inventory for the Origins of Life*. Nature, **1992**, *355*, 125-132.

C. F. Chyba; K. P. Hand, *Astrobiology: The Study of the Living Universe*. Annu. Rev. Astron. Astrophys., **2005**, *43*, 31-74.

P. Ü. Civcir, *A Theoretical Study of Tautomerism of Cytosine, Thymine, Uracil and their 1-Methyl Analogues in the Gas and Aqueous Phases using AM1 and PM3*. J. Mol. Struc. - Theo. Chem., **2000**, *532*, 157-169.

A. J. Cohen; P. Mori-Sanchez; W. Yang, *Insights into Current Limitations of Density Functional Theory*. Science, **2008**, *321*, 792-794.

C. A. Cole; N. Wehres; Z. Yang; D. L. Thomsen; T. P. Snow; V. M. Bierbaum, *A Gas-Phase Formation Route to Interstellar Trans-Methyl Formate*. Astrophys. J. Lett., **2012**, *754*, L5-L8.

C. A. Cole; N. J. Demarais; Z. Yang; T. P. Snow; V. M. Bierbaum, *Heterocyclic Anions of Astrobiological Interest*. Astrophys. J., **2013**, *779*, 181-190.

C. A. Cole; Z.-C. Wang; T. P. Snow; V. M. Bierbaum, *Anionic Derivatives of Uracil: Fragmentation and Reactivity*. Phys. Chem. Chem. Phys., **2014**, *16*, 17835-17844.

C. A. Cole; Z.-C. Wang; T. P. Snow; V. M. Bierbaum, *Deprotonated Purine Dissociation: Experiments, Computations, and Astrobiological Implications*. J. Phys. Chem. A, **2015**, *119*, 334-343.

A. S. Coolidge, *The Vapor Density and Some Other Properties of Formic Acid*. J. Am. Chem. Soc., **1928**, *50*, 2166-2178.

M. A. Cordiner; J. V. Buckle; E. S. Wirstrom; A. O. H. Olofsson; S. B. Charnley, *On the Ubiquity of Molecular Anions in the Dense Interstellar Medium*. Astrophys. J., **2013**, *770*, 48-56.

A. Coustenis; A. Salama; B. Schulz; S. Ott; E. Lellouch; T. Encrenaz; D. Gautier; H. Feuchtgruber, *Titan's Atmosphere from ISO Mid-Infrared Spectroscopy*. Icarus, **2003**, *161*, 383-403.

A. Coustenis; R. K. Achterberg; B. J. Conrath; D. E. Jennings; A. Marten; D. Gautier; C. A. Nixon; F. M. Flasar; N. A. Teanby; B. Bezard; R. E. Samuelson; R. C. Carlson; E. Lellouch; G. L. Bjoraker; P. N. Romani; F. W. Taylor; P. G. J. Irwin; T. Fouchet; A. Hubert; G. S. Orton; V. G. Kunde; S. Vinatier; J. Mondellini; M. M. Abbas; R. Courtin, *The Composition of Titan's Stratosphere from Cassini/CIRS Mid-Infrared Spectra*. Icarus, **2007**, *189*, 35-62.

D. Cremer, Møller–Plesset perturbation theory. *Encyclopedia of Computational Chemistry*, John Wiley and Sons, Ltd.: 2002.

J. Cui; R. V. Yelle; V. Vuitton; J. H. Waite; W. T. Kasprzak; D. A. Gell; H. B. Niemann; I. C. F. Muller-Wodarg; N. Borggren; G. G. Fletcher; E. L. Patrick; E. Raaen; B. A. Magee, *Analysis of Titan's Neutral Upper Atmosphere from Cassini Ion Neutral Mass Spectrometer Measurements*. Icarus, **2009**, *200*, 581-615.

F. F. da Silva; C. Matias; D. Almeida; G. Garcia; O. Ingolfsson; H. D. Flosadottir; B. Omarsson; S. Ptasinska; B. Puschnigg; P. Scheier; P. Limao-Vieira; S. Denifl, *NCO^-, a Key Fragment Upon Dissociative Electron Attachment and Electron Transfer to Pyrimidine Bases: Site Selectivity for a Slow Decay Process*. J. Am. Soc. Mass Spectrom., **2013**, *24*, 1787-1797.

L. Dalila Fondren; J. McLain; D. M. Jackson; N. G. Adams; L. M. Babcock, *Studies of Reactions of a Series of Ions with Nitrogen Containing Heterocyclic Molecules Using a Selected Ion Flow Tube*. Int. J. Mass Spectrom., **2007**, *265*, 60-67.

G. Danger; F. Duvernay; P. Theule; F. Borget; J. C. Guillemin; T. Chiavassa, *Hydroxyacetonitrile ($HOCH_2CN$) as a Precursor for Formylcyanide (CHOCN), Ketenimine (CH_2CNH), and Cyanogen (NCCN) in Astrophysical Conditions*. Astron. Astrophys., **2013**, *549*, A93.

J. de Vries; R. Hoekstra; R. Morgenstern; T. Schlathoelter, *Ionization and Fragmentation Modes of Nucleobases after Collisions with Multiply Charged Ions*. Phys. Scr., **2004**, *T110*, 336-339.

N. J. Demarais; Z. Yang; O. Martinez; N. Wehres; T. P. Snow; V. M. Bierbaum, *Gas-Phase Reactions of Polycyclic Aromatic Hydrocarbon Anions with Molecules of Interstellar Relevance*. Astrophys. J., **2012**, *746*, 32-38.

C. H. DePuy; V. M. Bierbaum; G. K. King; R. H. Shapiro, *Hydrogen-Deuterium Exchange-Reactions of Carbanions with Deuterated Alcohols in the Gas-Phase*. J. Am. Chem. Soc., **1978**, *100*, 2921-2922.

C. H. DePuy; V. M. Bierbaum, *Gas Phase Sulfur Anions: Synthesis and Reactions of H_2NS^- and Related Ions*. Tetrahedron Lett., **1981**, *22*, 5129-5130.

C. H. DePuy; V. M. Bierbaum; R. Damrauer; J. A. Soderquist, *Gas-Phase Reactions of the Acetyl Anion*. J. Am. Chem. Soc., **1985**, *107*, 3385-3386.

C. H. DePuy; S. Gronert; A. Mullin; V. M. Bierbaum, *Gas-Phase S_N2 and E2 Reactions of Alkyl-Halides*. J. Am. Chem. Soc., **1990**, *112*, 8650-8655.

C. H. DePuy; S. Kato, *H/D Exchange Reactions*. In *Encyclopedia of Mass Spectrometry*, Armentrout, P. B.; Gross, M. L.; Caprioli, R., Eds. Elsevier: Ansterdam, 2003; Vol. 1, 670-674.

J. E. Dickens; W. M. Irvine; M. Ohishi; G. Arrhenius; S. Pitsch; A. Bauder; F. Muller; A. Eschenmoser, *A Search for Interstellar Oxiranecarbonitrile (C_3H_3NO)*. Origins Life Evol. Biospheres, **1996**, *26*, 97-110.

J. E. Dickens; W. M. Irvine; M. Ohishi; M. Ikeda; S. Ishikawa; A. Nummelin; A. Hjalmarson, *Detection of Interstellar Ethylene Oxide (c-C_2H_4O)*. Astrophys. J., **1997**, *489*, 753-757.

A. Douglas; G. Herzberg, *Note on CH^+ in Interstellar Space and in the Laboratory*. Astrophys. J., **1941**, *94*, 381.

T. H. Dunning Jr., *Gaussian Basis Sets for use in Correlated Molecular Calculations. I. The Atoms Boron through Neon and Hydrogen*. J. Chem. Phys., **1989**, *90*, 1007-1023.

F. Duvernay; T. Chiavassa; F. Borget; J. P. Aycard, *Experimental Study of Water-Ice Catalyzed Thermal Isomerization of Cyanamide into Carbodiimide: Implication for Prebiotic Chemistry*. J. Am. Chem. Soc., **2004**, *126*, 7772-7773.

P. Ehrenfreund; S. Rasmussen; J. Cleaves; L. Chen, *Experimentally Tracing the Key Steps in the Origin of Life: The Aromatic World*. Astrobiology, **2006**, *6*, 490-520.

P. Ehrenfreund; M. A. Sephton, *Carbon Molecules in Space: from Astrochemistry to Astrobiology*. Faraday Disc., **2006**, *133*, 277-288.

B. Eichelberger; T. P. Snow; C. Barckholtz; V. M. Bierbaum, *Reactions of H, N, and O Atoms with Carbon Chain Anions of Interstellar Interest: An Experimental Study*. Astrophys. J., **2007**, *667*, 1283-1289.

B. R. Eichelberger; T. P. Snow; V. M. Bierbaum, *Collision Rate Constants for Polarizable Ions*. J. Am. Soc. Mass Spectrom., **2003**, *14*, 501-505.

E. El Hammi; E. Warkentin; U. Demmer; F. Limam; N. M. Marzouki; U. Ermler; L. Baciou, *Structure of Ralstonia eutropha Flavohemoglobin in Complex with Three Antibiotic Azole Compounds*. Biochem., **2011**, *50*, 1255-1264.

N. D. Epiotis; R. L. Yates; F. Bernardi; S. Wolfe, *Theoretical-Analysis of Factors Determining Conformations and Stabilities of Oxycarbanions and Thiocarbanions*. J. Am. Chem. Soc., **1976**, *98*, 5435-5439.

K. M. Ervin, *Experimental Techniques in Gas-Phase Ion Thermochemistry*. Chem. Rev., **2001**, *101*, 391-444.

K. M. Ervin, *Capture Collisions of Polyynide Anions with Hydrogen Atoms: Effect of the Ion Dipole, Quadrupole, and Anisotropic Polarizability*. Int. J. Mass Spectrom., **2014**, *in press*.

C. Favre; D. Despois; N. Brouillet; A. Baudry; F. Combes; M. Guelin; A. Wootten; G. Wlodarczak, *$HCOOCH_3$ as a Probe of Temperature and Structure in Orion-KL*. Astron. Astrophys., **2011**, *532*, A32.

F. C. Fehsenfeld; C. J. Howard; E. E. Ferguson, *Thermal Energy Reactions of Negative Ions with H Atoms in the Gas Phase*. J. Chem. Phys., **1973**, *58*, 5841-5842.

F. C. Fehsenfeld, *Interactions between Ions and Molecules*. NATO Advanced Study Institutes Series. Series B, Physics. Plenum Press, New York, **1975**, 387.

S. Feil; K. Gluch; S. Matt-Leubner; P. Scheier; J. Limtrakul; M. Probst; H. Deutsch; K. Becker; A. Stamatovic; T. D. Mark, *Partial Cross Sections for Positive and Negative Ion Formation Following Electron Impact on Uracil*. J. Phys. B, **2004**, *37*, 3013-3020.

W. Y. Feng; C. Lifshitz, *Thermal-Reactions of Protonated Formic Acid Clusters $(HCOOH)_nH^+$ (n=1-3)*. J. Phys. Chem., **1994**, *98*, 3658-3663.

J. B. Fenn; M. Mann; C. K. Meng; S. F. Wong; C. M. Whitehouse, *Electrospray Ionization–Principles and Practice*. Mass Spectrom. Rev., **1990**, *9*, 37-70.

E. E. Ferguson; F. C. Fehsenfeld; A. L. Schmeltekopf, *Flowing Afterglow Measurements of Ion-Neutral Reactions*. Academic Press, Inc.: New York, NY, 1969; Vol. 5.

E. E. Ferguson; F. C. Fehsenfeld; A. L. Schmeltekopf, *Ion-Molecule Reaction Rates Measured in a Discharge Afterglow*. Adv. Chem. Ser., **1969**, 83-91.

M. Ferus; R. Michalcikova; V. Shestivska; J. Sponer; J. E. Sponer; S. Civis, *High-Energy Chemistry of Formamide: A Simpler Way for Nucleobase Formation*. J. Phys. Chem. A, **2014**, *118*, 719-736.

R. Flammang; M. Plisnier; G. Bouchoux; Y. Hoppilliard; S. Humbert; C. Wentrup, *Unimolecular Chemistry of Oxazole and Isoxazole Radical Cations in the Gas-Phase - Combined Experimental and Molecular-Orbital Study*. Org. Mass Spectrom., **1992**, *27*, 317-325.

A. I. Florescu-Mitchell; J. B. A. Mitchell, *Dissociative Recombination*. Phys. Rep., **2006**, *430*, 277-374.

C. E. Folsome; J. Lawless; M. Romiez; C. Ponnampe, *Heterocyclic Compounds Indigenous to Murchison Meteorite*. Nature, **1971**, *232*, 108-109.

C. G. Freeman; P. W. Harland; M. J. McEwan, *Ion-Molecule Reactions of Formic Acid .1. Proton-Transfer Reactions*. Aust. J. Chem., **1978**, *31*, 2157-2160.

M. J. Frisch; G. W. Trucks; H. B. Schlegel; G. E. Scuseria; M. A. Robb; J. R. Cheeseman; J. A. Montgomery; T. Vreven; K. N. Kudin; J. C. Burant; J. M. Millam; S. S. Iyengar; J. Tomasi; V. Barone; B. Mennucci; M. Cossi; G. Scalmani; N. Rega; G. A. Petersson; H. Nakatsuji; M. Hada; M. Ehara; K. Toyota; R. Fukuda; J. Hasegawa; M. Ishida; T. Nakajima; Y. Honda; O. Kitao; H. Nakai; M. Klene; X. Li; J. E. Knox; H. P. Hratchian; J. B. Cross; V. Bakken; C. Adamo; J. Jaramillo; R. Gomperts; R. E. Stratmann; O. Yazyev; A. J. Austin; R. Cammi; C. Pomelli; J. W. Ochterski; P. Y. Ayala; K. Morokuma; G. A. Voth; P. Salvador; J. J. Dannenberg; V. G. Zakrzewski; S. Dapprich; A. D. Daniels; M. C. Strain; O. Farkas; D. K. Malick; A. D. Rabuck; K. Raghavachari; J. B. Foresman; J. V. Ortiz; Q. Cui; A. G. Baboul; S. Clifford; J. Cioslowski; B. B. Stefanov; G. Liu; A. Liashenko; P. Piskorz; I. Komaromi; R. L. Martin; D. J. Fox; T. Keith; A. Laham; C. Y. Peng; A. Nanayakkara; M. Challacombe; P. M. W. Gill; B. Johnson; W. Chen; M. W. Wong; C. Gonzalez; J. A. Pople, Gaussian 03, Revision C.02. Gaussian Inc. Wallingford, CT 2003.

M. J. Frisch; G. W. Trucks; H. B. Schlegel; G. E. Scuseria; M. A. Robb; J. R. Cheeseman; G. Scalmani; V. Barone; B. Mennucci; G. A. Petersson; H. Nakatsuji; M. Caricato; X. Li; H. P. Hratchian; A. F. Izmaylov; J. Bloino; G. Zheng; J. L. Sonnenberg; M. Hada; M. Ehara; K. Toyota; R. Fukuda; J. Hasegawa; M. Ishida; T. Nakajima; Y. Honda; O. Kitao; H. Nakai; T. Vreven; Jr; J. E. Peralta; F. Ogliaro; M. Bearpark; J. J. Heyd; E. Brothers; K. N. Kudin; V. N. Staroverov; R. Kobayashi; J. Normand; K. Raghavachari; A. Rendell; J. C. Burant; S. S. Iyengar; J. Tomasi; M. Cossi; N. Rega; J. M. Millam; M. Klene; J. E. Knox; J. B. Cross; V. Bakken; C. Adamo; J. Jaramillo; R. Gomperts; R. E. Stratmann; O. Yazyev; A. J. Austin; R. Cammi; C. Pomelli; J. W. Ochterski; R. L. Martin; K. Morokuma; V. G. Zakrzewski; G. A. Voth; P. Salvador; J. J. Dannenberg; S. Dapprich; A. D. Daniels; Farkas; J. B. Foresman; J. V. Ortiz; J. Cioslowski; D. J. Fox, Gaussian 09 Revision A.02. Gaussian Inc. Wallingford, CT: 2009.

E. Garand; T. I. Yacovitch; D. M. Neumark, *Slow Photoelectron Velocity-Map Imaging Spectroscopy of C_2N^-, C_4N^-, and C_6N^-*. J. Chem. Phys., **2009**, *130*, 64304.

R. T. Garrod; E. Herbst, *Formation of Methyl Formate and Other Organic Species in the Warm-Up Phase of Hot Molecular Cores*. Astron. Astrophys., **2006**, *457*, 927-936.

J. M. Garver; Z. Yang; S. Kato; S. W. Wren; K. M. Vogelhuber; W. C. Lineberger; V. M. Bierbaum, *Gas Phase Reactions of 1,3,5-Triazine: Proton Transfer, Hydride Transfer, and Anionic sigma-Adduct Formation*. J. Am. Soc. Mass Spectrom., **2011**, *22*, 1260-1272.

W. D. Geppert; M. Hamberg; R. D. Thomas; F. Osterdahl; F. Hellberg; V. Zhaunerchyk; A. Ehlerding; T. J. Millar; H. Roberts; J. Semaniak; M. af Ugglas; A. Kallberg; A. Simonsson; M. Kaminska; M. Larsson, *Dissociative Recombination of Protonated Methanol*. Faraday Disc., **2006**, *133*, 177-190.

D. Gerlich; M. Smith, *Laboratory Astrochemistry: Studying Molecules Under Inter-and Circumstellar Conditions*. Phys. Scripta, **2006**, *73*, C25-C31.

A. J. Gianola; T. Ichino; S. Kato; V. M. Bierbaum; W. C. Lineberger, *Thermochemical Studies of Pyrazolide*. J. Phys. Chem. A, **2006**, *110*, 8457-8466.

F. A. Gianturco; F. Sebastianelli; R. Lucchese; I. Baccarelli; N. Sanna, *Ring-Breaking Electron Attachment to Uracil: Following Bond Dissociations via Evolving Resonances*. J. Chem. Phys., **2008**, *128*, 174302.

G. Gioumousis; D. P. Stevenson, *Reactions of Gaseous Molecule Ions with Gaseous Molecules. 5. Theory*. J. Chem. Phys., **1958**, *29*, 294-299.

R. Glaser; B. Hodgen; D. Farrelly; E. McKee, *Adenine Synthesis in Interstellar Space: Mechanisms of Prebiotic Pyrimidine-Ring Formation of Monocyclic HCN-Pentamers*. Astrobiology, **2007**, *7*, 455-470.

C. Gonzalez; H. B. Schlegel, *An Improved Algorithm for Reaction Path Following*. J. Chem. Phys., **1989**, *90*, 2154-2161.

C. Gonzalez; H. B. Schlegel, *Reaction Path Following in Mass-Weighted Internal Coordinates*. J. Phys. Chem., **1990**, *94*, 5523-5527.

L. Gorb; A. Kaczmarek; A. Gorb; A. J. Sadlej; J. Leszczynski, *Thermodynamics and Kinetics of Intramolecular Proton Transfer in Guanine. Post Hartree-Fock Study*. J. Phys. Chem. B, **2005**, *109*, 13770-13776.

J. M. Gregson; J. A. McCloskey, *Collision-Induced Dissociation of Protonated Guanine*. Int. J. Mass Spectrom., **1997**, *165*, 475-485.

S. Gronert; C. H. DePuy; V. M. Bierbaum, *Deuterium-Isotope Effects in Gas-Phase Reactions of Alkyl-Halides - Distinguishing E2 and S_N2 Pathways*. J. Am. Chem. Soc., **1991**, *113*, 4009-4010.

S. Gronert, *Estimation of Effective Ion Temperatures in a Quadrupole Ion Trap*. J. Am. Soc. Mass Spectrom., **1998**, *9*, 845-848.

S. Gronert, *Mass Spectrometric Studies of Organic Ion/Molecule Reactions*. Chem. Rev., **2001**, *101*, 329-360.

S. Gronert, *Quadrupole Ion Trap Studies of Fundamental Organic Reactions*. Mass Spectrom. Rev., **2005**, *24*, 100-120.

J. D. Gu; J. Leszczynski, *A DFT Study of the Water-Assisted Intramolecular Proton Transfer in the Tautomers of Adenine*. J. Phys. Chem. A, **1999**, *103*, 2744-2750.

H. Gupta; C. A. Gottlieb; V. Lattanzi; J. C. Pearson; M. C. McCarthy, *Laboratory Measurements and Tentative Astronomical Identification of H_2NCO^+*. Astrophys. J. Lett., **2013**, *778*, L1-L5.

V. P. Gupta; P. Tandon; P. Rawat; R. N. Singh; A. Singh, *Quantum Chemical Study of a New Reaction Pathway for the Adenine Formation in the Interstellar Space*. Astron. Astrophys., **2011**, *528*, A129.

V. P. Gupta; P. Tandon; P. Mishra, *Some New Reaction Pathways for the Formation of Cytosine in Interstellar Space - A Quantum Chemical Study*. Adv. Space Res., **2013**, *51*, 797-811.

J. N. Harvey, *Understanding the Kinetics of Spin-Forbidden Chemical Reactions*. Phys. Chem. Chem. Phys., **2007**, *9*, 331-343.

R. Hayatsu, *Orgueil Meteorite - Organic Nitrogen Contents*. Science, **1964**, *146*, 1291-1293.

R. Hayatsu; M. H. Studier; L. P. Moore; E. Anders, *Purines and Triazines in Murchison Meteorite*. Geochim. Cosmochim. Ac., **1975**, *39*, 471-488.

W. M. Haynes, *CRC Handbook of Chemistry and Physics*. 93 ed.; Taylor & Francis: 2012.

E. Herbst; W. Klemperer, *The Formation and Depletion of Molecules in Dense Interstellar Clouds*. Astrophys. J., **1973**, *185*, 505-534.

E. Herbst; T. J. Millar, *The Chemistry of Cold Interstellar Cloud Cores*. Smith, I. W. M., Ed. Imperial College Press, World Scientific Publishing Co.: Singapore, 2008; 1-54.

E. Herbst; E. F. van Dishoeck, *Complex Organic Interstellar Molecules*. Annu. Rev. Astron. Astrophys., **2009**, *47*, 427-480.

E. Herbst; E. Roueff; D. Talbi, *Radiative Association and the Formation of Interstellar Propylene*. Molec. Phys., **2010**, *108*, 2171-2177.

E. Herbst; J. T. Yates, *Introduction: Astrochemistry*. Chem. Rev., **2013**, *113*, 8707-8709.

E. Herbst, *Three Milieux for Interstellar Chemistry: Gas, Dust, and Ice*. Phys. Chem. Chem. Phys., **2014**, *16*, 3344-3359.

J. M. Hollis; F. J. Lovas; P. R. Jewell, *Interstellar Glycolaldehyde: The First Sugar*. Astrophys. J., **2000**, *540*, L107-L110.

J. M. Hollis; S. N. Vogel; L. E. Snyder; P. R. Jewell; F. J. Lovas, *The Spatial Scale of Glycolaldehyde in the Galactic Center*. Astrophys. J., **2001**, *554*, L81-L85.

J. M. Hollis; A. J. Remijan; P. R. Jewell; F. J. Lovas, *Cyclopropenone (c-H_2C_3O): A New Interstellar Ring Molecule*. Astrophys. J., **2006**, *642*, 933-939.

A. Horn; H. Mollendal; O. Sekiguchi; E. Uggerud; H. Roberts; E. Herbst; A. A. Viggiano; T. D. Fridgen, *The Gas-Phase Formation of Methyl Formate in Hot Molecular Cores*. Astrophys. J., **2004**, *611*, 605-614.

A. Horn; H. Mollendal; J.-C. Guillemin, *A Quantum Chemical Study of the Generation of a Potential Prebiotic Compound, Cyanoacetaldehyde, and Related Sulfur Containing Species*. J. Phys. Chem. A, **2008**, *112*, 11009-11016.

C. J. Howard; F. C. Fehsenfeld; M. McFarland, *Negative Ion-Molecule Reactions with Atomic Hydrogen in the Gas Phase at 296 K*. J. Chem. Phys., **1974**, *60*, 5086-5089.

T.-Y. Huang; J. F. Emory; R. A. J. O'Hair; S. A. McLuckey, *Electron-Transfer Reagent Anion Formation via Electrospray Ionization and Collision-Induced Dissociation*. Anal. Chem., **2006**, *78*, 7387-7391.

Y. Q. Huang; H. I. Kenttämaa, *Theoretical Estimations of the 298 K Gas-Phase Acidities of the Pyrimidine-Based Nucleobases Uracil, Thymine, and Cytosine*. J. Phys. Chem. A, **2003**, *107*, 4893-4897.

Y. Q. Huang; H. Kenttamaa, *Theoretical Estimations of the 298 K Gas-Phase Acidities of the Purine-Based Nucleobases Adenine and Guanine*. J. Phys. Chem. A, **2004**, *108*, 4485-4490.

R. Hudson; M. Moore, *Reactions of Nitriles in Ices Relevant to Titan, Comets, and the Interstellar Medium: Formation of Cyanate Ion, Ketenimines, and Isonitriles*. Icarus, **2004**, *172*, 466-478.

E. P. L. Hunter; S. G. Lias, *Evaluated Gas Phase Basicities and Proton Affinities of Molecules: An Update*. J. Phys. Chem. Ref. Data, **1998**, *27*, 413-656.

Y. Ikezoe; S. Matsuoka; M. Takebe, *Gas Phase Ion-Molecule Reaction Rate Constants through 1986*. Tokyo: Maruzan Company, Ltd.: 1987.

W. M. Irvine; J. Ellder; A. Hjalmarson; E. Kollberg; O. E. H. Rydbeck; G. O. Sorensen; B. Bak; H. Svanholt, *Searches for Inter-Stellar Imidazole and Cyanoform*. Astron. Astrophys., **1981**, *97*, 192-194.

K. Ishii; A. Tajima; T. Taketsugu; K. Yamashita, *Theoretical Elucidation of the Unusually High HNC/HCN Abundance Ratio in Interstellar Space: Two-Dimensional and Two-State Quantum Wave Packet Dynamics Study on the Branching Ratio of the Dissociative Recombination Reaction* $HCNH^+ + e^- \rightarrow HNC/HCN + H$. Astrophys. J., **2006**, *636*, 927-931.

L. P. Jameson; S. V. Dzyuba, *Aza-BODIPY: Improved Synthesis and Interaction with Soluble A Beta 1-42 Oligomers*. Bioorg. Med. Chem. Lett., **2013**, *23*, 1732-1735.

Y. A. Jeilani; N. Huyen Thi; D. Newallo; J.-M. D. Dimandja; N. Minh Tho, *Free Radical Routes for Prebiotic Formation of DNA Nucleobases from Formamide*. Phys. Chem. Chem. Phys., **2013**, *15*, 21084-21093.

Y. A. Jeilani; H. T. Nguyen; B. H. Cardelino; M. T. Nguyen, *Free Radical Pathways for the Prebiotic Formation of Xanthine and Isoguanine from Formamide*. Chem. Phys. Lett., **2014**, *598*, 58-64.

D. Jewitt, *Rosetta Mission: When the Dust has Settled*. Nature Phys., **2015**, *11*, 96-97.

A. M. Kamel; B. Munson, *Collision-Induced Dissociation of Purine Antiviral Agents: Mechanisms of Ion Formation using Gas-Phase Hydrogen/Deuterium Exchange and Electrospray Ionization Tandem Mass Spectrometry*. Eur. J. Mass Spectrom., **2004**, *10*, 239-257.

D. Kaur; S. Khanna; R. P. Kaur, *The Role of Conjugative Interactions in Acidic and Basic Character of Five Membered Aromatic Heterocyclics*. J. Molec. Struc.-Theochem., **2010**, *949*, 14-22.

O. Kikuchi; T. Watanabe; Y. Satoh; Y. Inadomi, *Ab Initio GB Study of Prebiotic Synthesis of Purine Precursors from Aqueous Hydrogen Cyanide: Dimerization Reaction of HCN in Aqueous Solution*. J. Mol. Struc.-Theo. Chem., **2000**, *507*, 53-62.

J. Kissel; F. R. Krueger, *The Organic-Component in Dust from Comet Halley as measured by the Puma Mass-Spectrometer onboard Vega-1*. Nature, **1987**, *326*, 755-760.

H. Knicker; P. G. Hatcher; A. W. Scaroni, *Solid-State N-15 NMR-Spectroscopy of Coal*. Energy & Fuels, **1995**, *9*, 999-1002.

K. Kobayashi; Y. Takano; H. Masuda; H. Tonishi; T. Kaneko; H. Hashimoto; T. Saito, *Possible Cometary Organic Compounds as Sources of Planetary Biospheres*. In *Space Life Sciences: Search for Signatures of Life, and Space Flight Environmental Effects on the Nervous System*, Horneck, G.; Levasseur Regourd, A. C.; Rabin, B. M.; Slenzka, K. B., Eds. 2004; Vol. 33, 1277-1281.

S. K. Koehn; N. L. Tran; S. Gronert; W. M. Wu, *The Stability of Aryl Carbanions Derived from Pyridine N-Oxide: The Role of Resonance in Stabilizing Aryl Anions*. J. Am. Chem. Soc., **2010**, *132*, 390-395.

H. Koizumi; P. B. Armentrout, *The Kinetic Energy Dependence of Association Reactions. A New Thermokinetic Method for Large Systems*. J. Chem. Phys., **2003**, *119*, 12819-12829.

H. Koizumi; F. Muntean; P. B. Armentrout, *Reaction of Cu^+ with Dimethoxyethane: Competition between Association and Multiple Dissociation Channels*. J. Chem. Phys., **2004**, *120*, 756-766.

Y. J. Kuan; S. B. Charnley; H. C. Huang; W. L. Tseng; Z. Kisiel, *Interstellar Glycine*. Astrophys. J., **2003**, *593*, 848-867.

Y. J. Kuan; C. H. Yan; S. B. Charnley; Z. Kisiel; P. Ehrenfreund; H. C. Huang, *A Search for Interstellar Pyrimidine*. Mon. Not. Roy. Astron. Soc., **2003**, *345*, 650-656.

Y. J. Kuan; S. B. Charnley; H. C. Huang; Z. Kisiel; P. Ehrenfreund; W. L. Tseng; C. H. Yan, *Searches for Interstellar Molecules of Potential Prebiotic Importance*. Adv. Space. Res., **2004**, *33*, 31-39.

Y. J. Kuan; H. C. Huang; S. B. Charnley; W. L. Tseng; L. E. Snyder; P. Ehrenfreund; Z. Kisiel; S. Thorwirth; R. K. Bohn; T. L. Wilson, *Prebiologically Important Interstellar Molecules*. Bioastronomy 2002: Life among the Stars, **2004**, 185-188.

S. Kumari; C. L. Devi; S. Prabhakar; K. Bhanuprakash; M. Vairaman, *Estimation of Gas-Phase Acidities of Deoxyribonucleosides: An Experimental and Theoretical Study*. J. Am. Soc. Mass Spectrom., **2010**, *21*, 136-143.

V. G. Kunde; A. C. Aikin; R. A. Hanel; D. E. Jennings; W. C. Maguire; R. E. Samuelson, *C_4H_2, HC_3N and C_2N_2 in Titan's Atmosphere*. Nature, **1981**, *292*, 686-688.

J. C. Laas; R. T. Garrod; E. Herbst; S. L. W. Weaver, *Contributions from Grain Surface and Gas Phase Chemistry to the Formation of Methyl Formate and its Structural Isomers*. Astrophys. J., **2011**, *728*, 71-79.

P. Langevin, *A Fundamental Formula of Kinetic Theory*. Annal. Chim. Physi., **1905**, *5*, 245-288.

V. Lattanzi; C. A. Gottlieb; P. Thaddeus; S. Thorwirth; M. C. McCarthy, *The Rotational Spectrum of the NCO^- Anion*. Astrophys. J., **2010**, *720*, 1717-1720.

P. A. Lawson; D. S. Osborne, Jr.; N. G. Adams, *Dissociative Electron-Ion Recombination of the Interstellar Species Protonated Glycolaldehyde, Acetic Acid, and Methyl Formate*. J. Phys. Chem. A, **2012**, *116*, 2880-2884.

C. Lee; W. Yang; R. G. Parr, *Development of the Colle-Salvetti Correlation-Energy Formula into a Functional of the Electron Density*. Phys. Rev. B, **1988**, *37*, 785-789.

D. G. Leopold; J. Ho; W. C. Lineberger, *Photoelectron Spectroscopy of Mass-Selected Metal Cluster Anions. I. Cu_n^-, n= 1–10*. J. Chem. Phys., **1987**, *86*, 1715-1726.

S. Lepp; A. Dalgarno, *Polycyclic Aromatic Hydrocarbons in Interstellar Chemistry*. Astrophys. J., **1988**, *324*, 553-556.

M. Levy; S. L. Miller; J. Oro, *Production of Guanine from NH_4CN Polymerizations*. J. Molec. Evol., **1999**, *49*, 165-168.

Z. Lin; D. Talbi; E. Roueff; E. Herbst; N. Wehres; C. A. Cole; Z. Yang; T. P. Snow; V. M. Bierbaum, *Can Interstellar Propene (CH_3CHCH_2) be Formed via Gas-Phase Reactions?* Astrophys. J., **2013**, *765*, 80-84.

F. P. Lossing, *Free Radicals by Mass Spectrometry. XLV. Ionization Potentials and Heats of Formation of C_3H_3, C_3H_5, and C_4H_7 Radicals and Ions*. Can. J. Chem., **1972**, *50*, 3973-3981.

Y. A. Mankelevich; M. N. Ashfold; H. Umemoto, *Molecular Dissociation and Vibrational Excitation on a Metal Hot Filament Surface*. J. Phys. D: Appl. Phys., **2014**, *47*, 025503.

D. J. D. Marais; J. A. Nuth, III; L. J. Allamandola; A. P. Boss; J. D. Farmer; T. M. Hoehler; B. M. Jakosky; V. S. Meadows; A. Pohorille; B. Runnegar; A. M. Spormann, *The NASA Astrobiology Roadmap*. Astrobiology, **2008**, *8*, 715-730.

N. Marcelino; J. Cernicharo; M. Agúndez; E. Roueff; M. Gerin; J. Martín-Pintado; R. Mauersberger; C. Thum, *Discovery of Interstellar Propylene (CH_2CHCH_3): Missing Links in Interstellar Gas-Phase Chemistry*. Astrophys. J. Lett., **2007**, *665*, L127-L130.

R. E. March; J. F. Todd, *A Historical Review of the Early Development of the Quadrupole Ion Trap*. In *Quadrupole Ion Trap Mass Spectrometry*, 2 ed.; 2005; Vol. 165, 1-33.

R. E. March, *Quadrupole Ion Traps*. Mass Spec. Rev., **2009**, *28*, 961-989.

O. Martinez; Z. Yang; N. B. Betts; T. P. Snow; V. M. Bierbaum, *Experimental Determination of the Rate Constant for the Associative Detachment Reaction $H^- + H \rightarrow H_2 + e^-$ at 300 K*. Astrophys. J. Lett., **2009**, *705*, L172-L175.

Z. Martins; O. Botta; M. L. Fogel; M. A. Sephton; D. P. Glavin; J. S. Watson; J. P. Dworkin; A. W. Schwartz; P. Ehrenfreund, *Extraterrestrial Nucleobases in the Murchison Meteorite*. Earth Planet. Sci. Lett., **2008**, *270*, 130-136.

C. K. Materese; M. Nuevo; P. P. Bera; T. J. Lee; S. A. Sandford, *Thymine and Other Prebiotic Molecules Produced from the Ultraviolet Photo-Irradiation of Pyrimidine in Simple Astrophysical Ice Analogs*. Astrobiology, **2013**, *13*, 948-962.

M. McCarthy; C. Gottlieb; H. Gupta; P. Thaddeus, *Laboratory and Astronomical Identification of the Negative Molecular Ion C_6H^-*. Atrophys. J. Lett., **2006**, *652*, L141-L144.

M. J. McEwan; G. B. I. Scott; N. G. Adams; L. M. Babcock; R. Terzieva; E. Herbst, *New H and H_2 Reactions with Small Hydrocarbon Ions and their Roles in Benzene Synthesis in Dense Interstellar Clouds*. Astrophys. J., **1999**, *513*, 287-293.

A. McKellar, *Evidence for the Molecular Origin of some Hitherto Unidentified Interstellar Lines*. Pub. Astron. Soc. Pac., **1940**, *52*, 187-192.

D. M. Mehringer; L. E. Snyder; Y. T. Miao, *Detection and Confirmation of Interstellar Acetic Acid*. Astrophys. J., **1997**, *480*, L71-L74.

M. Meltzer, *The Cassini-Huygens Visit to Saturn: An Historic Mission to the Ringed Planet*. Springer Praxis Books: Chichester, UK, 2015.

K. M. Merz; E. C. Aguiar; J. B. P. da Silva, *Adenine Formation without HCN*. J. Phys. Chem. A, **2014**, *118*, 3637-3644.

Y. T. Miao; D. M. Mehringer; Y. J. Kuan; L. E. Snyder, *Complex Molecules in Sagittarius B2(N) - The Importance of Grain Chemistry*. Astrophys. J., **1995**, *445*, L59-L62.

A. Milano; M. R. Pasca; R. Provvedi; A. P. Lucarelli; G. Manina; A. Ribeiro; R. Manganelli; G. Riccardi, *Azole Resistance in Mycobacterium Tuberculosis is Mediated by the MmpS5-MmpL5 Efflux System*. Tuberculosis, **2009**, *89*, 84-90.

S. L. Miller; H. C. Urey, *Organic Compound Synthesis on the Primitive Earth*. Science, **1959**, *130*, 245-251.

B. F. Minaev; M. I. Shafranyosh; Y. Y. Svida; M. I. Sukhoviya; I. I. Shafranyosh; G. V. Baryshnikov; V. A. Minaeva, *Fragmentation of the Adenine and Guanine Molecules Induced by Electron Collisions*. J. Chem. Phys., **2014**, *140*, 175101.

H. Mollendal; A. Konovalov, *Microwave Spectrum of 2-Aminooxazole, a Compound of Potential Prebiotic and Astrochemical Interest*. J. Phys. Chem. A, **2010**, *114*, 2151-2156.

C. Møller; M. S. Plesset, *Note on an Approximation Treatment for Many-Electron Systems*. Phys. Rev., **1934**, *46*, 618-622.

B. Moriyama; S. A. Henning; J. Leung; O. Falade-Nwulia; P. Jarosinski; S. R. Penzak; T. J. Walsh, *Adverse Interactions Between Antifungal Azoles and Vincristine: Review and Analysis of Cases*. Mycoses, **2012**, *55*, 290-297.

A. Moser; K. Range; D. M. York, *Accurate Proton Affinity and Gas-Phase Basicity Values for Molecules Important in Biocatalysis*. J. Phys. Chem. B, **2010**, *114*, 13911-13921.

J. L. Neill; A. L. Steber; M. T. Muckle; D. P. Zaleski; V. Lattanzi; S. Spezzano; M. C. McCarthy; A. J. Remijan; D. N. Friedel; S. L. W. Weaver; B. H. Pate, *Spatial Distributions and Interstellar Reaction Processes*. J. Phys. Chem. A, **2011**, *115*, 6472-6480.

C. C. Nelson; J. A. McCloskey, *Collision-Induced Dissociation of Adenine*. J. Am. Chem. Soc., **1992**, *114*, 3661-3668.

C. C. Nelson; J. A. McCloskey, *Collision-Induced Dissociation of Uracil and its Derivatives*. J. Am. Soc. Mass Spectrom., **1994**, *5*, 339-349.

K. E. Nelson; M. P. Robertson; M. Levy; S. L. Miller, *Concentration by Evaporation and the Prebiotic Synthesis of Cytosine*. Origin Life Evol. Bio., **2001**, *31*, 221-229.

M. T. Nguyen; T. K. Ha; R. A. M. Oferrall, *An Ab Initio Study of the Cyclization and Rearrangement of Vinylketene, Imidoylketene, and Formylketene*. J. Org. Chem., **1990**, *55*, 3251-3256.

J. Novozamsky; W. Schutte; J. Keane, *Further Evidence for the Assignment of the XCN Band in Astrophysical Ice Analogs to OCN^- Spectroscopy and Deuterium Shift*. Astron. Astrophys., **2001**, *379*, 588-591.

M. Nuevo; S. N. Milam; S. A. Sandford; J. E. Elsila; J. P. Dworkin, *Formation of Uracil from the Ultraviolet Photo-Irradiation of Pyrimidine in Pure H_2O Ices*. Astrobiology, **2009**, *9*, 683-695.

K. I. Oberg; E. F. van Dishoeck; H. Linnartz, *Photodesorption of Ices I: CO, N_2, and CO_2*. Astron. Astrophys., **2009**, *496*, 281-293.

Y. Okumura; Y. Sugiyama; K. Okazaki, *Evolution Prediction of Coal-Nitrogen in High Pressure Pyrolysis Processes*. Fuel, **2002**, *81*, 2317-2324.

L. E. Orgel, *Prebiotic Chemistry and the Origin of the RNA World*. Crit. Rev. Biochem. Mol. Biol., **2004**, *39*, 99-123.

J. Oro, *Synthesis of Adenine from Ammonium Cyanide*. Biochem. Biophys. Res. Commun., **1960**, *2*, 407-412.

J. Oro, *Mechanism of Synthesis of Adenine from Hydrogen Cyanide Under Possible Primitive Earth Conditions*. Nature, **1961**, *191*, 1193-1194.

J. Oro, *Comets and Formation of Biochemical Compounds on Primitive Earth*. Nature, **1961**, *190*, 389-390.

Y. Osamura; K. Fukuzawa; R. Terzieva; E. Herbst, *A Molecular Orbital Study of the $HC_3NH^+ + e^-$ Dissociative Recombination and Its Role in the Production of Cyanoacetylene Isomers in Interstellar Clouds*. Astrophys. J., **1999**, *519*, 697-704.

N. Otero; L. Estevez; M. Mandado; R. A. Mosquera, *An Electron-Density-Based Study on the Ionic Reactivity of 1,3-Azoles*. Eur. J. Org. Chem., **2012**, 2403-2413.

G. Pascoli; H. Lavendy, *Are C_nN^- clusters really bent?* Chem. Phys. Lett., **1999**, *312*, 333-340.

W. Paul; H. Steinwedel, *Ein Neues Massenspektrometer Ohne Magnetfeld*. Z. Naturforsch., **1953**, *8*, 448-450.

A. A. Pavlov; M. T. Hurtgen; J. F. Kasting; M. A. Arthur, *Methane-Rich Proterozoic Atmosphere?* Geol., **2003**, *31*, 87-90.

J. C. Pearson; K. Sastry; E. Herbst; F. C. Delucia, *The Millimeter-Wave and Submillimeter-Wave Spectrum of Propylene (CH_3CHCH_2)*. J. Mol. Spectrosc., **1994**, *166*, 120-129.

Z. Peeters; O. Botta; S. B. Charnley; R. Ruiterkamp; P. Ehrenfreund, *The Astrobiology of Nucleobases*. Astrophys. J., **2003**, *593*, L129-L132.

Z. Peeters; O. Botta; S. B. Charnley; Z. Kisiel; Y. J. Kuan; P. Ehrenfreund, *Formation and Photostability of N-Heterocycles in Space - I. The Effect of Nitrogen on the Photostability of Small Aromatic Molecules*. Astron. Astrophys., **2005**, *433*, 583-590.

A. Pena-Gallego; J. Rodriguez-Oteroa; E. M. Cabaleiro-Lago, *A DFT Study of the 4+2 Cycloadditions of Conjugated Ketenes (Vinylketene, Imidoylketene and Formylketene) with Formaldimine. The Pericyclic or Pseudopericyclic Character from Magnetic Properties*. Tetrahedron, **2007**, *63*, 4937-4943.

A. A. Penzias; P. M. Solomon; R. W. Wilson; K. B. Jefferts, *Interstellar Carbon Monosulfide*. Astrophys. J., **1971**, *168*, L53-L58.

G. Petersson; A. Bennett; T. G. Tensfeldt; M. A. Al-Laham; W. A. Shirley; J. Mantzaris, *A Complete Basis Set Model Chemistry. I. The Total Energies of Closed-Shell Atoms and Hydrides of the First-Row Elements*. J. Chem. Phys., **1988**, *89*, 2193-2218.

N. G. Petrik; R. J. Monckton; S. P. Koehler; G. A. Kimmel, *Distance-Dependent Radiation Chemistry: Oxidation versus Hydrogenation of CO in Electron-Irradiated $H_2O/CO/H_2O$ Ices*. J. Phys. Chem. C, **2014**, *118*, 27483-27492.

S. Pilling; A. F. Lago; L. H. Coutinho; R. B. de Castilho; G. G. B. de Souza; A. Naves de Brito, *Dissociative Photoionization of Adenine following Valence Excitation*. Rapid Commun. Mass Spectrom., **2007**, *21*, 3646-3652.

S. Pilling; D. P. P. Andrade; A. C. Neto; R. Rittner; A. N. de Brito, *DNA Nucleobase Synthesis at Titan Atmosphere Analog by Soft X-rays*. J. Phys. Chem. A, **2009**, *113*, 11161-11166.

S. Pilling; D. P. P. Andrade; E. M. do Nascimento; R. R. T. Marinho; H. M. Boechat-Roberty; L. H. de Coutinho; G. G. B. de Souza; R. B. de Castilho; R. L. Cavasso; A. F. Lago; A. N. de Brito, *Photostability of Gas- and Solid-Phase Biomolecules within Dense Molecular Clouds due to Soft X-rays*. Month. Not. Royal Astron. Soc., **2011**, *411*, 2214-2222.

M. W. Powner; B. Gerland; J. D. Sutherland, *Synthesis of Activated Pyrimidine Ribonucleotides in Prebiotically Plausible Conditions*. Nature, **2009**, *459*, 239-242.

M. W. Powner; S. L. Zheng; J. W. Szostak, *Multicomponent Assembly of Proposed DNA Precursors in Water*. J. Am. Chem. Soc., **2012**, *134*, 13889-13895.

B. Pullman; A. Pullman, *Electronic Delocalization and Biochemical Evolution*. Nature, **1962**, *196*, 1137-1142.

D. Quan; E. Herbst; Y. Osamura; E. Roueff, *Gas-Grain Modeling of Isocyanic Acid (HNCO), Cyanic Acid (HOCN), Fulminic Acid (HCNO), and Isofulminic Acid (HONC) in Assorted Interstellar Environments*. Astrophys. J., **2010**, *725*, 2101-2109.

F. Raulin, *Question 2: Why an Astrobiological Study of Titan will Help Us Understand the Origin of Life*. Origins Life Evol. Bio., **2007**, *37*, 345-349.

S. Rayat; R. Glaser, *5-cyanoimino-4-oxomethylene-4,5-dihydroimidazole and Nitrosative Guanine Deamination. A Theoretical Study of Geometries, Electronic Structures, and N-protonation*. J. Org. Chem., **2003**, *68*, 9882-9892.

G. E. Reid; R. A. J. O'Hair; M. L. Styles; W. D. McFadyen; R. J. Simpson, *Gas Phase Ion-Molecule Reactions in a Modified Ion Trap: H/D Exchange of Non-Covalent Complexes and Coordinatively Unsaturated Platinum Complexes*. Rapid Commun. Mass Spectrom., **1998**, *12*, 1701-1708.

A. J. Remijan; J. Hollis; F. Lovas; M. Cordiner; T. Millar; A. Markwick-Kemper; P. Jewell, *Detection of C_8H^- and Comparison with C_8H toward IRC+10216*. Astrophys. J. Lett., **2007**, *664*, L47-L50.

A. J. Remijan; L. E. Snyder; B. A. McGuire; H.-L. Kuo; L. W. Looney; D. N. Friedel; G. Y. Golubiatnikov; F. J. Lovas; V. V. Ilyushin; E. A. Alekseev; S. F. Dyubko; B. J. McCall; J. M. Hollis, *Observational Results of a Multi-telescope Campaign in Search of Interstellar Urea $[(NH_2)_2CO]$*. Astrophys. J., **2014**, *783*, 77-92.

J. M. Rice; G. O. Dudek, *Mass Spectra of Nucleic Acid Derivatives. 2. Guanine, Adenine and Related Compounds*. J. Am. Chem. Soc., **1967**, *89*, 2719-2725.

S. T. Ridgway; D. N. B. Hall; S. G. Kleinmann; D. A. Weinberger; R. S. Wojslaw, *Circumstellar Acetylene in Infrared-Spectrum of IRC $+10^o$ 216*. Nature, **1976**, *264*, 345-346.

M. P. Robertson; S. L. Miller, *An Efficient Prebiotic Synthesis of Cytosine and Uracil*. Nature, **1995**, *375*, 772-774.

M. T. Rodgers; S. Campbell; E. M. Marzluff; J. L. Beauchamp, *Low-Energy Collision-Induced Dissociation of Deprotonated Dinucleotides - Determination of the Energetically Favored Dissociation Pathways and the Relative Acidities of the Nucleic-Acid Bases*. Int. J. Mass Spectrom. Ion Proc., **1994**, *137*, 121-149.

R. Rodriguez-Fernandez; S. A. Vazquez; E. Martinez-Nunez, *Collision-Induced Dissociation Mechanisms of Li(uracil)$^+$*. Phys. Chem. Chem. Phys., **2013**, *15*, 7628-7637.

H. Rosemeyer, *The Chemodiversity of Purine as a Constituent of Natural Products*. Chem. Biodivers., **2004**, *1*, 361-401.

E. Roueff; E. Herbst, Molecular Ions in Astrophysics. *J. Phys. Conf. Ser.*, Van Der Zande, W. J., Ed. 2009; Vol. 192.

D. Roy; K. Najafian; P. v. R. Schleyer, *Chemical Evolution: The Mechanism of the Formation of Adenine under Prebiotic Conditions*. Proc. Natl. Acad. Sci. U. S. A., **2007**, *104*, 17272-17277.

H. Sabbah; L. Biennier; I. R. Sims; Y. Georgievskii; S. J. Klippenstein; I. W. M. Smith, *Understanding Reactivity at Very Low Temperatures: The Reactions of Oxygen Atoms with Alkenes*. Science, **2007**, *317*, 102-105.

R. Saladino; C. Crestini; S. Pino; G. Costanzo; E. Di Mauro, *Formamide and the Origin of Life*. Phys. Life Rev., **2012**, *9*, 84-104.

J. Y. Salpin; S. Guillaumont; J. Tortajada; L. MacAleese; J. Lemaire; P. Maitre, *Infrared Spectra of Protonated Uracil, Thymine and Cytosine*. ChemPhysChem, **2007**, *8*, 2235-2244.

S. A. Sandford; M. Nuevo; C. K. Materese, Formation of Nucleobases from the UV Irradiation of Pyrimidine in Astrophysical Ice Analogs. *Lunar and Planetary Science Conference* Houston, TX, 2014.

M. J. Scanlan; I. H. Hillier, *An Ab Initio Study of Tautomerism of Uracil, Thymine, 5-Fluorouracil, and Cytosine*. J. Am. Chem. Soc., **1984**, *106*, 3737-3745.

D. Schroder; M. Engeser; M. Bronstrup; C. Daniel; J. Spandl; H. Hartl, *Ion Chemistry of the Hexanuclear Methoxo-Oxovanadium Cluster $V_6O_7(OCH_3)_{12}$*. Int. J. Mass Spectrom., **2003**, *228*, 743-757.

N. A. Senger; C. E. Bliss; J. R. Keeffe; S. Gronert; W. Wu, *Stabilities of Uracil and Pyridone-based Carbanions: a Systematic Study in the Gas Phase and Solution and Implications for the Mechanism of Orotidine-5 '-Monophosphate Decarboxylase*. Tetrahedron, **2013**, *69*, 5287-5292.

R. Shapiro, *Prebiotic Cytosine Synthesis: A Critical Analysis and Implications for the Origin of Life*. Proc. Nat. Acad. Sci. U. S. A., **1999**, *96*, 4396-4401.

K. Shen; Y. Fu; J.-N. Li; L. Liu; Q.-X. Guo, *What are the pKa Values of C-H Bonds in Aromatic Heterocyclic Compounds in DMSO?* Tetrahedron, **2007**, *63*, 1568-1576.

A. Simakov; G. B. S. Miller; A. J. C. Bunkan; M. R. Hoffmann; E. Uggerud, *The Dissociation of Glycolate – Astrochemical and Prebiotic Relevance*. Phys. Chem. Chem. Phys., **2013**, *15*, 16615-16625.

V. P. Sinditskii; V. Y. Egorshev; V. V. Serushkin; S. A. Filatov, *Combustion of Energetic Materials Controlled by Condensed-Phase Reactions*. Combust. Explo. Shock Wave., **2012**, *48*, 81-99.

D. Smith; P. Španěl, *The SIFT and FALP Techniques; Applications to Ionic and Electronic Reaction Studies and their Evolution to the SIFT-MS and FA-MS Analytical Methods*. Int. J. Mass Spectrom., **2014**, *in press*.

I. W. M. Smith; D. Talbi; E. Herbst, *The Production of HCN Dimer and more Complex Oligomers in Dense Interstellar Clouds*. Astron. Astrophys., **2001**, *369*, 611-615.

I. W. M. Smith, *Laboratory Astrochemistry: Gas-Phase Processes*. In *Ann. Rev. Astron. Astrophys.*, Faber, S. M.; VanDishoeck, E., Eds. 2011; Vol. 49, 29-66.

T. P. Snow; B. J. McCall, *Diffuse Atomic and Molecular Clouds*. Annu. Rev. Astron. Astrophys., **2006**, *44*, 367-414.

T. P. Snow; V. M. Bierbaum, *Ion Chemistry in the Interstellar Medium*. Annu. Rev. Anal. Chem., **2008**, *1*, 229-259.

T. P. Snow; M. Stepanovic; N. B. Betts; B. R. Eichelberger; O. Martinez Jr; V. M. Bierbaum, *Formation of Gas-Phase Glycine and Cyanoacetylene via Associative Detachment Reactions*. Astrobiology, **2009**, *9*, 1001-1005.

T. P. Snow; M. Stepanovic; N. B. Betts; B. R. Eichelberger; O. Martinez, Jr.; V. M. Bierbaum, *Formation of Gas-Phase Glycine and Cyanoacetylene via Associative Detachment Reactions*. Astrobiology, **2009**, *9*, 1001-1005.

L. E. Snyder; D. Buhl, *Observations of Radio Emission from Interstellar Hydrogen Cyanide*. Astrophys. J., **1971**, *163*, L47-L52.

L. E. Snyder; D. Buhl, *Interstellar Isocyanic Acid*. Astrophys. J., **1972**, *177*, 619-623.

B. T. Soifer; R. C. Puetter; R. W. Russell; S. P. Willner; P. M. Harvey; F. C. Gillett, *4–8 Micron Spectrum of the Infrared Source W33-A*. Astrophys. J., **1979**, *232*, L53-L57.

J. E. Sponer; J. Sponer; M. Fuentes-Cabrera, *Prebiotic Routes to Nucleosides: A Quantum Chemical Insight into the Energetics of the Multistep Reaction Pathways*. Chem. Euro. J., **2011**, *17*, 847-854.

J. E. Sponer; A. Mladek; J. Sponer; M. Fuentes-Cabrera, *Formamide-Based Prebiotic Synthesis of Nucleobases: A Kinetically Accessible Reaction Route*. J. Phys. Chem. A, **2012**, *116*, 720-726.

G. Stafford; P. Kelley; J. Syka; W. Reynolds; J. Todd, *Recent Improvements in and Analytical Applications of Advanced Ion Trap Technology*. Int. J. Mass Spectrom. Ion Proc., **1984**, *60*, 85-98.

J. Stevenson; J. Lunine; P. Clancy, *Membrane Alternatives in Worlds without Oxygen: Creation of an Azotosome*. Sci. Adv., **2015**, *1*, 1400067-1400075.

P. G. Stoks; A. W. Schwartz, *Uracil in Carbonaceous Meteorites*. Nature, **1979**, *282*, 709-710.

P. G. Stoks; A. W. Schwartz, *Nitrogen-Heterocyclic Compounds in Meteorites – Significance and Mechanisms of Formation*. Geochim. Cosmochim. Ac., **1981**, *45*, 563-569.

P. G. Stoks; A. W. Schwartz, *Basic Nitrogen-Heterocyclic Compounds in the Murchison Meteorite*. Geochim. Cosmochim. Ac., **1982**, *46*, 309-315.

T. Su; W. J. Chesnavich, *Parametrization of the Ion-Polar Molecule Collision Rate-Constant by Trajectory Calculations*. J. Chem. Phys., **1982**, *76*, 5183-5185.

J. Sultan, *Collision Induced Dissociation of Deprotonated Guanine: Fragmentation of Pyrimidine Ring and Water Adduct Formation*. Int. J. Mass Spectrom., **2008**, *273*, 58-68.

P. Swings; L. Rosenfeld, *Considerations Regarding Interstellar Molecules*. Astrophys. J., **1937**, *86*, 483-486.

J. Tabet; S. Eden; S. Feil; H. Abdoul-Carime; B. Farizon; M. Farizon; S. Ouaskit; T. D. Mark, *20-150 keV Proton Impact-Induced Ionization of Uracil: Fragmentation Ratios and Branching Ratios for Electron Capture and Direct Ionization*. Phys. Rev. A: At., Mol., Opt. Phys., **2010**, *81*, 012711.

B. Tercero; L. Margules; M. Carvajal; R. A. Motiyenko; T. R. Huet; E. A. Alekseev; I. Kleiner; J. C. Guillemin; H. Mollendal; J. Cernicharo, *Microwave and Submillimeter Spectroscopy and First ISM Detection of ^{18}O-Methyl Formate*. Astron. Astrophys., **2012**, *538*, A119.

P. Thaddeus; J. M. Vrtilek; C. A. Gottlieb, *Laboratory and Astronomical Identification of Cyclopropenylidene, C_3H_2*. Astrophys. J., **1985**, *299*, L63-L66.

P. Thaddeus; C. A. Gottlieb; H. Gupta; S. Bruenken; M. C. McCarthy; M. Agundez; M. Guelin; J. Cernicharo, *Laboratory and Astronomical Detection of the Negative Molecular Ion C_3N^-*. Astrophys. J., **2008**, *677*, 1132-1139.

R. L. Thompson; K. Damodaran; D. Luebke; H. Nulwala, *Aprotic Heterocyclic Anion Triazolide Ionic Liquids - A New Class of Ionic Liquid Anion Accessed by the Huisgen Cycloaddition Reaction*. Synlett, **2013**, 1093-1096.

D. M. Tideswell; G. A. Fuller; T. J. Millar; A. J. Markwick, *The Abundance of HNCO and Its Use as a Diagnostic of Environment*. Astron. Astrophys., **2010**, *510*, A85.

P. W. Tiedemann; J. W. Riveros, *Ion-Molecule Reactions of Acids and Esters with Alcohols. Gas Phase Analogs of Acidic Esterification Processes*. J. Am. Chem. Soc., **1974**, *96*, 185-189.

A. G. G. M. Tielens, *The Molecular Universe*. Rev. Mod. Phys., **2013**, *85*, 1021-1081.

J. F. Todd, *Ion Trap Mass Spectrometer—Past, Present, and Future (?)*. Mass Spec. Rev., **1991**, *10*, 3-52.

J. F. J. Todd; S. J. Barber; I. P. Wright; G. H. Morgan; A. D. Morse; S. Sheridan; M. R. Leese; J. Maynard; S. T. Evans; C. T. Pillinger; D. L. Drummond; S. C. Heys; S. E. Huq; B. J. Kent; E. C. Sawyer; M. S. Whalley; N. R. Waltham, *Ion Trap Mass Spectrometry on a Comet Nucleus: the Ptolemy Instrument and the Rosetta Space Mission*. J. Mass Spec., **2007**, *42*, 1-10.

M. G. Trainer; A. A. Pavlov; H. L. DeWitt; J. L. Jimenez; C. P. McKay; O. B. Toon; M. A. Tolbert, *Organic Haze on Titan and the Early Earth*. Proc. Nat. Acad. Sci., **2006**, *103*, 18035-18042.

D. W. Trainor; D. O. Ham; F. Kaufman, *Gas Phase Recombination of Hydrogen and Deuterium Atoms*. J. Chem. Phys., **1973**, *58*, 4599-4609.

F. Turecek; X. H. Chen, *Protonated Adenine: Tautomers, Solvated Clusters, and Dissociation Mechanisms*. J. Am. Soc. Mass Spectrom., **2005**, *16*, 1713-1726.

F. Van Broekhuizen; K. Pontoppidan; H. Fraser; E. van Dishoeck, *A 3-5 Micrometer VLT Spectroscopic Survey of Embedded Young Low Mass Stars II: Solid OCN^-*. Astron. Astrophys., **2005**, *441*, 249-260.

W. Van Der Velden; A. W. Schwartz, *Search for Purines and Pyrimidines in the Murchison Meteorite*. Geochim. Cosmochim. Ac., **1977**, *41*, 961-968.

E. F. Van Dishoeck, *Astrochemistry of Dust, Ice and Gas: Introduction and Overview*. Faraday Disc., **2014**, *168*, 9-47.

J. M. Van Doren; S. E. Barlow; C. H. DePuy; V. M. Bierbaum, *The Tandem Flowing Afterglow-SIFT-DRIFT*. Int. J. Mass Spectrom. Ion Proc., **1987**, *81*, 85-100.

E. Vigren; M. Hamberg; V. Zhaunerchyk; M. Kaminska; J. Semaniak; M. Larsson; R. D. Thomas; M. af Ugglas; I. Kashperka; T. Millar, *Dissociative Recombination of Protonated Formic Acid: Implications for Molecular Cloud and Cometary Chemistry*. Astrophys. J., **2010**, *709*, 1429-1434.

S. Vijayakumar; P. Kolandaivel, *Isomerization of C_3H_3NO Isomers: Ab Initio Study*. Mol. Phys., **2006**, *104*, 1401-1411.

S. M. Villano; A. J. Gianola; N. Eyet; T. Ichino; S. Kato; V. M. Bierbaum; W. C. Lineberger, *Thermochemical Studies of N-methylpyrazole and N-methylimidazole*. J. Phys. Chem. A, **2007**, *111*, 8579-8587.

J. d. Vries; R. Hoekstra; R. Morgenstern; T. Schlathölter, *Multiple Ionization and Fragmentation of the DNA Base Thymine by Interaction with C^{q+} ions*. Euro Phys. J. D, **2003**, *24*, 161-164.

V. Vuitton; R. Yelle; M. McEwan, *Ion Chemistry and N-Containing Molecules in Titan's Upper Atmosphere*. Icarus, **2007**, *191*, 722-742.

V. Vuitton; P. Lavvas; R. Yelle; M. Galand; A. Wellbrock; G. Lewis; A. Coates; J.-E. Wahlund, *Negative Ion Chemistry in Titan's Upper Atmosphere*. Planet. Space Sci., **2009**, *57*, 1558-1572.

V. Vuitton; R. Yelle; P. Lavvas, *Composition and Chemistry of Titan's Thermosphere and Ionosphere*. Philos. Trans. A Math Phys. Eng. Sci., **2009**, *367*, 729-741.

J. Waite; D. Young; T. Cravens; A. Coates; F. Crary; B. Magee; J. Westlake, *The Process of Tholin Formation in Titan's Upper Atmosphere*. Science, **2007**, *316*, 870-875.

V. Wakelam; E. Herbst; F. Selsis, *The Effect of Uncertainties on Chemical Models of Dark Clouds*. Astron. Astrophys., **2006**, *451*, 551-562.

V. Wakelam; E. Herbst; J.-C. Loison; I. Smith; V. Chandrasekaran; B. Pavone; N. Adams; M.-C. Bacchus-Montabonel; A. Bergeat; K. Béroff, *A Kinetic Database for Astrochemistry (KIDA)*. Astrophys. J. Sup. Ser., **2012**, *199*, 21-30.

C. Walsh; N. Harada; E. Herbst; T. Millar, *The Effects of Molecular Anions on the Chemistry of Dark Clouds*. Astrophys. J., **2009**, *700*, 752-761.

J. Wang; J. Gu; N. Minh Tho; G. Springsteen; J. Leszczynski, *From Formamide to Adenine: A Self-Catalytic Mechanism for an Abiotic Approach*. J. Phys. Chem. B, **2013**, *117*, 14039-14045.

T. Wang; J. H. Bowie, *Can Cytosine, Thymine and Uracil be Formed in Interstellar Regions? A Theoretical Study*. Org. Biomolec. Chem., **2012**, *10*, 652-662.

N. Watanabe; A. Kouchi, *Measurements of Conversion Rates of CO to CO_2 in Ultraviolet-Induced Reaction of Amorphous $D_2O(H_2O)$/CO Amorphous Ice*. Astrophys. J., **2002**, *567*, 651-655.

C. Wentrup; H. Briehl; P. Lorencak; U. J. Vogelbacher; H. W. Winter; A. Maquestiau; R. Flammang, *Primary Ethynamines ($HC{\equiv}CNH_2$, $PhC{\equiv}CNH_2$), Aminopropadienone ($H_2NCH{=}C{=}C{=}O$), and Imidoylketene ($HN{=}CHCH{=}C{=}O$) - Preparation and Identification of Molecules of Cosmochemical Interest*. J. Am. Chem. Soc., **1988**, *110*, 1337-1343.

R. W. Wilson; K. B. Jefferts; A. A. Penzias, *Carbon Monoxide in Orion Nebula*. Astrophys. J., **1970**, *161*, L43-L44.

D. E. Woon *The Astrochymist*. http://www.astrochymist.org/ (accessed February 23, 2015).

S. Yamamoto; S. Saito; M. Ohishi; H. Suzuki; S. Ishikawa; N. Kaifu; A. Murakami, *Laboratory and Astronomical Detection of the Cyclic C_3H Radical*. Astrophys. J., **1987**, *322*, L55-L58.

B. Yang; R. Wu; G. Berden; J. Oomens; M. Rodgers, *Infrared Multiple Photon Dissociation Action Spectroscopy of Proton-Bound Dimers of Cytosine and Modified Cytosines: Effects of Modifications on Gas-Phase Conformations*. J. Phys. Chem. B, **2013**, *117*, 14191-14201.

Z. Yang; B. Eichelberger; M. Y. Carpenter; O. Martinez Jr; T. P. Snow; V. M. Bierbaum, *Experimental and Theoretical Studies of Reactions Between H atoms and Carbanions of Interstellar Relevance*. Astrophys. J., **2010**, *723*, 1325-1330.

Z. Yang; B. Eichelberger; O. Martinez Jr; M. Stepanovic; T. P. Snow; V. M. Bierbaum, *The Influence of Spin Effects on the Gas Phase Reactions of Carbanions with N and O Atoms*. J. Am. Chem. Soc., **2010**, *132*, 5812-5819.

Z. Yang; T. P. Snow; V. M. Bierbaum, *Computational Studies of Gas Phase Reactions of Carbon Chain Anions with N and O Atoms*. Phys. Chem. Chem. Phys., **2010**, *12*, 13091-13098.

Z. Yang; C. A. Cole; O. Martinez, Jr.; M. Y. Carpenter; T. P. Snow; V. M. Bierbaum, *Experimental and Theoretical Studies of Reactions Between H atoms and Nitrogen-Containing Carbanions*. Astrophys. J., **2011**, *739*, 19-29.

Z. Yang; M. T. Rodgers, *Tautomerization in the formation and collision-induced dissociation of alkali metal cation-cytosine complexes*. Physical Chemistry Chemical Physics, **2012**, *14*, 4517-4526.

M. K. Yim; J. C. Choe, *Dimerization of HCN in the Gas Phase: A Theoretical Mechanistic Study*. Chem. Phys. Lett., **2012**, *538*, 24-28.

A. Zhachkina; M. Liu; X. Sun; F. S. Amegayibor; J. K. Lee, *Gas-Phase Thermochemical Properties of the Damaged Base O(6)-Methylguanine versus Adenine and Guanine*. J. Org. Chem., **2009**, *74*, 7429-7440.

C. M. Zimmermann; G. P. Jackson, *Gas Chromatography Tandem Mass Spectrometry for Biomarkers of Alcohol Abuse in Human Hair*. Ther. Drug Monit., **2010**, *32*, 216-223.

E. L. Zins; C. Pirim; L. Vettier; M. Chaboud; L. Krim, *May Interstellar Leucine React with NO Radicals Present in Interstellar/Interplanetary Medium? An Ion-Trap Mass Spectrometry Study*. Int. J. Mass Spectrom., **2013**, *348*, 47-52.

NIST Chemistry WebBook, NIST Standard Reference Database Number 69. National Institute of Standards and Technology, webbook.nist.gov, accessed 2010-2014.

Finnigan LCQ Series Hardware Manual 97344-97023 Revision B. *Thermo Electron Corporation*, Technical Publications: San Jose, CA, 2005.